EVALUATING THE LOW-LEVEL JET AND OZONE TRANSPORT IN CENTRAL TEXAS: PHASE 2 – INFLUENCE OF OTHER CONSTITUENTS ON OZONE

GRANT ACTIVITIES NO. 582-08-86246-FY10-08
DELIVERABLE 9 –FINAL REPORT FOR 2010
ARLYN ANDREWS, SAM OLTMANS AND LAURA PATRICK
DUE FEBRUARY 28, 2010

ABSTRACT

KWKT tower in Moody, Texas has been the home to NOAA's CO, CO_2 and meteorological continuous-monitoring equipment since 2006. Additional instrumentation was installed in April, 2009 and the tower now hosts a number of continuous-sampling instruments at multiple levels (6m, 30m, 122m and 457m above ground level (AGL)), that measure ozone (O_3), carbon dioxide (CO_2), carbon monoxide (CO), and meteorological components (temperature, relative humidity, wind direction and wind speed) every 30 seconds. The purpose of the second phase of this grant was to continue measurements of ozone in Central Texas through October 31, 2010 in order to determine the influence on ozone levels in Central Texas of air that carries ozone and precursors from upwind sources. In order to accomplish this mission, we characterize the frequency, strength, and direction of the nocturnal low-level jet in central Texas through all seasons of the year. In addition to continuous tower measurements, a flask-sampling intensive was conducted during late August and September, in pursuance of identification of O_3 precursors that may have urban and industrial sources. Instrumentation at the site, data collection and quality assurance, and instrument calibration is discussed in detail. Major accomplishments, as well as difficulties, of the project are discussed. General seasonal trends are presented and we characterize the low-level jet, which includes quantification of diurnal and seasonal nighttime median wind, ozone, CO, and CO_2 values. We also evaluate the effect of the low-level jet on transport of O_3 and O_3 precursors from urban and industrial sources. Conclusions from this study are that the nighttime low-level jet exists, but only occasionally brings high ozone concentrations into the tower area during the summer months. However, during the other seasons, high ozone pulses coming in the nighttime jet are more frequent. Whether the high ozone pulses from those cities affect the surface-level ozone is dependent on whether vertical mixing is present at the time of the pulse. In addition to study conclusions, recommendations for further study and unresolved issues are also discussed.

INTRODUCTION

PURPOSE

The purpose of the second phase of Grant Activities No. 582-08-86246-FY10-08 was to extend the KWKT-TV tower (near Moody, Texas—please note this site is distinct from the Moody Tower site on the University of Houston's downtown campus) measurements of ozone in Central Texas through October 30, 2010 to determine the influence on ozone levels in Central Texas of air that carries ozone and precursors from upwind sources. Phase two of this project has two objectives. The first is to continue to characterize the frequency, strength, and direction of the nocturnal low level jet in central Texas through all seasons of the year. The second objective is to evaluate the effect of the low level jet upon daytime and nighttime transport of ozone from urban and industrial sources upwind of the KWKT-TV tower with particular attention paid to the influence of other co-transported constituents on ozone production or loss, and especially source identification.

The National Oceanic and Atmospheric Administration Earth System Research Laboratory Global Monitoring Division (NOAA/ESRL/GMD) currently has a lease to operate sensors installed on and at the base of the KWKT-TV tower near Moody, Texas. The tower is instrumented at two levels (30m and 457m) for measuring winds, temperature, relative humidity, and at three levels (30m, 122m and 457m) for measuring Carbon Monoxide (CO) and Carbon Dioxide (CO_2). During Phase One of this study, ozone sensors were installed at the 457- meter and 30-meter levels where the measurements noted above are also made. In addition, an ozone analyzer and meteorological sensor package of instruments to measure wind speed, wind direction, temperature and humidity were installed near the surface (6 m above ground level). Phase one also included the launch of ozonesondes during the peak ozone season (August 25 – September 14, 2009) to measure the vertical profile of winds and ozone through the jet.

While the continuously measured CO and CO_2 that are currently observed along with ozone at two tower levels provide continuous and important information on possible sources contributing to the ozone measured at the tower, they are limited in the ability to distinguish among various emission regions and types of emission sources. This phase of the grant focused on providing additional information from analysis of flask measurements. On a near daily basis, flask samples are taken from the tower and analyzed for a wide range of gases. These flask samples provide a powerful tool for identifying various emission sources. An intensive campaign during summer 2010 was performed with higher frequency flask sampling and expanded analysis that included $^{14}CO_2$, a strong marker for pollution, and non-methane hydrocarbons (NHMCs). The constituents measured in the flasks provide information about upwind sources that may help to characterize high ozone events.

Data gathered at this site has the potential to assist researchers in investigating the transport of ozone and ozone precursors to central Texas from urban and industrial sites, for emissions from new power plants, and as a benchmark for evaluation of other regional-scale phenomena at several different levels in the boundary layer of the troposphere. The project provides support for analysis and interpretation of this unique data set, which could yield important insights into regional scale ozone transport in central Texas. The success of the project could also validate the need for follow-up studies.

BACKGROUND

Ozone formed at ground level during ozone pollution episodes mixes through the depth of the boundary layer during the course of the day. Typically the ozone concentrations near the surface erode during the night as a nocturnal inversion forms and decouples the surface from the upper air. However, it has been found that a residual layer of high ozone persists throughout the night above the nocturnal surface layer. This layer of enhanced ozone is then available the next morning to be mixed down to the surface where this residual ozone serves as an initiator for the daytime ozone chemistry.

The development and subsequent evolution of this nocturnal layer has been studied with episodic aircraft measurements but has not been monitored on a continuous basis over an extended period of time. Continuous ozone measurements were collected near the surface and at altitudes of 30 and 457m on a tall-tower near Waco, Texas in order to better understand the formation and transport of the elevated ozone layer and its contribution to surface ozone formation both locally and on a regional scale.

During the summer of 2006, wind, CO and CO_2 data were collected at the KWKT-TV tall tower site. When combined with back trajectory data, the wind speeds and directions measured at the tower helped identify source regions and industrial sources in central Texas. Preliminary analysis of the 2006 data has also identified unique ratios between CO and CO_2 that allow discrimination between electric generating units and other industrial sources.

As part of TEXAQS 2006, a prototype analyzer was installed at the 457 m level on the KWKT tower along with an analyzer measuring at the near-surface height of 6 meters. The analyzers operated from July-December 2006. These measurements confirmed the maintenance of the nighttime residual ozone layer at the top of the tower, particularly during the summer months. Several high ozone episodes (O_3 > 80 ppb) were recorded during this campaign. Preliminary analysis (Andrews et al., 2009) indicated influence on the high ozone readings by transport from large urban regions (Houston and Dallas). Additional instrumentation was added to the

tower site during April 2009 to measure ozone concentrations at 6m (surface), 30m and 457m. A meteorological measurement system was also installed at 6m to monitor conditions at the surface in order to create a more complete vertical profile. With the instrument additions at the surface, 30 and 457 meters, the measurements provide detailed information on the vertical wind speed and direction of the jet during both day and night. The continuous measurements have provided a wealth of information on the transport patterns impacting the tower site and the strong variations in transport that contribute to the observed ozone distribution. The instrumentation added in 2009 is a positive addition to the CO/CO_2 and meteorological measurements that have existed on the tower for several years. During 2010, instrumentation was maintained, refurbished, and/or replaced, but the basic instrument design remained similar to that of 2009. All site instrumentation is described in detail in the following section.

INSTRUMENTATION

All the ozone instrumentation installed at the WKT site in April 2009 is based on UV absorption at 254 nm. Table 1 shows the instrumentation that existed at KWKT tower before April 2009 and new instrumentation that was installed for this work. Two ozone instrument models are now in use at the site, one larger unit housed in the trailer at the surface and a smaller, more portable, weatherproof model in two tower locations. A meteorological measurement system, similar to those previously existing at the 30m and 457 m-tower levels was also installed at the surface. The continuous CO and CO_2 analyzers have been operating at the site for several years and are briefly described. Flask samples, which are regularly taken at the site and were taken at an increased rate during the Ozone Season Flask Intensive, are collected with programmable flask packages and sent back to NOAA/ESRL/GMD in Boulder for analysis. The flask instrumentation and the analysis process are detailed as well.

SURFACE (6M) OZONE INSTRUMENT

A Thermo Scientific Ozone Analyzer, Model 49*i* O_3 Analyzer (Photo 1) was installed in the instrumentation trailer at the base of the tower. An inlet for this instrument was installed at 6 m AGL (Photo2). The Model 49*i* Ozone Analyzer is capable of taking observations at up to 1-minute time resolution. This system is currently implemented at 12 NOAA long-term surface ozone monitoring sites. A general description excerpted from the Thermo Scientific brochure for the Model 49*i* is as follows:

> *The Thermo Scientific Ozone Analyzer, Model 49i utilizes UV Photometric technology to measures the amount of ozone in the air*

> *from ppb levels up to 200ppm. The Model 49i is a dual cell photometer, the concept adopted by the NIST for the national ozone standard.*
>
> *Dual range and auto range are standard features in this instrument. Because the instrument has both sample and reference flowing at the same time a response time of 20 seconds can be achieved. Temperature and pressure correction are standard features. User settable alarm levels for concentration and for a wide variety of internal diagnostics are available from an easy to follow menu structure.*

The analyzer, which can be operated remotely by computer, measures in the range from 0.05 to 200 ppm with a precision of 1 ppb, so is well-suited for any surface-layer ozone conditions. Table 2 gives instrument specifications as provided by Thermo Scientific for the Model 49i Ozone Analyzer. The instrument also has very little drift and will run without maintenance for long periods of time, as proven at other NOAA monitoring sites.

TOWER (30M AND 457M) OZONE INSTRUMENTS

Ozone instrumentation was installed at the 30 m and 457m locations in April 2009, but both instruments were replaced in May 2010. The continuous measurements are made using a compact, light-weight analyzer manufactured by 2B Technologies of Boulder, Colorado. For the latest instrument installation in May 2010, we procured a Model 205 Ozone Monitor, whereas last year the instrument was a Model 202 Ozone Monitor. The upgrade to a dual-beam, rather than a single-beam instrument was based on a desire for increased precision and decreased noise. For 1-minute measurements the precision of the 2B analyzer (Photo 3) is the greater of 1 ppb or 2% of the reading. This is similar to the surface TEI 49*i*, in which the comparable precision would be 1.0 ppb. The accuracy of the 2B analyzer for continuous observations over a several-month operating period is also on the order of 1-2 ppb. More information about the analyzer is as follows from the 2B brochure:

> *The Model 205 Ozone Monitor makes use of two detection cells to improve precision, baseline stability and response time. In the Dual Beam instrument, UV light intensity measurements ozone-scrubbed air and unscrubbed air are made simultaneously.*

The 2B Technologies Model 205 Ozone Monitor™ is designed to enable accurate and precise measurements of ozone ranging from low ppb (precision of ~1 ppb) up to 100,000 ppb (0-100 ppm) based on the well-established technique of absorption of UV light at 254 nm. The Model 205 Ozone Monitor has been approved by the EPA as a Federal Equivalent Method (FEM) based on a modification of the Model 202.

The Model 205 Ozone Monitor™ is light weight (4.7 lb., 2.1 kg.) and has low power consumption (12V DC, 0.33 amp, 4.0 Watt) relative to conventional instruments and is therefore well suited for applications such as:

Vertical profiling using balloons, kites, RPVs and light aircraft where space and weight are highly limited

Long-term monitoring at remote locations where power is highly limited

The lightweight analyzer has low power requirements, a flow meter, and back-up pump which made it useful for our application on the tower. The instrument has a temperature operating range of 0-50°C, (but can operate at -20-50°C with modifications).

As part of the 2010 effort, a 2B ozone analyzer (blue unit in Photo 4) was procured and built into a weather-proof, temperature- regulated case for installation at the 457-m tower level. The instrument that had previously operated at the 457-m level was refurbished as a spare. Supplemental components were added to enhance the long-term performance and data transmission such as:

Thermostatically-controlled Air blower and heaters
Large particle filter
Zeroing cycle (to quantify drift)
Computer control board
Improved catalyst (MnO_2)
Power supply (convert 110VAC to 12VDC)
Upgraded pump with a 2-year minimum lifetime

All of the ozone analyzers at the time of installation or repair have been calibrated against a NIST-traceable standard. The analyzers were compared with a network standard TEI49i ozone analyzer maintained by NOAA/ESRL/GMD either through direct comparison or by comparison with a TEI49C Ozone Calibrator calibrated against the NOAA/GMD standard. The NOAA/GMD

network standard is against the NOAA/GMD standard. The NOAA/GMD network standard is regularly compared against the Standard Photometer (SP) maintained by NIST at Gaithersburg, MD. All reported data are on the NIST scale.

METEOROLOGICAL INSTRUMENTATION

An additional meteorological measurement system was installed at the surface level. This system combines several sensors, a Vaisala HMP45AC temp humidity sensor, a Met One Instruments Model T200A Platinum resistance temperature sensor, a Gill Instruments Wind Observer II, and a Met One Instruments Radiation Shield model 077. The specifications and other details on these instruments can be found at:

HMP45AC temperature/humidity sensor (Vaisala):
http://www.campbellsci.com/hmp45c-l
Model T200A Platinum resistance temperature sensor (Met One instruments):
http://www.metone.com/documents/T-200A_DS.PDF
Radiation Shield model 077 (Met One instruments):
http://www.metone.com/documents/077AspiratorTemp.pdf
Wind Observer II, Ultrasonic Anemometer (Gill Instruments):
http://www.gill.co.uk/products/anemometer/wind_ob2.htm

The Vaisala temperature/relative humidity probe has an accuracy of approximately 1% and can measure a range from 0.8% to 100% relative humidity. The Wind Observer II gives wind directions and wind speeds of up to 65 m/s with an accuracy of 2%. These combination meteorological systems have been operating at other sites and on the tower for many years with good success.

CONTINUOUS CO AND CO_2 ANALYZERS

The CO_2 and CO analysis system at WKT was been developed for deployment at sites in the NOAA Earth System Research Laboratory's (ESRL) Carbon Tracker Tall Tower Observing Network. The design is largely derived from the original CO_2 and meteorological sampling equipment deployed at the NOAA ITN, LEF, WKT and AMT tall tower sites (Zhao, Bakwin et al. 1997; Bakwin, Tans et al. 1998), but with modifications to minimize sensitivity to environmental conditions (such as room temperature). The precision and long-term stability of the systems in the field are typically better than 0.1 ppm for CO_2 and 6 ppb for CO, as determined from repeated measurements of a suite of standard gases and comparison with flask samples of air collected at the sites. The instrumentation is fully automated and includes sensors for

measuring a variety of engineering parameters, such as temperature, pressure and flow data, that are inputs for automated quality control algorithms. Each analyzer has three sample inlets for profile sampling, and a complete profile is obtained every 15 minutes.

The CO instrument used at WKT is the Thermo Electron Corporation 48C trace-level CO Analyzer:

> *The Model 48C Gas Filter Correlation (GFC) CO Analyzer measures low CO concentrations. The Model 48C is based on the principle that carbon monoxide (CO) absorbs infrared radiation at a wavelength of 4.6 microns. Because infrared absorption is a nonlinear measurement technique, it is necessary for the instrument electronics to transform the basic analyzer signal into a linear output. The Model 48C uses an exact calibration curve to accurately linearize the instrument output over any range up to a concentration of 10,000ppm. The sample is drawn into the analyzer through the SAMPLE bulkhead. The sample flows through the optical bench. Radiation from an infrared source is chopped and then passed through a gas filter alternating between CO and N_2. The radiation then passes through a narrow bandpass interference and enters the optical bench where absorption by the sample gas occurs. The infrared radiation then exits the optical bench and falls on an infrared detector.*

The LI CO_2/H_2O Gas Analyzer is the CO_2 instrument used at WKT:

> *The LI-7000 CO_2/ H_2O Gas Analyzer is a high performance, dual cell, differential gas analyzer. It uses a dichroic beam splitter and two separate detectors to measure infrared absorption by CO_2 and H_2O in the same gas stream. At the heart of the LI-7000 is an innovative optical bench that can be dismantled and cleaned by the user without the need for factory recalibration.*

PROGRAMMABLE FLASK AND COMPRESSOR PACKAGES

The Summer Flask Sampling Intensive occurred from 27 August to 9 October 2010 and employed Programmable Flask and Compressor Packages designed by the Carbon Cycle Greenhouse Gases Group (CCGG) at NOAA. While this sampling system was initially designed specifically for use on small aircraft, it is now also being operated at unattended tall-tower and surface NOAA sites. At the KWKT tall-tower site, flask samples are usually acquired at a rate of one package (12 samples-6 pairs on 6 days) per week, but the frequency of sampling was considerably increased during the Intensive.

The sampling system (Photo 5) consists of a programmable compressor package (PCP) and a programmable flask package (12-pack or PFP). A PCP includes two pumps that have been plumbed in series. The 12-pack is composed of twelve 0.7L borosilicate glass flasks, a stainless-steel manifold system, glass valves sealed with Teflon O-rings, and a data logging and control system.

For each sample, the inlet line and internal manifold are first flushed with 25 liters of ambient air. The valves on both ends of the selected flask are then opened and the flask is flushed with 10 more liters of ambient air to displace the dry, low-CO_2 (~330 μmol/mol) fill gas with which the flasks are shipped. The downstream valve is closed and pressurization begins. An additional ~1.55L of sample will be added once the downstream flask valve has been closed.

The 12-pack is sent back to NOAA/ESRL in Boulder, CO, for analysis of as many as 55 trace gases. The greenhouse gases are measured by the Measurement of Atmospheric Gases that Influence Climate Change (MAGICC) system, which consists of custom-made gas inlet systems, gas-specific analyzers, and system-control software. Photo 6 shows the MAGICC lab set-up at NOAA that analyzes up to 55 greenhouse gases. A portion of sample flows into a gas chromatograph (GC), which uses an electron capture detector to measure N_2O and SF_6 with a repeatability of 0.4 ppb and 0.03 ppt respectively (Dlugokencky et al., in preparation, 2010). Instrument precision for N_2O is ~0.2 ppb. Another ~50 ml of sample is diverted to a second GC, where pulsed-discharge He ionization isolates H_2 before detection, providing a precision of ±0.4 ppb for H_2 (Novelli et al., 2009). Two instruments are currently used to measure CO, however individual flasks are not measured on both. CO is also determined by either resonance fluorescence at ~150 nm with a precision of ±0.4 ppb, or by UV absorption spectroscopy with precision ~ 1 ppb (Novelli et al., 1998). Long-term comparison of the two systems show the GC and fluorescence measurements agree within ~ 1 ppb. A fourth ~50 ml aliquot of sample is diverted to a GC analyzer for flame-ionization detection of CH_4 with a precision of ±1.2 ppb (Dlugokencky et al., 1994). Finally, a non-dispersive infrared analyzer measures the last 100 ml of sample for CO_2 with a precision of ±0.03 ppm (Conway et al., 1994). Flask sample responses are calibrated versus whole air working reference gases which, in turn, are calibrated with respect to primary international standards maintained by NOAA/GMD.

More than 30 halocarbons, hydrocarbons and sulfur containing trace gases are also routinely measured at NOAA using a separate analysis system. The gases are measured using a GC/mass spectrometric (GCMS) technique that requires ~200 ml aliquots from each flask. Each sample is pre-concentrated with a cryogenic trap near liquid nitrogen temperatures. Analytes desorbed at ~140°C are then separated by temperature-programmed GC column (combination 25m x 0.25mm DB5 and 30m x 0.25mm Gaspro), followed by detection with mass spectrometry to monitor compound-specific ion mass to charge ratios. Flask sample responses are calibrated

versus whole air working reference gases which, in turn, are calibrated with respect to gravimetric primary standards (NOAA scales: CFC-11 on NOAA-1992, CFC-12 on NOAA-2001, HFC-134a on NOAA-1995, benzene on NOAA-2006 and all other hydrocarbons (besides methane) on NOAA-2008). Absolute uncertainties for analyses reported here are <5%.

After analysis on the NOAA MAGICC and GCMS systems, the flask packages are typically sent to the University of Colorado INSTAAR Laboratory for measurement of the stable isotopes of carbon dioxide ($\delta^{13}C$ of CO_2 and $\delta^{18}O$ of CO_2).

For the Ozone Season Flask Intensive, samples were also measured for Radiocarbon ($^{14}CO_2$, the $^{14}C/^{12}C$ ratio of CO_2). Carbon dioxide emitted during fossil fuel combustion is completely devoid of radiocarbon (the half-life of radiocarbon is 5730 years), so radiocarbon measurements can be used to estimate the amount of observed CO_2 resulting from fossil fuel contribution. The high precision $^{14}CO_2$ measurements are made through a combination of effort at the University of Colorado INSTAAR Laboratory for AMS Radiocarbon Preparation and Research (NSRL) and the accelerator mass spectrometer at University of California at Irvine. The process begins by: (a) extracting the CO_2 from whole air, using a cryogenic extraction system [*Turnbull et al., 2009*]; (b) reducing the CO_2 to elemental graphite over Fe catalyst with $Mg(ClO_4)_2$ to remove water; and (c) making the ^{14}C measurement with a high-count accelerator mass spectrometer (AMS) (Turnbull et al. 2007).

Finally, samples from the Ozone Season Flask Intensive were also sent to another INSTAAR laboratory for GCMS analysis of Non-Methane Hydrocarbons (NHMCs). The INSTAAR GCMS is designed to measure some compounds that are not reported by the NOAA GCMS laboratory. These include ethane, isoprene, iso-butane, n-pentane, and n-hexane. Ratios among hydrocarbons can provide information about the origin and age of upwind pollution.

The regular PFP hardware was modified for the summer 2010 campaign to allow for larger samples to be collected. This modification allowed the system to take three flask samples at 2.1 standard liters simultaneously versus two samples back to back at 0.7 liters. The improved hardware also allowed for multi-package setup (up to three PFP units attached to the system at a time) for increased flexibility in event sampling. The flushing limits were increased to 50 liters for the manifold flushing and an increase in sample flushing to 15 liters per flask. Also the collection times for the samples were modified to capture periods of high pollution manually along with the regularly scheduled sampling time which collects air at the tower which targets well-mixed afternoon conditions (20:30 GMT = 15:30 CDT =14:30 CST). The manual sampling mode was used to collect several early morning samples during pollution episodes. Morning samples were meant to provide information about air aloft that would mix down to the surface later in the day. Forty samples were selected for VOC and Radiocarbon analysis with an

emphasis on sampling during pollution events, accompanied by clean boundary air conditions on neighboring days. Elevated levels of O_3 and CO were used to identify polluted air.

GRANT TASK FULFILLMENT

In order to execute the study and fulfill the tasks of the grant, tower ozone instrumentation was refurbished and replaced, measurements were collected and Quality Assured/Quality Controlled (QA/QC'd), and an Ozone Season Flask Intensive was conducted during late August through early September. Since the 2010 Notice to Commence was issued, monthly status reports, four preliminary reports and this summarizing report were emailed to the Project Leader. Table 3 shows the tasks and deliverable due dates and the following section summarizes accomplishments and details difficulties encountered of fulfillment of a few select tasks.

TASK 3, TASK 4 AND TASK 6 - DATA COLLECTION BETWEEN JANUARY 2010 AND OCTOBER 2010, AND TASK 2 – MONTHLY REPORTS

ACCOMPLISHMENTS

Task 3, Task 4 and Task 6 of the grant included collecting hourly measurements from all the instruments. Hourly measurements for April 1, 2009 through December, 2010 have been collected. The measurements collected at the site are automatically saved in a single data system for all instruments except the surface ozone analyzer, which is separately accessed on a remote computer application each week and the data downloaded.

At the end of each season, the data was QA/QC'd and analyzed to determine the day and night average wind speed, modal wind directions, and average ozone concentrations measured at the tower. The hourly averages were created for the meteorological data. Some finer resolution (one-minute) tower ozone data was produced, as well as the ozone hourly averages. The CO and CO_2 continuous measurement data was also QA/QC'd and archived on the ftp site as hourly averages.

The procedures to QA/QC the data were specific to each instrument output. Therefore, four different processes were used for the QA/QC of the data. For surface ozone data, computer programs were written to initially QA/QC the data and data not meeting quality requirements was removed, though this is quite rare for this instrument because it is so stable and protected from the elements. The data was then adjusted with calibration factors that were created with an initial NIST-standardized calibrator and the occasional remote calibration of the instrument. The surface data was then plotted and visually checked for any outliers.

The tower ozone instruments were initially calibrated against the NIST-standardized ozone calibrator in the laboratory. Both instruments have a "zero cycle" that removes all the ozone from the instrument intake each day for 10 minutes. Over time, these zero values are used to calculate whether the instrument is drifting. If drift occurs, the data is adjusted for this value. The process for quality assurance with the tower ozone instruments involved writing programs that removed the zero cycle data and removed any instrument spikes or obvious outliers to the dataset. The 30-second data was then visually inspected and one-minute and hourly averages created from the resulting data.

The wind direction files were processed into one-hour modes and the wind speed files into one-hour averages. Wind direction at each level was checked for reasonableness against the other layers. Although at times, wind directions are expected to vary, the overall wind direction during the night (when the winds are stronger) is often similar for the three levels, indicative of good quality measurements at all levels.

The CO and CO_2 data were filtered with previously-created computer code and then visually checked. Flags are added to the carbon data to give the user a quality reference. The carbon data for 30m, 122m and 457m were processed into data files. The created files include hourly averages and the original data resolution, which is variable for the different levels. The data is offered in several formats and on a publically-available ftp site.

Since data has been continuously collected since April 2009, Task 3, Task 4 and Task 6 could be more easily accomplished this year than last grant year. Programs for processing were already written and a procedure for data QA/QC had already been established last year, so the time required for these tasks was much shorter. All data, which are output from the instruments in Greenwich Mean Time (GMT), were translated into Texas Local Standard Time for ease of the data user. The data for CO, CO_2, wind speed and direction, and ozone were QA/QC'd and posted on the data ftp site (ftp://ftp.cmdl.noaa.gov/ozwv/towers/wkt/).

In addition to the completion of the three tasks, Deliverables 3, 4, and 6 (Preliminary Reports 3.1, 4.1 and 6.1 respectively) were generated and delivered to the Project Manager via email. Monthly reports, which were included in Task 2, regarding the status of the instrumentation and data collection were written and sent via email for each month of the grant period.

DIFFICULTIES IN COMPLETING TASK

The only difficulty encountered during the completion of Task 3 was the release of one-minute ozone data at the 30-m and 457-m levels. During the winter of 2009 and early 2010, the

performance of the surface ozone instrument was quite good. However, the tower ozone instruments, at 30m and 457m, both became quite noisy during this time period. After speaking with representatives from 2B Technologies (the company that manufactures the primary components for the tower-mounted instruments), we determined that the optical bench lamp temperatures were not staying warm enough to make steady measurements. However, after analyzing the collected data, we found that the one-hour averages of the data (with a filter to remove some noise) are actually quite consistent with ground measurements, so we feel confidence in using them. We will not release the one-minute data (not required by grant) during this period for these two levels, as it is not useful to the general public.

The instruments performed well overall during the Task 4 time period (Data Collection between May and June 2010). During May, new tower ozone instruments were mounted (see following section: Task 5 – Replace or Refurbish Tower Ozone Instruments), and were recording reasonable values 95% of the time. Before the new instruments were put up (early May), there is a missing two-week period of data at 457-m level due to no communication with that level's met box.

Task 6 was a period that included four months of data collection (July through October 2010). There were a few instrument issues during this time and some periods of no communication with instruments. Most of the issues did not increase the difficulty of processing the data, but did create some periods of missing data. During data analysis of July and August, we found that water was getting in the surface ozone instrument filter from condensation due to the air conditioner and giving some periods of false data. This condensation issue was remedied by wrapping the inlet line in heating pads. The data did have to be visually inspected and the questionable data removed manually because many of the ozone values were in a reasonable range (but not matching up to the two tower instrument data) and not being picked out by the data filtering program.

TASK 5 - REPLACE OR REFURBISH TOWER OZONE INSTRUMENTS

ACCOMPLISHMENTS

Task 5, Replace or Refurbish the Tower Ozone Instruments, was carried out in May 2010. Between October 2009 and May 2010, the 30-meter and 457-meter instruments became increasingly noisy in their 30-second readings. Although we were able to filter the data and produce good one-hour averages, it was beneficial to install new instruments. A brand-new

instrument was installed at 457 meters and a refurbished instrument was installed at 30 meters.

After investigation of the noisy data between October and May and speaking with 2B Technologies (the designer of the instruments), we determined the noise was likely due to the lamp in the optical bench not remaining warm enough to stay stable during the winter months. The brand-new 457-m replacement instrument was designed with an increased number of heaters and a more precise thermostat to counter this problem. Before installation on the tower, the lamp and heater functionality were tested in a cold room. A larger blower for cooling (instead of a small fan) and new software that identifies the daily zero cycles were also built into the new instrument. As an additional safeguard against noisy data, this new instrument was a Model 205 Dual Beam instead of single beam like the previous ones on the tower. In a dual-beam setup the reference path and a sample path are measured at the same time, after which solenoids switch the optical cells on the next sample (every 2 seconds). Additionally, a working instrument was taken off the Boulder Atmospheric Observation (BAO) tower and refurbished. This instrument was used to replace the ozone instrument at the 30-m level. During a climb on May 27, 2010, the two instruments were mounted on the tower and replaced the older instruments.

DIFFICULTIES IN COMPLETING TASK

Difficulties encountered during this task were primarily after the instruments were mounted on the tower. The weather, which is usually the largest deterrent to a successful tower climb was good the day we installed the instruments. During August, there was an outage of power to the "met box", the system that collects the ozone, wind, temperature and relative humidity data readings. The box was switched out on September 10, 2010. Another issue that appeared was the outage of a fan on the refurbished instrument that went up at the 30-m level. When the fan died, the instrument began to give intermittent data. When the temperature was over ~50°C inside the metal ozone box, the instrument would not give reasonable values. So, there was intermittent data from the end of July through mid-August and then was replaced in early September. Since that time, it has been reading well.

TASK 8 – OZONE SEASON FLASK SAMPLING INTENSIVE TOWER SITE

ACCOMPLISHMENTS

We report data from forty five flask samples collected from 27 August – 9 October 2010. Of these, forty one were mid-afternoon samples collected at 20:30 GMT (15:30 CDT, 14:30 CST). The remaining four samples were collected at 10:00 GMT (5:00 CDT, 4:00 CST) during the period 30 September through 3 October 2010. We investigated whether these samples, together with in situ ozone data from 457m agl, will provide information about concentrations of polluted air aloft that can mix down to the surface later in the day.

We were fortunate to sample several pollution events with distinct source regions during the intensive. Trajectories from the NOAA model HYSPLIT (Appendix A) were used along with images from the Texas AIRNow (Appendix B) website in order to decide which samples to send for Radiocarbon/VOC analysis. We also took into account ozone data from the TCEQ website for Killeen Skylark Field. Thirty six samples were selected for NMHC analysis, and thirty eight samples were selected for radiocarbon analysis.

The data for the Summer Flask Sampling Intensive is posted on the data ftp site (ftp://ftp.cmdl.noaa.gov/ozwv/towers/wkt/).

DIFFICULTIES IN COMPLETING TASK

Difficulties in this task occurred when Hurricane Hermine passed by the site on September 7 (Appendix B) and caused a power outage. A NOAA technician visited the site on 9-10 September to restart the system and supervise climbers who were replacing ozone and met equipment on the tower. Flask and in situ data are unavailable for the period from ~12:00 GMT 7 September 2010 to 0:00 GMT on 10 September.

The NOAA GCMS data analysis software was being updated during and after the flask sampling intensive. We were therefore unable to include NOAA GCMS data in the Preliminary Report for this task. Those data are available now and have been posted on the data ftp site.

There was a substantial delay (> 4 months) between sample collection and the availability of the radiocarbon data. At the time the grant proposal was written, we did not anticipate such a lengthy delay. Thus, we requested an extension of the deadline for the final report. The radiocarbon data are now available and have been posted on the data ftp site along with other flask measurements.

TREND ANALYSIS AND FINDINGS

The purpose of the second phase of this grant was to continue measurements of ozone in Central Texas through October 31, 2010 in order to determine the influence on ozone levels in Central Texas of air that carries ozone and precursors from upwind sources. In order to accomplish this mission, we characterize the frequency, strength, and direction of the nocturnal low-level jet in central Texas through all seasons of the year.

In order to characterize the nighttime low level jet, wind speeds and directions, ozone, CO, and CO_2 values were analyzed for diurnal and seasonal trends. Nighttime and daytime measurements were separated to identify whether the nighttime and/or daytime data showed differing seasonal patterns. Seasons were separated for this 2010 Final Report differently than they were in 2009, based this year on dominant wind patterns: spring (March, April, May), summer (June, July), fall (August, September, October) and winter (November, December, January and February). Winter wraps around, so winter was separated into actual year. Winter 2010 is equal to January and February 2010 and also November and December 2010 (when data is available). 2009 data is reanalyzed for comparison to 2010 data and is created from January, February, November and December 2009.

Findings are presented and included are subsections on the Flask Sampling Intensive and one with examples that help demonstrate findings. HYSPLIT model back trajectories were created for special cases, particularly during very high or very low concentration ozone events.

WIND SPEEDS

Wind speeds were monitored at 6 m, 30m and 457m, and were collected as 30-second averages. The data were analyzed and QA/QC'd before being made publically available on the ftp site. Measured wind speeds vary with altitude and wind direction, seasonally, and diurnally.

ALTITUDEVARIATION

Wind speed varies with height at any location, generally increasing as height increases. The variation of wind speeds with altitude, particularly high speeds aloft and lower speeds near the surface, contributes to the formation of a nighttime boundary layer (NBL). Figure 1 shows the monthly wind speed percentiles for the 6-m, 30-m and 457-m levels for 2009 and 2010. At KWKT tower, the hourly-averaged wind speeds were much faster in all months at the 457-m level than at the surface or 30m-levels (Figure 1), which was an expected result. The lower

levels also showed less monthly variability in wind speed than the highly variable winds at the 457-m level.

Figure 2 shows the 2010 monthly wind speed percentiles measured at the 457-m level, which have been separated into daytime (a) and nighttime (b) data. Although the wind speeds at 457 meters can almost double at night, the lower tower levels measured nighttime wind speeds that were similar or only slightly higher than daytime values.

DIURNAL AND SEASONAL VARIATION

The magnitude of these daytime-to-nighttime wind speed differences varies seasonally and is important to understanding the behavior of the low-level nighttime jet. During all months of the year, the nighttime wind speeds at 457 meters were increased over their daytime values (Figure 2). June, July and August nighttime speeds increased by the largest percentages and were almost double their daytime values. However, the wind speed magnitudes are lower during these months than they are during the colder months. The months of November through April have faster median winds, while the data for May through October show much slower winds. In fact, the slowest median winds are found in September at ~6 m/s and are less than half the median speed found for November, which is the month with the fastest speeds.

Investigation of the diurnal wind variation must include a seasonal analysis because as seen in Figure 2, the diurnal variation can vary by month. Figure 3 shows the 457-m wind speed percentiles for the four seasons. The diurnal cycles were analyzed in one-hour increments for each season to yield median values. At 457 meters, in all seasons, the lowest wind speeds occur at mid-day and the highest wind speeds at night. The faster nighttime winds are a somewhat expected result, occurring because of the formation of the nighttime lower-level jet. This is not, however, only a warm season phenomena, but exists year-round.

Yielding further evidence that a nighttime boundary layer exists and that the jet is present, Figure 4 shows the same diurnal averages for each season at 30 meters. At this height, the slowest speeds occur primarily in the early morning (~6 a.m. or 7 a.m.), except for during winter. During winter, which has the largest diurnal fluctuation at 30m and 457m, the minimum speed occurs at 5 p.m. and the speed peaks around 3-5 a.m. It is probable that during spring, summer and fall, there is a strong nighttime boundary layer leading to slow winds near the ground at night and wind speeds increasing aloft.

Also in Figures 3 and 4, the winter(d) and spring(a) plots show high variability, but summer and fall show much less variation in wind speed. The multidirectional winds of the winter and spring are likely the primary cause of this wind speed variability. The wind speeds, like the wind directions are much less variable during these months.

DEPENDENCY ON WIND DIRECITION

Figure 5 shows the measured 457-m wind speeds and their correlating wind directions. The speeds decrease in May, are lowest in September and begin to increase again through the winter months. The directions correspond to the wind speeds because the lowest, least variable speeds occur during the months that the flow is primarily from the WSW. During April and October, the shift away from and towards, respectively, a more multidirectional flow correlates with higher variability and increased occurrences of higher wind speeds.

MONTHLY AVERAGES

Table 4 of wind speed means supports the results we have found in the previous graphics (Figures 1-5). September shows the lowest mean wind speed at the 457-m level. April through October, except for August, at the 30-m level show the nighttime wind speeds drop below the daytime averages possibly pointing to a stronger nighttime boundary layer during these months. The 6-m mean wind speeds are generally very similar during the daytime and nighttime, sometimes dropping a little during the night, but during the months of April through October, they drop more than in the colder months.

DIFFERENCES FROM 2009 DATA

Most results of the data analysis for 2010 were similar to those of 2009. However, there were some differences in the results. In 2009, the midday summer wind speeds were slower and less variable than spring or fall wind speeds. The 2010 data shows that the wind speeds at 457m were the slowest and least variable during the fall season. However, May, September, and October are found to have the slowest median winds for 2010, which is similar to 2009, in which May and September had the slowest wind speeds. May, September and October are also the months found to have more high ozone days than other months (not necessarily the highest median ozone) as discussed later.

Another difference appears in the wind speed data for November and December. In 2009, October had the fastest winds at 457 meters, but in 2010, the fastest winds were during November and December. The general pattern between the two years at 457-m level is also quite different. In 2010, the winds gradually decrease over the spring months and the minimum speeds occur in fall (August, September and October) and then pick up again in November and December. In 2009, the wind speeds did not show a particular pattern.

CO_2

CO_2 mixing ratios were monitored at the 30 m, 122m and 457m tower levels. Samples, carried down from the three tower levels through a long intake line, were analyzed at variable time intervals. The data were automatically and visually QA/QC'd before being made publically available on the ftp site. The measured CO_2 varies with altitude, seasonally, diurnally, but does not appear to be highly correlated with wind direction.

ALTITUDE VARIATION

KWKT tower is located in a rural area comprised primarily of farmland with some riparian zones. In rural areas, CO_2 levels are dependent on plant respiration and photosynthesis, emissions from the ground, and also global CO_2 levels. The CO_2 hourly-averaged percentiles for summer (June and July) at each of the three tower levels are shown in Figure 6. As expected, maximum CO_2 values were found during the day at the tower level closest to the surface, the 30-meter level. In addition to higher concentrations near the surface, CO_2 was found to have more pronounced diurnal cycles at altitudes closest to the surface.

DIURNAL AND SEASONAL VARIATION

Since CO_2 flux is strongly correlated with leaf temperature, during the times of day with the highest irradiation, CO_2 uptake is the highest. During the night, CO_2 is then released from the plants. The largest daytime-to-nighttime CO_2 differences at the 30-m level (the lowest level of CO_2 measurement) occur during July. The summer plots in Figure 6 demonstrate the CO_2 uptake-and-release relationship with plant-life and reflect that CO_2 uptake has a strong dependency on irradiation and photosynthesis. During mid-day, when solar insolation is highest, the CO_2 drops as plants uptake the CO_2. At 6 a.m., before the sun rises to a high angle, the CO_2 has been released from the plants and reached its maximum level for the day (Figure 6a).

In addition to terrestrial CO_2 uptake, another process that is occurring at mid-day is vertical mixing, which is inhibited during the night by the formation of the nighttime boundary layer. The CO_2 diurnal cycle is very diluted at the 457-m level, pointing to the layer's separateness from the surface and the lack of mixing during the night. The peak at this level occurs at 8 a.m. during the summer season (Figure 6c), after vertical mixing has increased, but before any uptake at the surface can begin. The 457-m peak at 8 a.m. correlates well with the time that summer CO_2 values become similar at all tower levels, indicating well-mixed air. During the daily CO_2 peak, carbon monoxide mixing ratios also show a morning peak (and O_3 shows a concurrent decrease) at the 457-meter level due to this increase in vertical mixing. However,

CO is much more variable due to its anthropogenic sources and this morning peak may not be the maximum for the day.

Figure 7 shows CO_2 mixing ratios at 30, 122 and 457 meters for a) Feb 10-13 and b) June 25-28 for 2010. Figure 7b corroborates the idea that the maximum peak at 457 meters is due to the vertical mixing. The figure demonstrates that on most days in June the vertical mixing begins at ~5 a.m. The mixing is suggested by the suddenly decreasing CO_2 at 30-m and 122-m levels and the concurrent rise at 457 meters. The air near the tower becomes fully vertically mixed at approximately 8 a.m., when the CO_2 concentrations measured at the three levels become similar. During February, a similar feature is seen in the data, but at a later time in the day. In Figure 7a, the CO_2 levels become homogenous around noon for most of the days. The seasonal analysis for 2010 (Figure 10) supports that the 457-m diurnal maximum for winter (February is included) occurs at noon. During fall, the time of day that the air becomes well mixed shifts to 10 a.m., which is between the summer and winter times.

The well-mixed portion of a day on winter days is less than that on summer days. However, more mixing is seen during February nights, which is shown in Figure 7a by small nighttime peaks in 457-m CO_2 that correspond with small dips at the 30-m and 122-m levels. More vertical motion is counter to what is expected in wintertime, because thermal gradients are lessened in the wintertime and continental tropospheric stability is greater than in the summertime (Korty and Schneider, 2007). The explanation for much of the nighttime mixing may be that the 457-m nighttime winds in wintertime are much faster. If the nighttime boundary layer is also weaker, because of decreased thermal gradient present in winter, wind shear may be the cause of increased mixing at night.

Figure 8 shows the winter diurnal minimum-to-maximum difference to be much smaller than in the summer. During the typical winter day, the CO_2 values at the 457-m level stays near 395 ppm, not wavering very much during the day. During the summer, the daily minimum-to-maximum is ~ 8ppb, which is likely due to the uptake and release of CO_2 by plant life at the surface. In addition to terrestrial uptake and release, surface emissions are a further source of CO_2 and are investigated further in a following section, The Ozone Season Flask Intensive.

DEPENDENCY ON WIND DIRECTION

The measured CO_2 averages do not appear to be highly correlated with a particular wind direction. Pollution events and very high CO_2 can come from the primary seasonal direction, but no particular direction appears to yield regular amounts of higher CO_2 than another. During the summer season, when the wind is coming primarily from the WSW direction, the higher concentrations come from WSW. During winter, fall and spring, more of the high events come

from northerly directions because the wind shifts more from that direction. Often, when high concentrations of CO_2 are seen they can be traced as having come through one of the major cities (Dallas, Austin, San Antonio and Houston in a few cases).

MONTHLY AVERAGES

CO_2 averages for January through October are shown in Table 5 and support previous figures and conclusions. The 30-m level is the closest of the three levels to the ground and the measured CO_2 values show the largest day-to-night difference due to diurnal uptake and release of CO_2 by plants. The maximum 30-m day-to-night differences are in June and July, which is supported by Figure 6a.

On most nights, the nighttime boundary layer (NBL) likely includes both the 30-m and 122-m levels. These two lower levels have increasing values at night that are closer in value than when compared to 457 meters. From the values and Figure 7 it appears these two lower levels are within the NBL and 457 meters is clearly measuring separate air. The air at 457-m has traveled far and has had little contact with the ground due to inhibited vertical nighttime mixing.

The averages also show nighttime increases at the 457-m level during March, April, May and June, but not during the other months, during which CO_2 decreases at night. October shows the largest decrease from daytime to nighttime at the 457-m level. The winter months, with less vertical mixing and less of an uptake-and-release of CO_2 near the surface, show decreases at night at this level.

DIFFERENCES BETWEEN 2009 AND 2010

Analysis found differences between the two years of measurements though they have the same overall seasonal patterns. Figure 8 shows 2009 and 2010 CO_2 percentiles for the three different levels. 2010 shows generally higher CO_2 median values for all seasons. The two years also show peak median values in different months. 2009 has a CO_2 peak in March, but 2010 has a peak in February. Both years show May to have a sudden decrease in median CO_2, likely due to the combination of increased day duration, increased sun angle and rapid plant growth. Both years then show a slight increase in June and then a decrease again in July. 2009 has a CO_2 minimum in September, but 2010 shows its minimum in August.

Figures 9 and 10 show the diurnal CO_2 cycle analyzed by season for the 457-m level. All seasons in 2010 show higher CO_2, but are generally very similar except for summer. During spring, fall and winter, the daily seasonal maximums occur at the same time both years, although the minimums vary slightly from year to year for all seasons. Summer of 2010 has a much larger day-to-night difference than 2009, which only has a diurnal range of 3 ppm. The minimum and

the maximum values are respectively lower and higher than 2009, yielding a diurnal range of ~8 ppm. Although the overall CO_2 values are higher, one would expect a fairly similar diurnal range. Several factors could be influencing this much larger diurnal range in 2010, including vertical mixing and surface plant growth and/or emissions. Analysis shows during 2010, there was a much larger production-uptake cycle, but also slower wind speeds at 30 meters, which could allow for more vertical mixing to the 457-m level.

CO

Carbon monoxide is an ozone precursor and involved in the formation of ozone, in the presence of NO_x and VOCs. CO is a product of vehicle exhaust and industrial emissions, so typically peaks during the day in urban areas. Carbon monoxide is one of the important trace gases because its concentration in the troposphere directly influences the concentrations of tropospheric hydroxyl (OH). During the day, CO in the atmosphere reacts strongly with hydroxyl radicals to form carbon dioxide and HO_2 radicals, which can then react with NO_x to form O_3 (the rate is dependent on atmospheric temperature).

Carbon monoxide mixing ratios were monitored at the 30 m, 122m and 457m tower levels. Samples, carried down from the three tower levels through a long intake line, were analyzed at variable time intervals. The data were automatically and visually QA/QC'd before being made publically available on the ftp site. The measured CO varies with altitude, seasonally, diurnally, and appears to be correlated with wind direction.

DIURNAL VARIATION

CO concentrations are largely variable during the course of a day and a month (Figure 11) and calculated CO medians show no steady diurnal cycle at the 30-m or 122-m tower levels, though there are trends in day-to-night data. However, median CO concentrations at the 457-m tower level in Figure 12 show a slight diurnal cycle, increasing gradually during the daytime. Although Figure 12 shows only diurnal CO percentiles during spring (March, April and May), all seasons appear to have this gradual increase during the daytime. Although it is probable that this increase is related to transport from an urban area rather than photochemistry, as CO would theoretically decrease during the day due to reaction with OH.

Although diurnal cycles are not very discernable on a daily basis, Table 6 shows that there are day-to-night trends at each level. At 30 meters for, there are increases in mean CO from daytime to nighttime for all months of the year. At 457 meters, mean CO decreases from day to night for all months of the year. At the 122-m level, Table 6 shows mean CO increasing, staying

nearly the same, or decreasing at night. Although a trend is not clear at this level, the three months that show increases at night are the months of the year with the highest CO (February, March and April).

SEASONAL VARIATION

Figure 13 shows WKT 2009 and 2010 monthly CO percentiles for all three tower levels. In general, seasonal CO values are characterized by a peak in the spring, which decrease in the summer. The CO decreases throughout August and then rises again in September. One reason for the summer decrease of CO is the increase in the availability of the hydroxyl radical (OH) in the summer (from increasing UV). Another reason for the summer decrease of CO is that the seasonal cycles for CO and O_3 are influenced by the seasonal exchanges of different air mass types due to the seasonal shift of wind directions. In Figure 14, wind rose plots of CO show that southerly flow during the summer is lower in CO than northerly flow. The figure also shows that during the summer there is very littler northerly flow. Air masses originating over land, such as the northerly flow, contain higher concentrations of O_3 and CO, due to the higher continental background concentrations, and sometimes due to the contribution from regional pollution. In the months of summer, as the wind direction becomes predominantly SW/WSW, winds bring relatively “clean” air from the Gulf of Mexico. So months with this predominant flow, June through August, are associated with lower CO.

DEPENDENCY ON WIND DIRECTION

In Figure 14, the CO, plotted on wind roses versus wind direction measurements, shows some expected results. Since CO is primarily from anthropogenic emissions (volcanic activity and fires do also contribute), one might expect high CO values to come mainly from urban directions. The highest values do indeed come from the NE (~0-60°), SE (~180-150°) and SW (210-240°), which are the respective directions of Dallas, Houston and Austin. The maximum values of CO during the whole year were measured in February from the direction of Dallas.

General wind patterns can be seen influencing the measured CO values. The primary wind directions, which are NE and SW during the colder months, narrow to a single wind direction during May through August (August did not have much data at the 457-m level in 2010). The plots for February through April (the months with the highest mean CO) show the northern direction being a source, though this is not present in the following months. May through August had much cleaner air and almost all measurements were from a southerly direction. When the wind had much less variation in direction, it brought lower CO air from the WSW and SSW. July had the lowest mean CO of the year and WSW was its predominant direction. The northern influence began again in September and then continues throughout the winter.

CO/O_3 RELATIONSHIP

O_3 and CO are generally correlated due to the relationship between CO and O_3 precursors (NO_x and VOCs). The relationship of CO to O_3 was investigated with linear regression. The linear fit coefficients for O_3 and CO at WKT tower in 2009 and 2010 are plotted in Figure 15. The warm months of the year have positive correlation coefficients that are relatively high compared to the other months. July of both years has the highest correlation coefficients. August 2010 at 457 meters is an exception to the higher coefficients of the warmer months, likely because there was very little data at that level for the month. The 457-m level almost always has a higher correlation than the 30-m level. The cold months have lower positive coefficients, which turn negative during winter months. The reason for the shift in a positive relationship to a negative one has to do with the source of the air and the availability of CO.

For example, Figure 16 shows CO and O_3 scatterplots plus the associated linear fits for both daytime and nighttime at 30 meters and 457 meters. In February (a), the linear fit has a low coefficient that is negative for both levels and night and day. In February, the air has a continental source and has high CO as a result. In the continental dry, cold air, there is little OH to react with CO. In this situation, you could not predictably use this coefficient to predict the concentration of O_3 from CO. However, you could see the tendency towards higher O_3 corresponding with lower CO values. In July (b), the CO concentrations are very low. In fact, the maximum CO concentrations in July 2010 are the same as the minimum CO found in February (~120 ppb). The CO and O_3 are both low in the "clean" marine-sourced air to begin with, but additionally, OH is highest in summer due to moisture and sunlight. These cleaner conditions for CO are controlled by loss. These months with the highest linear fit coefficients show that during times of cleaner air, there is a stronger relationship between CO/O_3 and the O_3 value might be predicted based on the measured CO concentration. Isolating only the measurements from a southerly direction could prove an even stronger relationship.

DIFFERENCES BETWEEN 2009 AND 2010

The two years of CO measurements were largely similar in their overall pattern (likely due to the air flow pattern being similar), but there were some differences. The general pattern of increase of CO from the minimum in summer through late winter and then the rapid decrease in June through August exists in both years. Looking at Figure 13, there are a few obvious differences. September of 2009 has a large deviation from the gradual increase of CO that 2010 shows. There were large wildfires in California during this time, which was a likely contributor to the high September 2009 CO values. Another difference in the two years is that in 2009 the month with the maximum median CO was February, but was April in 2010. Additionally, the month with the minimum median CO was August in 2009 and July in 2010.

Other, not as obvious differences were also found. Seasonal analysis showed that the day-to-night differences in CO were of a larger magnitude during 2010. Interestingly, although not necessarily expected, the seasonal averages, except for summer, were relatively close to each other in magnitude. Summer of 2010 though, was much lower than the mean CO in 2009.

OZONE

Ozone is continuously monitored at the KWKT tall tower site at the 6-m, 30-m and 457-m levels. The surface instrument outputs measurement information at 1-minute intervals, and the two tower instruments output data at a rate of 30-second averages of three 10-second measurements. The data were analyzed and QA/QC'd before being made publically available on the ftp site. The measured ozone values vary with altitude, seasonally, diurnally and with wind direction.

ALTITUDE VARIATION

Figure 17 shows O_3 percentiles at 6-m, 30-m and 457-m levels during summer (June and July). Ozone generally increases as altitude increases, during both day and night. However, the difference between 457-m and the lower levels is much more pronounced at night. Often, due to mixing during the day, 30 and 457 meters have nearly similar O_3 values. The lowest level, at 6 meters, has loss to the surface, so there is more loss at this level during both day and night. The loss seems somewhat consistent, as the relative nighttime difference between the surface (6m) and 30-m level was steady between 15-23% for all months of the year.

DIURNAL VARIATION

Ozone tower measurements have a diurnal cycle with a minimum in early morning and a maximum in the late afternoon (Figure 17). Ozone formation occurs as the result of volatile organic compound (VOC) oxidation in the presence of nitrogen oxides (NO and NO_2) and sunlight, so the high levels in the late afternoon are the result of the solar-driven production. The low levels in the morning are caused by a combination of factors: deposition on surfaces, the reaction between NO and ozone to produce NO_2 and O_2, and vertical mixing becomes slower at night. The slower, nighttime mixing due to a nighttime boundary layer (NBL), exists at the 6-m and 30-m tower levels, but does not appear to affect the 457m tower level. The difference in wind speeds from the ground to the top of the NBL inhibits ozone from vertically mixing with the faster moving upper-layer of air and replenishing whatever ozone has been deposited or chemically consumed in the NBL. As a result, the higher nighttime speeds aloft lower the range of diurnal ozone values at 457 meters (Figure 17c).

SEASONAL VARIATION

Ozone, due to its dependency on UV, should have a seasonal cycle at the WKT site. The nighttime monthly ozone percentiles are in Figure 18. The ozone data does not correlate with UV levels as May through July decrease, when they should theoretically be increasing, highlighting the important role that transport also plays in seasonal variability at this site. August through October ozone values do not follow a decreasing pattern into the winter that UV does and actually increase. Daytime figures show the same result.

Figure 19 shows O_3 percentiles at 457-m level for all seasons. The spring, summer and fall seasons show a diurnal cycle, with a peak in the afternoon, but the minimum is not early in the a.m. The minimum occurs, as explained in the CO_2 section, when the air becomes well-mixed near the tower. When the 457-m level with higher ozone and more precursors, such as higher CO (the precursors in the lower levels have deposited out during the night), mix with the lower levels, there is a dip in the 457-m O_3. Winter shows no particular diurnal pattern, which is consistent because the UV is lowest at this time of year.

Figure 20 shows the hourly-averaged ozone for selected months of 2010. During February (Figure 20a), ozone concentrations generally peaked near 40 ppbv, and reached 60 ppbv twice during the month. However, during March, the daily peak concentrations are higher and have increased night and day average values (Table 7). Ozone values reach above 60 ppbv more than half the days of the month. The monthly ozone for April (Figure 20b) shows the effects of increasing solar day length and angle, as well as seasonally transitioning wind patterns (less northerly flow, increasing southerly flow). During April, the daily maximums peaked above 80 ppbv several times, but generally peaked above 60 ppbv. However, in April, concentrations were less predictable, with several days of relatively high ozone and then several days of fairly low ozone peaks (~40 ppbv). The pattern is more variable than in March, where daily peak values more predictably between 40-65ppbv. The increase in variability is due to the increased low-ozone flow from the Gulf of Mexico (see Wind Direction section for more details).

The monthly ozone plots for May and June (Figure 20c) reflect the transitioning wind patterns to a more southerly flow. In the month of May, there are two days that reach above 80 ppbv and about half of the days have ozone peaks around 60 ppbv. There are only three days that peak below 40ppbv, whereas in June, most of the days peak at or below 40 ppbv. In fact, June average ozone values are lower than those in January and February, months that we would typically expect to be the lowest due to the low SZA and short day length. This is due to the increasingly southern winds that are coming directly from the Gulf and are relatively “clean”. The July figure is much like the June plot with low daytime and nighttime ozone for weeks at a time.

At the end of August (Figure 20d), this trend ends as the ozone becomes higher for about six days. When daily ozone mixing ratios oscillate between periods of high and low, it is on a period of about 4-7 days rather than weeks (like in June and July). The last week of August leads back into a season of higher ozone. October's plot, Figure 20e, has many days that peak above 60 ppbv, a few above 80 ppbv and none below 40 ppbv. The higher values are due to the increasing air flow from urban directions.

WIND DIRECTION

Monthly wind-direction plots indicate that the wind directions shift and may be largely responsible for deviations from a primarily UV-controlled cycle. For instance, September should theoretically have a lower median value as the UV decreases, but it has a slightly higher median than August. Figure 21 shows ozone plotted on wind roses. The ozone wind directions show that July and August (the last portion of August was missing at this level) have a primarily S/SW component for nighttime values, but September wind directions shift more from S/SE and N/NE. When the winds come from these directions, they may go through Austin (S), Houston (SE) or Dallas (NE) and if so, they will likely have higher CO and/or O_3. March, which has the highest ozone, has many values from the NE. According to HYSPLIT back trajectories, these high values very often come through Dallas before reaching the tower.

AVERAGE VALUES

Table 7 shows the mean day and night ozone values for 2010 at all three tower levels. For all months except January through March, at the 457-m level, O_3 decreases at night, but to a much smaller degree then do the lower levels. Day-to-night differences are approximately 2-8 ppbv at 457 meters, whereas the lower levels have differences of 10-15 ppbv. The relative differences also show this nighttime drop more at the lower levels. For example, the September 457-m ozone daytime average is 48.6 ppb and only lowers to 46.1 ppb (5.1% relative difference) at night. This is in contrast to the 30-m level during the same month, at which the ozone daytime average is 45.1 ppb and lowers to 30.1 ppb during the nighttime (33.3% relative difference).

January through March show very slight increases at night of 0.4-1.5 ppbv (relative differences ~1-3%). March has the highest average nighttime ozone values, though April and October have high values as well.

The ozone mixing ratios increase as the altitude increases, except in May and October where the 457-m ozone mixing ratio is lower than at 30 meters during the daytime. During the daytime, ozone's increase with height is much less than the nighttime, because of the absence of the nighttime boundary layer and increased vertical mixing. The table also illustrates how

close the top two levels are during the daytime, showing that the vertical mixing is good during the daytime.

DIFFERENCES BETWEEN 2009 AND 2010

Figure 22 shows the monthly ozone percentiles for 2009 and 2010. The two years show very different patterns. The 457-m (Figure 18c) June 2009 median is not representative because of missing data (a 10-day stretch of low-ozone), which would effectively lower the median significantly. Although, there is nothing to compare for January through April of 2009 for the 457-m level, the months of June, July, August and September are lower. July is much lower and is the lowest month of 2010, but October is the lowest value of recorded data for 2009. The two other levels have similar patterns to their respective top levels for each year, but are slightly lower towards the surface.

WIND DIRECTION

Measured wind speeds, ozone, and CO are influenced by wind direction. Wind directions were monitored at the 6m, 30m and 457m tower levels, and were collected as 30-second averages of 1-second readings. The data were analyzed and QA/QC'd before being made publically available on the ftp site. The measured wind directions vary with altitude, seasonally and diurnally. Although discussed in other sections, we will discuss wind direction briefly and investigate some calculated values to add to the general directions we have observed.

ALTITUDE VARIATION

Wind direction varies with altitude, because most of the year, the median wind becomes increasingly clockwise with increasing altitude. At the 6-m level, the wind direction is always between 150° and 180°. Although this is roughly in the direction of Houston, back trajectories show that these winds do not travel that far in one day. However, back trajectories at 6 meters can come from Houston, but usually only after 4 or 5 days of travel. The 30-m and 457-m winds came from a much wider range of directions (130°-230°) during 2010. The 457-m level is always more westerly than either of the other levels.

DIURNAL VARIATION

Wind direction has day-to-night differences at the tower for some months of 2010. The 30-m and 457-m level showed very little variation between day and night for January through April, but showed a clockwise shift during nights of May through December. Using monthly medians, the day-to-night wind shifts were from 15 to 45 degrees, but were more often in the range of 20° clockwise. The largest day-to-night wind direction shift of 2010 was at the 457-m level in June, and generally, the day-to-night differences are largest at the 457-m level.

SEASONAL VARIATION

Seasonal variation does exist in the wind directions. Figure 23 shows the wind direction percentiles for 2009 and 2010 for 6-m, 30-m, and 457-m level. For the months of May through August 2010 at the 457-m level, the medians fall in the range of 180°-215° and have a very small range of variation compared to the other months. The wind direction of these warmer months is associated with "clean" air that has low CO and low O_3 concentrations. Based on HYSPLIT back trajectories, the air during the "clean" months was coming from the Gulf of Mexico (~180°).

The months of September through March have a much wider range of wind direction measurements, which is also seen in the wind direction roses shown in the previous sections. These months are also associated with much higher mean O_3 and CO than May through August.

MEDIAN VALUES

Table 8 shows the median wind direction for all months of 2010. For many months of the year, the smallest day-to-night wind direction shift is located at the 6-m level. The largest day-to-night shifts were generally at 457-m level, with the largest day-to-night wind direction shift during August. Additionally, for the 30-m and 457-m levels, the wind direction shifts from day-to-night were in a clockwise direction. When comparing the wind speeds against this median wind direction information, there is no clear correlation between the two.

Figure 24 shows the day and night median wind directions for each month and helps to visualize the information in Table 8. A few interesting details can be seen in this figure. May through August daytime winds have nearly the same median wind directions at each of the three tower levels. The 457-m level has similar wind directions for both June and July at night, as well. Both of these months had the "cleanest" air of 2010 because the CO and O_3 were both very low during those months. February, the month with the most southeasterly component to the winds at the 30-m and 457-m levels, had the highest CO values of 2010 (likely coming from the vicinity of Houston). August had a westerly component at night (~225°), but because of little data at this level for that month, this may not be representative.

DIFFERENCES BETWEEN 2009 AND 2010

Referring again to Figure 23, which shows the wind direction percentiles for 2009 and 2010 for 6-m, 30-m, and 457-m level, there are differences between the two years. In the summer of 2009 wind directions are somewhat more variable than in 2010. In September and October of 2009 the wind direction is much more variable, particularly at the lower levels.

FLASK SAMPLING INTENSIVE

Flask samples were collected from 27 August through 9 October in order to target the season where high ozone and carbon monoxide concentrations are typically observed at the tower. The following days exhibited high levels of ozone (shaded areas in Figure 25a):

- 27-28 August
- 4-5 September
- 13-19 September
- 27 September to 9 October

Data from the flask samples are shown in Figure 26 for a subset of species, and plots for all species are provided in Appendix 4. Mean and median values for each species are provided in Table 10 along with standard deviations. Strong correlations were observed among various species (Figure 27). In particular, carbon monoxide and acetylene were highly correlated (R^2= 0.77) and carbon monoxide was also strongly correlated with ozone observed on the tower (Figure 25b, R^2=0.69). A weaker relationship was observed between benzene and carbon monoxide (R^2 = 0.50). Molecular hydrogen is highly correlated with methyl chloride (R^2=0.71) and carbonyl sulfide (R^2=0.81), and bromoform with dibromomethane (R^2=0.87). Strong correlations also exist among the hydrocarbons (R^2 ~0.7 to 0.9) and weaker relationships ($R^2 \approx$ 0.5) among several of the modern refrigerants (e.g., HFCs, HCFCs). Fossil fuel CO_2 estimated from radiocarbon is moderately well-correlated with the combustion tracers (carbon monoxide, acetylene, benzene) and refrigerants such as CFC-11 and some of the HCFCs.

Figure 28 shows correlation plots for several species against CO and HFC-134a color coded according to pollution event. This type of analysis shows how correlations can change according to source region. For example, the samples from 27-28 August show higher carbon monoxide for a given value of acetylene than data from other polluted days (Figure 28b). The sample from 28 August was analyzed for radiocarbon, and it shows the highest carbon monoxide of any sample, but with a relatively lower value for fossil fuel CO_2. The acetylene and radiocarbon data for these samples are suggestive of a non-fossil fuel source of carbon monoxide for this sample, such as biomass burning or isoprene oxidation. Observed values for several refrigerants and other species (e.g. H_2, CH_3I) are relatively low for these data, while isoprene is relatively high. Data from the mid-September pollution event showed consistent levels of HFC-134a, HFC-142b, methyl iodide, hydrogen and dichloromethane, but a wide range of values for other species, such as isoprene, tetrachloroethylene (PCE) and HFC-125.

Sampling footprints were calculated using the Stochastic Time Inverted Lagranian Transport Model (STILT) (Lin et al., 2003) driven by reanalyzed weather forecast data from the North American Mesoscale Model. Examples are shown in Figure 29, and footprint images for most of

the samples are provided as an appendix. (Note: a few footprints are currently missing due to a problem with the model that occurs when simulating the first few days of the month. We hope to correct this error and provide an updated Appendix.). The footprints are time-resolved and provide estimates of the sensitivity of the measurement to upwind emissions. The footprints can be convolved with emissions inventories to estimate the contribution of various sources to an observed concentration (or mixing ratio) at the tower. The footprints are computed assuming a conservative tracer, so they can be applied to any long-lived gas. Chemical models can be applied to account for chemistry (production or loss) or loss to extend the utility of the footprint to reactive compounds. Figure 30 compares fossil fuel CO_2 derived from radiocarbon observations (CO_2-ff) with model estimates produced by convolving the STILT model footprints with two fossil fuel CO_2 inventories. Negative values of CO_2-ff result from imprecision in the radiocarbon measurement or uncertainty in the assumed background radiocarbon value. Although the correlation coefficient between the modeled and radiocarbon-based CO_2-ff estimates is rather low (0.22), a significant fraction of the remaining unexplained variance is due to imprecision in the radiocarbon measurement, which is significant at these low signal levels. The Vulcan inventory (green symbols in Figure 30a) covers only the continental USA, and thus does not include any emissions from Mexico. The Vulcan inventory has 0.1 deg x0.1 deg (~10 km x 10 km) resolution, while the CarbonTracker inventory (red symbols) has 1 deg x 1 degree resolution and included Mexico and Canada. The similarity between the two model results suggests that neither Mexico nor Canada contribute substantial CO_2 pollution to the observations during this time period, and that the relatively coarse resolution of the CarbonTracker inventory is sufficient for simulating observations at the Moody tall tower site, which is distant from large urban areas. The model results can be further analyzed according to source sector (Figure 31a) and geographic area (Figure 31b). We plan to extend this analysis to carbon monoxide and to use an improved transport simulation based on the WRF model (Nehrkorn et al.).

One of the tracers that was measured especially for this study was iso-butane. The ratio of i-butane to n-butane is higher for oil and gas well sources than for urban sources, while the lifetime of these compounds is relatively similar. Figure 32 summarizes the iso-butane and n-butane relationships observed during the flask sampling intensive. A strong inversion occurred at the tower on the afternoon of 26 September and was associated with very high hydrocarbon contributions. The n-butane to i-butane ratio indicates that the pollution event in late September through early October had a smaller contribution from oil and gas well sources than other polluted periods.

MAJOR STUDY QUESTIONS & ILLUSTRATIVE EXAMPLES

During the 20 months of ozone measurement at the KWKT tower, there have been many interesting events including the measurement of the 2009 California Wildfires, urban pollution from nearby large cities, and long periods of extremely "clean" Gulf air. In this section we provide a few illustrative cases for the primary questions of this study.

DOES THE NIGHTTIME CONTINENTAL JET EXIST AT KWKT TOWER?

The existence of a low-level nighttime continental jet is a feature consistently observed in the tower wind measurements. The nighttime boundary layer forms, leaving slower wind speeds in the lower layer, while in the overlying layer winds increase in speed. The measured wind speeds at 457 meters are generally double those at the lower tower levels (6-m and 30-m levels also measure wind speeds). This layer of faster winds effectively separates from the boundary layer inhibiting mixing to the lowest levels.

In many cases, this nighttime jet seems unassociated with higher ozone and in fact, often brings lower concentrations from the Gulf. There are numerous examples of the strong S/SW flow transporting ozone "clean" air from the Gulf of Mexico. The summer months are when air in the jet is the cleanest. In June and July, which are months with a strong S/SW jet, had the lowest ozone concentrations for the year. However, this jet can also bring polluted air from the vicinity of Austin or Houston as well, when the jet shifts through an urban area.

During the ozonesonde campaign at the tower site, the nighttime continental jet appeared in the vertical profiles, but did not appear to be associated with increased ozone values. Figure 33 shows an ozonesonde flight on Sept 10, 2009. The continental nighttime jet appears as the moister and faster southerly flow between 350 and 600 masl. In the figure, between these altitudes, the wind speeds increase and the wind direction shifts to the S/SW. However, the ozone concentrations during ozonesonde ascent and descent (2.5 hours later) show no increase at jet altitudes.

Figure 34a shows another week of September 2009, during which there were several days of relatively higher ozone values. The nighttime measurements at the 457-m level are very different than those at the surface and 30-m level. Through the use of HYSPLIT back trajectories (Figure 34b), the difference in wind speeds and slightly different southerly directions can account for this difference. Likely, there are more chemical and depositional processes at work at slower speeds, but there is also a difference in ozone concentrations due to how far the winds have travelled in a similar amount of time. For example, at 1900LT on September 2nd, the 457-m winds, came from the vicinity of Houston 24 hours earlier, whereas the 6-m and 30-m

level air came from only half as far away due to slower wind speeds. For “C”, the pattern is similar with the upper-level air coming from the vicinity of the Austin. For trajectory “D” the air parcels appear to bypass major population centers and ozone is much lower.

Figure 35 shows that for several days (September 26 – 30, 2009) the lower-level nighttime continental jet appears to be bringing higher ozone to the area. For example, on the evening of September 26, the wind direction shifts to S/SW and the 457m-wind speeds increase quite a bit. Ozone concentrations at the 457-m level stay the same in the early evening and then have high pulses during the night and early a.m. An ozonesonde was launched that night, but didn’t catch the period of high ozone. In Figure 35, evenings of September 26th and 27th have very similar events occurring, but the high ozone pulses do not affect the lower levels. On September 29th, there appears to be more vertical mixing, because the lower levels rise slightly during the night in response to the high ozone pulse above.

The nighttime continental jet is a persistent feature and appears to be particularly strong during the winter, as the winds are very fast at 457 meters. However, the winds are not as often from the S/SW. During the non-summer months, the 457-m winds are from many directions, and bring more high ozone pulses into the tower area.

Does the Nighttime Jet Affect Surface Level Ozone?

An important question for this study is whether high ozone transported by the nighttime jet affects the surface-level ozone. Several examples follow that illustrate cases where nighttime ozone transported to the tower at the 457-m level during the night appear to increase the surface-level ozone during the next day when increased vertical mixing (i.e. daybreak, high wind speeds, thermal instability) is coincident with the pulse of high ozone at the surface.

Figure 36 shows that on March 14th there was a well-mixed midday peak of high ozone, reaching 80 ppbv. Vertical mixing during this time of day (local time 2 p.m.), brought the ozone at 457-m and 30-m levels to a similar value. The 6-m value was typical in that it was ~15% lower than the other two levels. The CO_2 (Figure 36c) profile implies that this time of day on March 14th was well-mixed, at least at the 30-m and 457-m levels (6 meters is not equipped for CO_2).

Earlier that morning (~4 a.m. LT), the 457-m level showed a large pulse of high ozone air. Soon after the pulse at 457 meters, the 30-m level showed a pulse of higher ozone, which is atypical for nighttime air (30 meters is usually in the NBL and separate from 457 meters). When this lower-level pulse begins, the 457-m pulse decreases, indicating vertical mixing during the night, which appears to be more frequent during the winter months (see CO_2 section). After that, the ozone begins to rapidly increase for the day. It is likely that the nighttime influx of precursors

and pulse of high ozone set the stage for the day and the upcoming high peak at midday, particularly because the high ozone was able to mix down to the 30-m level during the night.

Figure 36b shows the hourly-averaged CO for the same time period. The figure shows possible correlation between O_3 and CO. At 3 a.m., just before the 4 a.m. peak of ozone (a), there is a large peak of CO, indicating polluted air being transported to the tower. When at 4 a.m., the ozone peaks, the CO shows a sharp decrease. At (b), when O_3 shows a peak at 30 meters, the CO shows a drop, but it may not necessarily be associated with the O_3, but rather the gradual decline of CO in the NBL. At the 4 p.m. (c) peak of ozone, however, the O_3 and CO both rise together, when all levels are well mixed.

Figure 36d shows the HYSPLIT back trajectory for March 14th, at 4a.m., 7 a.m. and 4 p.m. LT at the tower. The early morning back trajectory (A,B) shows how air parcels coming from the north are reversed by the Gulf-sourced marine winds and get diverted toward Austin (where it likely gained ozone and precursors) before reaching the tower. The 4 p.m HYSPLIT runs (C) do not show an obvious source for high midday ozone, as none of the midday back trajectories are from the vicinity of major cities. The high ozone at this time was likely due to chemical production that was enhanced by the precursors and high ozone at the 457-m level mixing down to the surface earlier that morning.

Figure 37a shows another example of ozone being mixed down from the 457-m level, which appears to lead to high ozone levels the next day. On April 12th, we measured high ozone the previous night which transitioned into very high ozone the next two following days. At 9 p.m. (a) on April 11 (the night before the very high O_3 day), the O_3 (Figure 37a) and CO (Figure 37b) both peak at the 457-m level. This comes after a large peak at 30 meters in the CO, but seems unrelated to vertical mixing as the 122-m level *follows* both those levels (it should come between the two if it were from mixing). CO_2 also shows some separation between the levels at this point as well. At 6 a.m. (b), the 457-m level peaks in both ozone and CO. This pulse of 457-m ozone is close to the beginning of vertical mixing (between 7-8 a.m. that morning (see CO_2 plot), so that polluted air is likely mixed down and contributes to very high O_3 for the next few days.

The HYSPLIT back-trajectories days show that the air parcel with higher ozone at 457 meters right before the vertical mixing began for the day came from the vicinity of Houston. When there is strong separation between levels (green vs red and blue trajectories), a pulse like this would not likely affect the tower air at the lower levels, which is seen in numerous plots. When an air parcel with high ozone does not mix down at the tower site, it very likely raises the ozone for the day at the location where the mixing begins for the day. In April, the mixing for the day begins regularly around 7-8 a.m. (this time changes with season, see CO_2 section), so the air

parcel would mix down towards the surface when it is further north. Forward trajectories of these particular air masses put them in the plains west of Dallas at that time (not shown).

May 28th through 30th is a period of relatively high ozone. On the 29th there was a pulse of higher ozone at 9 p.m. only at the 457-m level (see Figure 38a). The HYSPLIT trajectories (Figure 38b) indicate that the air at 457 meters passed in the vicinity of Austin on its way to the tower. Just a few hours before, all the air parcels came from the east. The 457-m air parcels then began to transition and headed to the south, eventually swinging through and past Austin towards the tower. So, in just a few hours, the winds changed from easterly to southwesterly. A few hours after the high pulse of high ozone wind (presumably from the vicinity of Austin), the lower tower level ozone values rise, rather than continuing their normal nightly decay. It is likely that this is because of vertical mixing, because the lower-level winds are still from the east.

In June, we measured another high O_3 day, which again likely resulted from the high ozone pulses at 457-m arriving in at a time of vertical mixing. Figure 39a shows one of the very few high ozone days in the summer months, June 4th. Again, a high ozone pulse at 457 meters comes at a time when the vertical mixing for the day is just beginning. HYSPLIT back trajectories in Figure 39b indicate the air mass at 457 meters had passed in the vicinity of Dallas before reaching the tower.

A number of other high ozone pulses during the night at 457 meters were recorded. For example, September is illustrative of how the time of the 457-m ozone pulse appearance affects ozone levels later that day. September 14th shows an early 2 a.m. pulse at 457 meters (Figure 40a). The HYSPLIT back-trajectories show that this air had come directly from the vicinity of Houston before reaching the tower area. The pulse passes over the tower before vertical mixing begins (CO_2 Figure 40c shows separate layers, and no vertical mixing at this early morning hour).

Two days later on September 16th, the pulse, similar in magnitude comes at an hour when vertical mixing is about to begin for the day (Figure 40c). The ozone increases to ~70 ppbv that day likely due to the increased ozone and precursors present at the beginning of the photochemical day. These two particular September cases demonstrate the importance of mixing vertical mixing in whether air pulses will contribute to the ozone values near the surface.

The number of high ozone days increases through the fall, which has slower nighttime wind speeds (but the 457-m level is still much faster than the lower levels, likely constituting a jet) and more transport through urban areas. Although the wind speeds are lower, measurements indicate the nighttime jet still exists and a nighttime boundary layer is present. The jet is simply

being shifted by the increasing winds from the northwest, so is more often going through Houston or Dallas.

CONCLUSIONS

KWKT tower in Moody, Texas has been the home to NOAA's CO, CO_2 and meteorological continuous-monitoring equipment since 2006. Additional instrumentation was installed in April, 2009 and the tower now hosts a number of continuous-sampling instruments at multiple levels (6m, 30m, 122m and 457m above ground level (AGL)), that measure ozone (O_3), carbon dioxide (CO_2), carbon monoxide (CO), and meteorological components (temperature, relative humidity, wind direction and wind speed) every 30 seconds.

The purpose of the second phase of this grant was to continue measurements of ozone in Central Texas through October 31, 2010 in order to determine the influence on ozone levels in Central Texas of air that carries ozone and precursors from upwind sources. Through the use of the tower instruments, by conducting both an ozonesonde and an intensive flask sampling campaign, we have been able to characterize the low-level nighttime jet, and identified and quantified CO, CO_2, O_3 and wind diurnal and seasonal trends at the tower location.

A significant finding from this study is that the nighttime low-level jet exists, but only occasionally brings high ozone concentrations into the tower area during the summer months. Although we see the existence of the nighttime jet, the ozonesonde intensive data did not show that the fast, southerly winds consistently enhance ozone concentrations at night, particularly during the summer (June and July here). Most of the summer nights investigated show the low-level nighttime jet generally transporting "clean" (low-ozone) air from the Gulf of Mexico. Additionally, when there is a pulse of high ozone associated with the jet there is a separation from the boundary layer that inhibits mixing to lower levels.

During the other seasons, high ozone pulses associated with the nighttime jet are more frequent. As the wind shifts from the summer flow to bringing a stronger influence of northerly flow, the nighttime jet tends to more often bring air to the tower from continental sources.

Whether the high ozone pulses from these sources affect the surface-level ozone is dependent on whether vertical mixing is present at the time of the pulse at the top of the tower. Although the average ozone values are highest in March, more high-ozone days occur during May and September than the other months. During this season, conditions for high ozone are present including more sunlight, more "dirty" air transported to the tower, increased wind speeds at 457 meters and increased vertical mixing (likely due to increased wind shear).

Data products from this study include CO, CO2, temperature, relative humidity, wind speed, wind direction and ozone. The QA/QC'd and processed data files for the duration of the study are found at ftp://ftp.cmdl.noaa.gov/ozwv/towers/wkt/. All data was processed in local time and hourly files. Additionally, ozone, CO and CO2 have smaller time increments available on the ftp site. Ozonesonde and flask sampling intensive data are also available on this publically-available ftp site.

RECOMMENDATIONS

A comprehensive transport modeling study over the entire period of observations would be helpful in quantifying how often the winds could be expected to pass through an urban area, which would assist in prediction of how often Central Texas might expect high ozone days. Additionally, studies involving forward trajectories could be helpful in estimating how often and where most of the pulses of high ozone measured at the top of the tower mix down to the surface (some high-ozone pulses do mix down at the tower, but more often they travel through, likely into the plains east of Dallas).

Prediction of high ozone events in Central Texas could also be aided by understanding the differences between 2009 and 2010 wind directions that were observed. Trends could be determined on a longer term if more than two years were present and we could understand whether the years were different for particular reasons (i.e. whether stronger Gulf flow correlates with El Nino events).

The CO/O3 relationship was explored in this paper, but a more complete understanding would be useful. An interesting feature present in the data is industrial plume signatures. Due to the high temperatures of combustion in industrial production, CO/CO_2 ratios have a specific signature. The O_3 data and CO/CO_2 ratios can be used to quantify the plumes, which may be useful to determining the area CO and O_3 budgets. Further analysis of the daily flask samples could also provide greater insight on source contributions to ozone measured on the tower.

An important piece that remains unresolved is that of NOx monitoring. NOx is important to this study in that it is a precursor for O_3. In urban areas, NO_2 can also be a temporary sink for O_3. After running the NO analyzer during the ozonesonde campaign, it became clear that a monitor with a lower threshold and better precision that meets the size and reliability requirements for operation on the tower would be necessary to quantify the NO at the rural tower site.

REFERENCES

A.E. Andrews et al., “Tall-tower observations of pollution from near-field sources in central Texas during the Texas Air Quality Study 2006”, Paper Number: A33B-0237, Fall Meeting of the American Geophysical Union, 15-19 Dec 2009.

Bakwin, P. S., P. P. Tans, et al. (1998). "Measurements of carbon dioxide on very tall towers: results of the NOAA/CMDL program." Tellus Series B-Chemical and Physical Meteorology 50(5): 401-415.

Korty, Robert L. and T. Schneider (2007). “A climatology of the tropospheric thermal stratification using saturation potential vorticity.” American Meteorological Society 20: 5977-5991.

Lin, J. C., C. Gerbig, S. C. Wofsy, A. E. Andrews, B. C. Daube, K. J. Davis, and C. A. Grainger (2003), A near-field tool for simulating the upstream influence of atmospheric observations: The Stochastic Time-Inverted Lagrangian Transport (STILT) model, *Journal of Geophysical Research-Atmospheres*, *108*(D16).

Nehrkorn, T., J. Eluszkiewicz, S. C. Wofsy, J. C. Lin, C. Gerbig, M. Longo, and S. Freitas (2010), Coupled Weather Research and Forecasting/Stochastic Time-Inverted Lagrangian Transport (WRF-STILT) model, *Meteor. Atmos. Phys., 107 (1-2),* 51–64, doi:10.1007/s00703-010-0068-x.

Oltmans, S.J. et al. (2001), Ozone in the Pacific tropical troposphere from ozonesonde observations, /J. Geophys. Res., 106, /32, 503-32,525.

Pérez, Isidro A.; Sánchez, María Luisa; García, María Ángeles; de Torre, Beatriz (2009). "Daily and annual cycle of CO2 concentration near the surface depending on boundary layer structure at a rural site in Spain" Theoretical and Applied Climatology 98(3-4): 269-277.

Wilson, K.W. and J.W. Birks (2006), Mechanism and elimination of a water vapor interference in the measurement of ozone by UV absorbance, Environmental Science and Technology, 40, 6361-6367.

Zhao, C. L., P. S. Bakwin, et al. (1997). "A design for unattended monitoring of carbon dioxide on a very tall tower." Journal of Atmospheric and Oceanic Technology 14(5): 1139-1145.

Instruments / Height AGL	Wind Speed / Wind Direction	Temperature	Relative Humidity	CO	CO_2	Ozone
457 meters	X	X	X	X	X	O+
122 meters				X	X	
30 meters	X	X	X	X	X	O+
Surface/6 m	O	O	O			O

Table 1) *KWKT instrumentation installed in April 2009 (O) and existed previous to April 2009 (X). The plus indicates the instruments were replaced in 2010 with updated instruments.*

Preset Ranges	0-0.05, 0.1, 0.2, 0.5, 1, 2, 5, 10, 20, 50,100 and 200 ppm	
	0-0.1, 0.2, 1, 2, 5, 10, 20, 50, 100, 200 and 400 mg/m^3	
Custom Ranges	0-0.05 to 200 ppm	
	0-0.1 to 400 mg/m^3	
Zero Noise	0.25 ppb RMS (60 second averaging time)	
Lower Detectable Limit	0.50 ppb	
Zero Drift (24 hour)	< 1.0 ppb	
Span Drift	<1% full scale per month	
Response Time	20 seconds (10 second lag time)	
Precision	1.0 ppb	
Linearity	+/-1% full scale	
Sample Flow Rate	1-3 liters/min.	
Operating Temperature	20°C - 30°C	
Power Requirements	100 VAC, 115 VAC, 220-240 VAC +/-10% @ 150W	
Size and Weight	16.75"(W) x 8.62"(H) x 23"(D), 55 lbs.	
	425 mm (W) x 219 mm (H) x 584 mm (D), 25 kg	
Outputs	Selectable Voltage, RS232/RS485, TCP/IP, 10 Status Relays, and Power Fail Indication (standard). 0-20 or 4-20 mA Isolated Current Outout (optional)	
Inputs	16 Digital Inputs (standard), 8 0-10vdc Analog Inputs (optional)	
Approvals and Certifications	US EPA Equivalent Method:	EQOA-0880-047
	MCerts Certified:	MC070096/00
	EN14626:	936/21203248/13 Report
	NF Certificate:	05/01

Table 2) *Instrument specifications provided by Thermo Scientific Instruments for the Model 49i Ozone Analyzer.*

Deliverable	Deliverable Due Date
Task 1 - Grant Activities Description **Deliverable 1.1:** TCEQ approved GAD. **Deliverable 1.2:** TCEQ approved Quality Assurance Plan (QAPP).	Within 14 days after this PGA is issued by TCEQ
Task 2 - Monthly Reports **Deliverable 2:** Monthly Status Report	By the 15th calendar day of each month during the grant period
Task 3 – Data Collection for a Period of Thirty (30) Days After the Notice to Commence is Issued **Deliverable 3:** Preliminary Report for Task 3	May 31, 2010.
Task 4 - Data Collection between May 2010 and June 2010 **Deliverable 4:** Preliminary Report for Task 4	July 31, 2010
Task 5 – Replace or Refurbish Tower Ozone Instruments **Deliverable 5:** Summary of Changes Made to Instrumentation	July 31, 2010
Task 6 - Data Collection between July 2010 and October 2010 **Deliverable 6:** Preliminary Report for Task 6	October 31, 2010
Task 7 – Explore the Feasibility of Making Nitrogen Oxide Measurements at the KWKT Tower Site **Deliverable 7:** Report on status of instrument development	Task 7 was removed
Task 8 - Summer Flask Sampling Intensive **Deliverable 8:** Preliminary Report of Flask Sampling	November 15, 2010
Task 9 – Draft Final Report **Deliverable 9:** Draft Final Report	February 28, 2011
Task 10 - Final Report **Deliverable 10:** TCEQ approved Final Report	March 31, 2010

Table 3) *Task and deliverable due dates for Grant Activities No. 582-08-86246-FY10-08.*

Wind speed	Jan Day	Jan Night	Feb Day	Feb Night
6m	5.0	5.0	5.5	5.1
30m	7.6	8.7	8.3	8.4
457m	9.6	11.8	9.8	11.6
Overall	7.4	8.5	7.9	8.4
	March Day	**March Night**	**April Day**	**April Night**
6m	4.9	4.8	4.0	3.7
30m	7.8	8.2	6.5	6.8
457m	10.4	13.3	9.2	13.2
Overall	7.7	8.8	6.6	7.9
	May Day	**May Night**	**June Day**	**June Night**
6m	3.3	2.6	3.4	2.5
30m	5.7	5.5	5.7	5.1
457m	6.8	9.2	7.6	11.2
Overall	5.2	5.8	5.6	6.2
	July Day	**July Night**	**Aug Day**	**Aug Night**
6m	3.1	2.2	2.6	2.1
30m	5.1	4.5	4.2	5.2
457m	7.1	10.0	5.0	8.8
Overall	5.1	5.6	4.0	5.4
	Sept Day	**Sept Night**	**Oct Day**	**Oct Night**
6m	2.9	2.1	2.6	2.3
30m	4.9	4.6	4.8	5.5
457m	6.1	7.1	6.3	9.6
Overall	4.6	4.6	4.5	5.8
	Nov Day	**Nov Night**	**Dec Day**	**Dec Night**
6m	4.3	4.5	4.7	5.0
30m	7.5	8.2	8.1	9.3
457m	10.5	14.7	10.6	14.9
Overall	7.4	9.1	7.8	9.7

Table 4) *Mean wind speeds at WKT levels for daytime and nighttime in 2010.*

CO_2 (ppm)	Jan Day	Jan Night	Feb Day	Feb Night
30m	397.3	399.4	398.7	401.9
122m	397.1	397.6	398.7	400.1
457m	395.3	394.7	397.4	397.1
Overall	396.6	397.2	398.3	399.7
	March Day	**March Night**	**April Day**	**April Night**
30m	395.5	402.4	392.7	404.0
122m	395.5	399.1	393.2	399.9
457m	395.0	395.3	393.1	395.2
Overall	395.3	399.0	393.0	399.7
	May Day	**May Night**	**June Day**	**June Night**
30m	389.6	401.9	391.7	405.5
122m	390.1	396.4	391.9	399.7
457m	390.1	392.3	391.3	392.0
Overall	389.9	396.9	391.6	399.1
	July Day	**July Night**	**Aug Day**	**Aug Night**
30m	389.4	406.1	387.9	399.3
122m	389.6	397.7	388.1	393.3
457m	389.4	389.1	387.1	386.8
Overall	389.5	397.6	388.0	393.1
	Sept Day	**Sept Night**	**Oct Day**	**Oct Night**
30m	390.3	403.6	389.5	397.6
122m	390.4	394.4	389.5	392.8
457m	390.0	387.9	389.2	388.9
Overall	390.2	395.3	389.4	393.1
	Nov Day	**Nov Night**	**Dec Day**	**Dec Night**
30m				
122m				
457m				
Overall				

Table 5) *Mean CO_2 at WKT levels for daytime and nighttime in 2010.*

CO (ppbv)	Jan Day	Jan Night	Feb Day	Feb Night
30m	151.5	153.0	169.0	172.6
122m	150.7	148.6	169.2	169.3
457m	143.4	138.7	160.1	157.0
Overall	148.5	146.8	166.1	166.3
	March Day	**March Night**	**April Day**	**April Night**
30m	157.1	161.2	158.9	163.3
122m	157.4	159.2	160.3	162.7
457m	154.5	151.1	158.1	156.8
Overall	156.4	157.2	159.1	160.9
	May Day	**May Night**	**June Day**	**June Night**
30m	140.4	142.3	108.7	110.6
122m	143.7	141.2	113.7	112.5
457m	139.4	135.0	107.2	101.7
Overall	141.1	139.5	109.9	108.3
	July Day	**July Night**	**Aug Day**	**Aug Night**
30m	97.0	100.2	111.5	119.8
122m	102.7	100.4	121.1	121.2
457m	95.1	89.9	113.4	108.7
Overall	98.3	96.9	115.3	116.6
	Sept Day	**Sept Night**	**Oct Day**	**Oct Night**
30m	118.8	124.9	124.8	132.3
122m	123.6	121.8	126.7	126.5
457m	119.0	115.2	123.9	118.9
Overall	120.5	120.6	125.1	125.9
	Nov Day	**Nov Night**	**Dec Day**	**Dec Night**
30m				
122m				
457m				
Overall				

Table 6) *Mean CO at WKT levels for daytime and nighttime in 2010.*

Ozone (ppbv)	Jan Day	Jan Night	Feb Day	Feb Night
6m	34.2	26.9	34.0	26.2
30m	40.3	35.2	40.0	33.7
457m	43.4	43.8	43.0	44.5
Overall	39.3	35.3	39.0	34.8
	March Day	**March Night**	**April Day**	**April Night**
6m	46.3	34.3	46.2	34.8
30m	52.9	43.3	52.7	42.7
457m	53.0	53.8	53.6	50.8
Overall	50.7	44.0	50.8	42.8
	May Day	**May Night**	**June Day**	**June Night**
6m	46.8	31.7	32.5	19.1
30m	53.3	39.6	36.5	23.5
457m	52.7	47.7	38.4	33.1
Overall	50.9	39.7	35.8	25.2
	Jul Day	**Jul Night**	**Aug Day**	**Aug Night**
6m	29.7	16.0	42.8	24.9
30m	34.3	19.3	44.0	29.1
457m	35.9	28.4	46.2	38.4
Overall	33.3	21.2	44.3	30.8
	Sep Day	**Sep Night**	**Oct Day**	**Oct Night**
6m	40.5	24.1	49.6	34.2
30m	45.6	30.1	55.9	41.9
457m	48.6	46.1	54.9	52.2
Overall	44.9	33.4	53.5	42.8
	Nov Day	**Nov Night**	**Dec Day**	**Dec Night**
6m	38.6	26.3		
30m	42.5	32.4	38.3	29.7
457m	43.4	41.5		
Overall	41.5	33.4		

Table 7) *Mean O_3 at WKT levels for daytime and nighttime in 2010.*

Wind direction (deg)	Jan Day	Jan Night	Feb Day	Feb Night
6m	170.4	171.7	171.0	167.3
30m	152.5	165.0	128.0	148.3
457m	185.1	194.3	175.4	188.1
Overall	172.4	177.0	162.4	168.0
	March Day	**March Night**	**April Day**	**April Night**
6m	181.3	172.7	157.2	161.6
30m	177.7	175.9	158.3	160.0
457m	186.4	188.2	157.7	165.9
Overall	182.4	178.9	160.5	162.5
	May Day	**May Night**	**June Day**	**June Night**
6m	161.9	157.4	153.8	167.3
30m	165.9	165.1	159.6	175.9
457m	175.4	192.0	186.0	208.1
Overall	173.3	171.5	173.8	183.8
	July Day	**July Night**	**Aug Day**	**Aug Night**
6m	156.4	158.2	158.3	177.3
30m	162.5	168.5	164.4	184.0
457m	186.1	206.1	189.0	227.4
Overall	175.0	177.6	183.4	169.2
	Sept Day	**Sept Night**	**Oct Day**	**Oct Night**
6m	150.1	154.8	166.5	170.6
30m	146.4	156.8	166.5	173.3
457m	144.8	180.1	184.5	204.2
Overall	158.8	163.9	179.1	182.7
	Nov Day	**Nov Night**	**Dec Day**	**Dec Night**
6m	180.6	173.1	180.4	172.1
30m	171.4	172.1	173.4	171.1
457m	191.6	200.1	196.6	217.4
Overall	184.0	181.8	190.4	186.9

Table 8) *Median wind direction at WKT levels for daytime and nighttime in 2010.*

Compound	Laboratory	units
tetrachloroethylene	gcms	ppt
acetylene	gcms	ppt
propane	gcms	ppt
benzene	gcms	ppt
carbon tetrachloride	gcms	ppt
CFC-113	gcms	ppt
CFC-115	gcms	ppt
CFC-11	gcms	ppt
CFC-12	gcms	ppt
CFC-13	gcms	ppt
dibromomethane	gcms	ppt
dichloromethane	gcms	ppt
methyl bromide	gcms	ppt
methyl chloride	gcms	ppt
methyl iodide	gcms	ppt
bromoform	gcms	ppt
chloroform	gcms	ppt
carbonyl disulfide	gcms	ppt
halon-1211	gcms	ppt
halon 1301	gcms	ppt
halon 2402	gcms	ppt
HCFC-142b	gcms	ppt
HCFC-22	gcms	ppt
HFC-125	gcms	ppt
HFC-134a	gcms	ppt
HFC-143a	gcms	ppt

Compound	Laboratory	units
HFC-152a	gcms	ppt
HFC-23	gcms	ppt
i-pentane	gcms	ppt
n-butane	gcms	ppt
n-pentane	gcms	ppt
carbonyl sulfide	gcms	ppt
carbon dioxide	magicc	ppm
methane	magicc	ppb
carbon monoxide	magicc	ppb
molecular hydrogen	magicc	ppt
nitrous oxide	magicc	ppb
sulfur hexafluoride	magicc	ppt
carbon-14/carbon in carbon dioxide	radiocarbon	per mil
carbon-13/carbon-12 in methane	sil	per mil
carbon-13/carbon-12 in carbon dioxide	sil	per mil
oxygen-18/oxygen-16 in carbon dioxide	sil	per mil
ethane (voc)	nmhc	ppt
propane (voc)	nmhc	ppt
i-butane (voc)	nmhc	ppt
acetylene (voc)	nmhc	ppt
n-butane (voc)	nmhc	ppt
i-pentane (voc)	nmhc	ppt
n-pentane (voc)	nmhc	ppt
n-hexane (voc)	nmhc	ppt
isoprene (voc)	nmhc	ppt

Table 9) *Species measured in NOAA Flask Samples.*

	Mean	Median	Standard Deviation	# of Samples
carbon dioxide	388.424	387.75	4.103	41
methane	1898.126	1900.95	55.303	41
carbon monoxide	121.947	122.52	24.923	41
molecular hydrogen	514.532	518.357	20.307	41
nitrous oxide	323.823	323.72	0.5	41
sulfur hexafluoride	7.287	7.28	0.09	41
carbon-13/carbon-12 in carbon dioxide	-8.289	-8.263	0.185	33
oxygen-18/oxygen-16 in carbon dioxide	-3.647	-2.579	3.008	33
HFC-134a	75.034	75.268	7.159	39
HCFC-22	242.503	237.338	21.193	39
CFC-12	532.76	532.679	1.503	39
methyl chloride	540.281	533.755	43.928	39
HCFC-142b	22.448	22.47	0.869	39
halon-1211	4.164	4.154	0.071	39
methyl bromide	7.617	7.378	1.01	39
CFC-11	242.159	241.928	0.936	39
methyl iodide	0.911	0.94	0.306	39
CFC-113	75.214	75.121	0.579	39
dichloromethane	36.822	37.767	6.847	39
chloroform	12.133	12.058	2.048	39
carbon tetrachloride	89.369	89.244	1.148	39
dibromomethane	1.031	0.958	0.287	39
tetrachloroethylene	4.913	4.061	4.268	39
bromoform	2.095	1.503	1.658	39
benzene	54.559	51.767	22.893	39
carbonyl sulfide	498.218	507.965	29.086	39
HFC-152a	16.551	15.466	5.611	39
carbonyl disulfide	5.097	4.085	3.487	39
propane	995.83	719.341	969.688	39
n-butane	311.216	220.01	388.88	39
i-pentane	138.213	112.495	124.793	39
n-pentane	110.456	88.212	131.557	39
halon 1301	3.201	3.215	0.084	39
halon 2402	0.442	0.442	0.014	39
HFC-143a	12.016	11.867	0.85	39
CFC-115	8.039	8.044	0.118	39
HFC-125	11.738	11.034	1.924	39
CFC-13	2.654	2.631	0.115	39

Table 10) *Flask sample statistics.*

	Mean	Median	Standard Deviation	# of Samples
CFC-13	2.654	2.631	0.115	39
HFC-23	23.624	23.511	0.612	39
acetylene	118.327	125.127	51.159	39
carbon-14/carbon in carbon dioxide	35.615	35.21	3.279	35
ethane (voc)	2328.689	2045.727	1394.117	33
propane (voc)	1049.973	769.188	922.489	33
i-butane (voc)	174.391	141.048	141.282	33
n-butane (voc)	323.374	240.188	370.436	33
i-pentane (voc)	148.884	127.354	118.304	33
n-pentane (voc)	112.814	100.794	115.364	33
n-hexane (voc)	52.455	43.626	42.095	33
isoprene (voc)	34.697	32.684	15.458	33
co2 fossil fuel from radiocarbon	2.255	2.28	1.147	35

Table 10 continued…) *Flask sample statistics.*

Photo 1) *The Model 49i Ozone Analyzer is larger and less portable than the tower instruments, but has better precision and is less likely to drift*

Photo 2*) The surface inlet mounted inside long conduit leads to a monitor that resides inside the instrument trailer. A radiation shield housing a T/RH probe is mounted next to the ozone inlet at the top of the conduit.*

Photo 3) *The Model 205 Ozone Monitor is small and lightweight with low power requirements.*

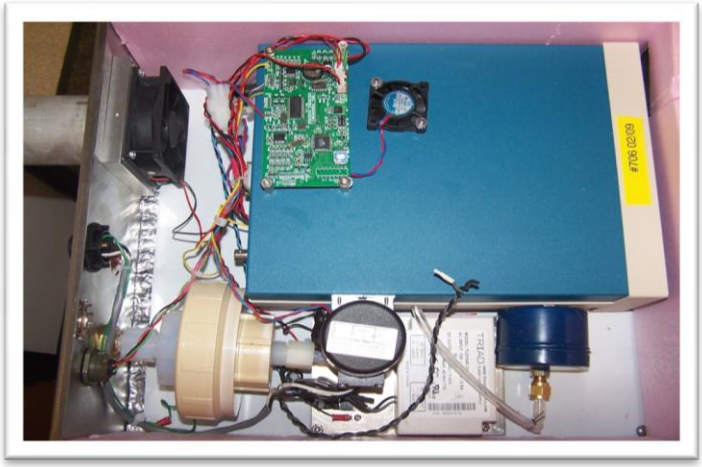

Photo 4*) Inside a tower-mounted ozone instrument.*

Photo 5) *Sampling system for flask measurements. On the left is the PFP, which contains 12 glass flasks. On the right is the PCP, which contains pumps for pressurizing the flasks.*

Photo 6) *MAGICC is the flask analysis system at NOAA that analyzes up to 55 greenhouse gases.*

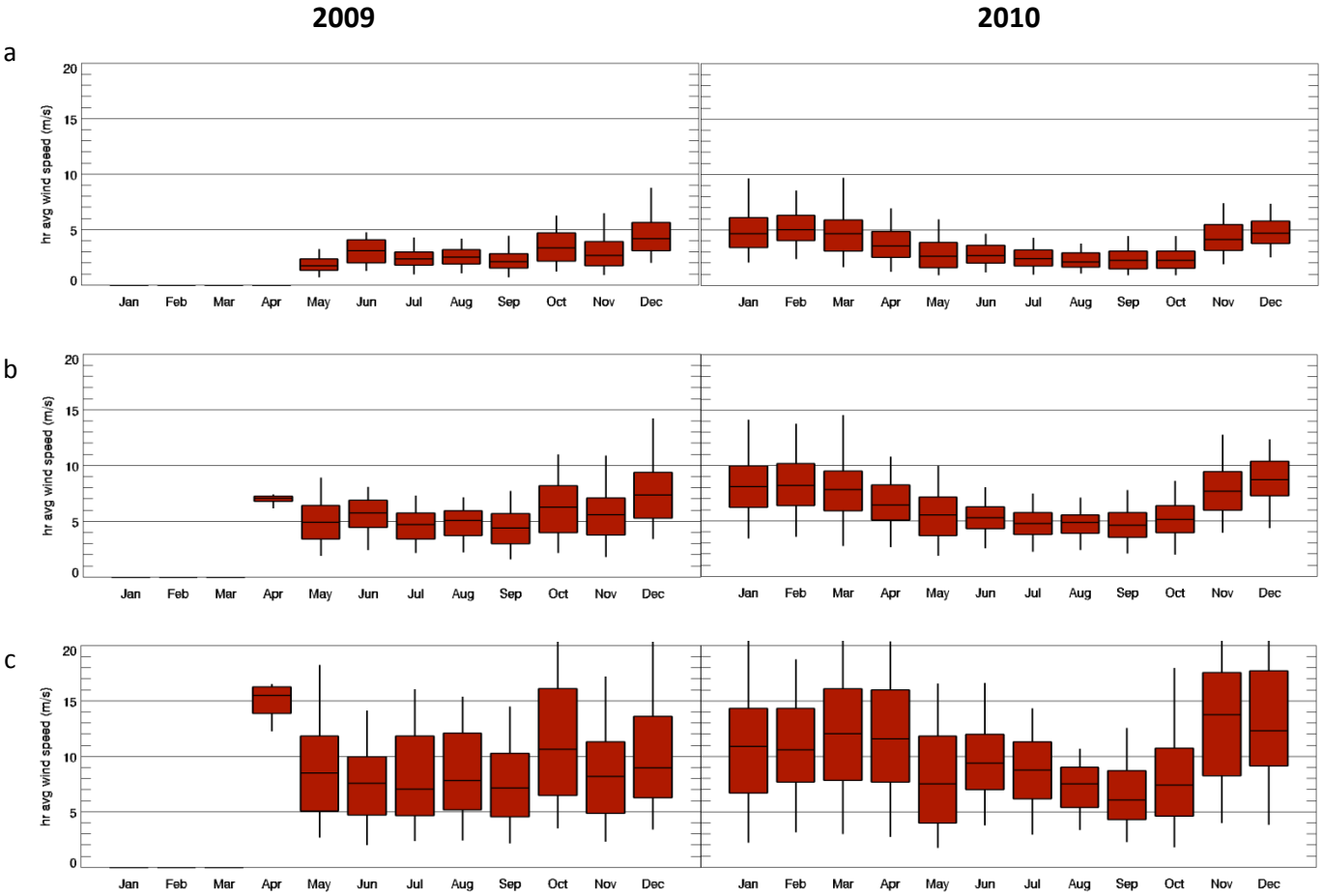

Figure 1) *WKT 2009 and 2010 wind speed percentiles 5th, 25th, 50th (median), 75th, 95th* ***a)*** *6m,* ***b)*** *30m, and* ***c)*** *457m.*

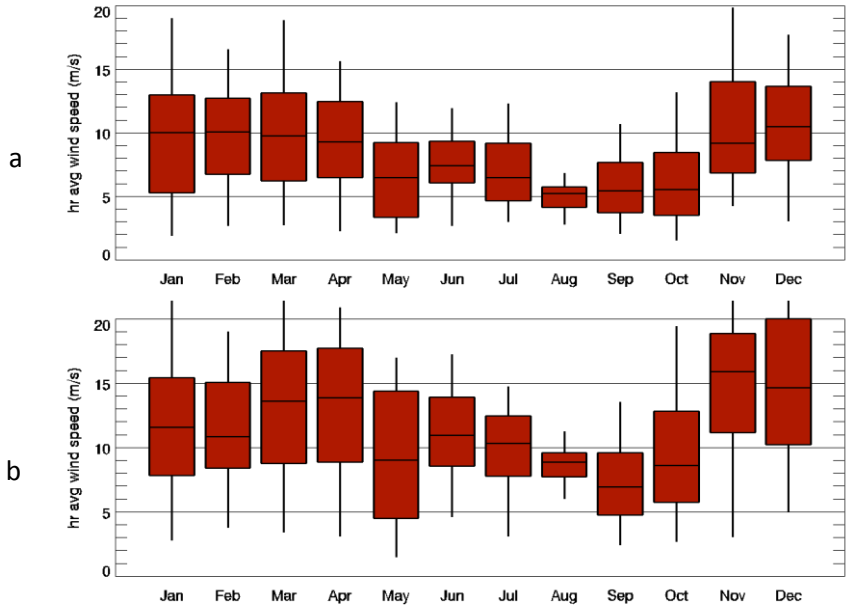

Figure 2) *WKT 2010 wind speed percentiles 5th, 25th, 50th (median), 75th, 95th at 457m for* ***a)*** *daytime, and* ***b)*** *nighttime.*

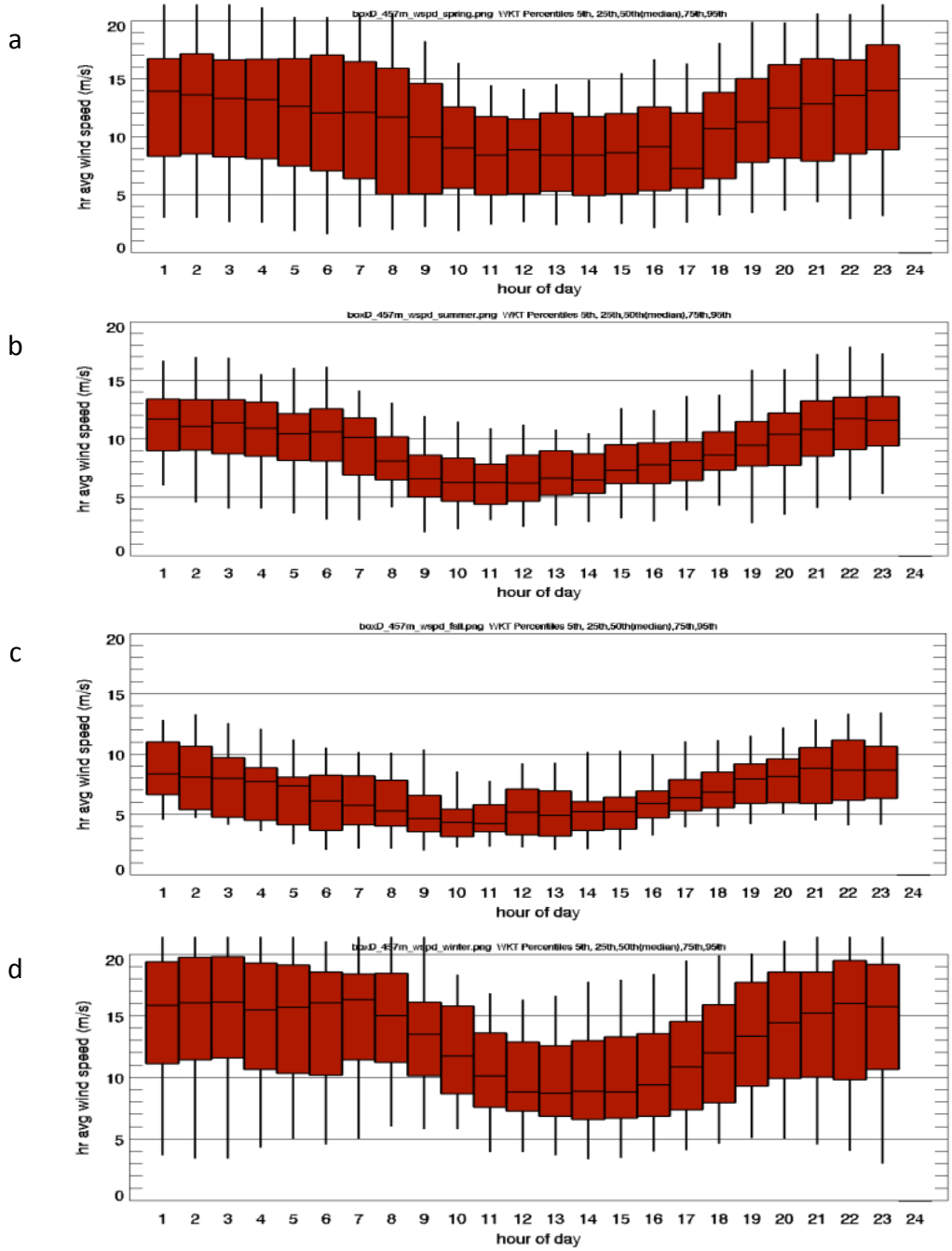

Figure 3) *WKT 2010 wind speed percentiles 5th, 25th,50th (median),75th,95th at 457m during* ***a)*** *spring(Mar, Apr, May),* ***b)*** *summer (Jun, Jul),* ***c)*** *fall (Aug, Sep, Oct), and* ***d)*** *winter (Nov, Dec, Jan, Feb).*

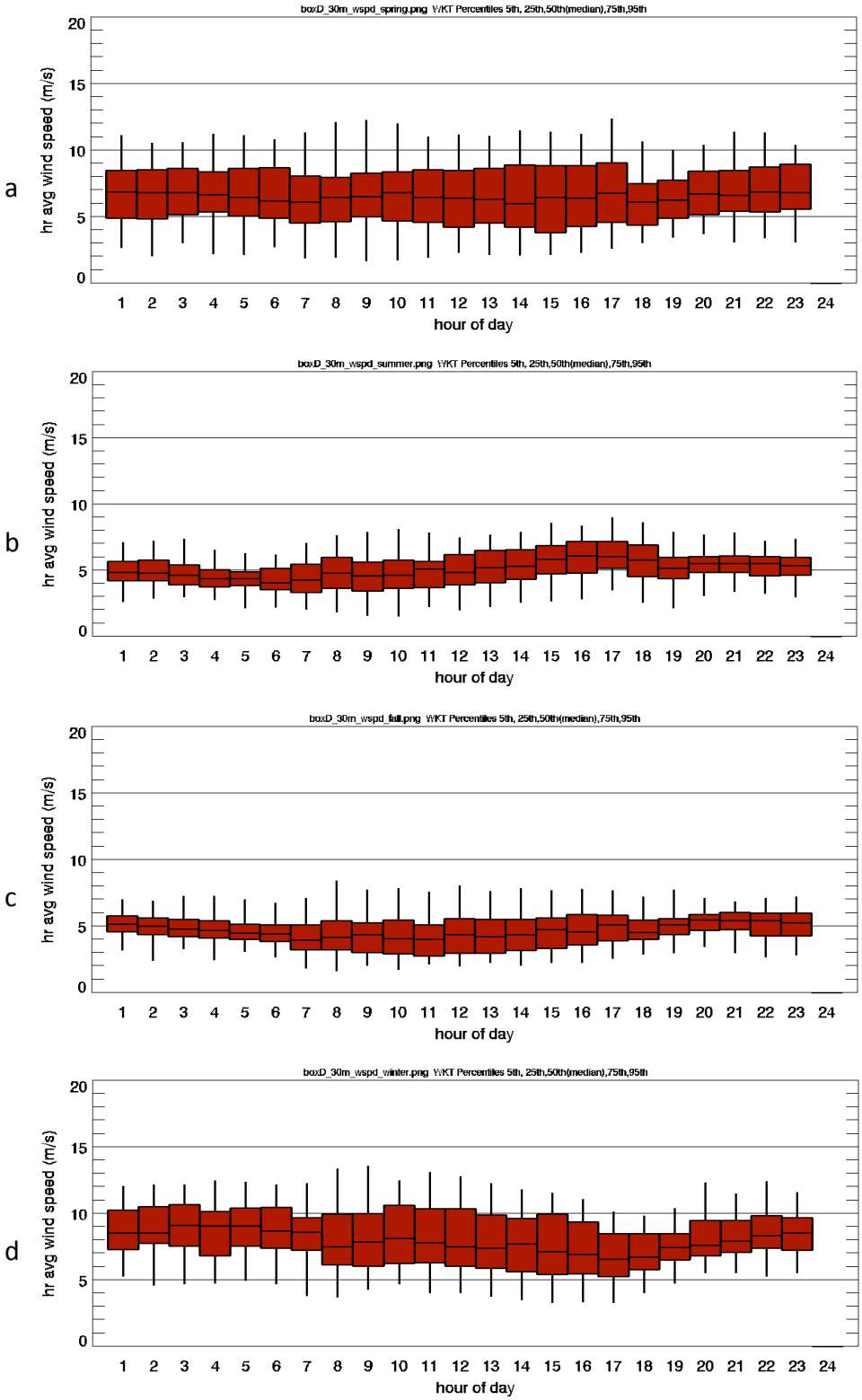

Figure 4) *WKT 2010 wind speed percentiles 5th, 25th,50th (median),75th,95th at 30m during* ***a)*** *spring(Mar, Apr, May),* ***b)*** *summer (Jun, Jul),* ***c)*** *fall (Aug, Sep, Oct), and* ***d)*** *winter (Nov, Dec, Jan, Feb).*

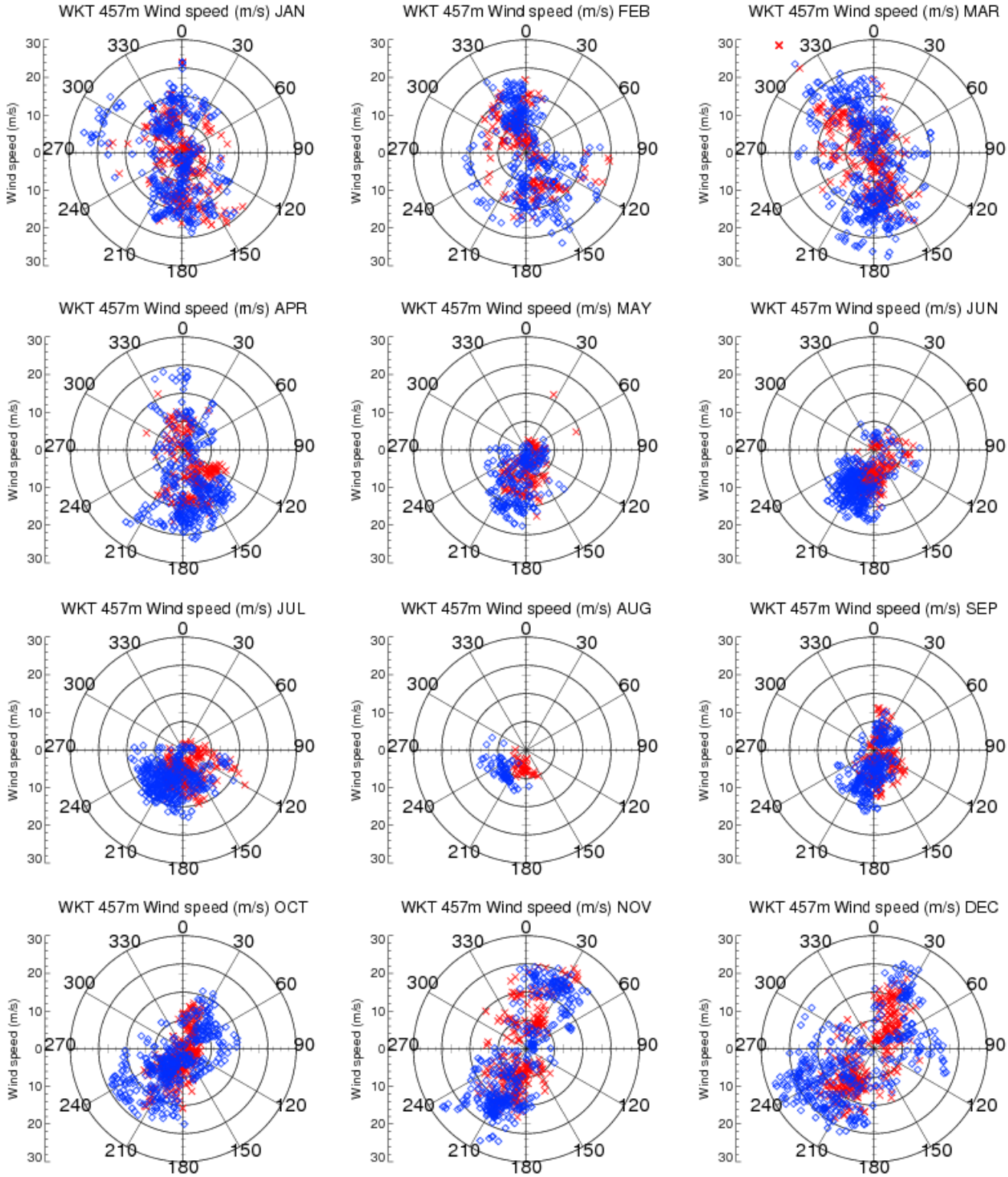

Figure 5) *Wind directions and correlating wind speeds at 457-m for Jan – Dec, 2010. Blue diamonds represent nighttime and red "x"s, daytime.*

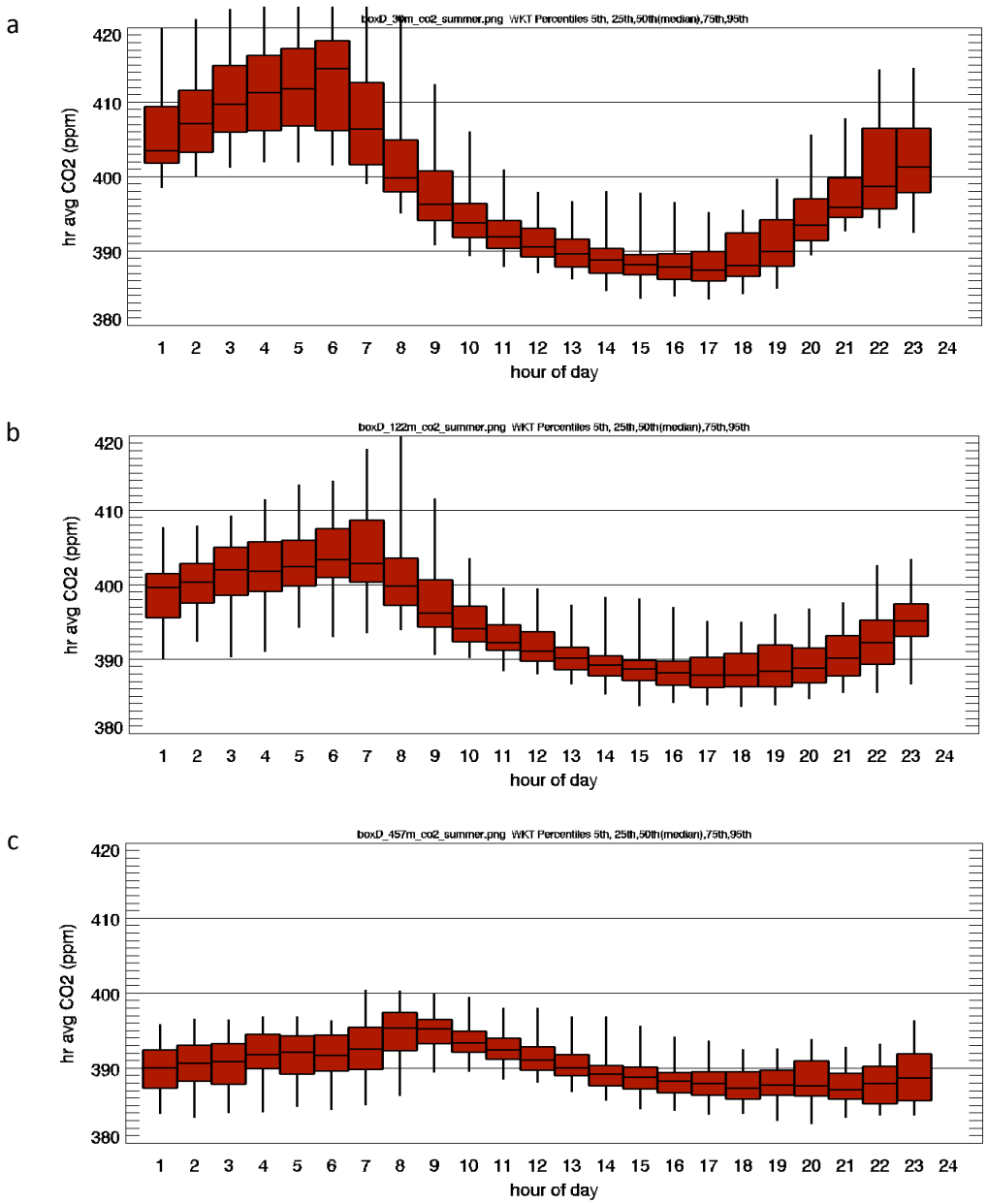

Figure6) *WKT 2010 CO_2 percentiles 5th, 25th, 50th (median), 75th, 95th* ***a)*** *30m,* ***b)*** *122m, and* ***c)*** *457m for June and July.*

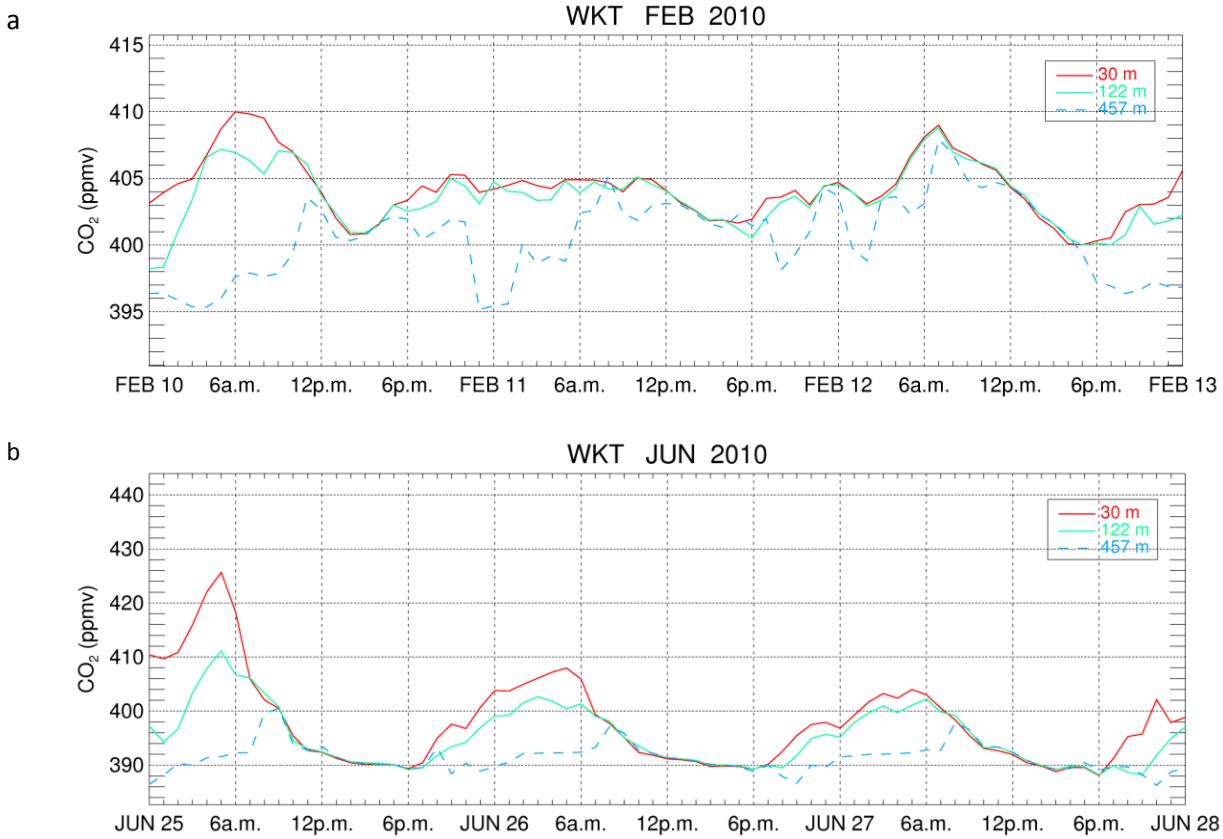

Figure 7) *Measured CO_2 values at 30m, 122m, and 457m for* ***a)*** *Feb 10th-13th, and* ***b)*** *June 25th-28th in 2010. Note that the y-axis is a much smaller range in February.*

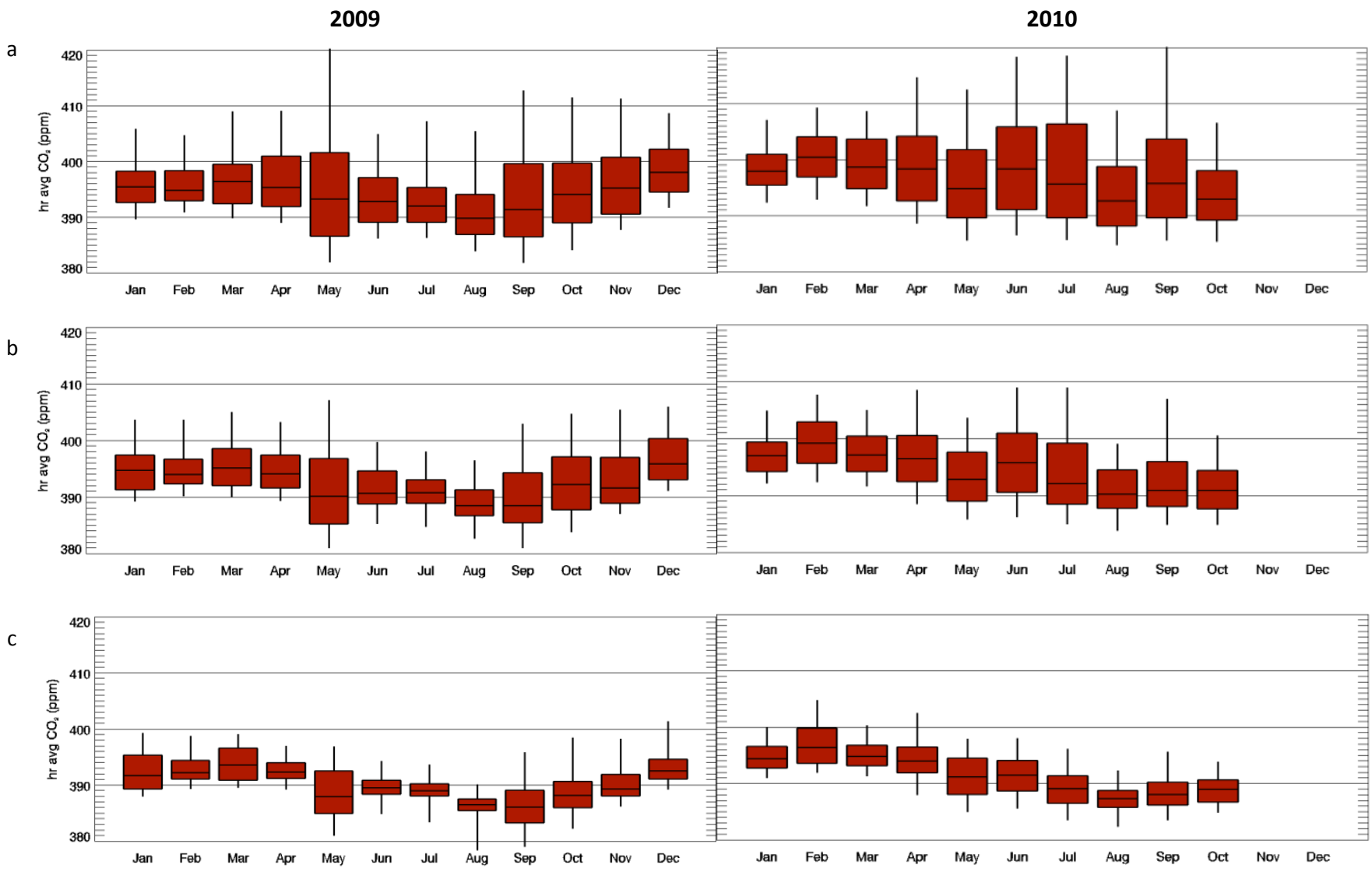

Figure 8) *WKT 2009 and 2010 CO_2 percentiles 5th, 25th, 50th (median), 75th, 95th* ***a)*** *30m,* ***b)*** *122m, and* ***c)*** *457m.*

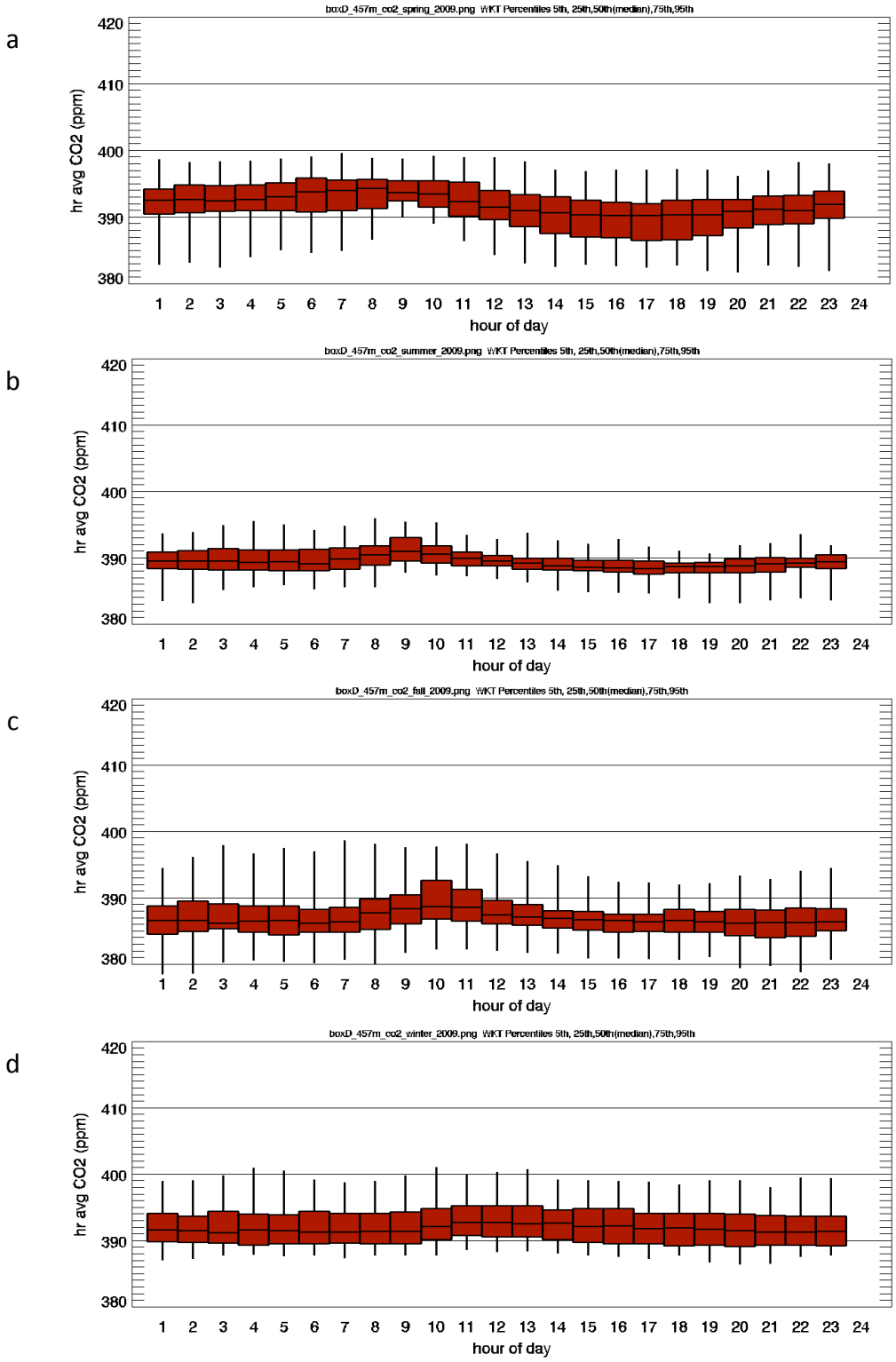

Figure 9) *WKT 2009 CO_2 percentiles 5th, 25th,50th (median),75th,95th at 457m during* ***a)*** *spring(Mar, Apr, May),* ***b)*** *summer (Jun, Jul),* ***c)*** *fall (Aug, Sep, Oct), and* ***d)*** *winter (Nov, Dec, Jan, Feb).*

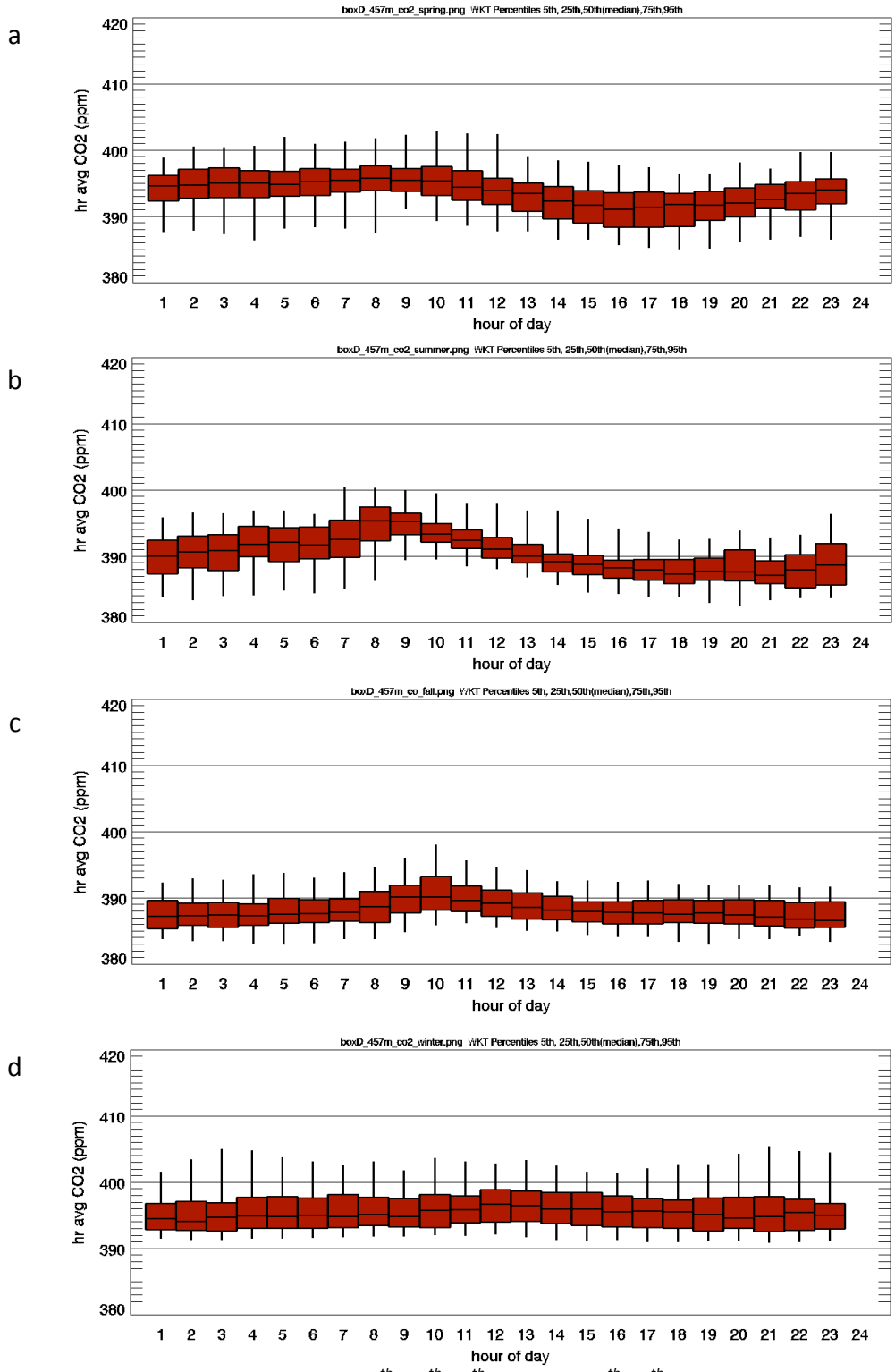

Figure 10) *WKT 2010 CO_2 percentiles 5th, 25th,50th (median),75th,95th at 457m during* ***a)*** *spring(Mar, Apr, May),* ***b)*** *summer (Jun, Jul),* ***c)*** *fall (Aug, Sep, Oct), and* ***d)*** *winter (Nov, Dec, Jan, Feb).*

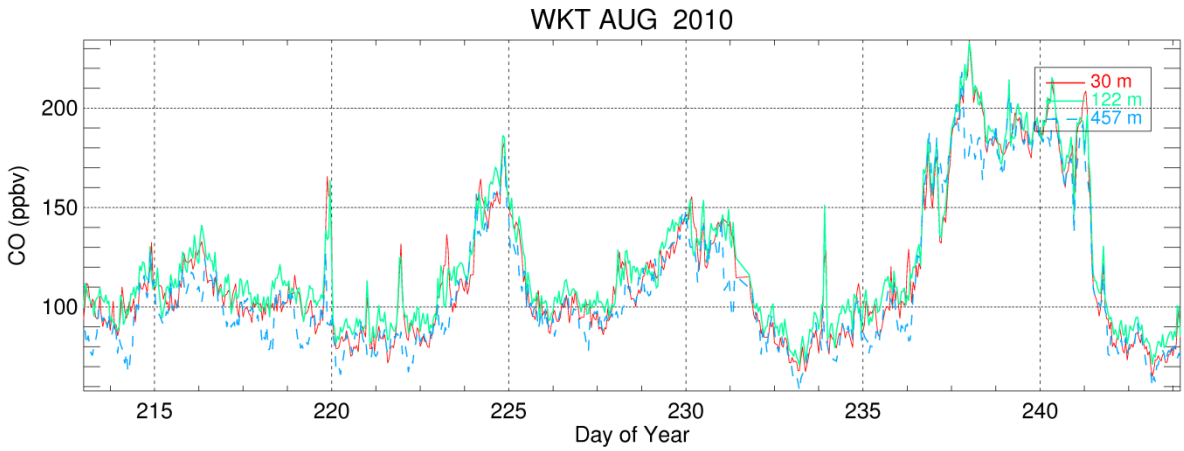

Figure 11) *August 2010 hourly-averaged CO at the 30-m (red), 122-m (green) and 457-m (blue) tower levels.*

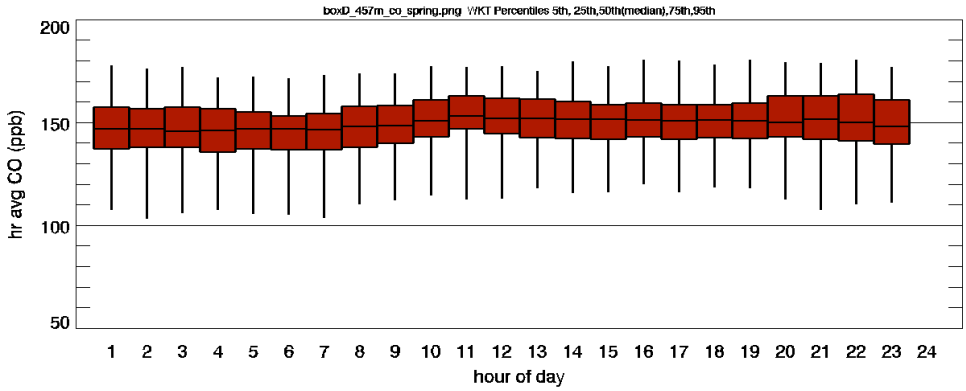

Figure 12) *WKT 2010 CO spring percentiles 5th, 25th, 50th (median), 75th, 95th* ***at*** *the 457-m level.*

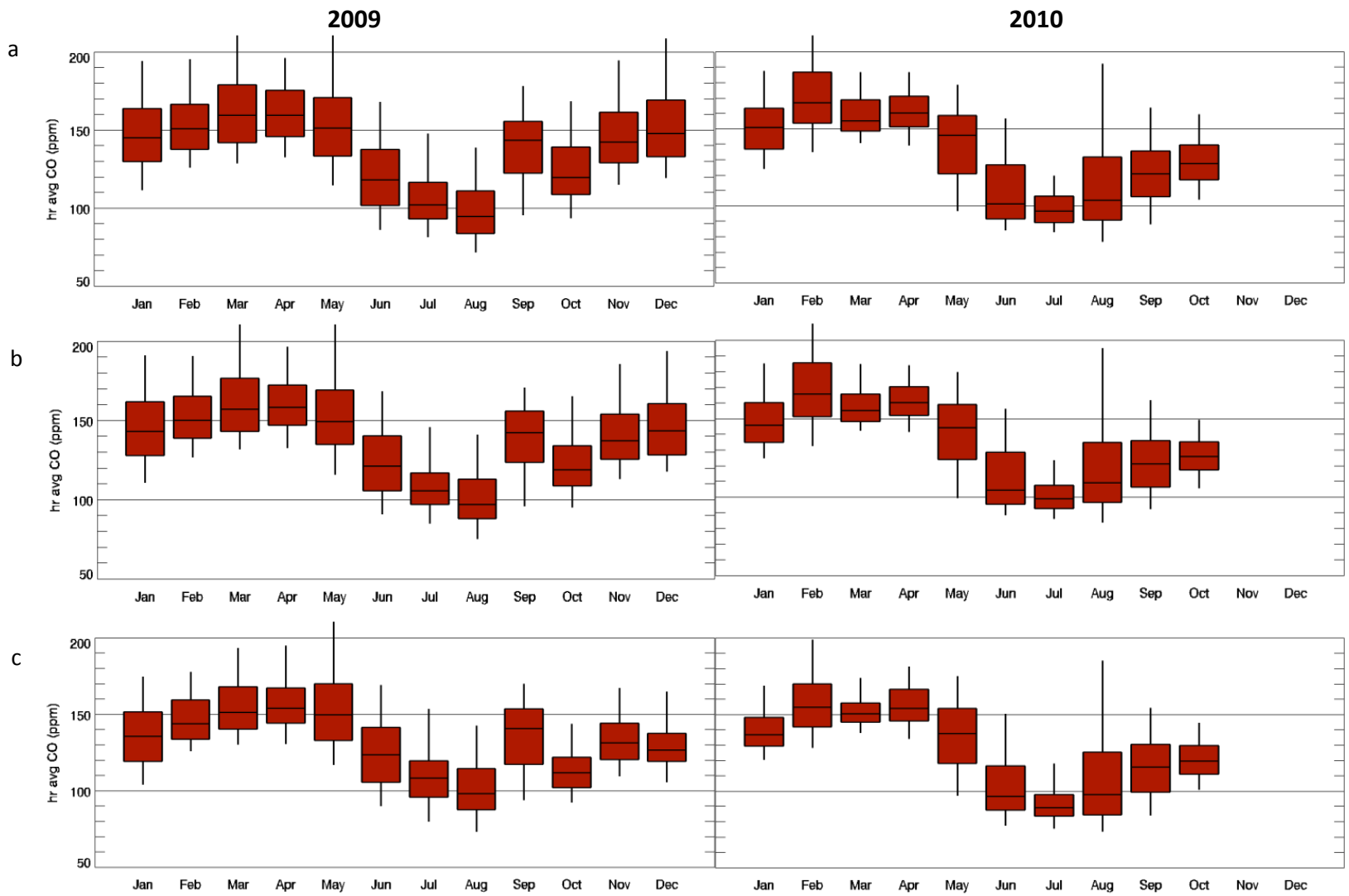

Figure 13) *WKT 2009 and 2010 CO percentiles 5th, 25th, 50th (median), 75th, 95th* ***a)*** *30m,* ***b)*** *122m, and* ***c)*** *457m.*

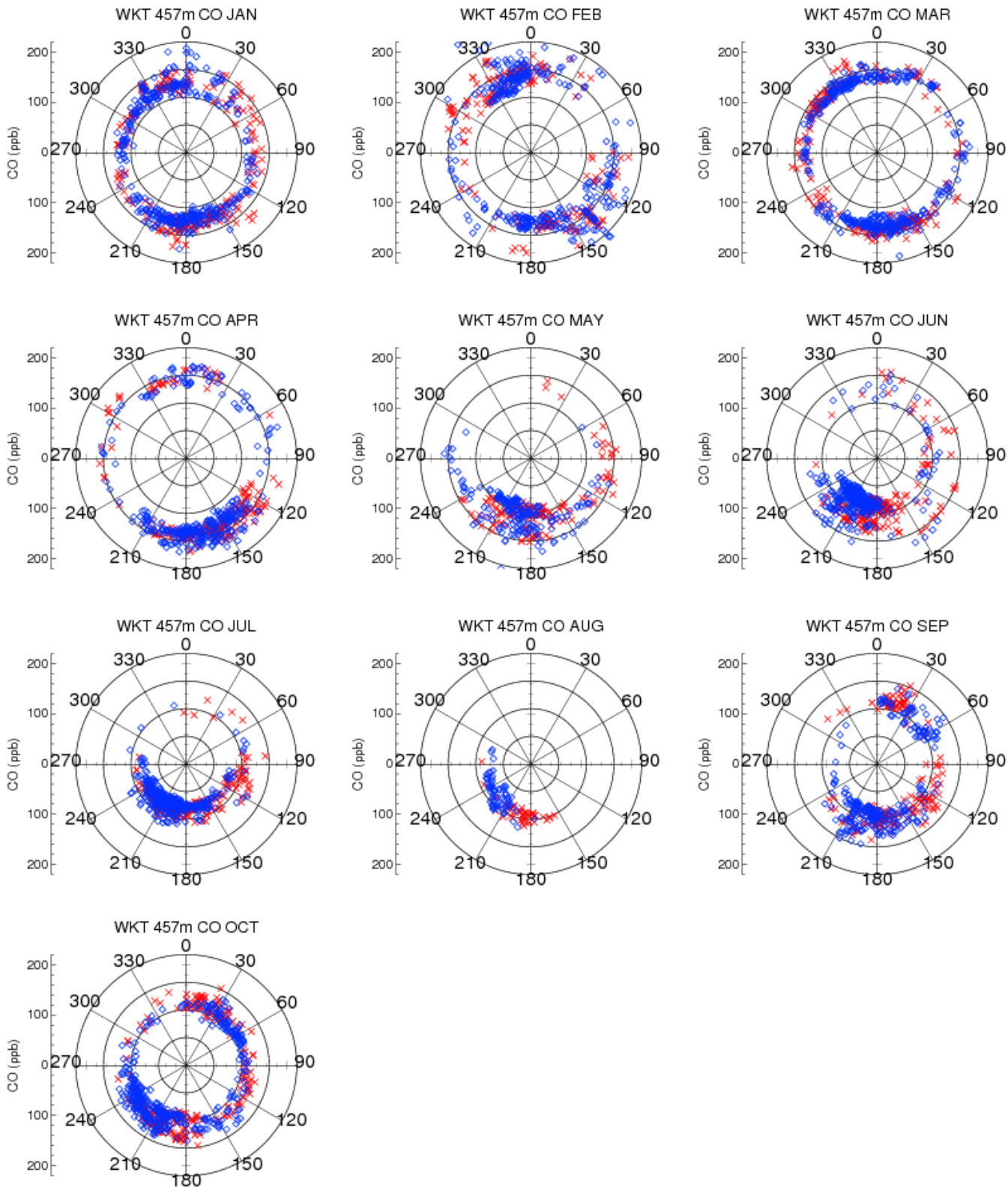

Figure 14) *Wind directions and correlating CO values at 457-m for Jan – Dec, 2010. Blue diamonds represent nighttime and red "x"s, daytime.*

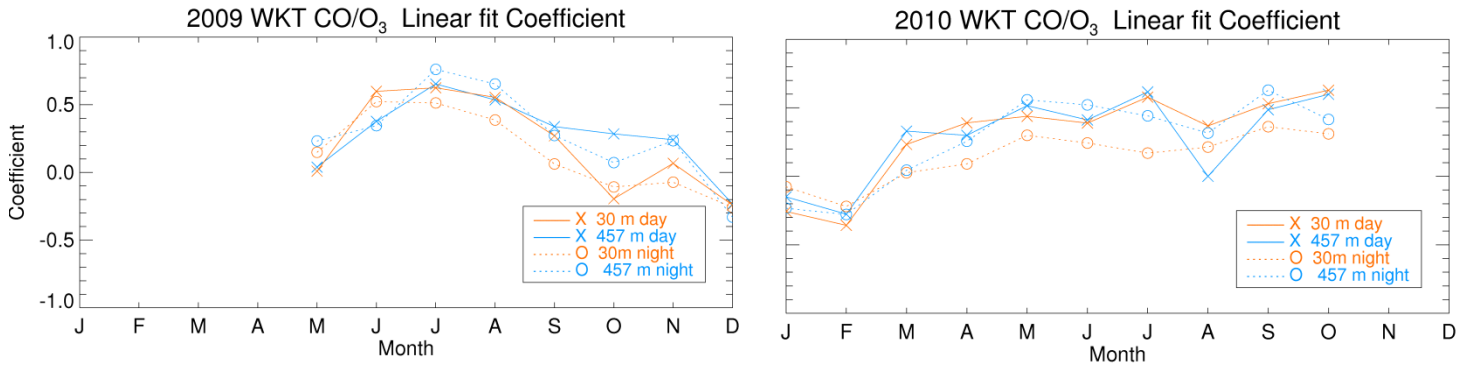

Figure 15) *WKT 2009 and 2010 day (solid) and night (dashed) CO/O_3 linear coefficients at the 30m (orange) and 457 (blue) tower levels. Daytime in this particular case was the well-mixed hours of 1p.m.-4p.m.*

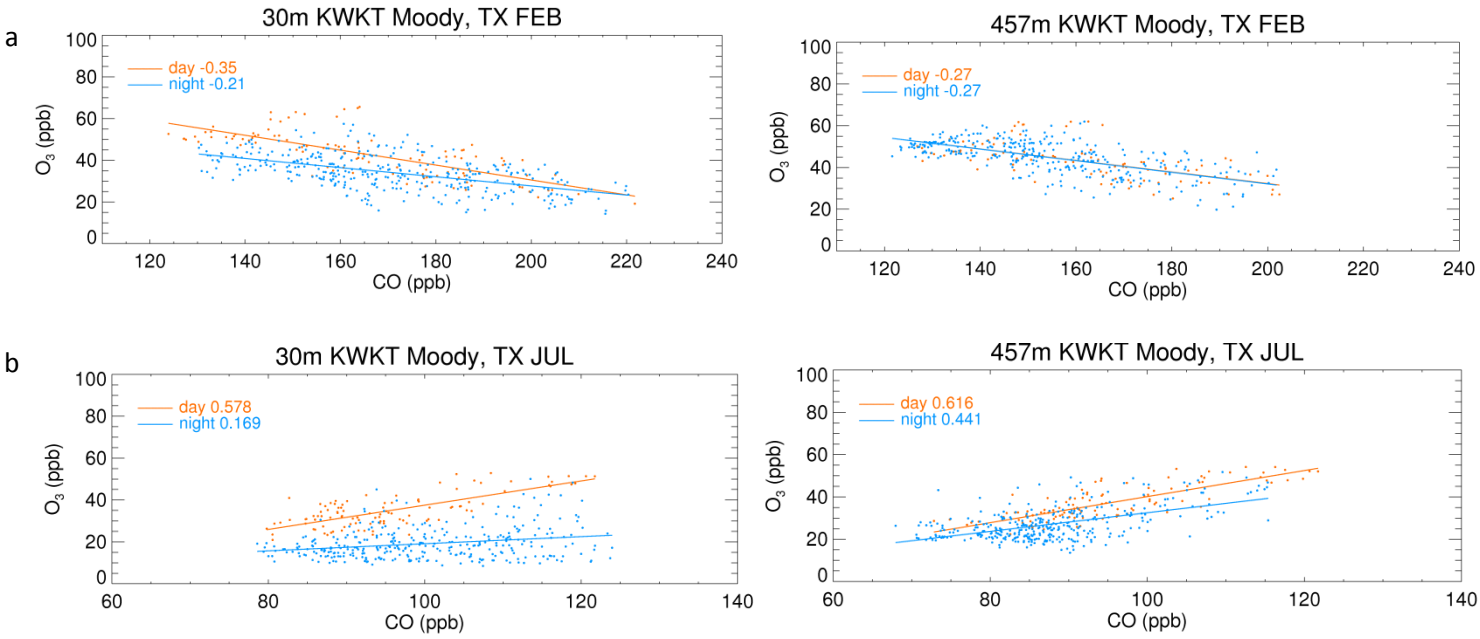

Figure 16) *WKT CO/O_3 scatter plots for a) February and b) July and their associated fits for night (blue) and day (orange) at 30m and 457m.Daytime in this particular case was the well-mixed hours of 1p.m.-4p.m.*

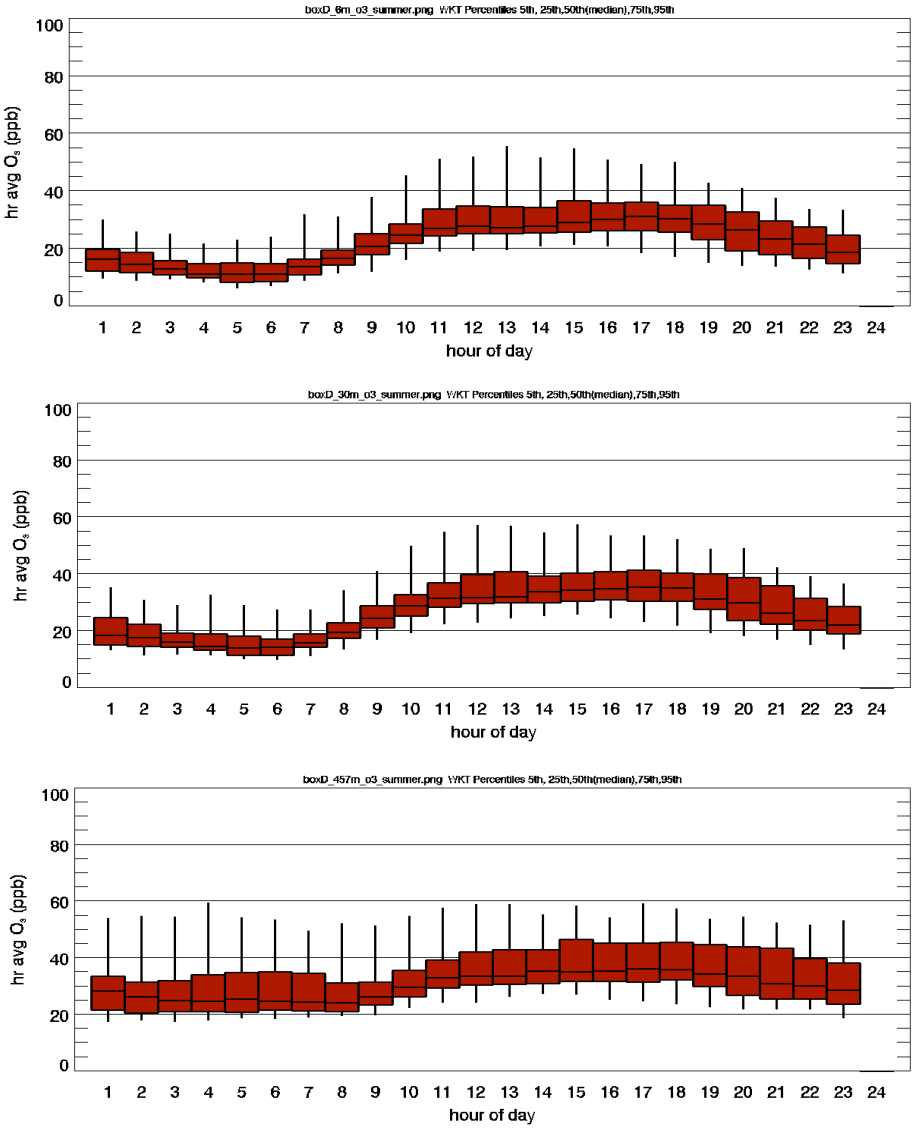

Figure 17) *WKT O_3 percentiles 5th, 25th, 50th (median), 75th, 95th during summer (June, July) at* ***a)*** *6m,* ***b)*** *30m, and* ***c)*** *457m.*

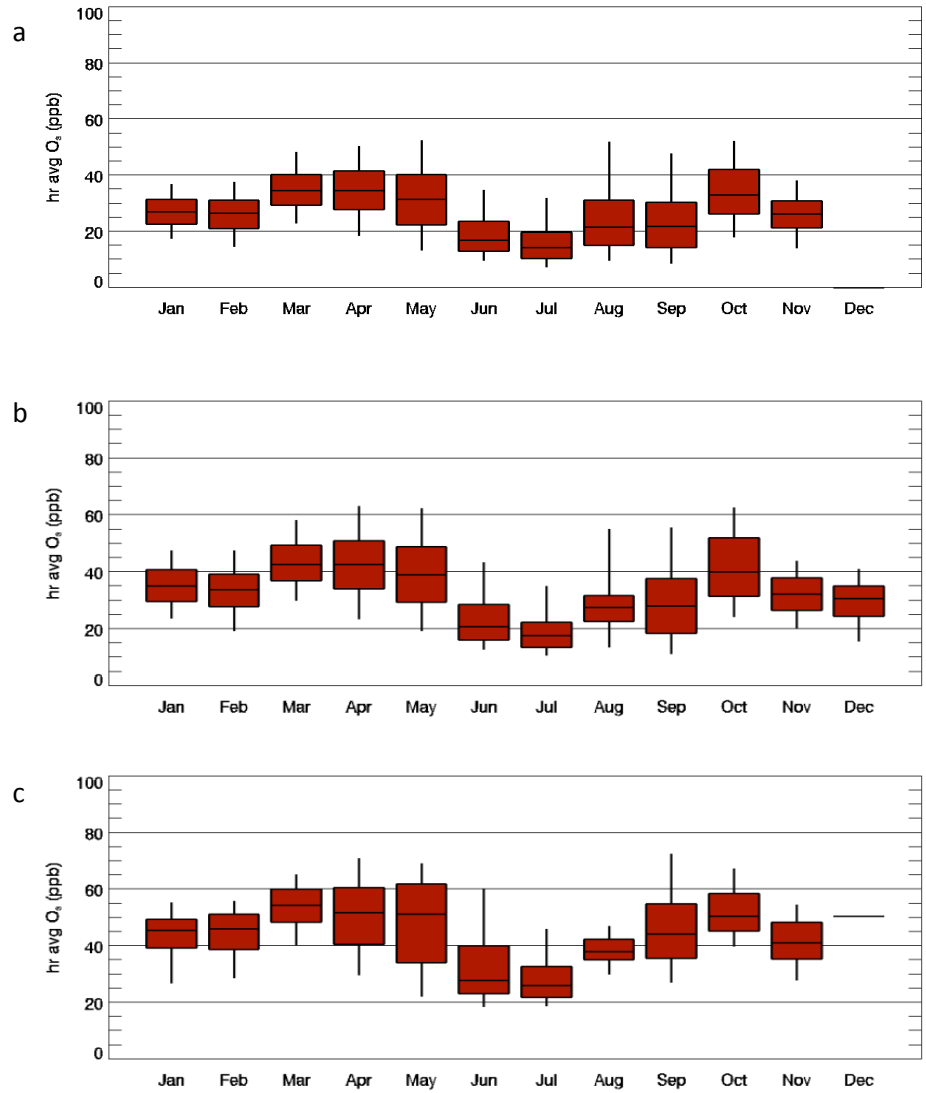

Figure 18) *Monthly WKT nighttime O_3 percentiles 5th, 25th,50th (median), 75th, 95th at* ***a)*** *6m,* ***b)*** *30m, and* ***c)*** *457m.*

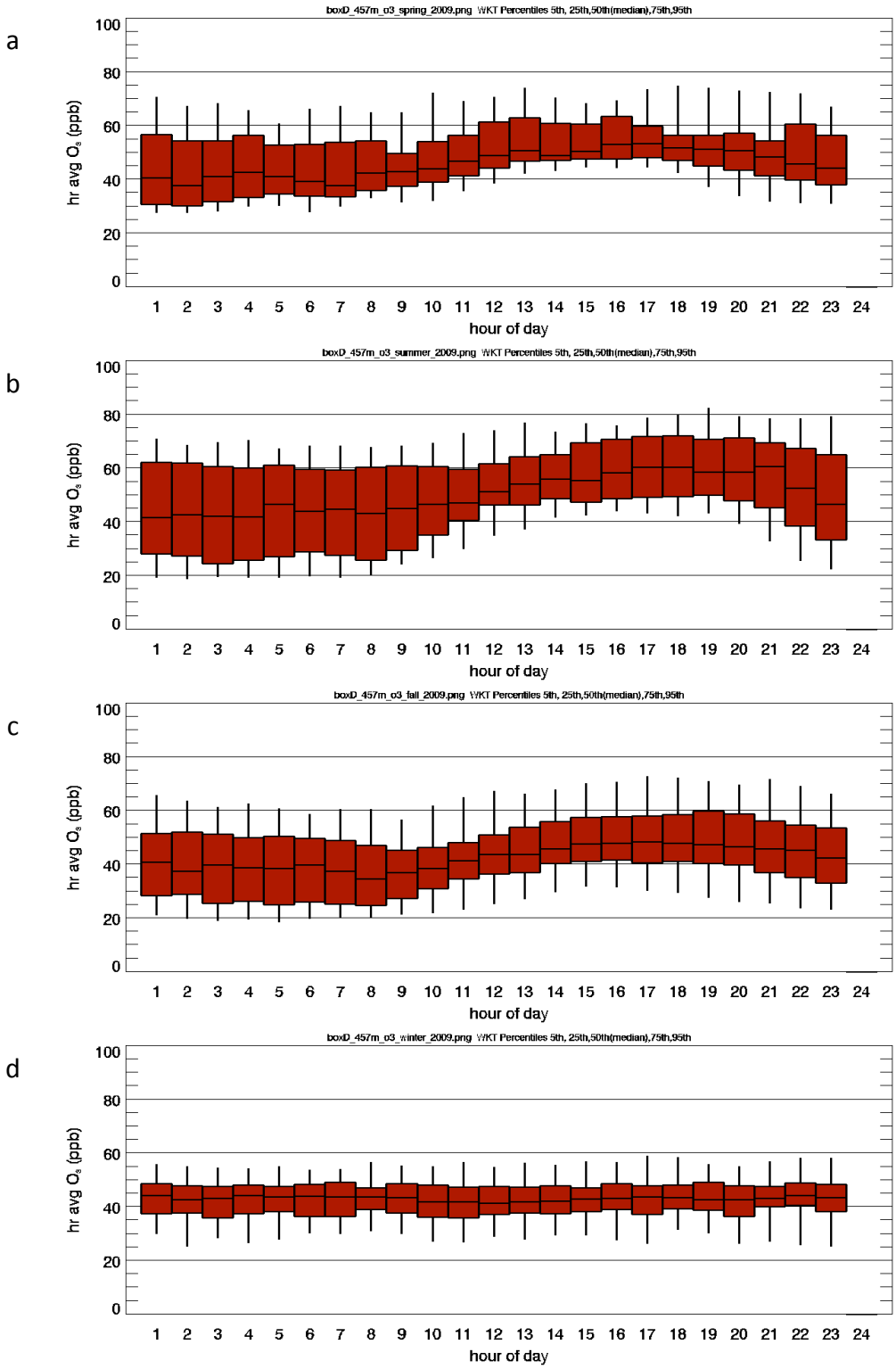

Figure 19) *2009 O_3 percentiles 5th, 25th,50th (median),75th,95th at 457m during* ***a)*** *spring (Mar, Apr, May),* ***b)*** *summer (Jun, Jul),* ***c)*** *fall (Aug, Sep, Oct), and* ***d)*** *winter (Nov, Dec, Jan, Feb).*

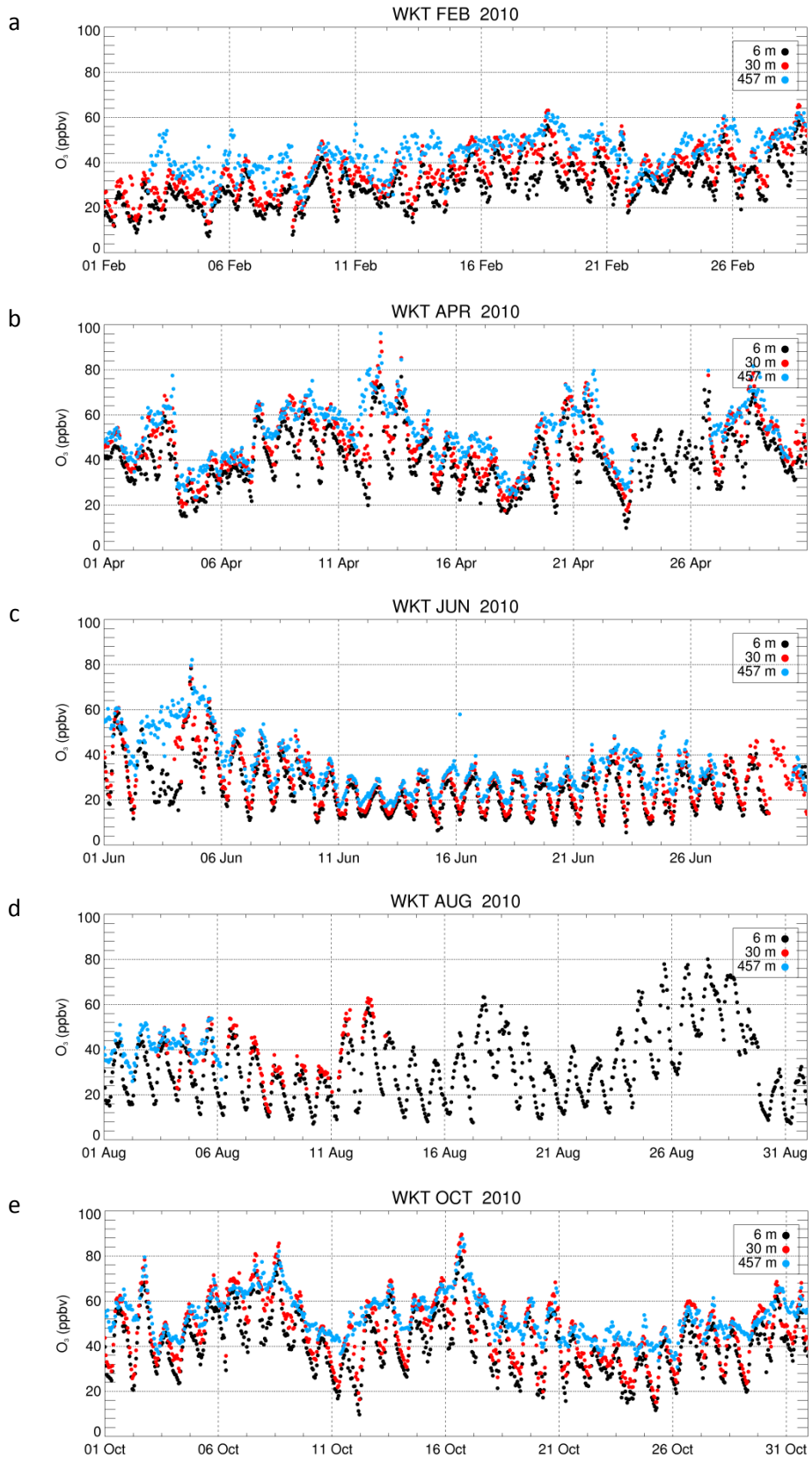

Figure 20) *Hourly-averaged O_3 for a) Feb, b) Apr, c) Jun, d) Aug, and e) Oct of 2010.*

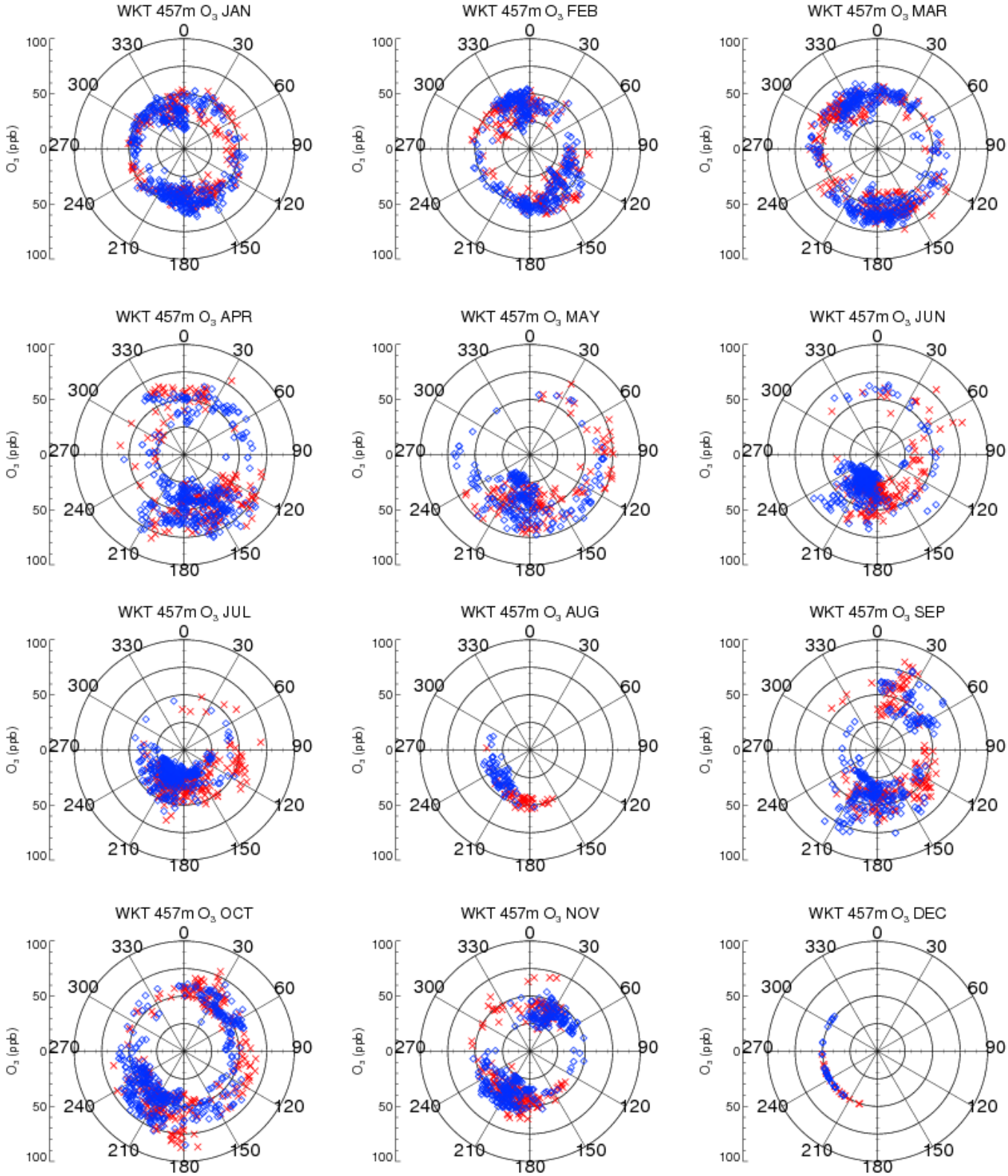

Figure 21) *wind directions and correlating ozone values at 457-m for Jan – Dec, 2010. Blue diamonds represent nighttime and red "x"s, daytime.*

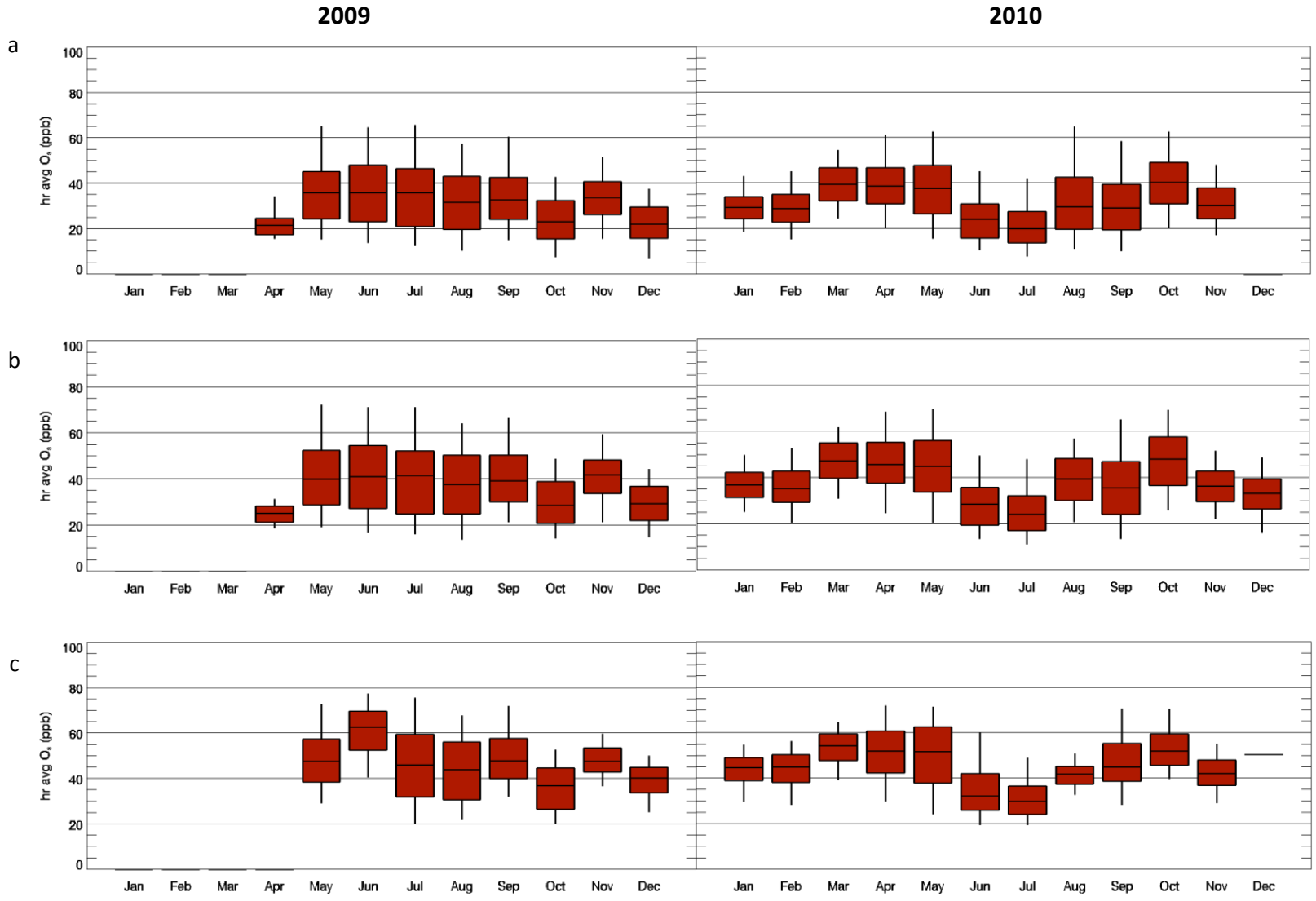

Figure 22) *WKT 2009 and 2010 O_3 percentiles 5th, 25th, 50th (median), 75th, 95th* ***a)*** *6,* ***b)*** *30m, and* ***c)*** *457m.*

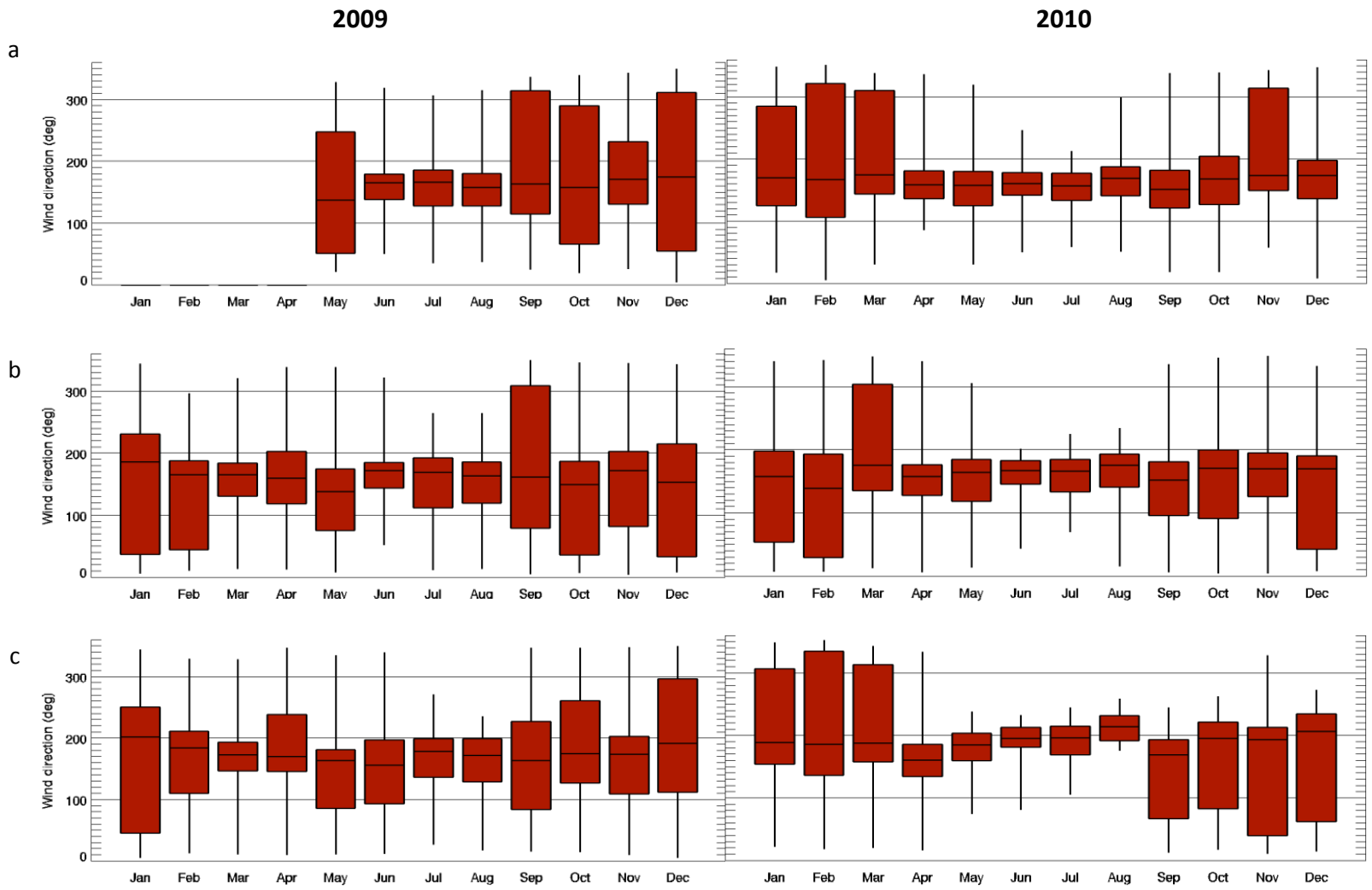

Figure 23) *WKT 2009 and 2010 wind direction percentiles 5th, 25th, 50th (median), 75th, 95th* ***a)*** *6m,* ***b)*** *30m, and* ***c)*** *457m.*

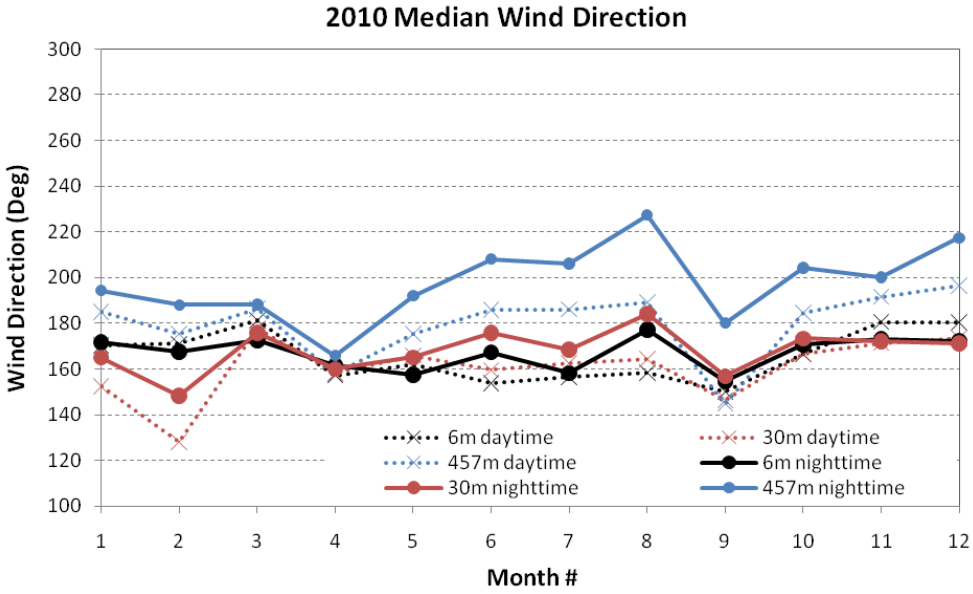

Figure 24) *Median wind directions for 2010 for both daytime and nighttime at 6m (black), 30m (red), and 457m (blue).*

Figure 25) a) *Time series plot of ozone for the hours corresponding to the flask samples. Only mid-day (20 GMT) samples are shown.* ***(b)*** *Correlation between CO observed in the flasks with hourly average ozone from the tower. Solid symbols are from the 30-m level. Open circles are from the 6-m level adjusted by the median difference between observations from 6-m and 30-m (filled circles represent days when data from the 30-m level are unavailable).*

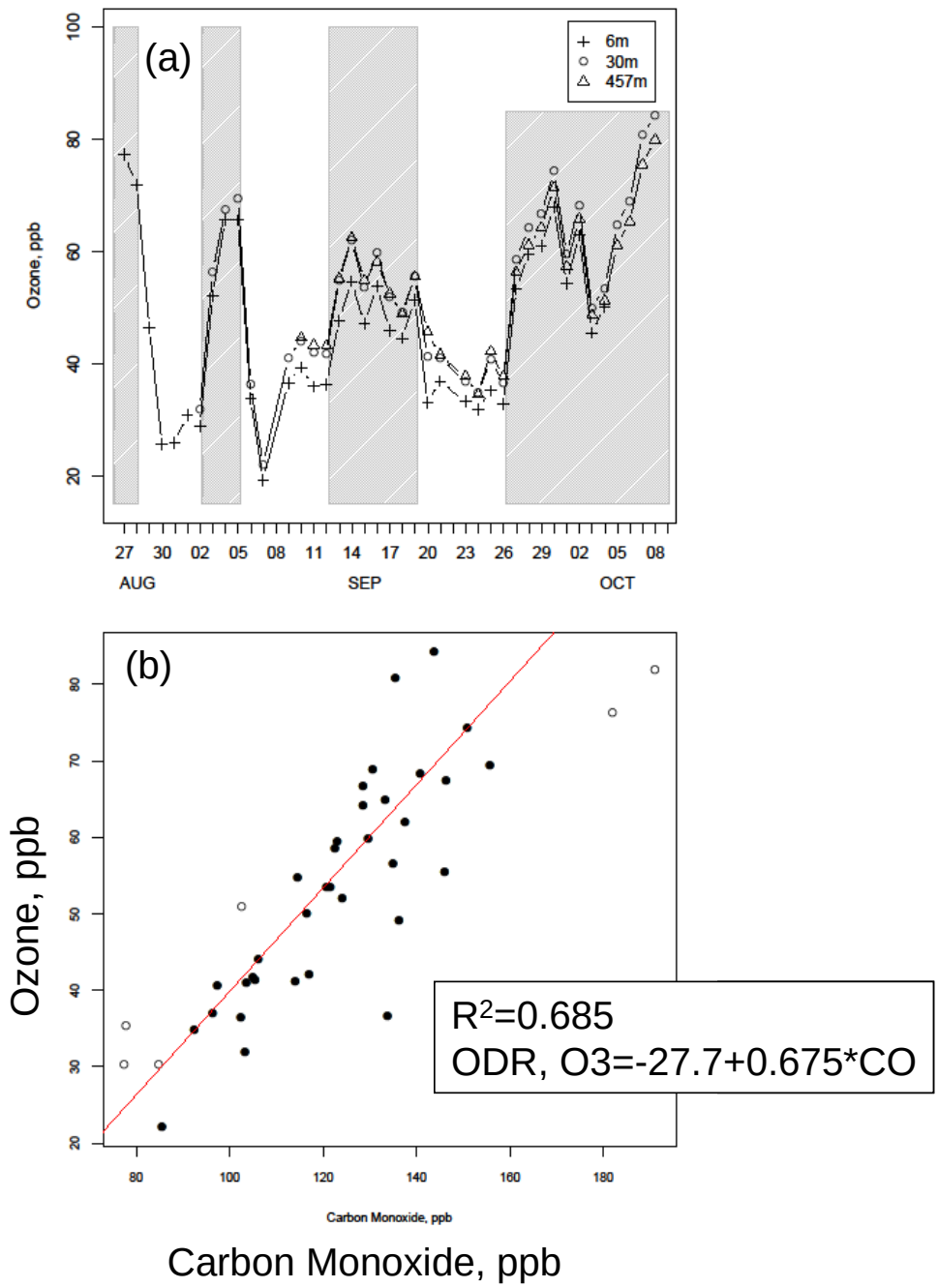

Figure 26) *Data from flask samples for selected species. Shaded areas indicate pollution episodes associated with high ozone. A strong inversion occurred on 26 September 2010 that lasted throughout the day. The tick marks on the plot correspond to 20 GMT, when most of the flask samples were collected.*

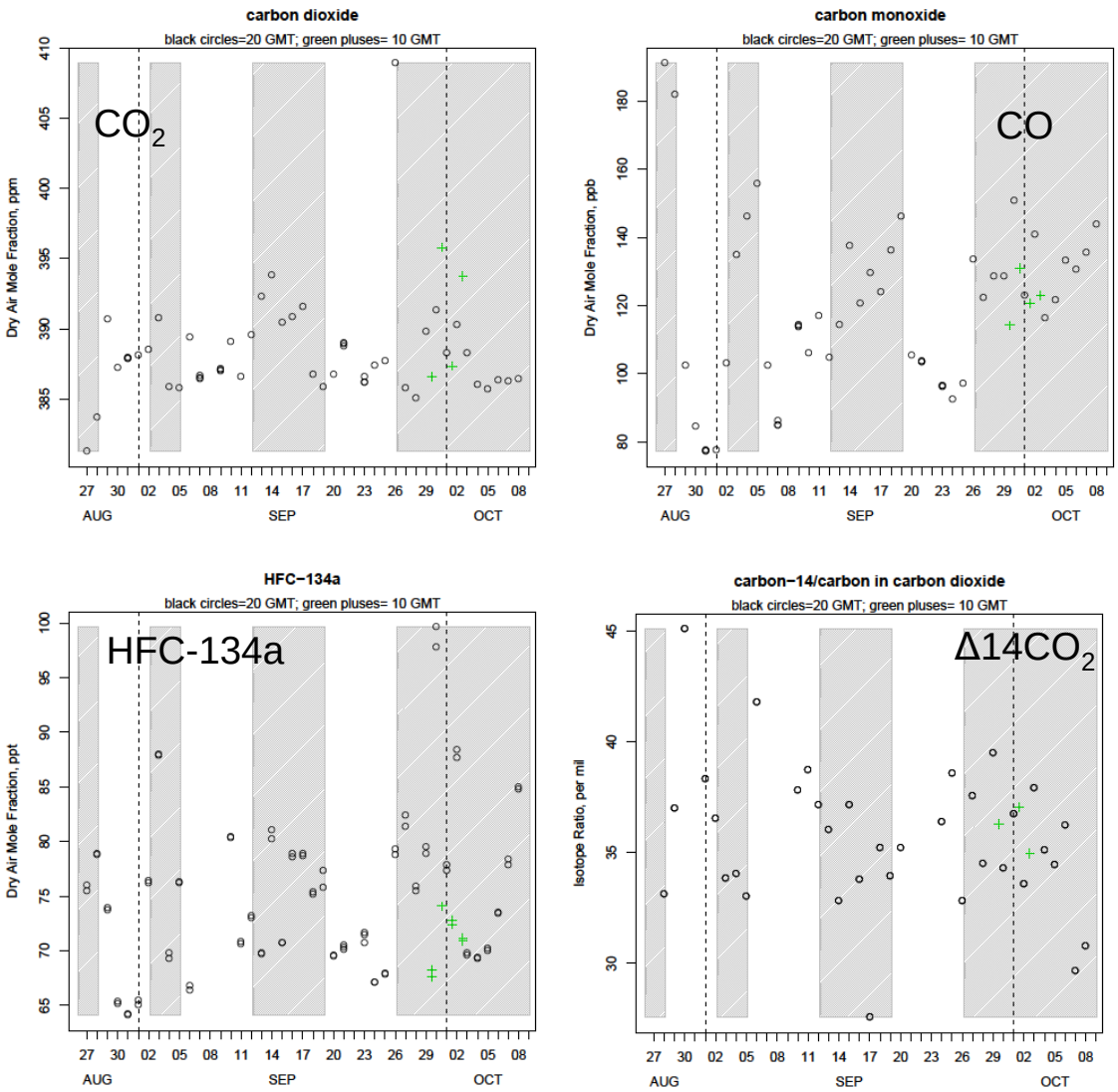

Figure 26 (continued):

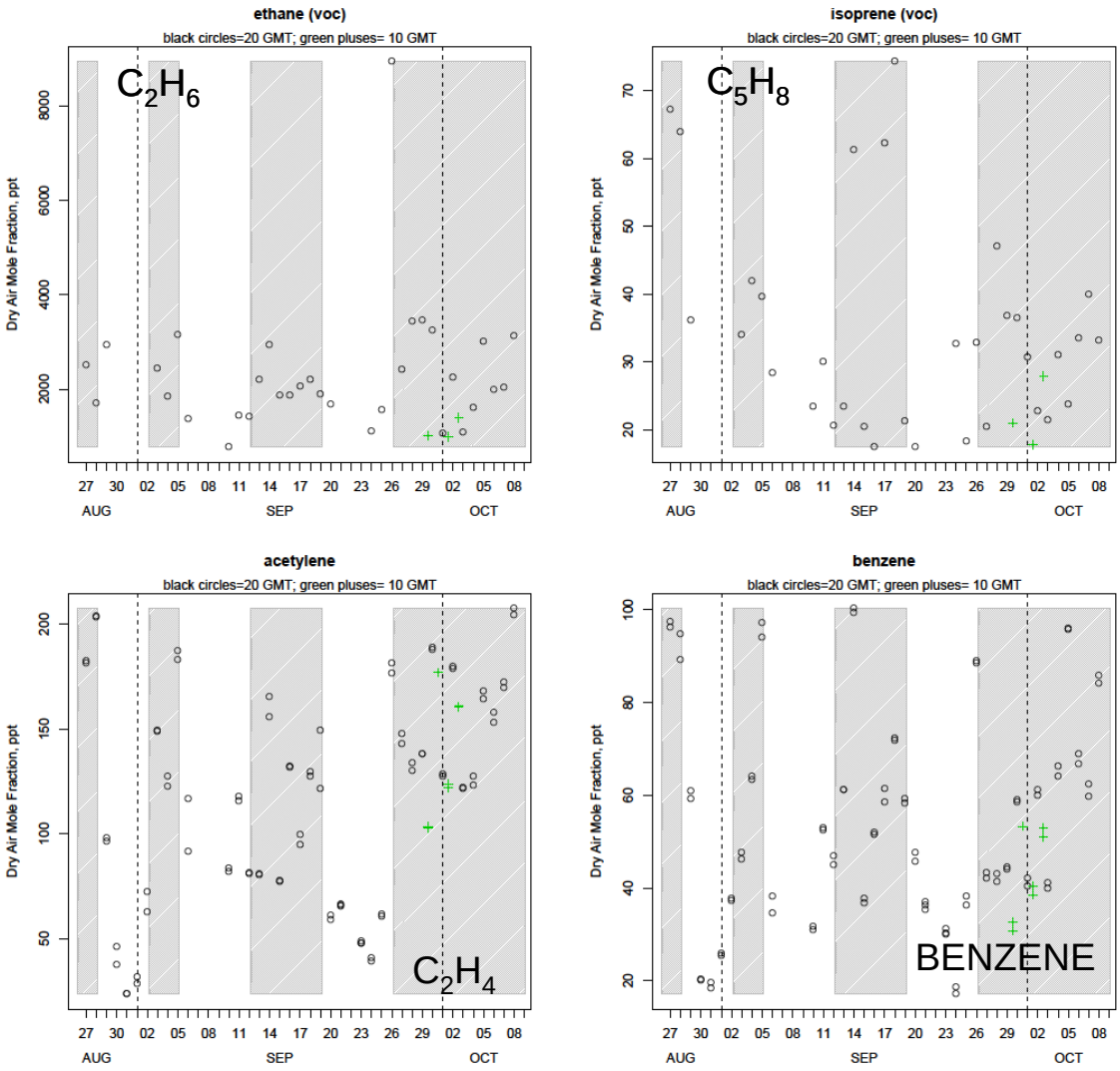

Figure 27) *Correlations among selected species measured in the flask samples. Five percent of the data with the highest and lowest measured values were removed for each species before computing the correlation coefficient. This was done to minimize the influence of outliers such as the single point with very high hydrocarbon values in the lower right panel.*

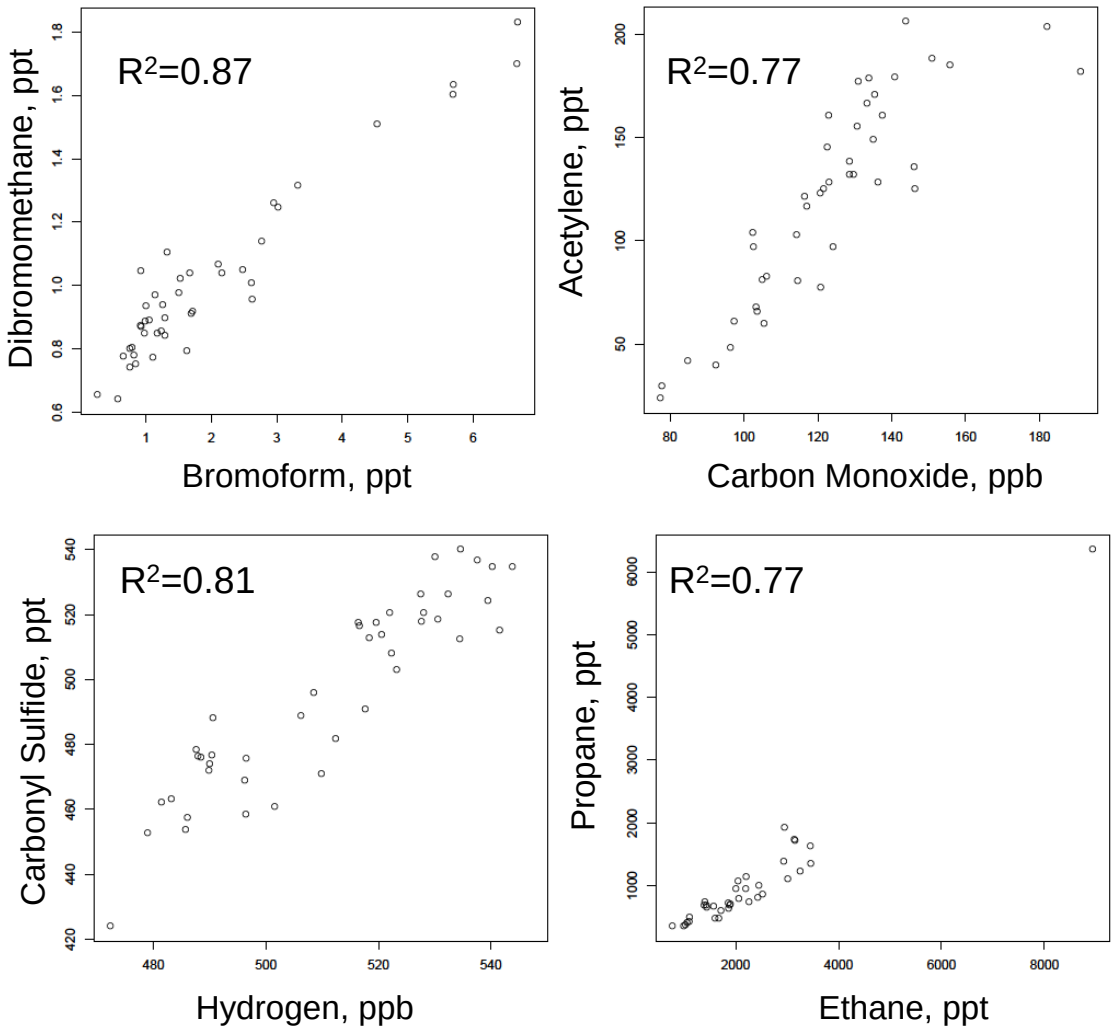

Figure 28) a) *Color-coded time series plot for carbon monoxide and corresponding correlation plots for various gases against carbon monoxide (b-j) and HFC-134a (k-m).*

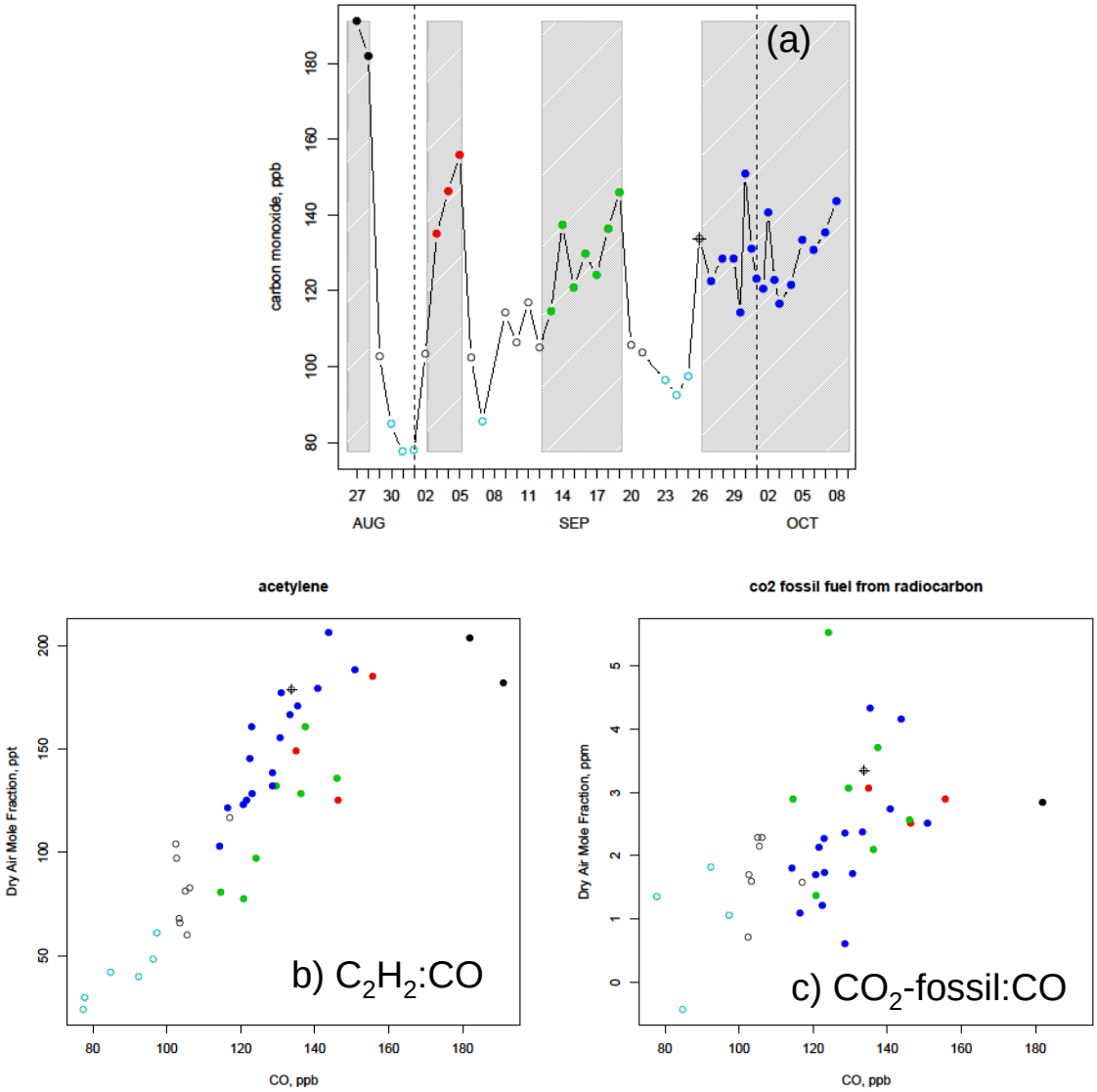

Figure 28 (continued):

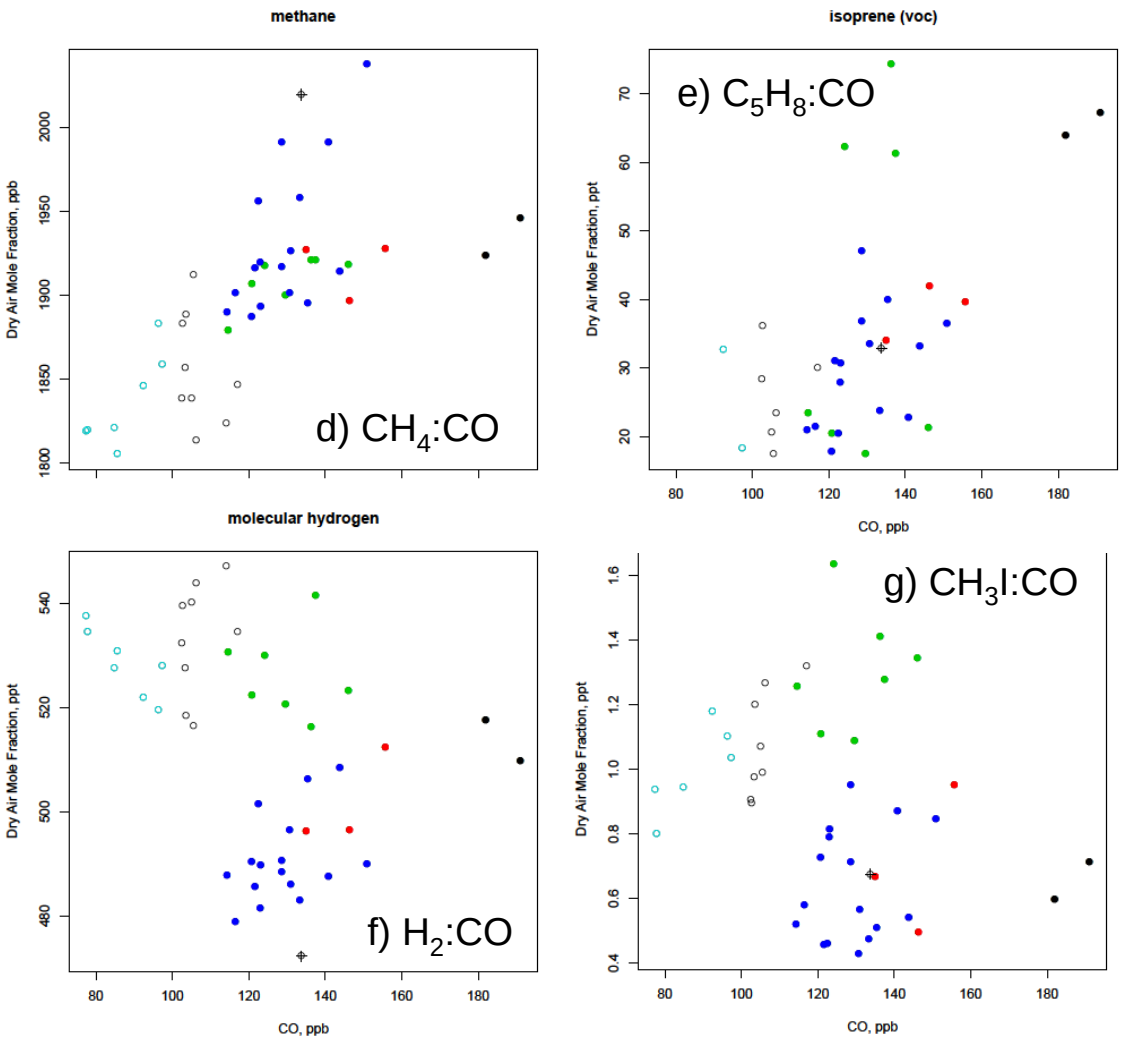

Figure 28 (continued):

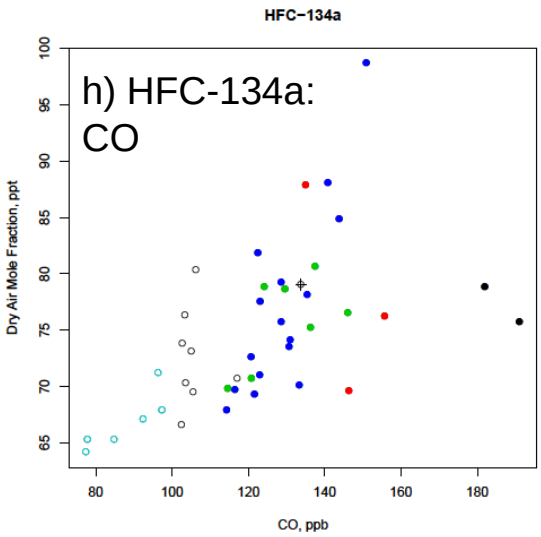

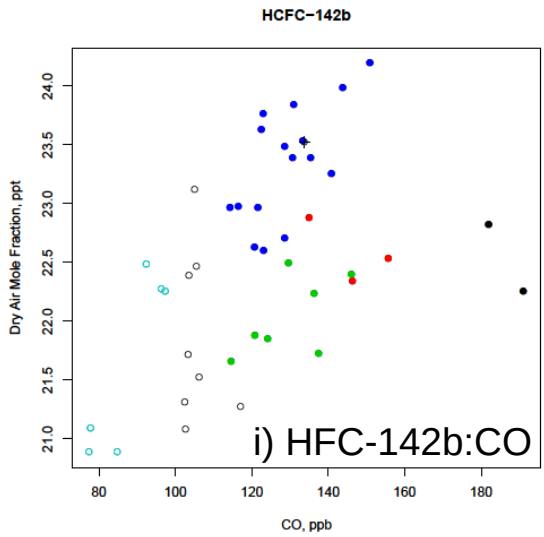

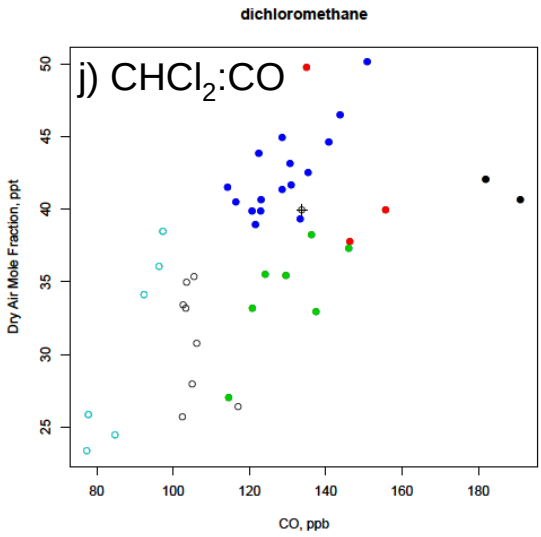

Figure 28 (continued):

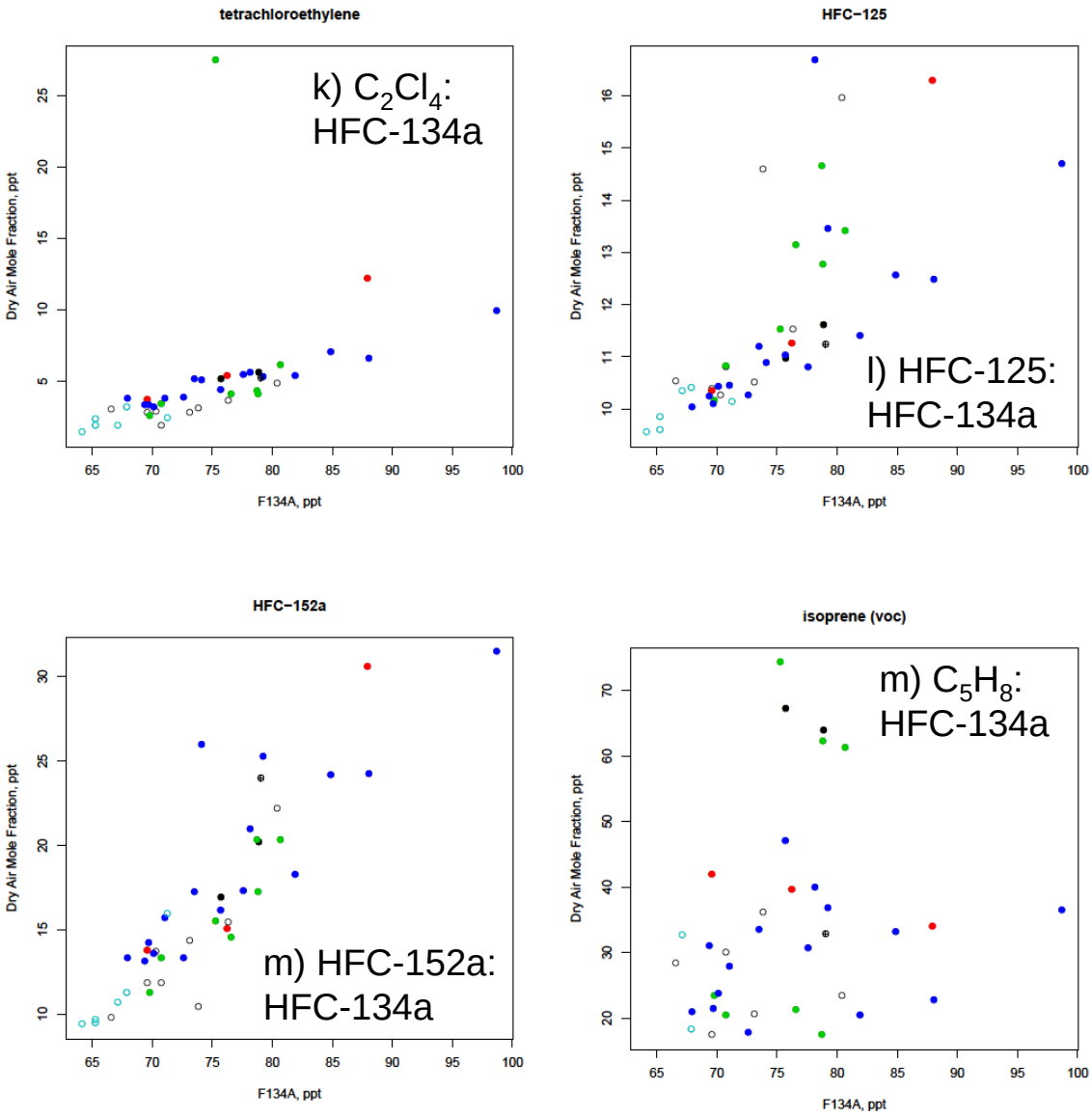

Figure 29) *STILT footprints for flask samples on selected polluted days for samples collected at 20:30 GMT.* ***a)*** *27 August,* ***b)*** *28 August,* ***c)*** *4 September,* ***d)*** *5 September,* ***e)*** *14 September,* ***f)*** *29 September,* ***g)*** *30 September,* ***h)*** *5 October,* ***i)*** *8 October.*

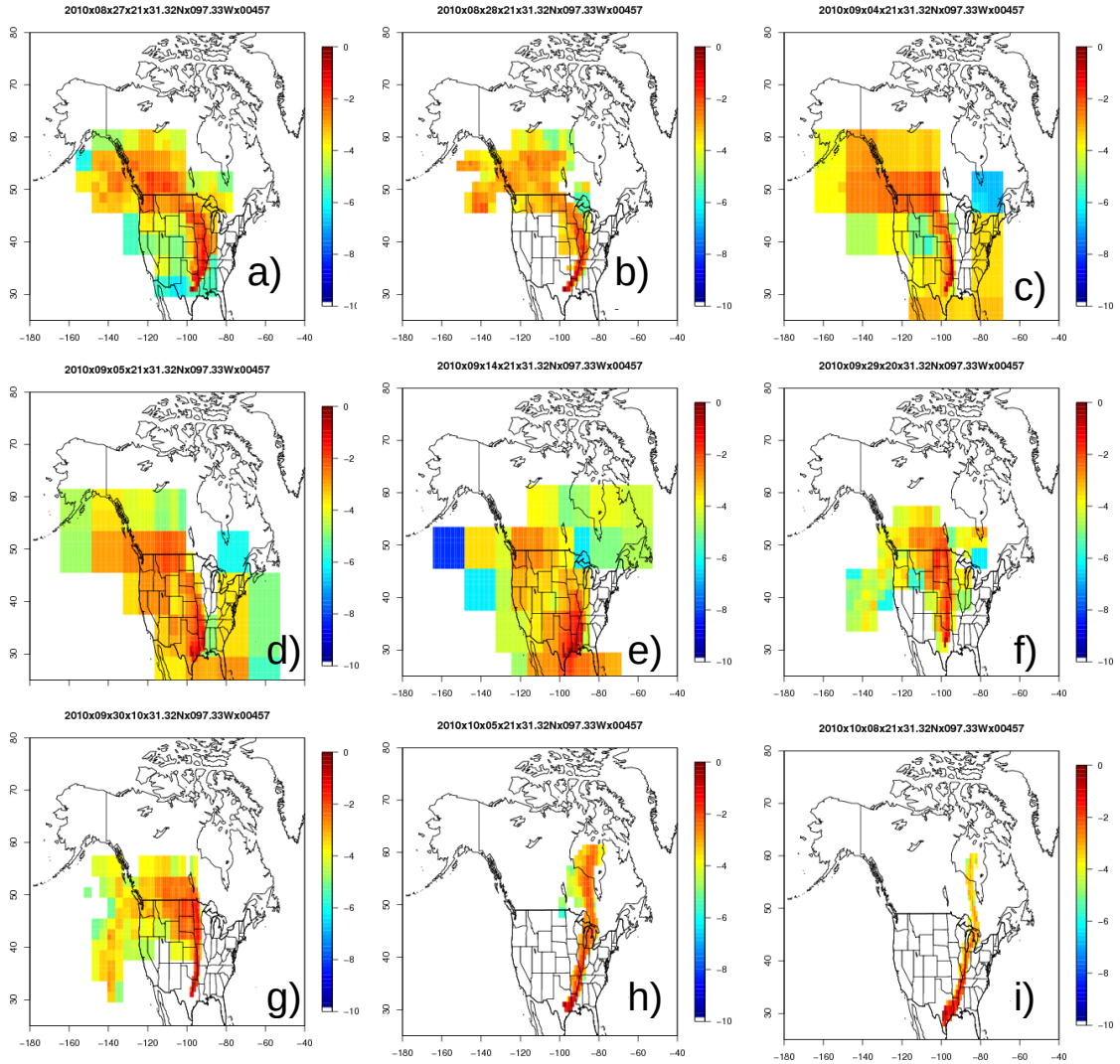

Figure 30) *Comparison of radiocarbon-based fossil fuel CO_2 (black squares) with model results for STILT footprints convolved with the NOAA CarbonTracker fossil fuel flux fields (red plus symbols; Peters et al., 2007) and the Vulcan CO_2 inventory (green crosses; USA only; Gurney et al., 2009).*

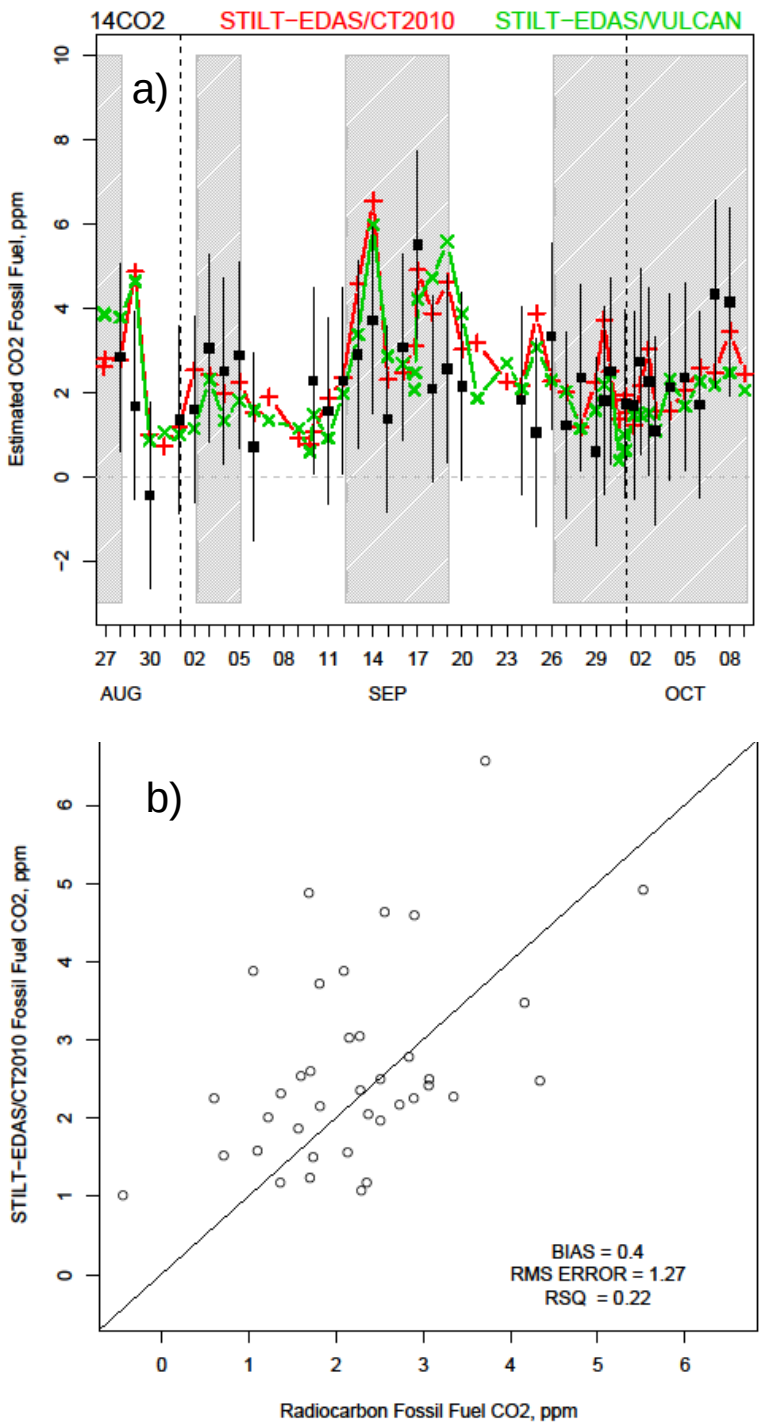

Figure 31) *Breakdown of modeled CO_2-ff by (a) sector and (b) region according to the Vulcan inventory. Shaded areas correspond to periods with high ozone.*

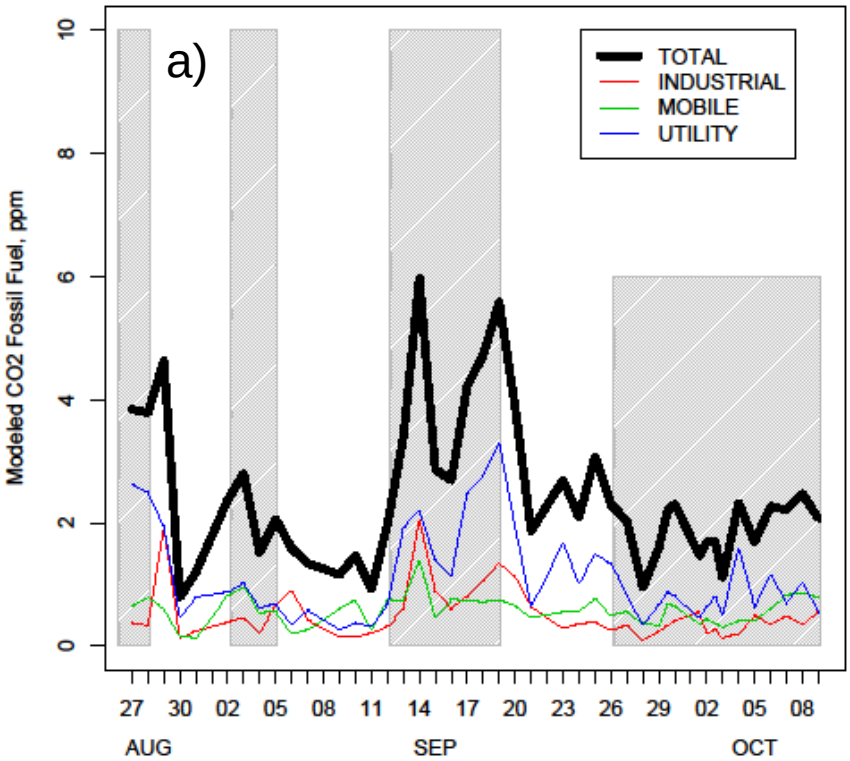

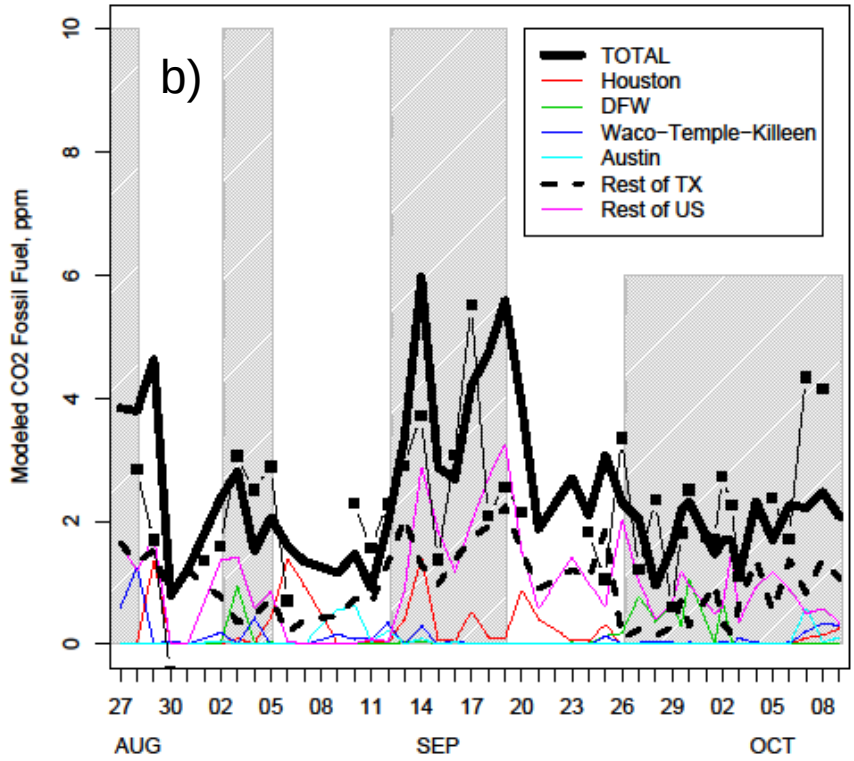

Figure 32) *Flask sample results for n-butane and iso-butane. Symbol size is proportional to n-butane/i-buane.*

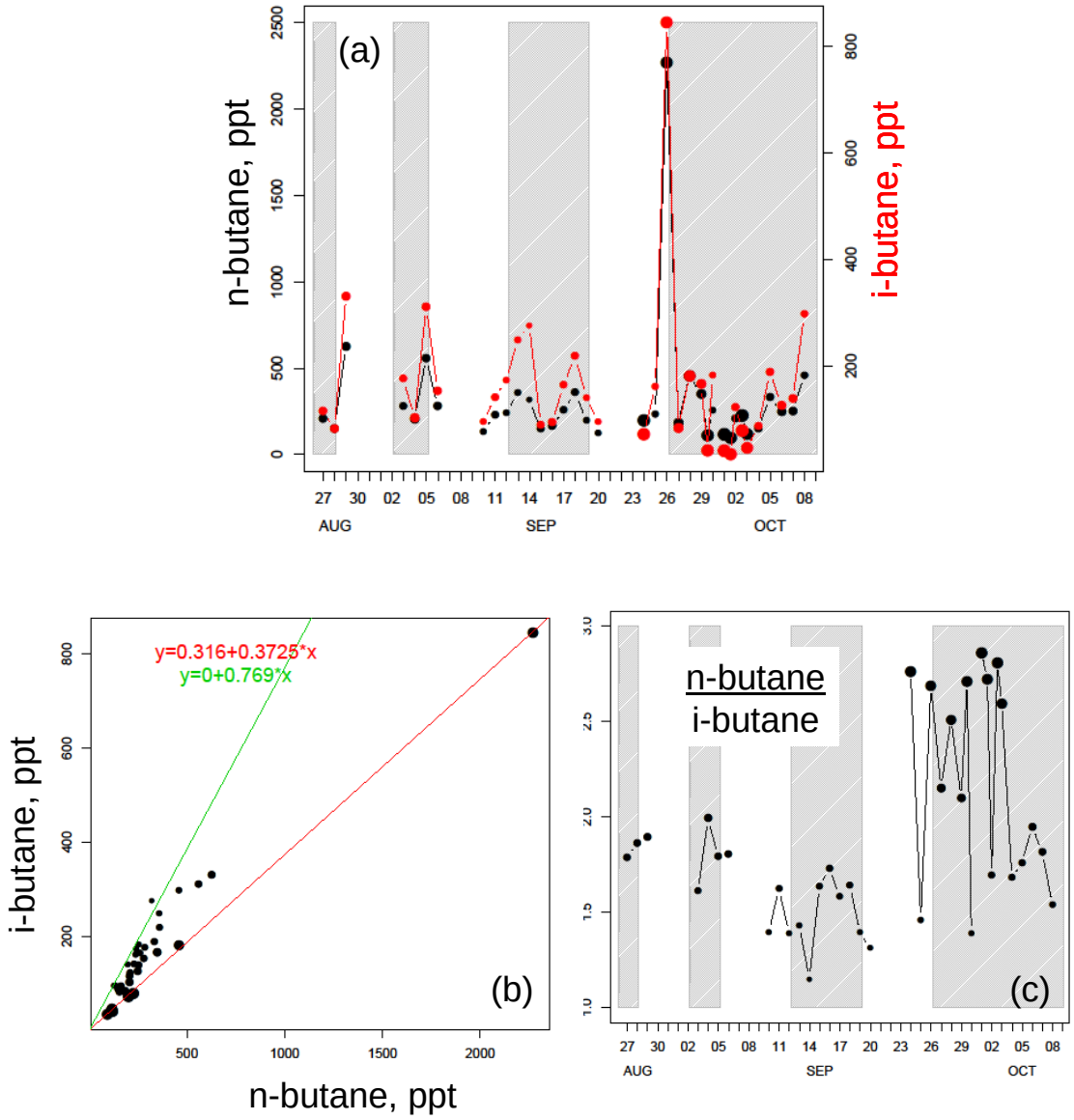

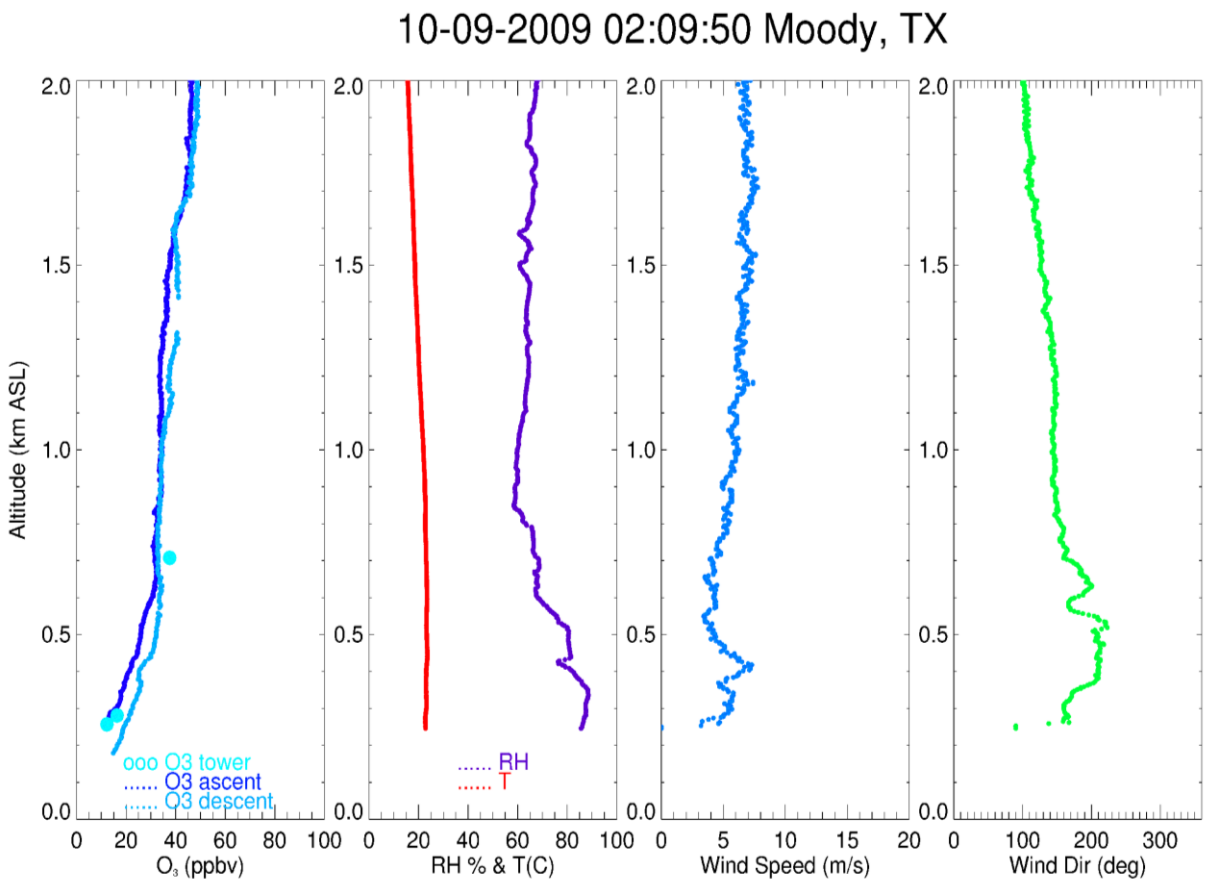

Figure 33) *An ozonesonde flight on Sept 10, 2009 shows the continental nighttime jet as the moister and faster southerly flow between 350 and 600 masl.*

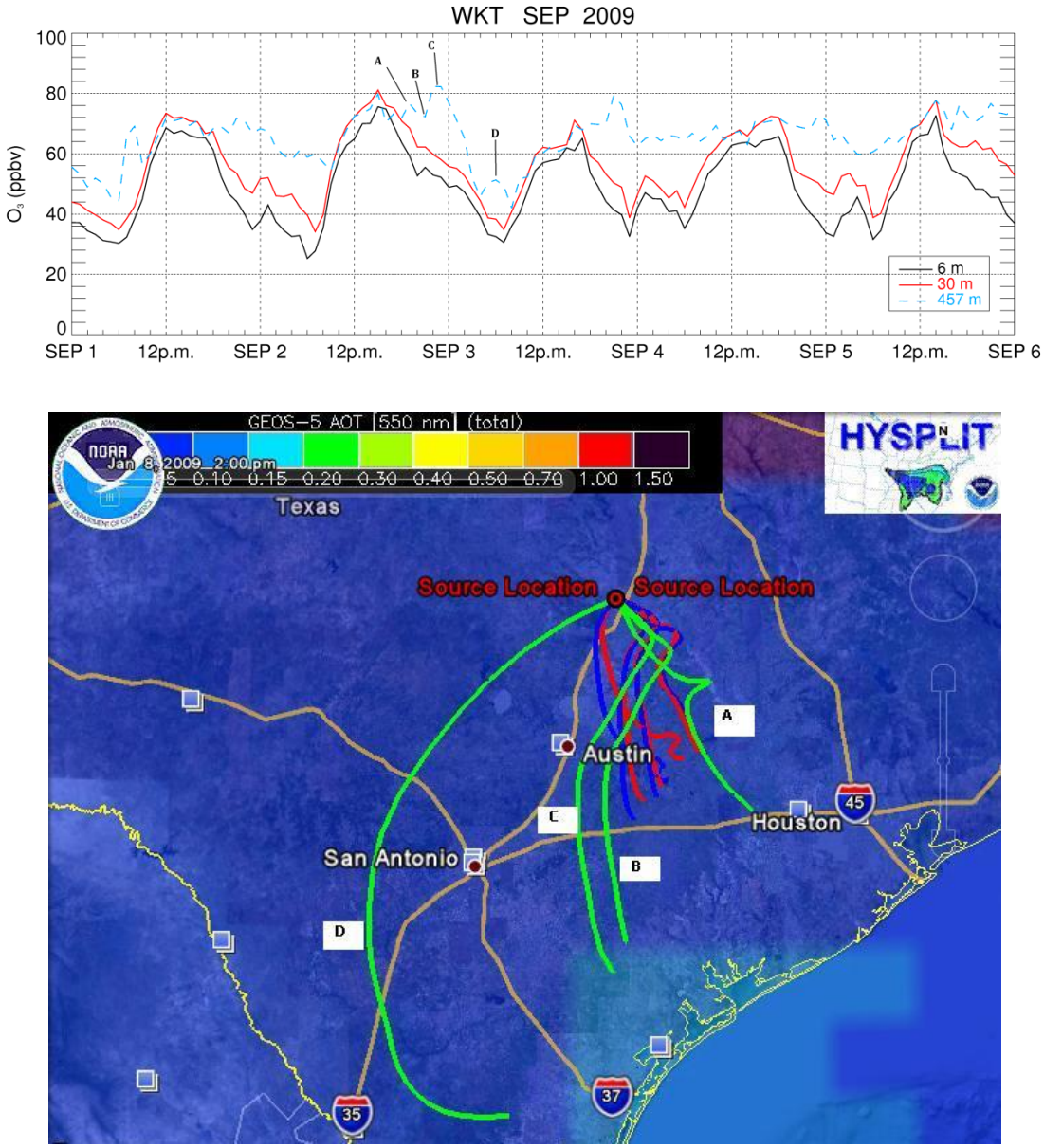

Figure 34) a) *Hourly-averaged ozone for September 1-5, 2009.* ***b)*** *HYSPLIT one day back trajectories of September 2nd run at different times,* ***A*** *– 1900 LT,* ***B*** *– 2000 LT,* ***C*** *– 2200 LT, and September 3rd at* ***D*** *– 0600 LT.*

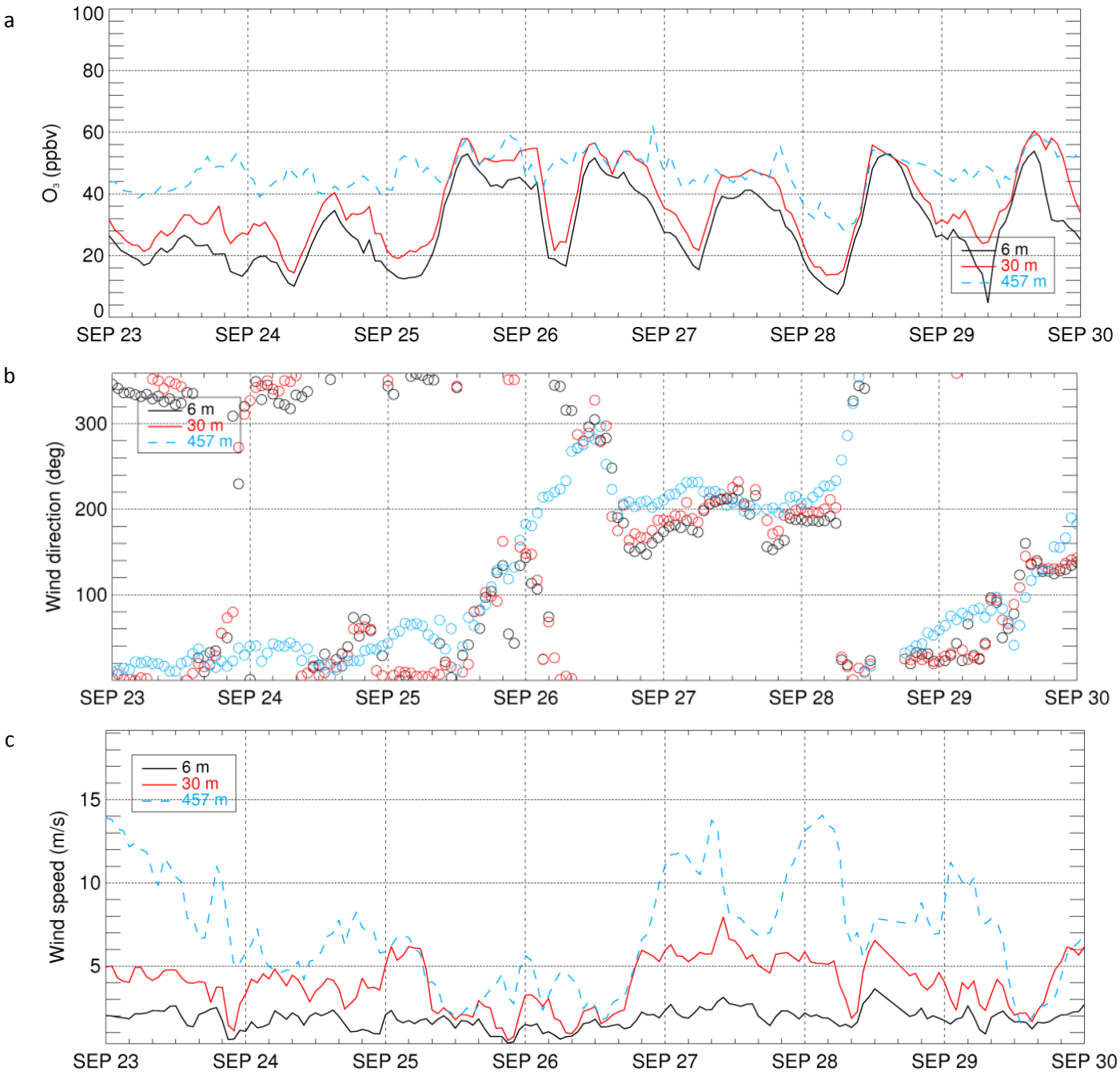

Figure 35) *Hourly averaged data for a) ozone, b) wind direction, and c) wind speed at 6m (black), 30m (red) and 457m (blue) for September 23-30, 2009.*

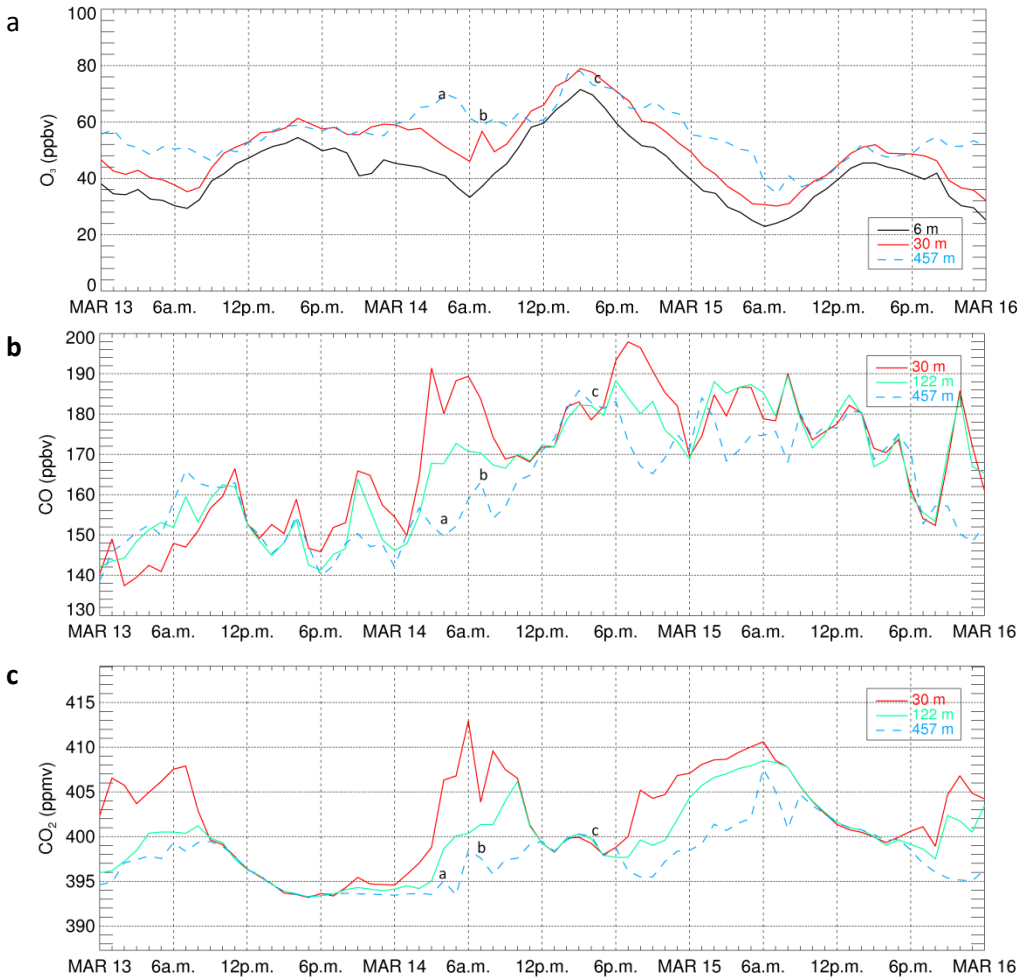

Figure 36) *March 14th shows hourly-averaged* ***a)*** *O_3,* ***b)*** *CO and* ***c)*** *CO_2 at times different run times a-c.* ***a*** *- 0400 LT,* ***b*** *- 0700 LT, and* ***c*** *- 1600 LT.*

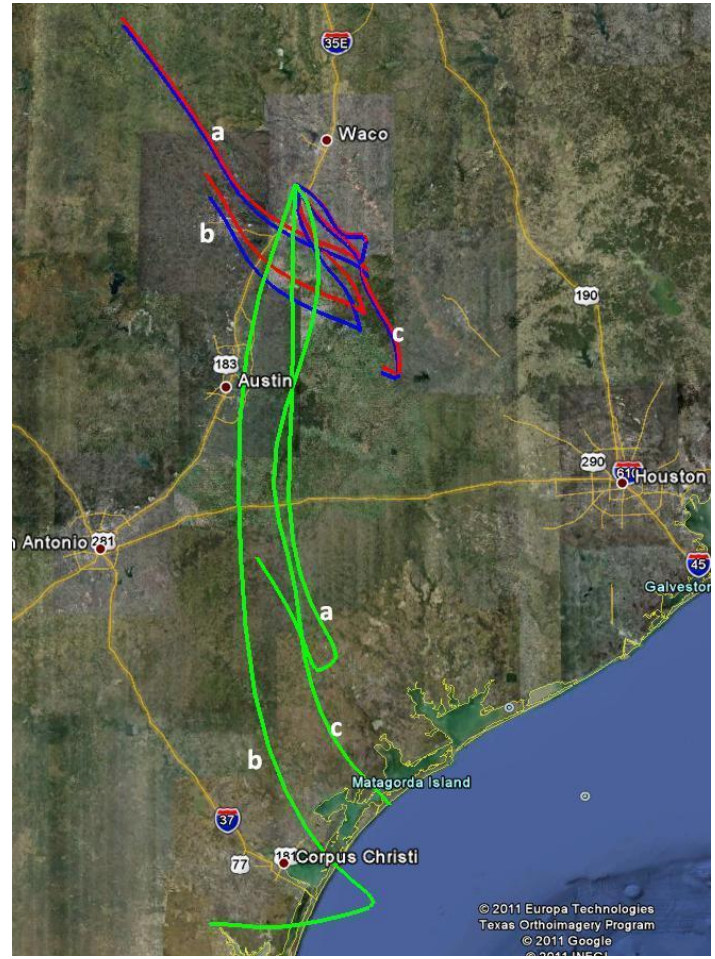

Figure 36d) *HYSPLIT back-trajectories for March 14,* ***a*** *- 0400 LT,* ***b*** *- 0700 LT, and* ***c*** *- 1600 LT. The 457-m level (green) comes from a different direction than the 6-m and 30-m (red and blue) levels.*

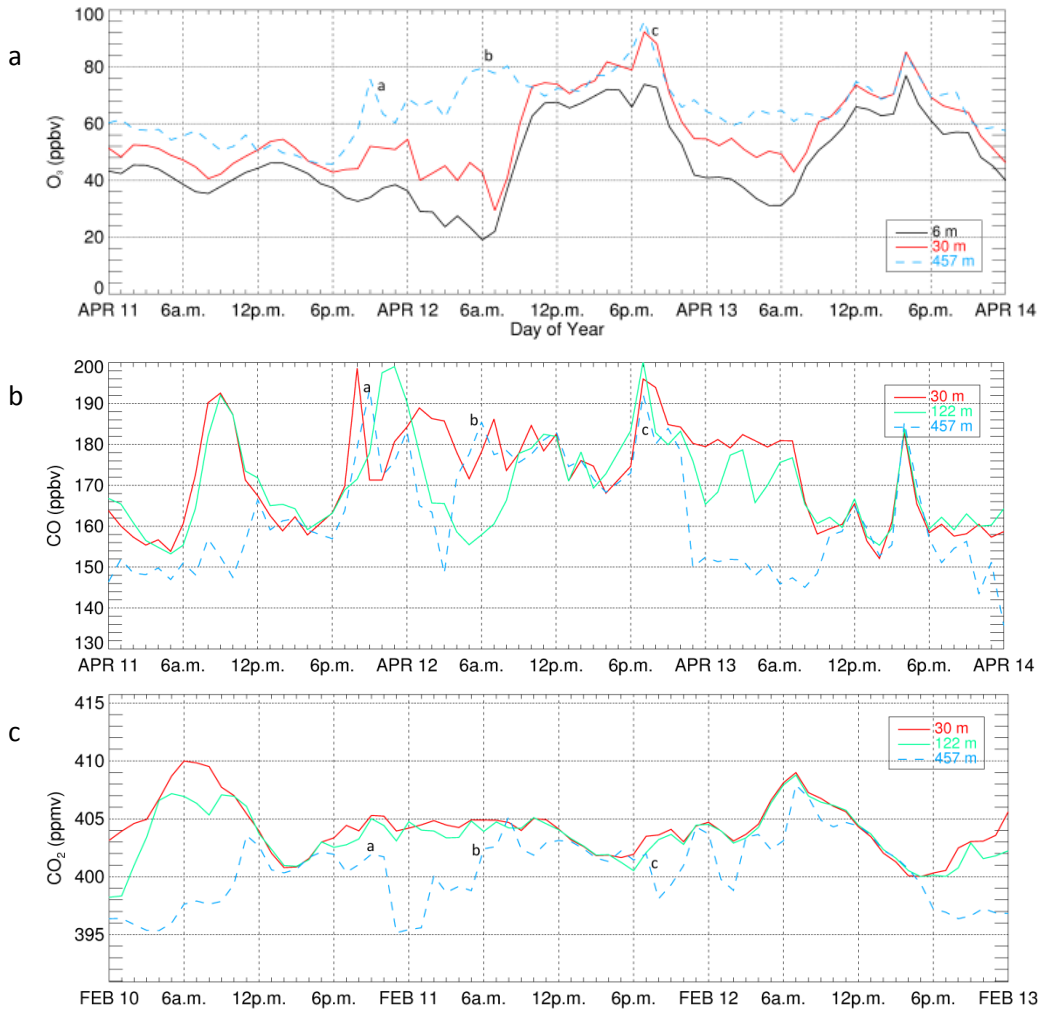

Figure 37) *April 11-12 shows hourly-averaged* ***a)*** *O_3,* ***b)*** *CO and* ***c)*** *CO_2 at times different runtimes a-c.* ***a*** *- 2100 LT April 11,* ***b*** *- 0600 LT April 12, and* ***c*** *- 1900 LT April 12.*

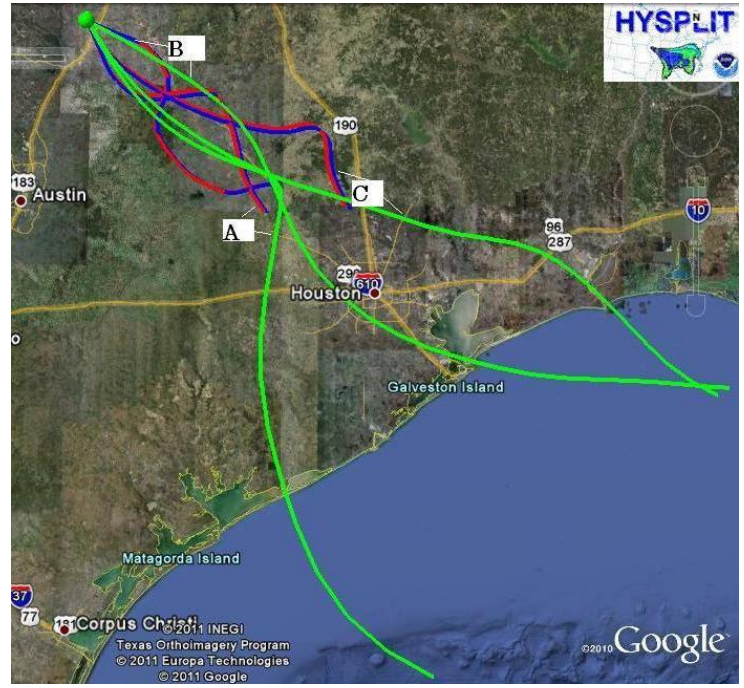

Figure 37d) *HYSPLIT back-trajectories for* ***a*** *- April 11,* ***2100 LT*** *and April 12* ***b*** *- 0600 LT and* ***c*** *- 1900 LT.*

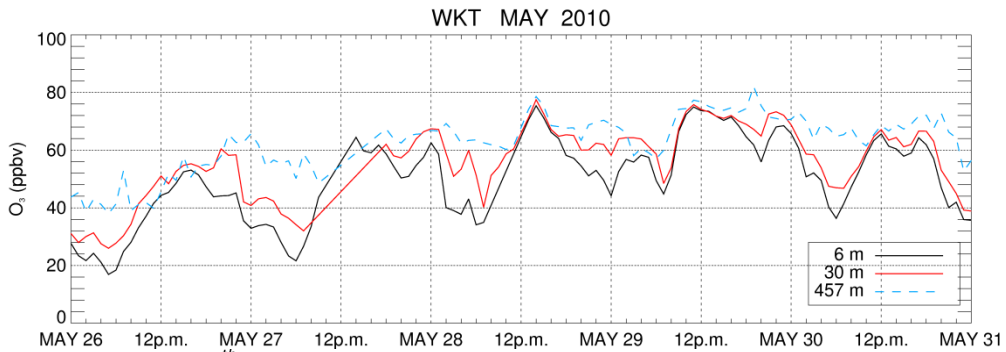

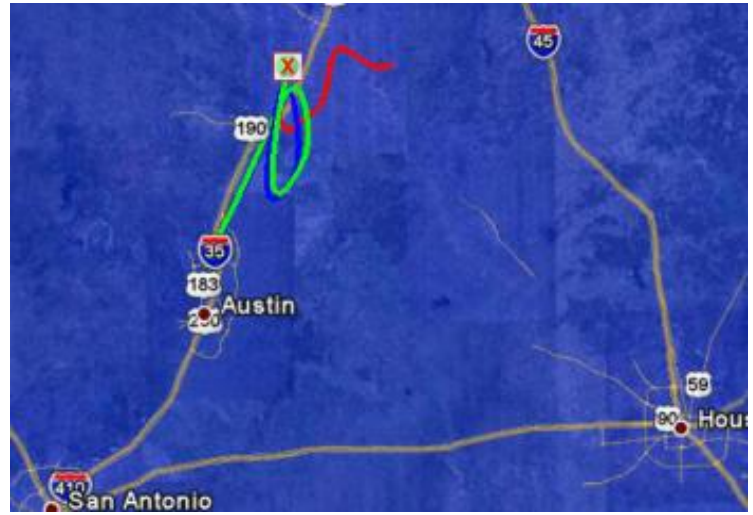

Figure 38) a) *May 29th shows a pulse of high ozone at 457 meters at ~1900 LT. As 457-m level shows a pulse, the other levels show gradual nighttime decay and then rise a few hours later.* ***b)*** *(right) HYSPLIT trajectory for May 29th, 1900 LT. The 457-m level (green) comes from further than the 6-m and 30-m (red and blue) levels and shows a nighttime pulse of high-ozone values likely from Austin.*

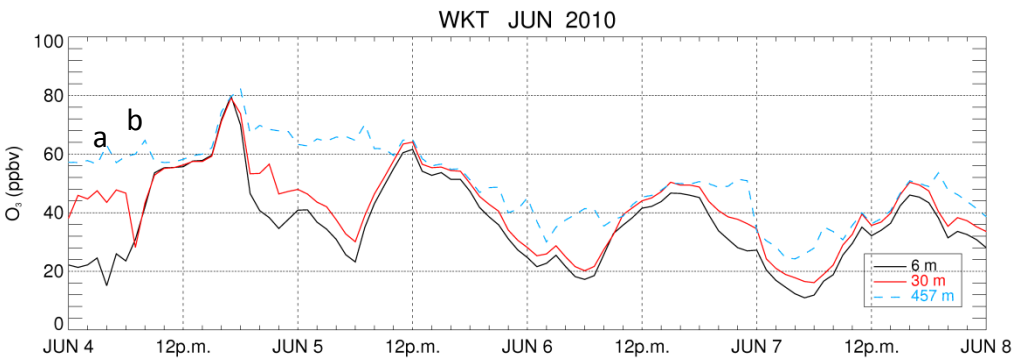

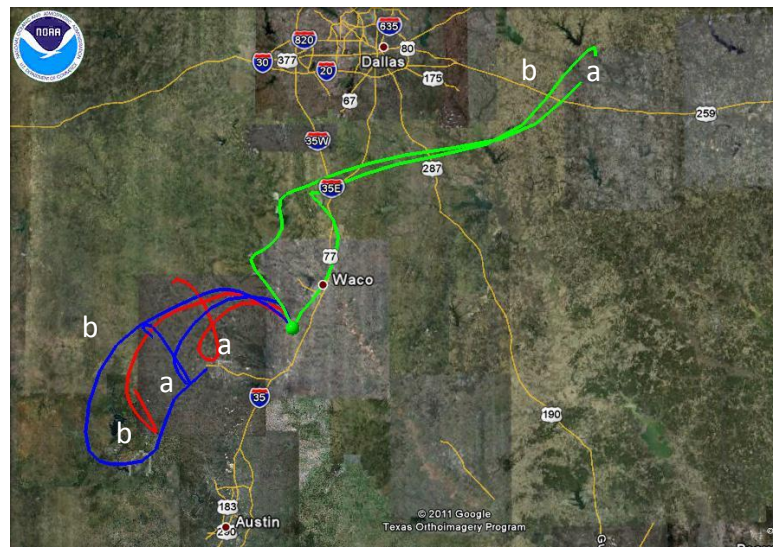

Figure 39) a) *June 4th and 5th had a two-day period with high ozone, before a long duration of low ozone at all levels.* ***b)*** *(right) HYSPLIT back-trajectory for June 4th at* ***a****- 0400 LT and* ***b****- 0800 LT .*

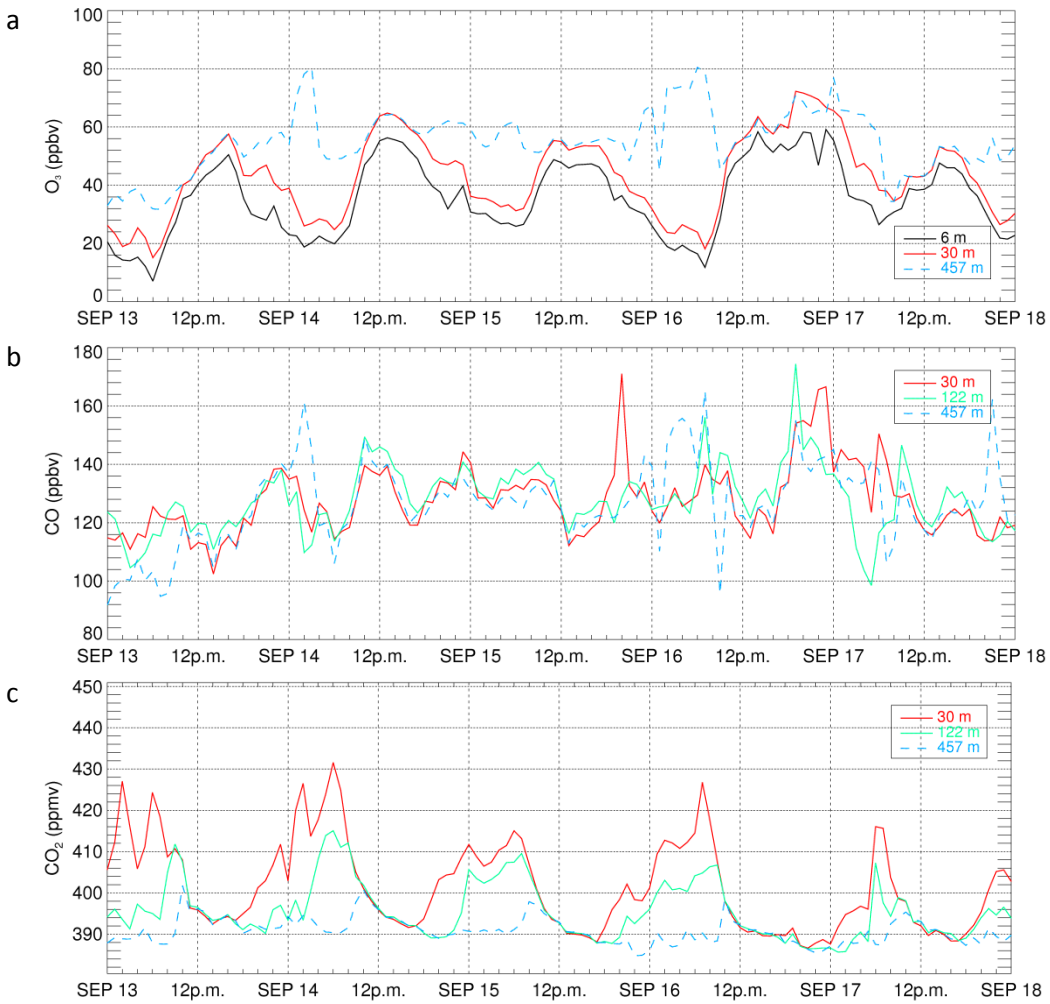

Figure 40) *Sept 14th shows* ***a)*** *a pulse of high ozone at 457 meters at ~0300 LT. As 457-m level shows a pulse, the other levels show gradual nighttime decay and then begin to rise at ~0800 LT (usual pattern). Sept 15th shows a small pulse, while Sept 16th shows a large pulse, which mixes into the other layers at daybreak. For the same time period* ***b)*** *CO, and* ***c)*** *CO_2.*

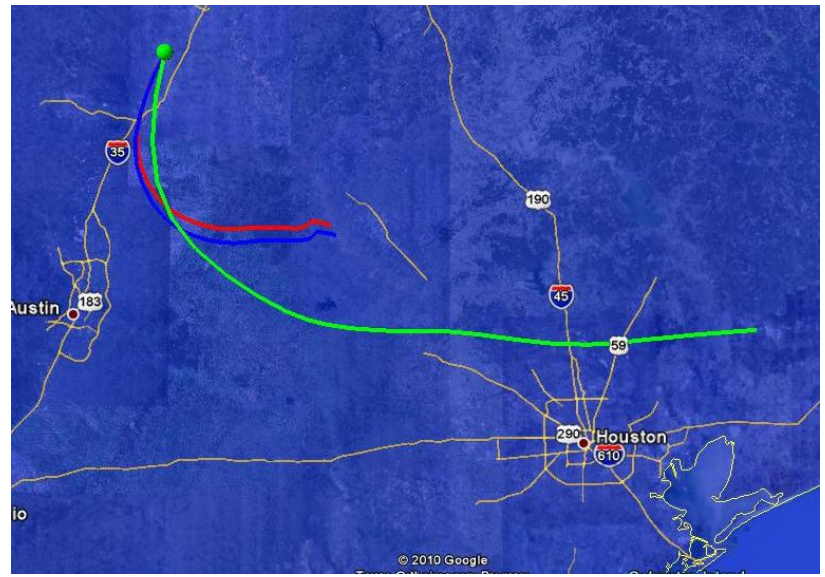

Figure 40d) *HYSPLIT trajectory for Sep 14, 0300 LT. The 457-m level (green) comes from further than the 6-m and 30-m (red and blue) levels and shows a nighttime pulse of high-ozone values likely originating in Houston.*

Appendix 1- HYSPLIT Trajectory Model Runs for Potential Pollution Events:

The back trajectories were run using the EDAS 40km meteorological data set in a 24 particle run for the location of the KWKT tower (31.32, -97.33)

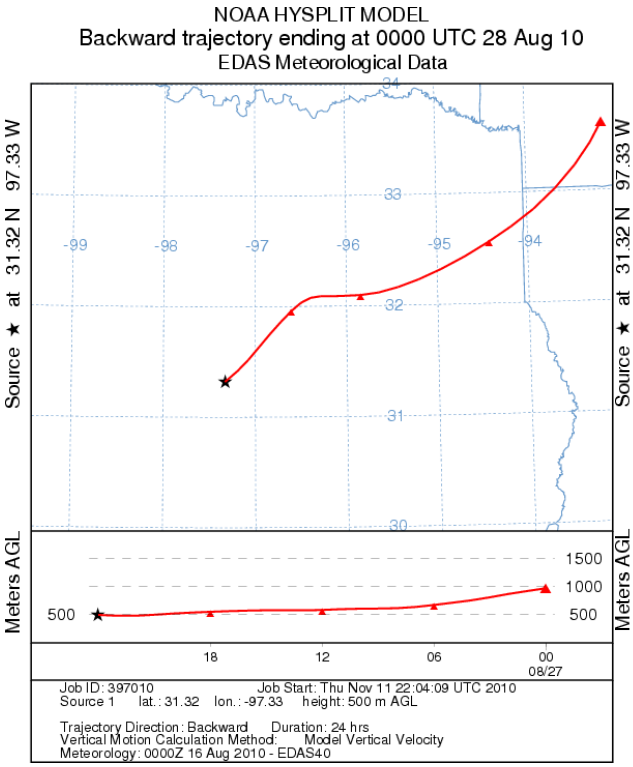

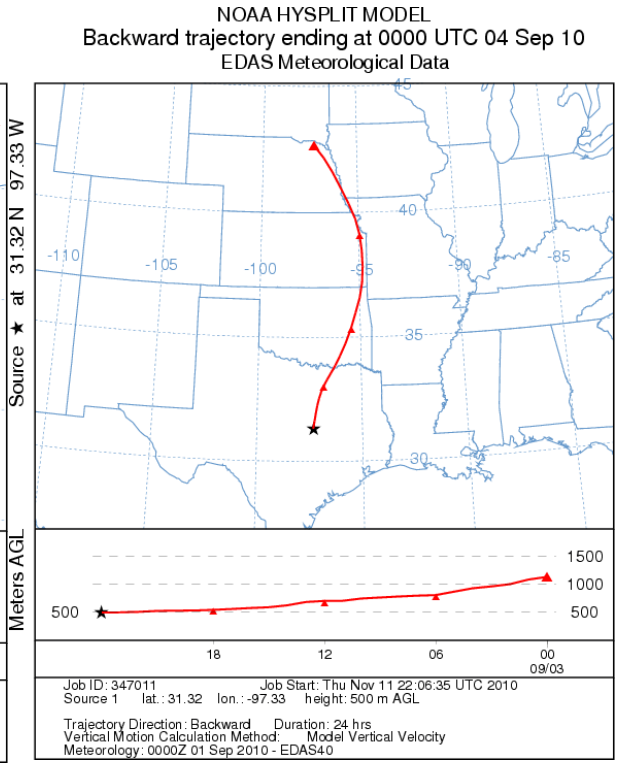

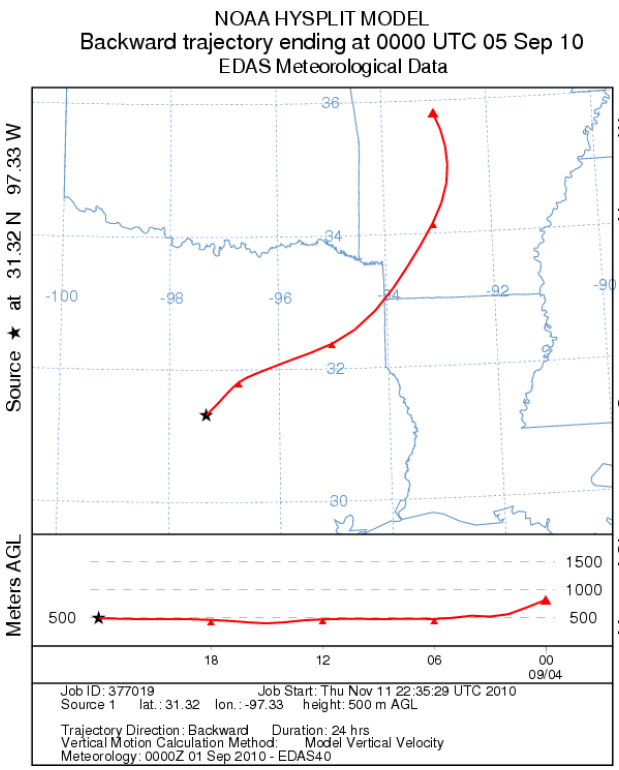
NOAA HYSPLIT MODEL
Backward trajectory ending at 0000 UTC 05 Sep 10
EDAS Meteorological Data
Source ★ at 31.32 N 97.33 W
Meters AGL
Job ID: 377019 Job Start: Thu Nov 11 22:35:29 UTC 2010
Source 1 lat.: 31.32 lon.: -97.33 height: 500 m AGL
Trajectory Direction: Backward Duration: 24 hrs
Vertical Motion Calculation Method: Model Vertical Velocity
Meteorology: 0000Z 01 Sep 2010 - EDAS40

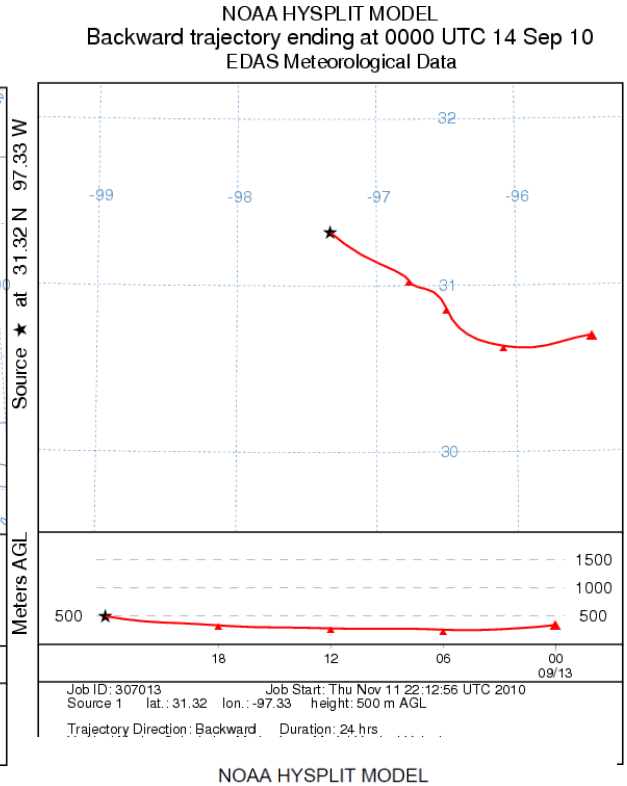
NOAA HYSPLIT MODEL
Backward trajectory ending at 0000 UTC 14 Sep 10
EDAS Meteorological Data
Source ★ at 31.32 N 97.33 W
Meters AGL
Job ID: 307013 Job Start: Thu Nov 11 22:12:56 UTC 2010
Source 1 lat.: 31.32 lon.: -97.33 height: 500 m AGL
Trajectory Direction: Backward Duration: 24 hrs

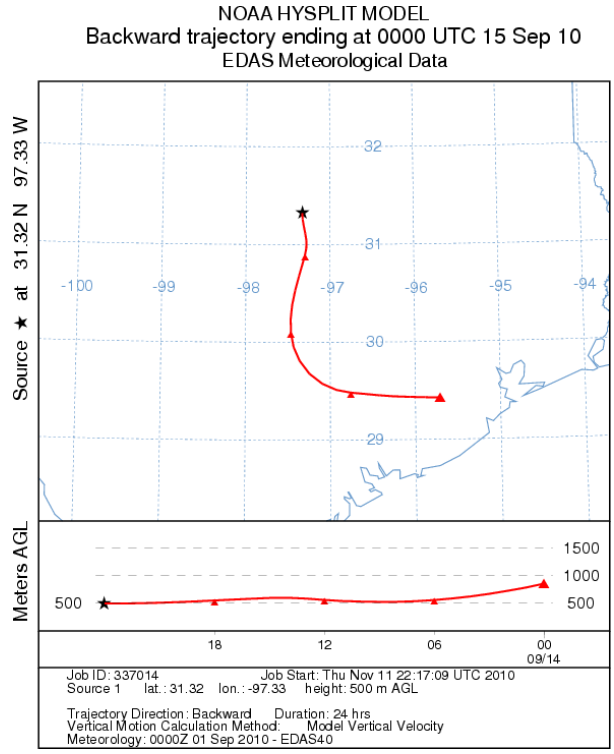
NOAA HYSPLIT MODEL
Backward trajectory ending at 0000 UTC 15 Sep 10
EDAS Meteorological Data
Source ★ at 31.32 N 97.33 W
Meters AGL
Job ID: 337014 Job Start: Thu Nov 11 22:17:09 UTC 2010
Source 1 lat.: 31.32 lon.: -97.33 height: 500 m AGL
Trajectory Direction: Backward Duration: 24 hrs
Vertical Motion Calculation Method: Model Vertical Velocity
Meteorology: 0000Z 01 Sep 2010 - EDAS40

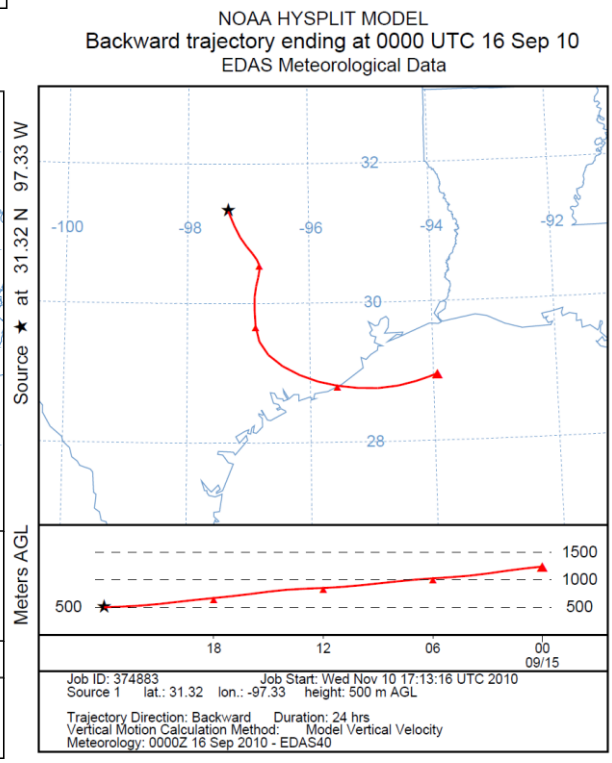
NOAA HYSPLIT MODEL
Backward trajectory ending at 0000 UTC 16 Sep 10
EDAS Meteorological Data
Source ★ at 31.32 N 97.33 W
Meters AGL
Job ID: 374883 Job Start: Wed Nov 10 17:13:16 UTC 2010
Source 1 lat.: 31.32 lon.: -97.33 height: 500 m AGL
Trajectory Direction: Backward Duration: 24 hrs
Vertical Motion Calculation Method: Model Vertical Velocity
Meteorology: 0000Z 16 Sep 2010 - EDAS40

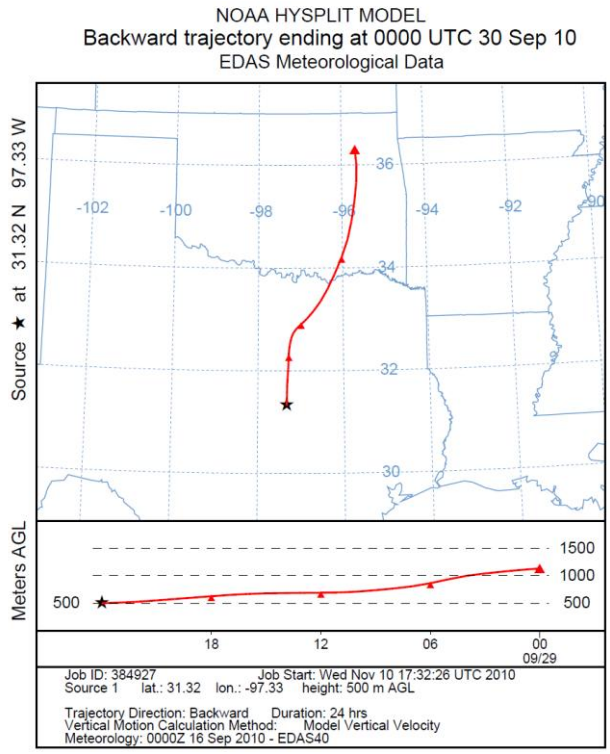
NOAA HYSPLIT MODEL
Backward trajectory ending at 0000 UTC 30 Sep 10
EDAS Meteorological Data
Source ★ at 31.32 N 97.33 W
Meters AGL
Job ID: 384927 Job Start: Wed Nov 10 17:32:26 UTC 2010
Source 1 lat.: 31.32 lon.: -97.33 height: 500 m AGL
Trajectory Direction: Backward Duration: 24 hrs
Vertical Motion Calculation Method: Model Vertical Velocity
Meteorology: 0000Z 16 Sep 2010 - EDAS40

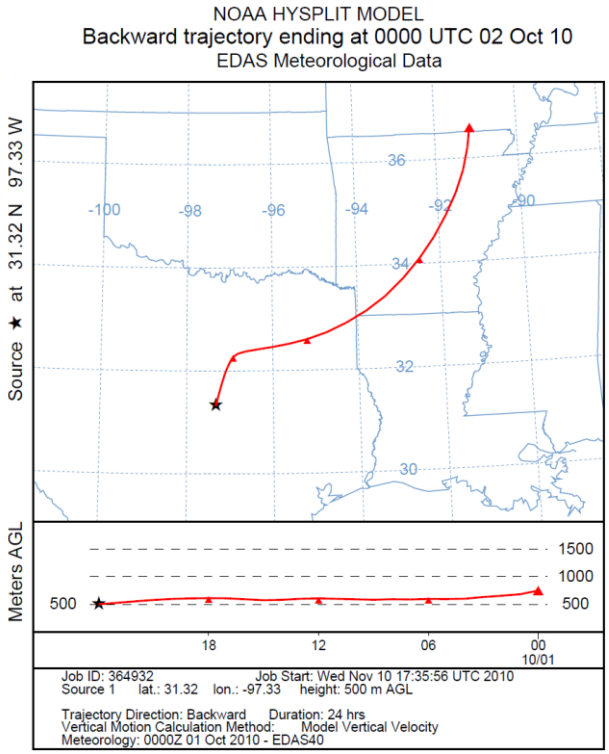
NOAA HYSPLIT MODEL
Backward trajectory ending at 0000 UTC 02 Oct 10
EDAS Meteorological Data
Source ★ at 31.32 N 97.33 W
Meters AGL
Job ID: 364932 Job Start: Wed Nov 10 17:35:56 UTC 2010
Source 1 lat.: 31.32 lon.: -97.33 height: 500 m AGL
Trajectory Direction: Backward Duration: 24 hrs
Vertical Motion Calculation Method: Model Vertical Velocity
Meteorology: 0000Z 01 Oct 2010 - EDAS40

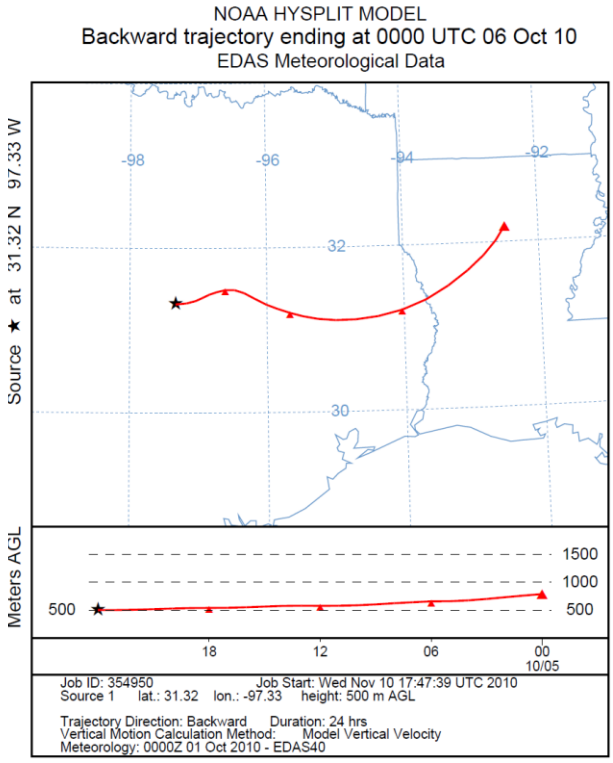
NOAA HYSPLIT MODEL
Backward trajectory ending at 0000 UTC 06 Oct 10
EDAS Meteorological Data
Source ★ at 31.32 N 97.33 W
Meters AGL
Job ID: 354950 Job Start: Wed Nov 10 17:47:39 UTC 2010
Source 1 lat.: 31.32 lon.: -97.33 height: 500 m AGL
Trajectory Direction: Backward Duration: 24 hrs
Vertical Motion Calculation Method: Model Vertical Velocity
Meteorology: 0000Z 01 Oct 2010 - EDAS40

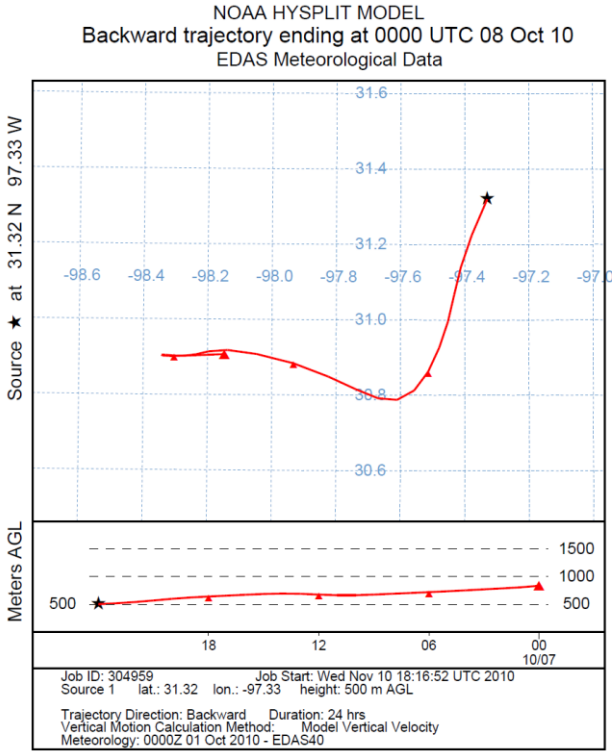
NOAA HYSPLIT MODEL
Backward trajectory ending at 0000 UTC 08 Oct 10
EDAS Meteorological Data
Source ★ at 31.32 N 97.33 W
Meters AGL
Job ID: 304959 Job Start: Wed Nov 10 18:16:52 UTC 2010
Source 1 lat.: 31.32 lon.: -97.33 height: 500 m AGL
Trajectory Direction: Backward Duration: 24 hrs
Vertical Motion Calculation Method: Model Vertical Velocity
Meteorology: 0000Z 01 Oct 2010 - EDAS40

Appendix 2: AIRNow Air Quality Ozone Concentration Maps (only for moderately polluted days)

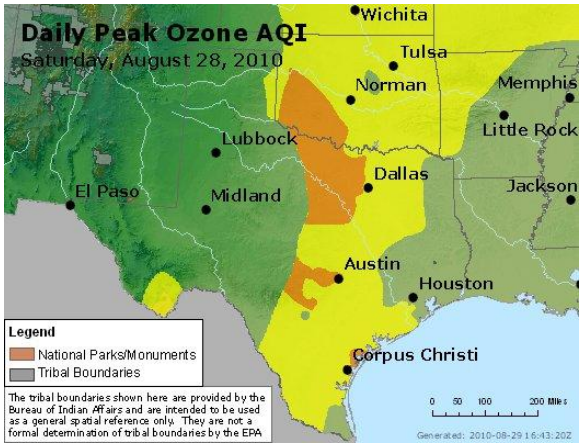

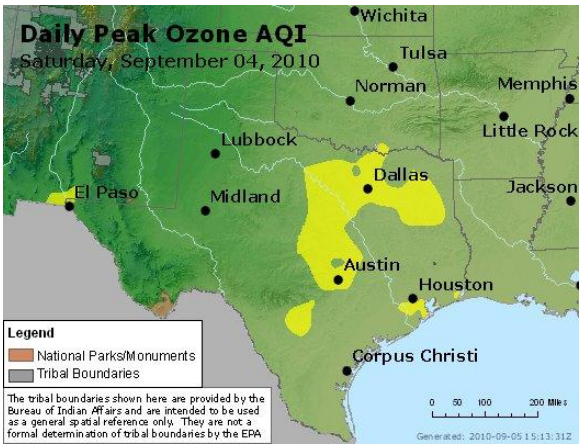

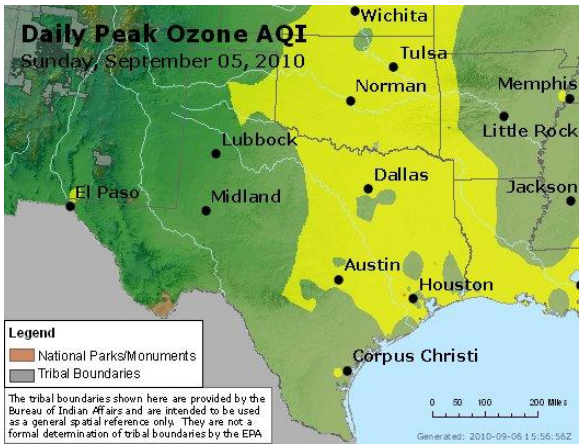

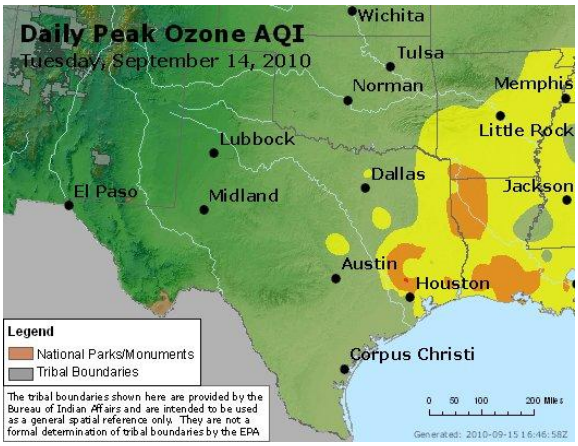

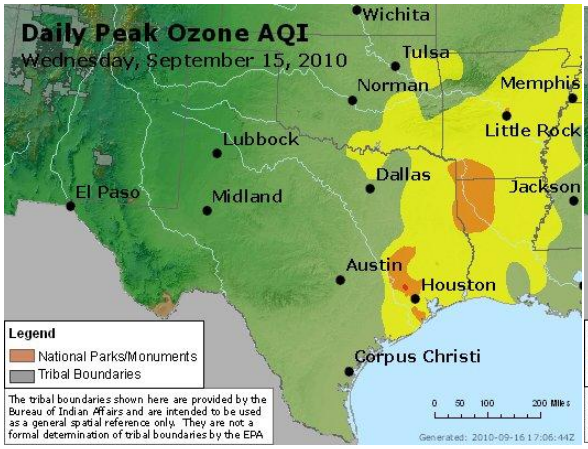

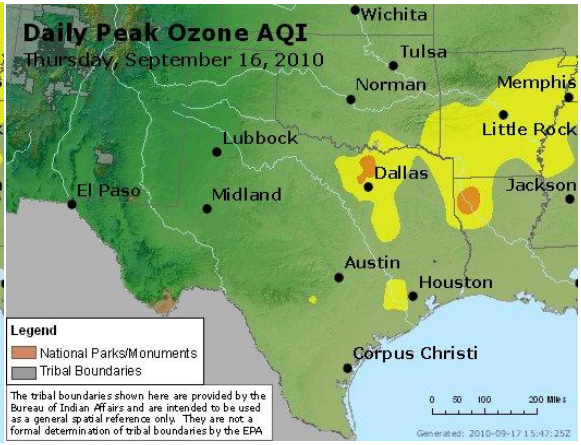

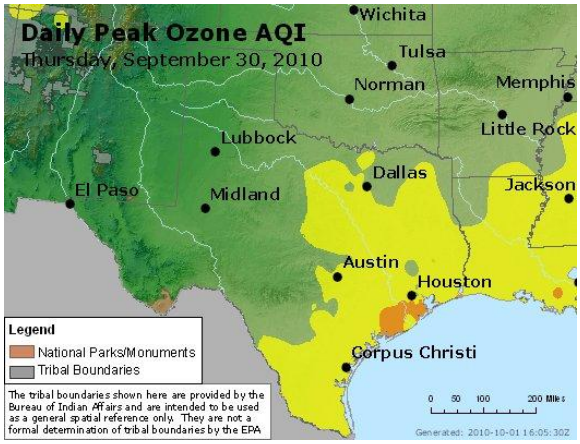
Daily Peak Ozone AQI
Thursday, September 30, 2010
Wichita
Tulsa
Norman
Memphis
Little Rock
Lubbock
Dallas
Jackson
El Paso
Midland
Austin
Houston
Corpus Christi
Legend
National Parks/Monuments
Tribal Boundaries
The tribal boundaries shown here are provided by the Bureau of Indian Affairs and are intended to be used as a general spatial reference only. They are not a formal determination of tribal boundaries by the EPA
0 50 100 200 Miles
Generated: 2010-10-01 16:05:30Z

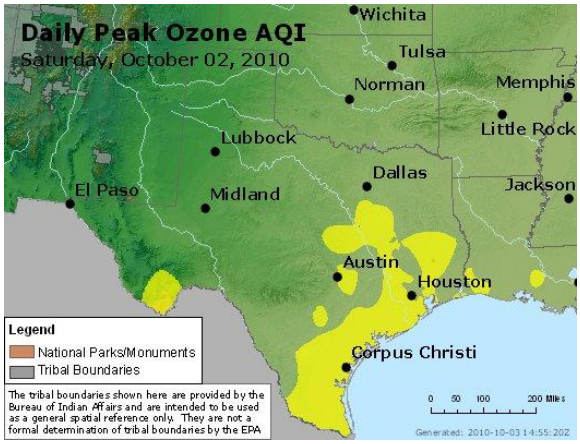
Daily Peak Ozone AQI
Saturday, October 02, 2010
Wichita
Tulsa
Norman
Memphis
Little Rock
Lubbock
Dallas
Jackson
El Paso
Midland
Austin
Houston
Corpus Christi
Legend
National Parks/Monuments
Tribal Boundaries
The tribal boundaries shown here are provided by the Bureau of Indian Affairs and are intended to be used as a general spatial reference only. They are not a formal determination of tribal boundaries by the EPA
0 50 100 200 Miles
Generated: 2010-10-03 14:55:20Z

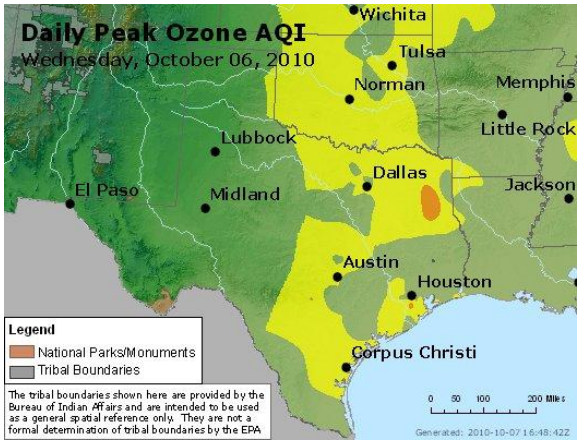
Daily Peak Ozone AQI
Wednesday, October 06, 2010
Wichita
Tulsa
Norman
Memphis
Little Rock
Lubbock
Dallas
Jackson
El Paso
Midland
Austin
Houston
Corpus Christi
Legend
National Parks/Monuments
Tribal Boundaries
The tribal boundaries shown here are provided by the Bureau of Indian Affairs and are intended to be used as a general spatial reference only. They are not a formal determination of tribal boundaries by the EPA
0 50 100 200 Miles
Generated: 2010-10-07 16:48:42Z

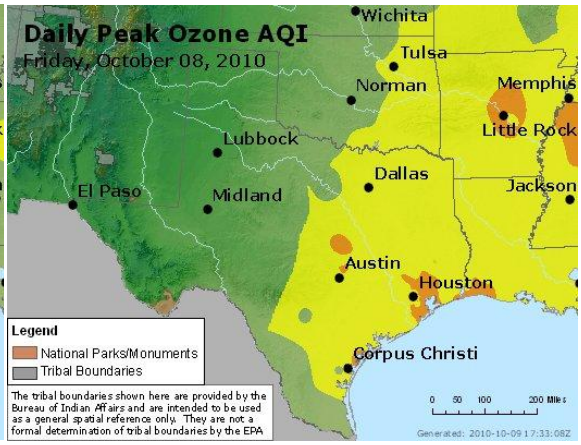
Daily Peak Ozone AQI
Friday, October 08, 2010
Wichita
Tulsa
Norman
Memphis
Little Rock
Lubbock
Dallas
Jackson
El Paso
Midland
Austin
Houston
Corpus Christi
Legend
National Parks/Monuments
Tribal Boundaries
The tribal boundaries shown here are provided by the Bureau of Indian Affairs and are intended to be used as a general spatial reference only. They are not a formal determination of tribal boundaries by the EPA
0 50 100 200 Miles
Generated: 2010-10-09 17:33:08Z

Appendix 3: TCEQ Flask Intensive Footprints

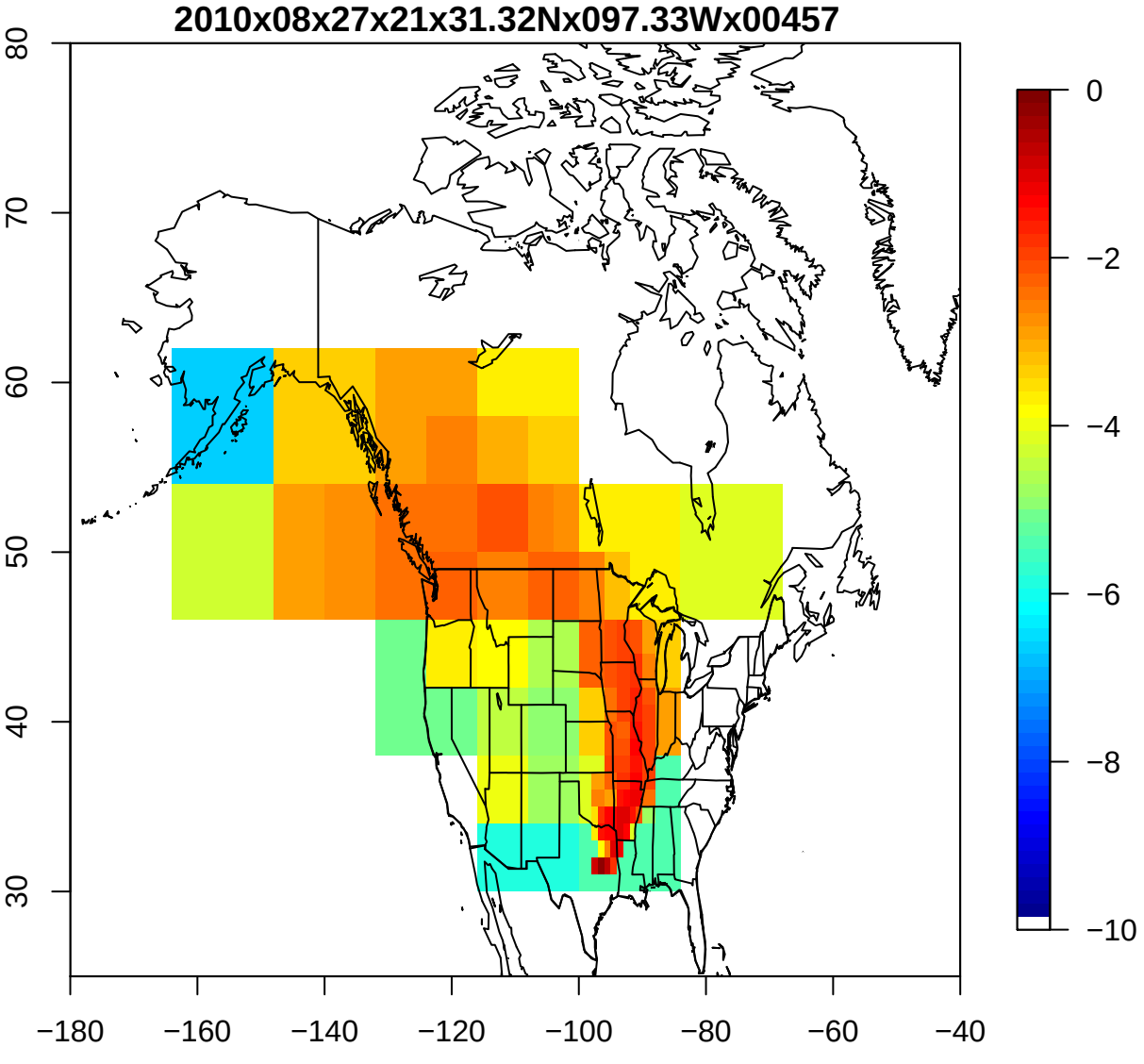

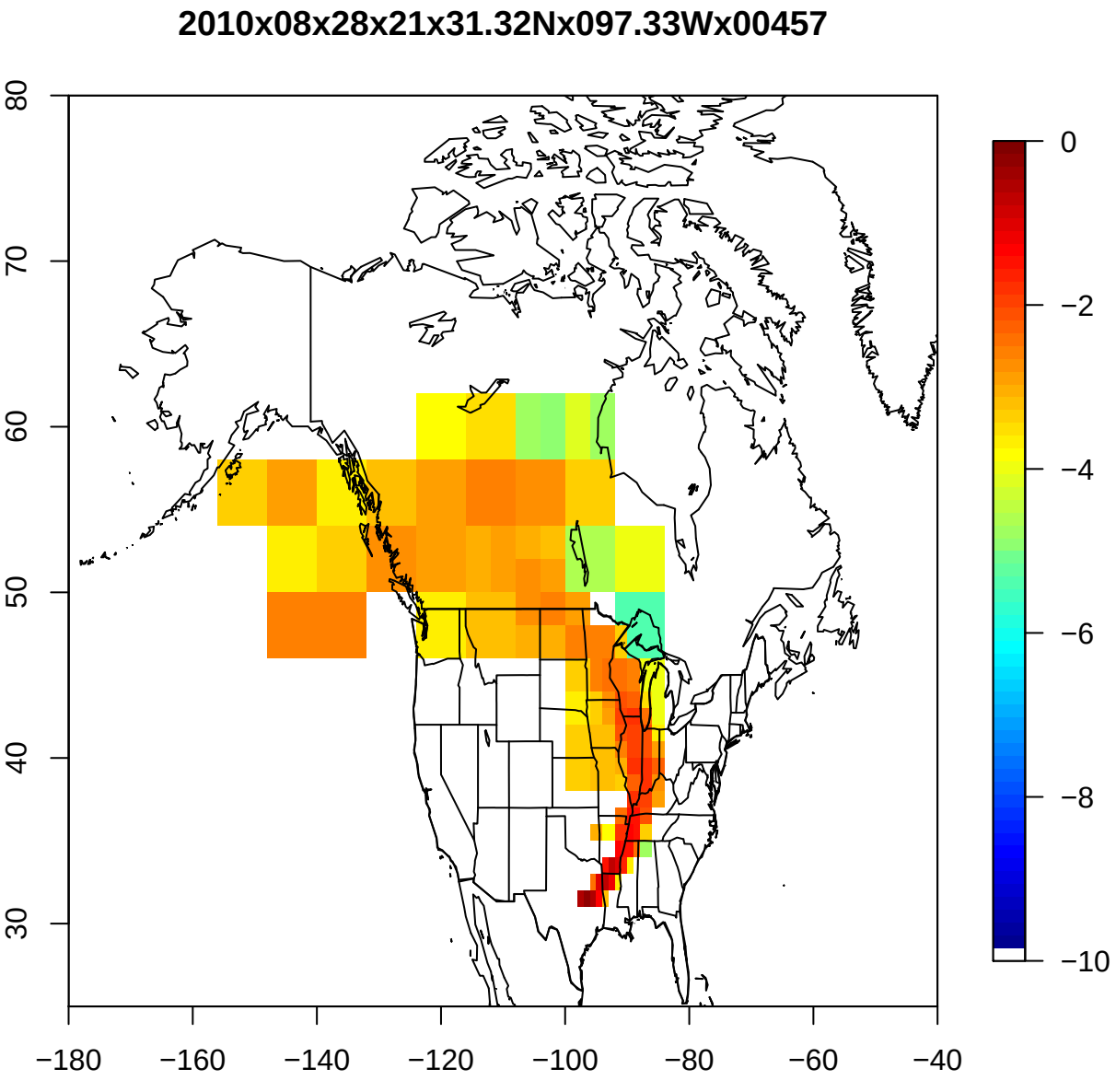
2010x08x28x21x31.32Nx097.33Wx00457
80
70
60
50
40
30
−180
−160
−140
−120
−100
−80
−60
−40
0
−2
−4
−6
−8
−10

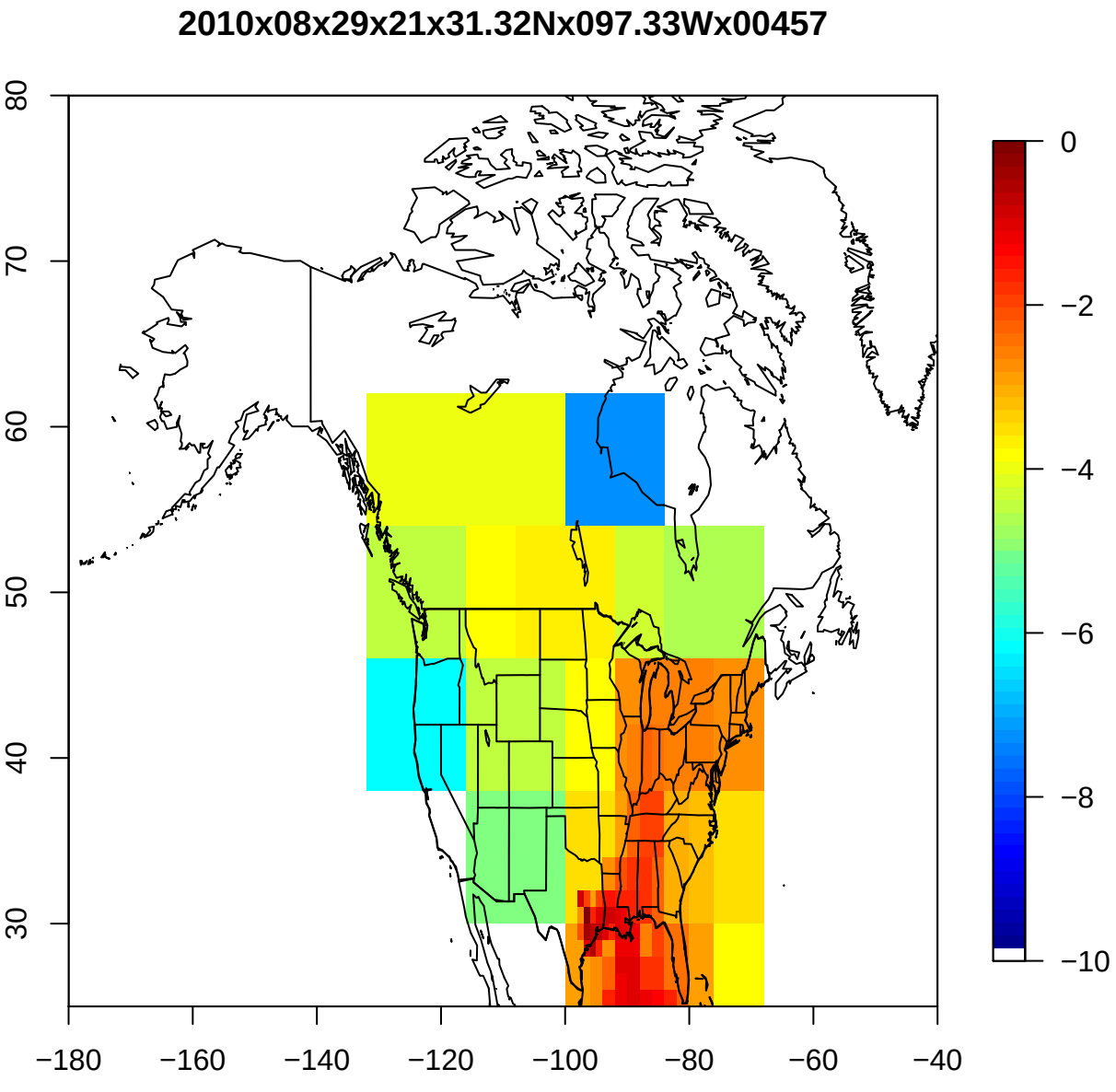
2010x08x29x21x31.32Nx097.33Wx00457
80
70
60
50
40
30
−180
−160
−140
−120
−100
−80
−60
−40
0
−2
−4
−6
−8
−10

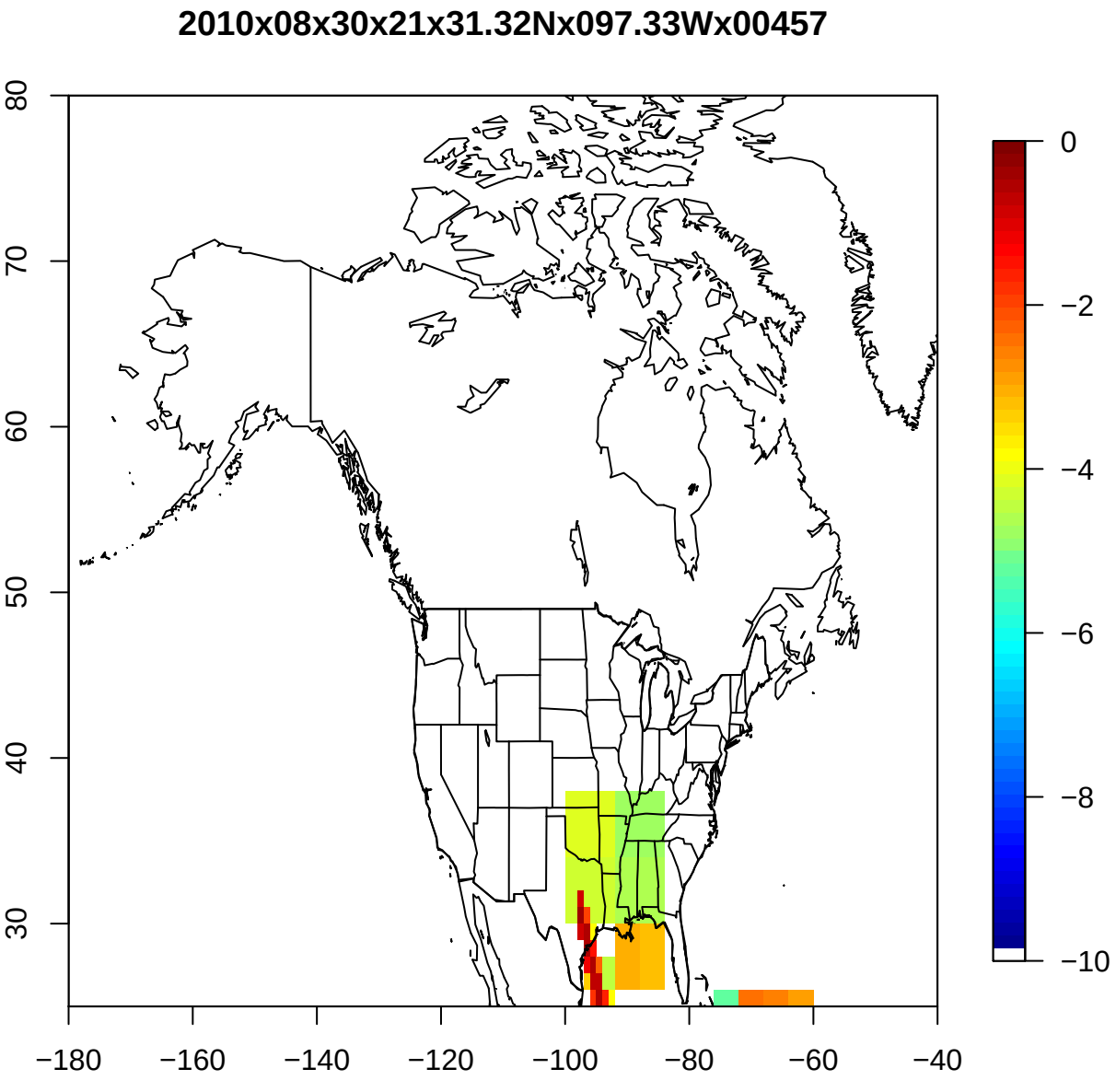
2010x08x30x21x31.32Nx097.33Wx00457
80
70
60
50
40
30
−180
−160
−140
−120
−100
−80
−60
−40
0
−2
−4
−6
−8
−10

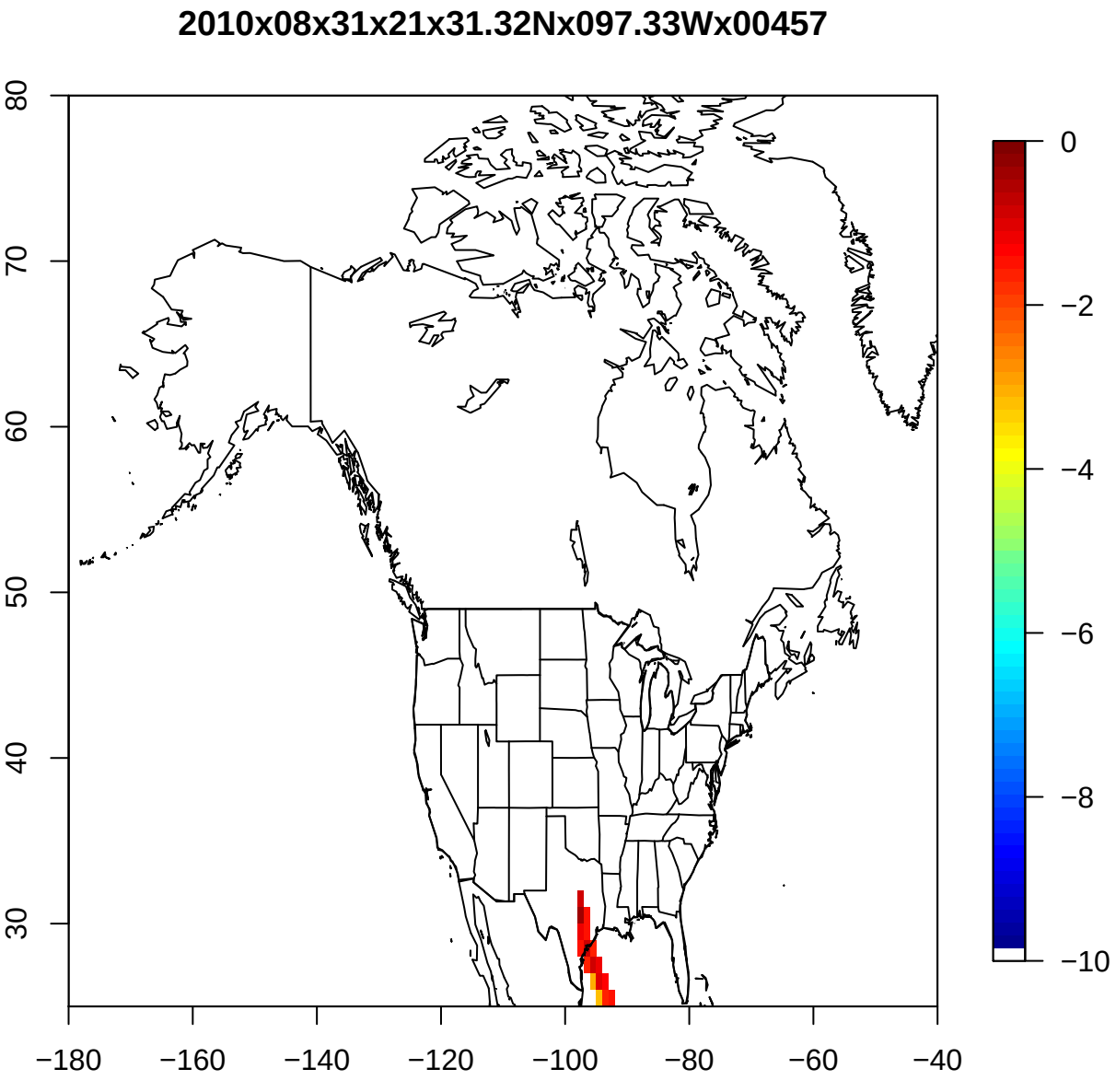
2010x08x31x21x31.32Nx097.33Wx00457
80
70
60
50
40
30
−180
−160
−140
−120
−100
−80
−60
−40
0
−2
−4
−6
−8
−10

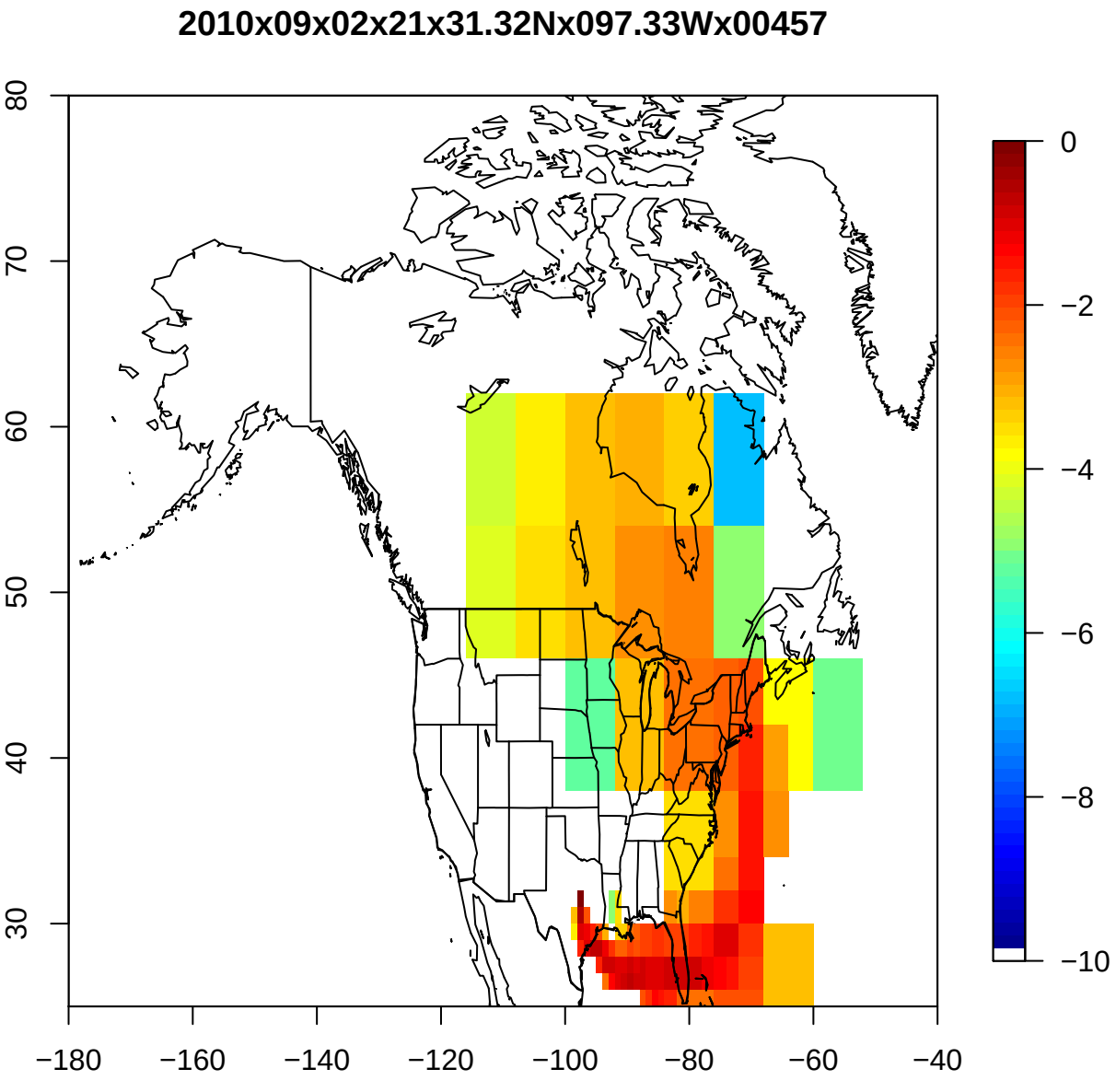
2010x09x02x21x31.32Nx097.33Wx00457
80
70
60
50
40
30
−180
−160
−140
−120
−100
−80
−60
−40
0
−2
−4
−6
−8
−10

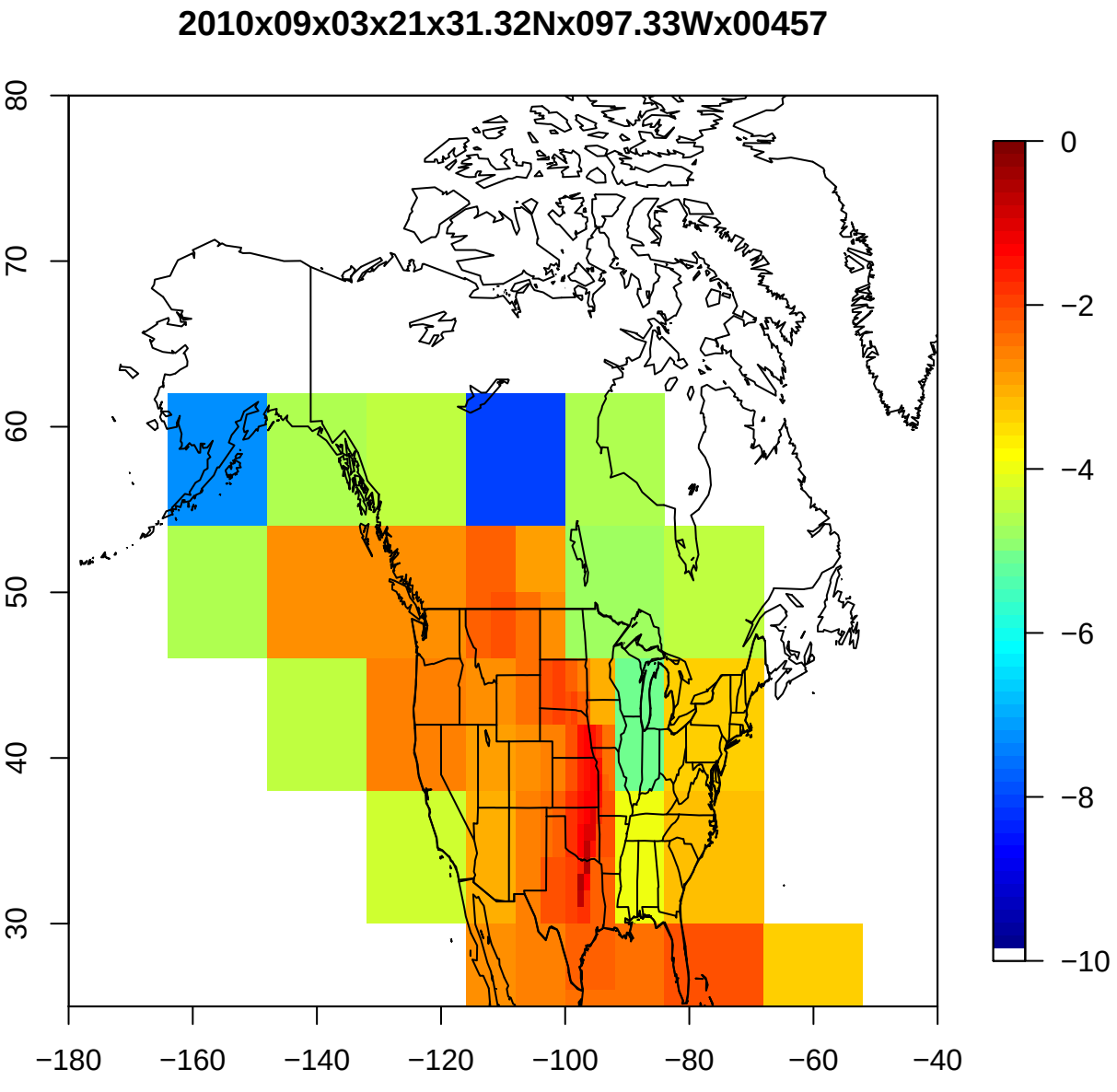
2010x09x03x21x31.32Nx097.33Wx00457
80
70
60
50
40
30
−180
−160
−140
−120
−100
−80
−60
−40
0
−2
−4
−6
−8
−10

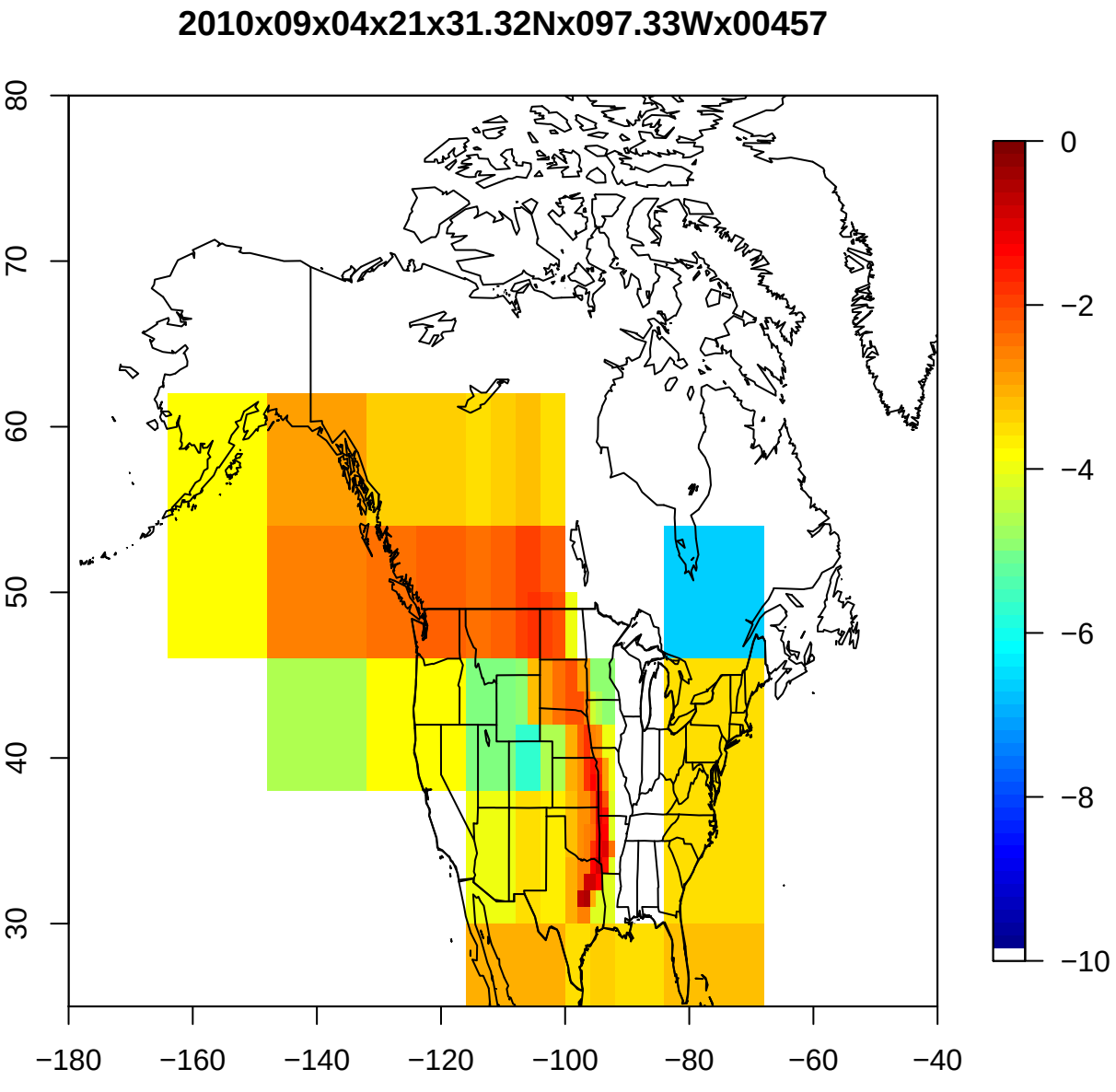
2010x09x04x21x31.32Nx097.33Wx00457
80
70
60
50
40
30
−180
−160
−140
−120
−100
−80
−60
−40
0
−2
−4
−6
−8
−10

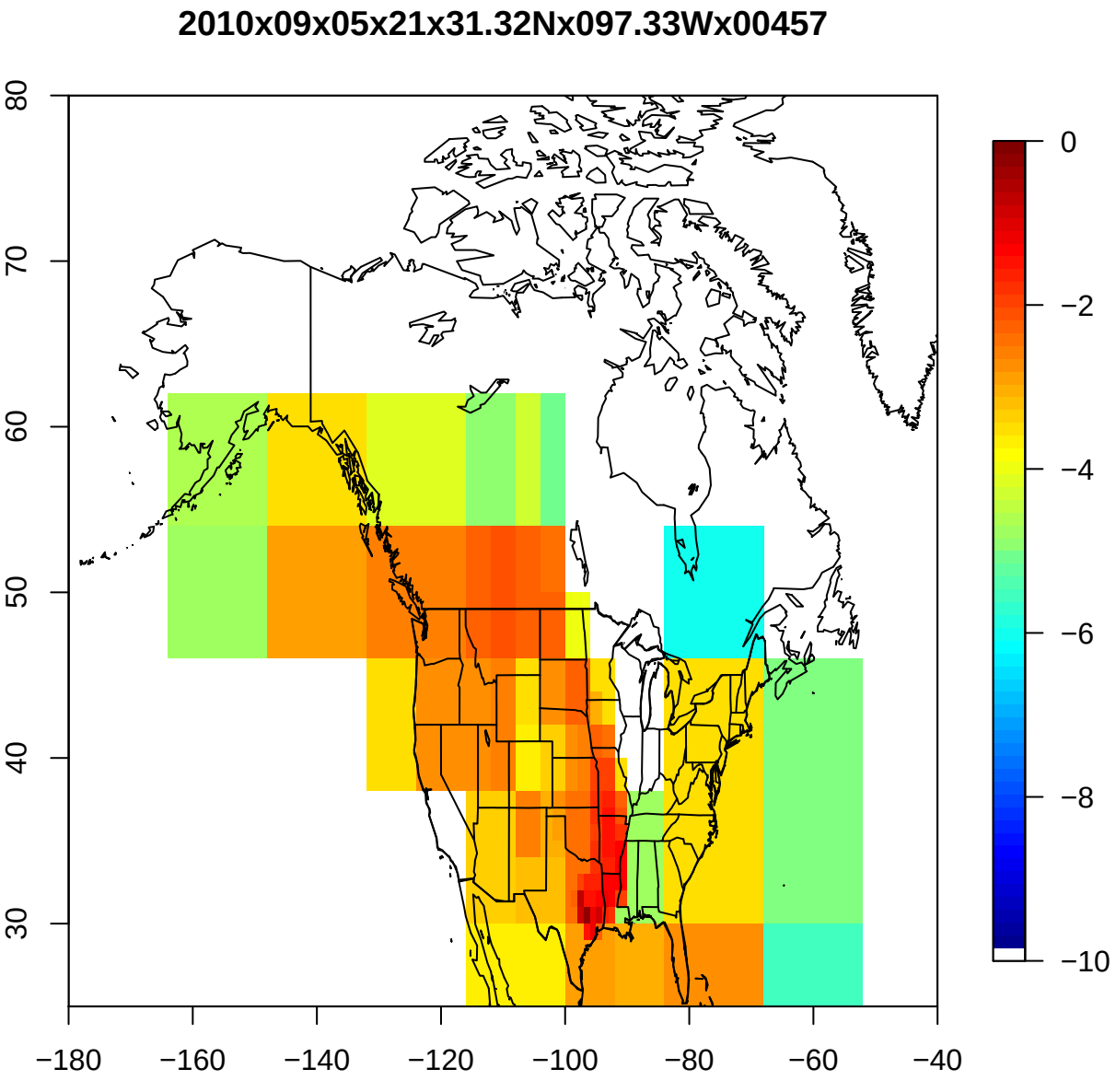
2010x09x05x21x31.32Nx097.33Wx00457
80
70
60
50
40
30
−180
−160
−140
−120
−100
−80
−60
−40
0
−2
−4
−6
−8
−10

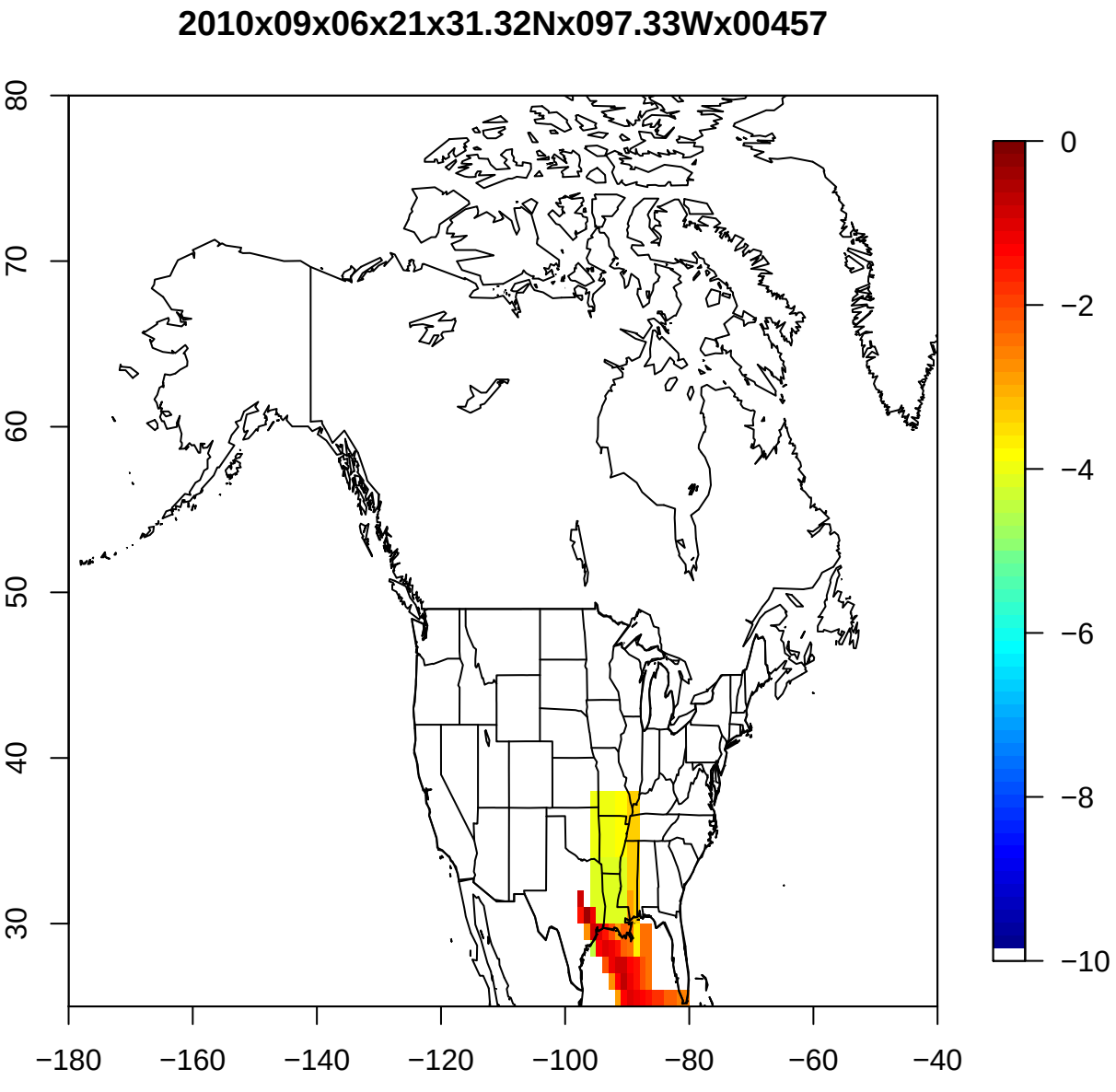
2010x09x06x21x31.32Nx097.33Wx00457
80
70
60
50
40
30
−180
−160
−140
−120
−100
−80
−60
−40
0
−2
−4
−6
−8
−10

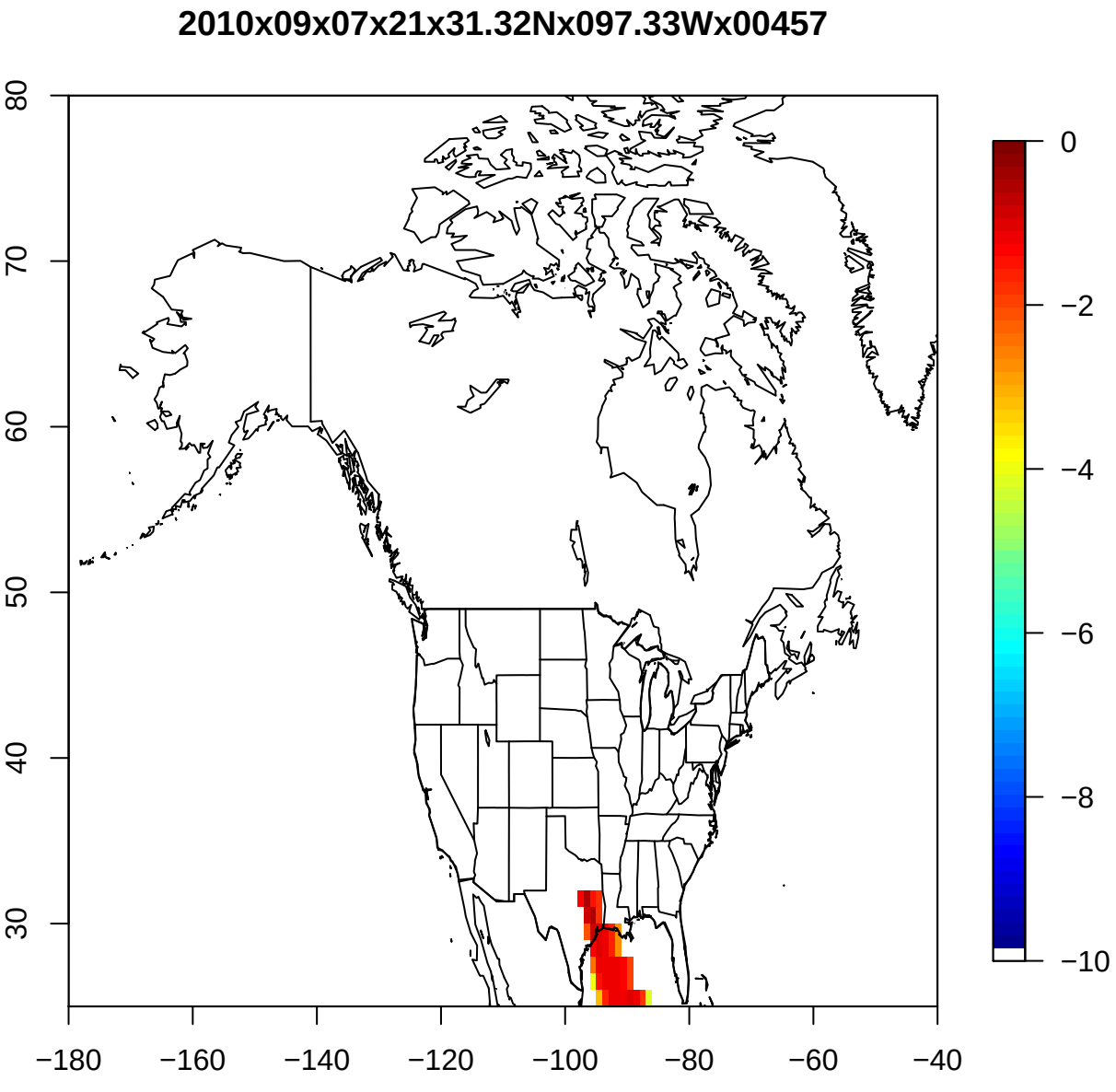
2010x09x07x21x31.32Nx097.33Wx00457
80
70
60
50
40
30
−180
−160
−140
−120
−100
−80
−60
−40
0
−2
−4
−6
−8
−10

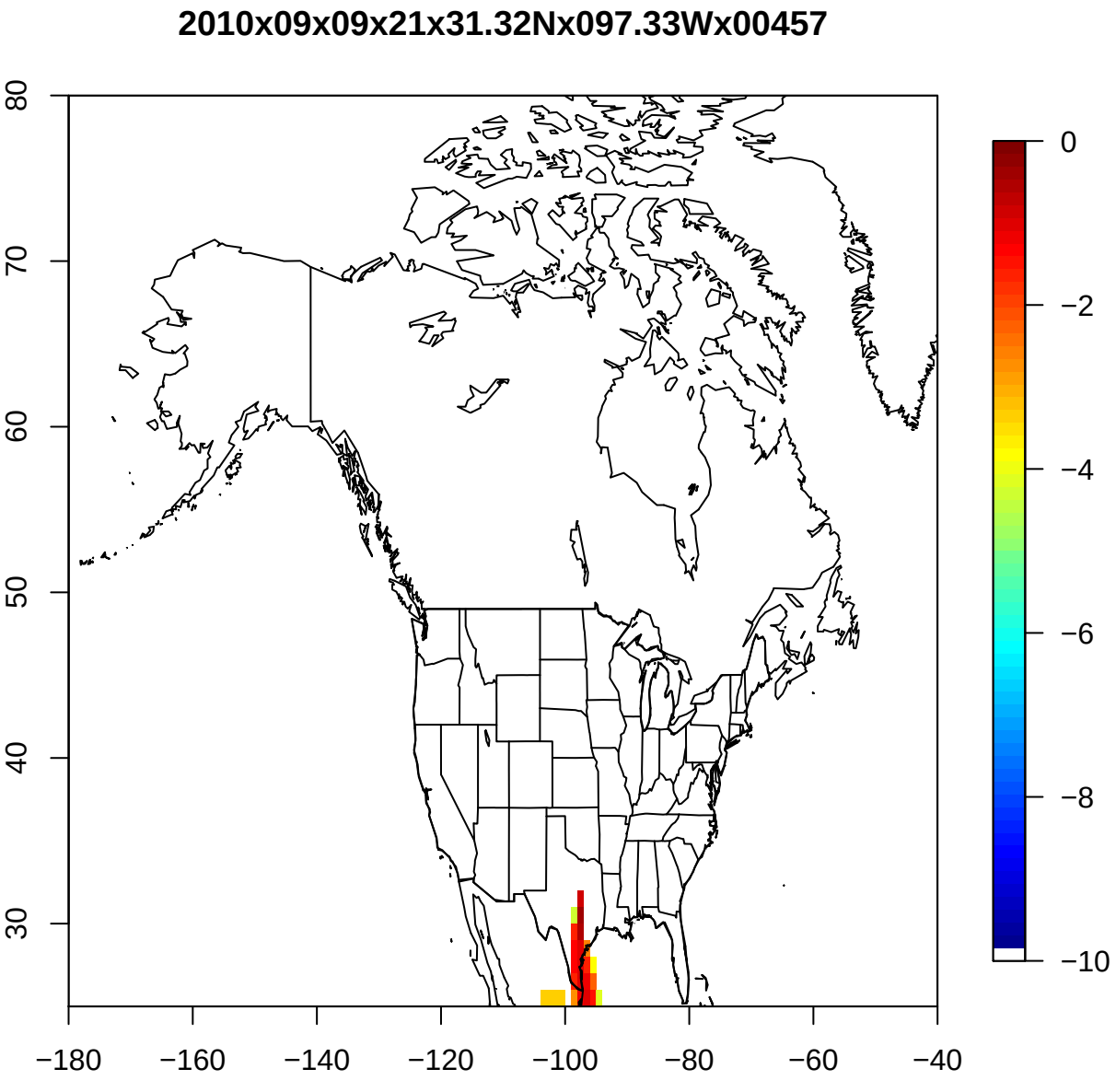
2010x09x09x21x31.32Nx097.33Wx00457
80
70
60
50
40
30
−180
−160
−140
−120
−100
−80
−60
−40
0
−2
−4
−6
−8
−10

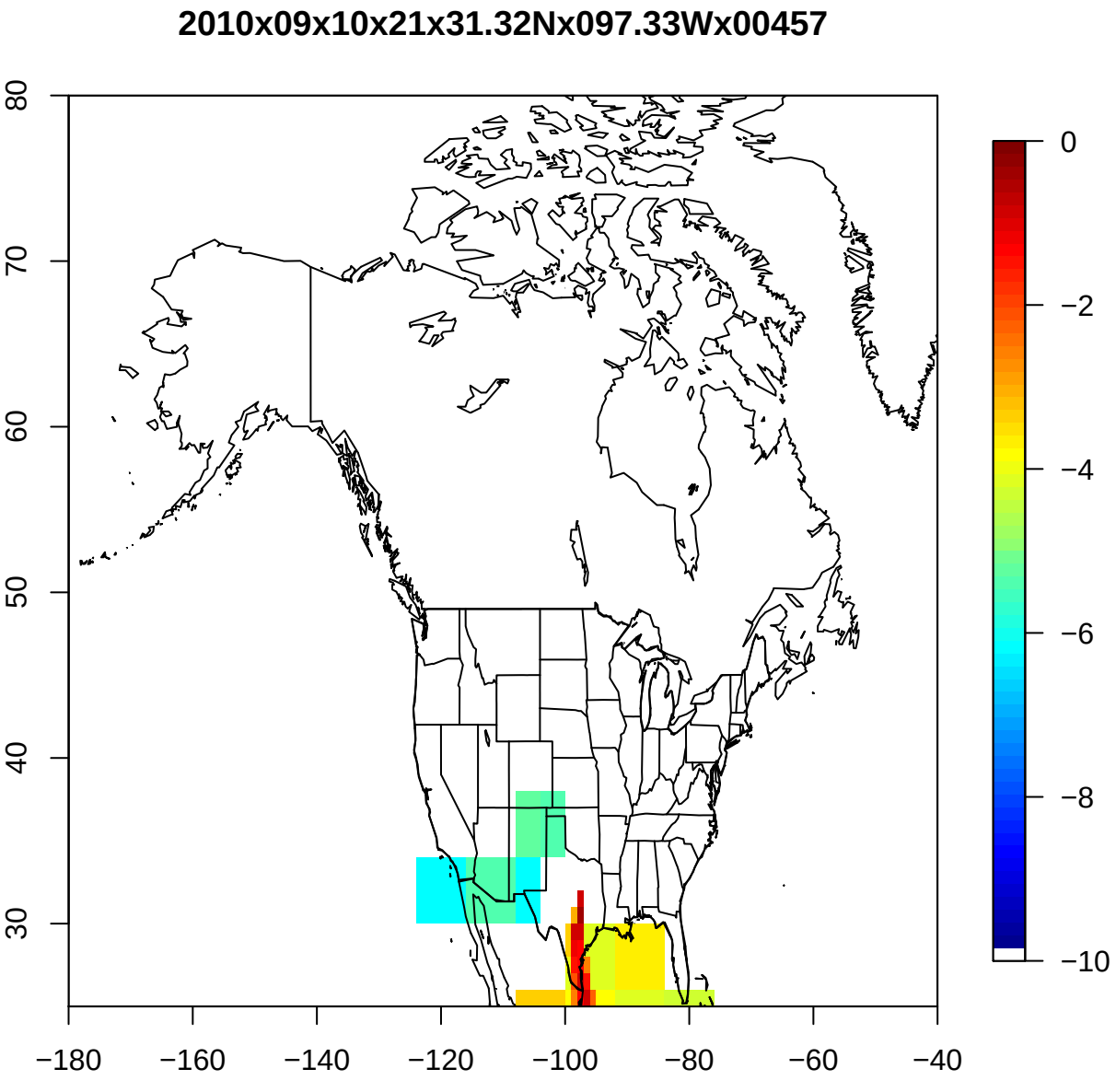
2010x09x10x21x31.32Nx097.33Wx00457
80
70
60
50
40
30
−180
−160
−140
−120
−100
−80
−60
−40
0
−2
−4
−6
−8
−10

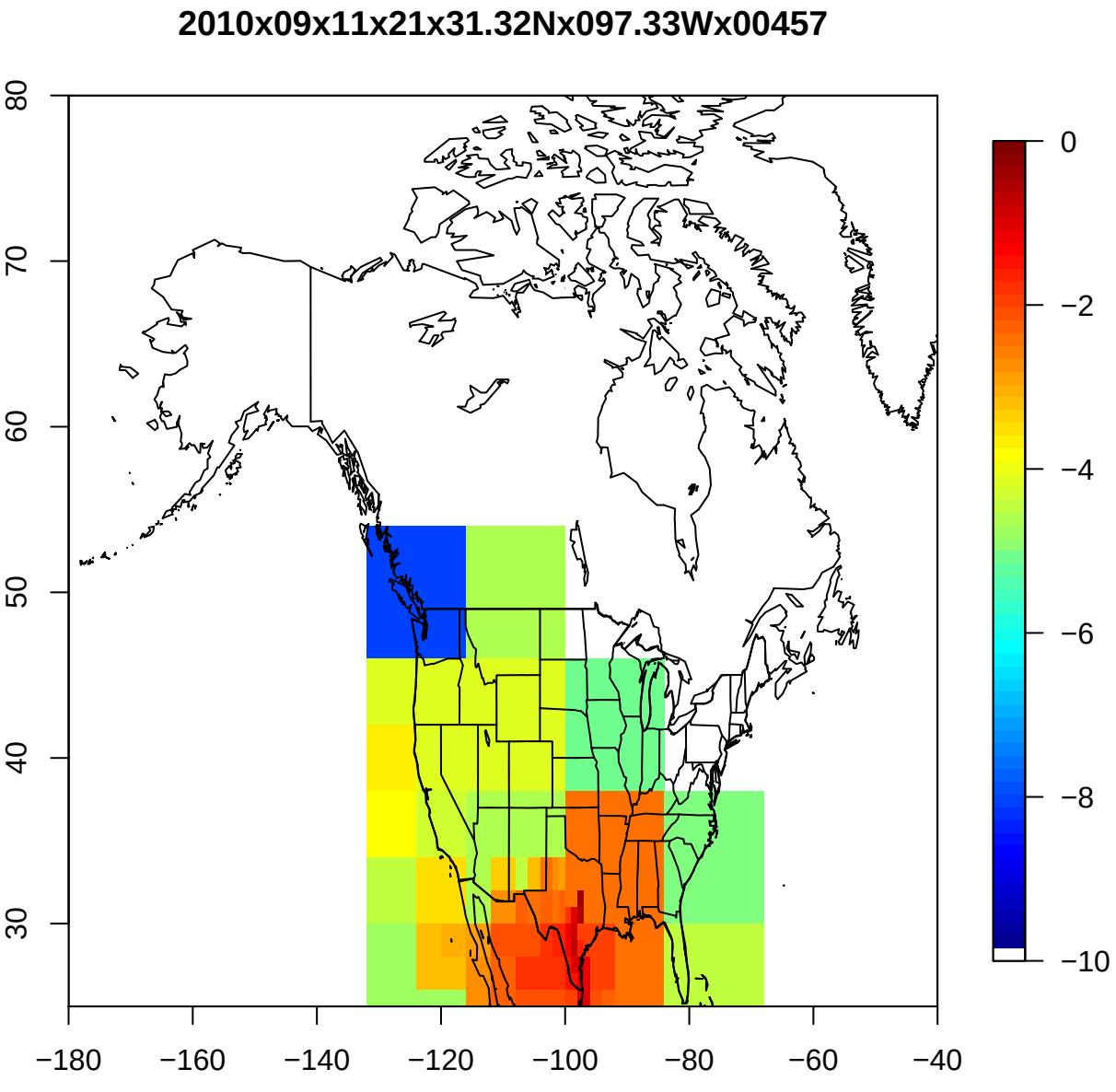
2010x09x11x21x31.32Nx097.33Wx00457
80
70
60
50
40
30
−180
−160
−140
−120
−100
−80
−60
−40
0
−2
−4
−6
−8
−10

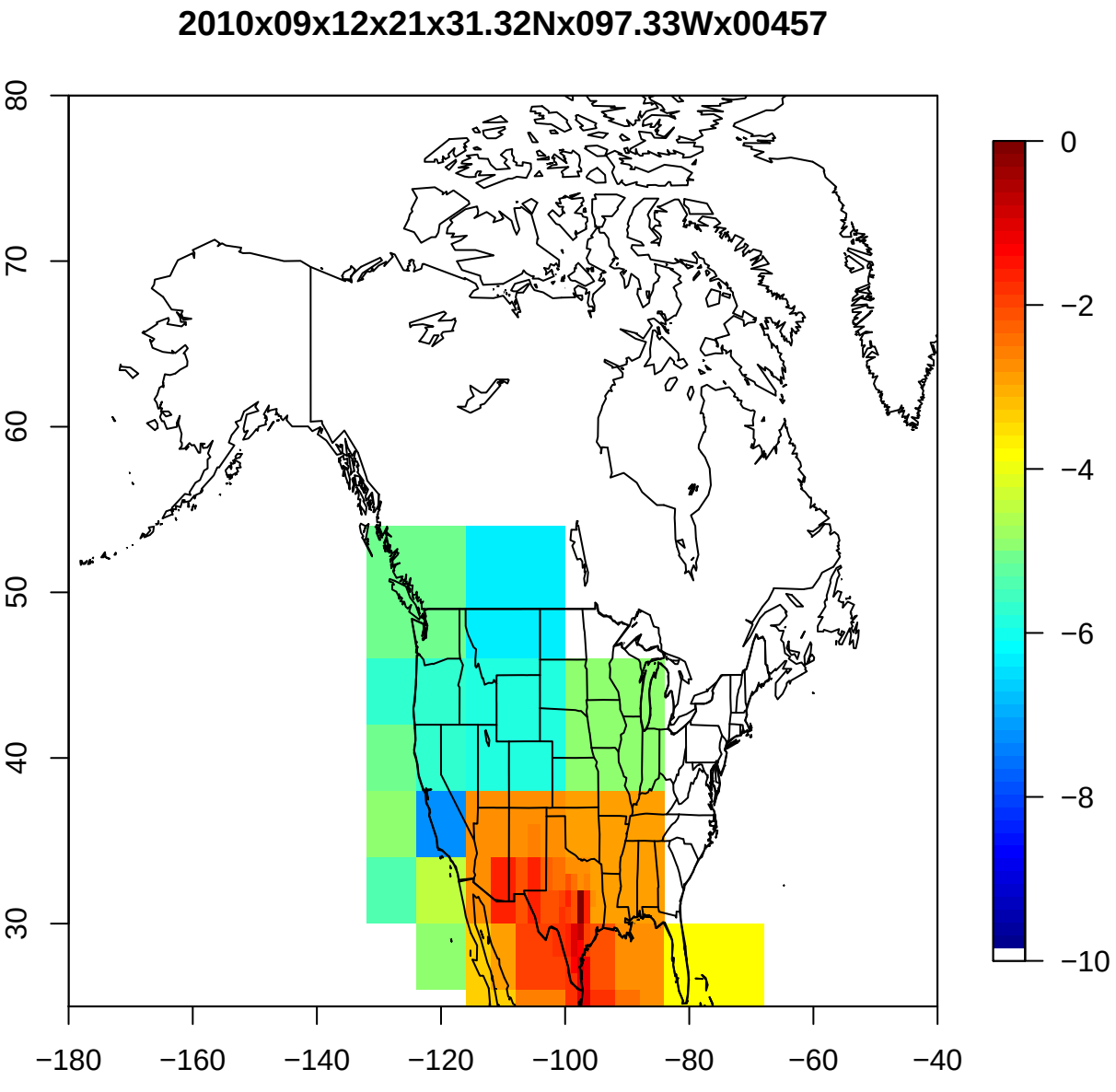
2010x09x12x21x31.32Nx097.33Wx00457
80
70
60
50
40
30
−180
−160
−140
−120
−100
−80
−60
−40
0
−2
−4
−6
−8
−10

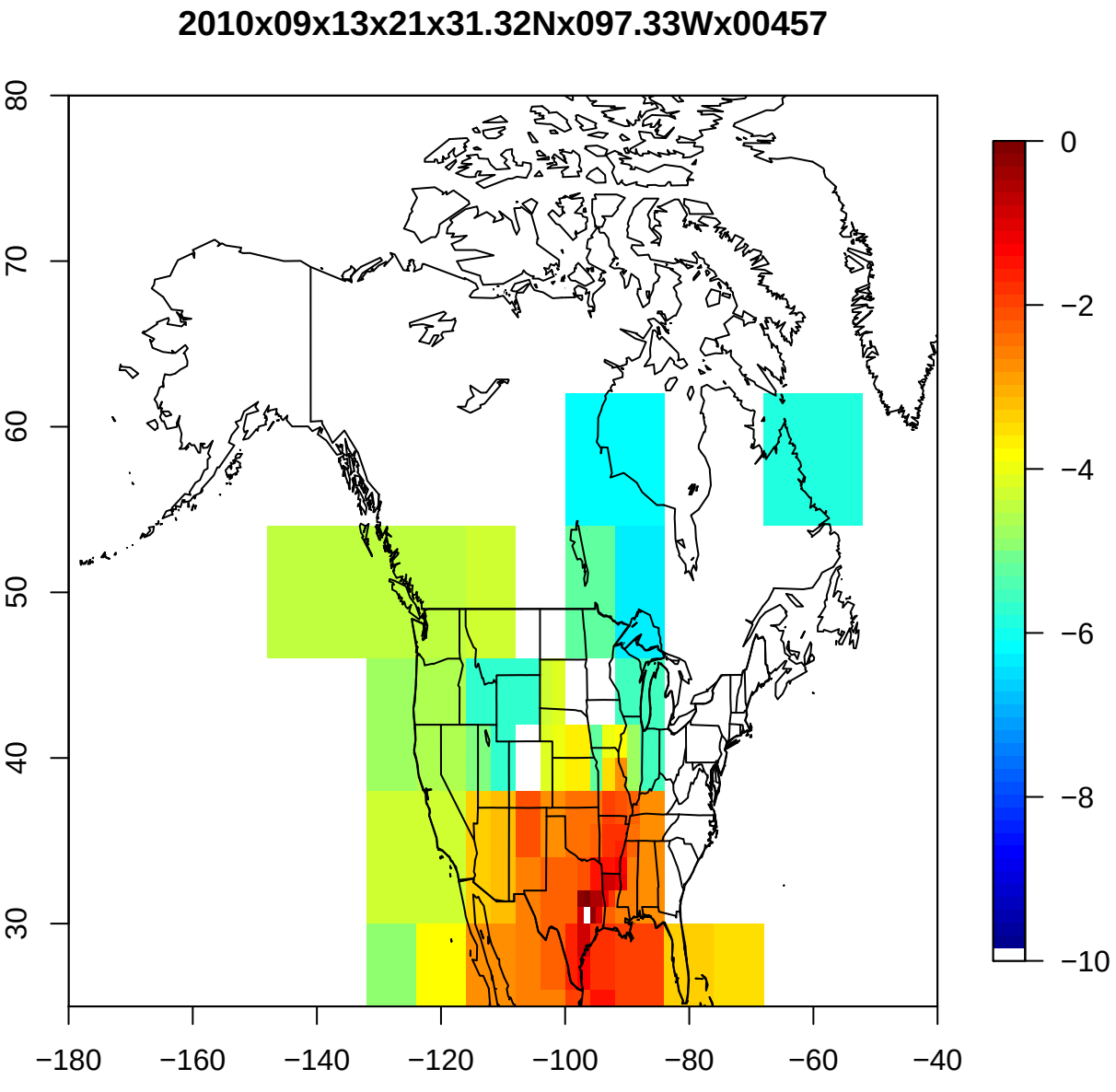
2010x09x13x21x31.32Nx097.33Wx00457
80
70
60
50
40
30
−180
−160
−140
−120
−100
−80
−60
−40
0
−2
−4
−6
−8
−10

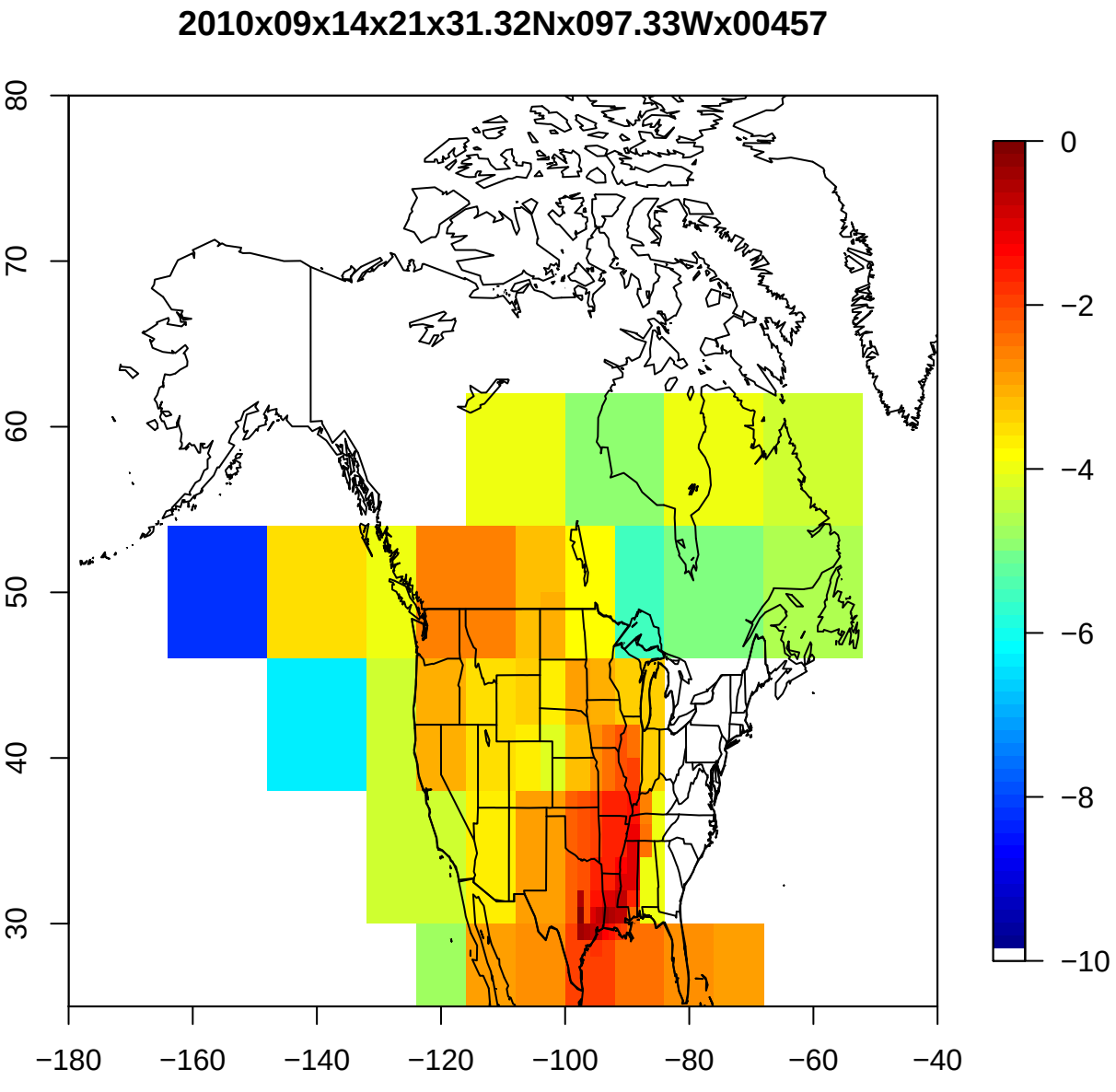
2010x09x14x21x31.32Nx097.33Wx00457
80
70
60
50
40
30
−180
−160
−140
−120
−100
−80
−60
−40
0
−2
−4
−6
−8
−10

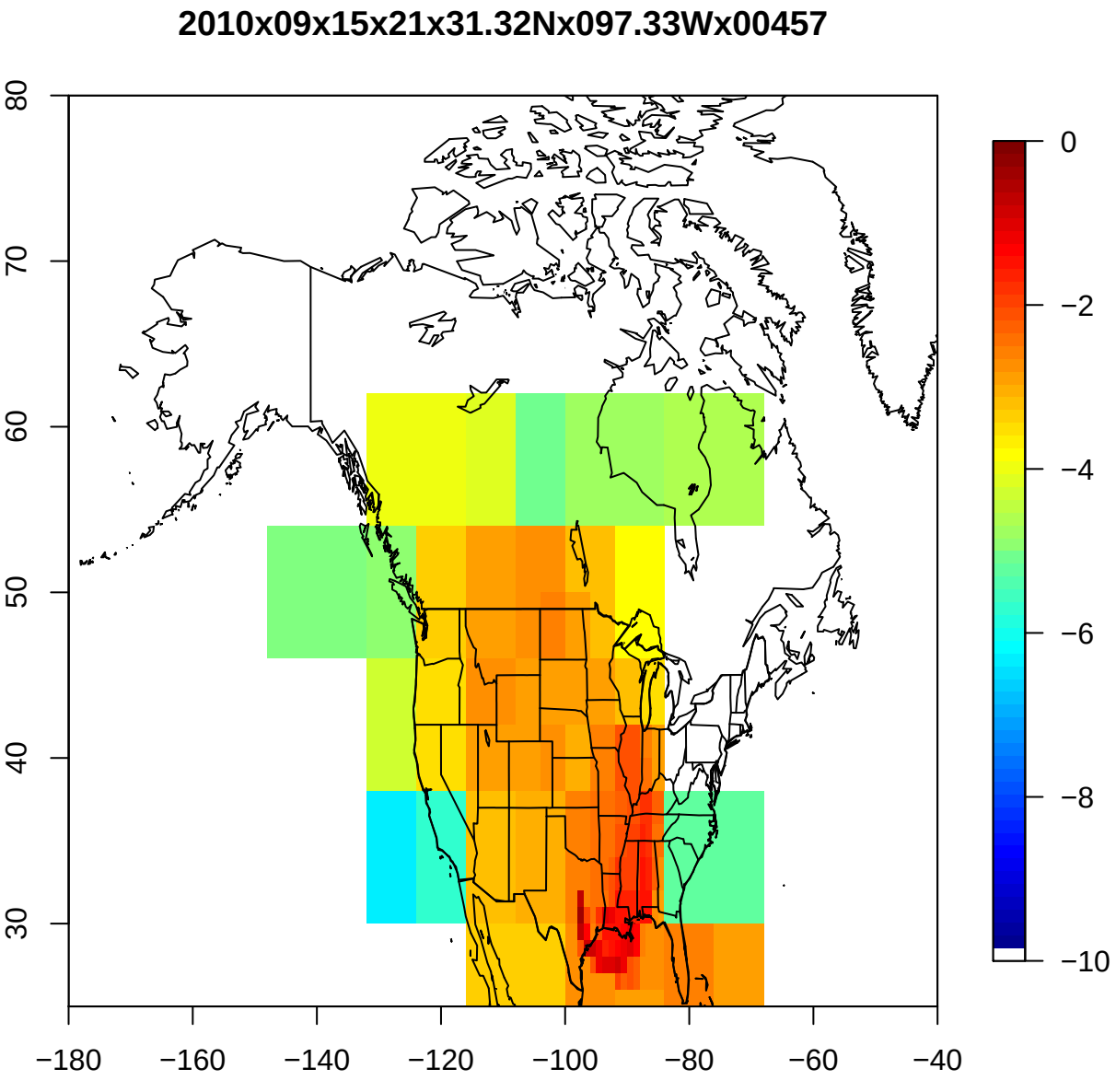
2010x09x15x21x31.32Nx097.33Wx00457
80
70
60
50
40
30
−180
−160
−140
−120
−100
−80
−60
−40
0
−2
−4
−6
−8
−10

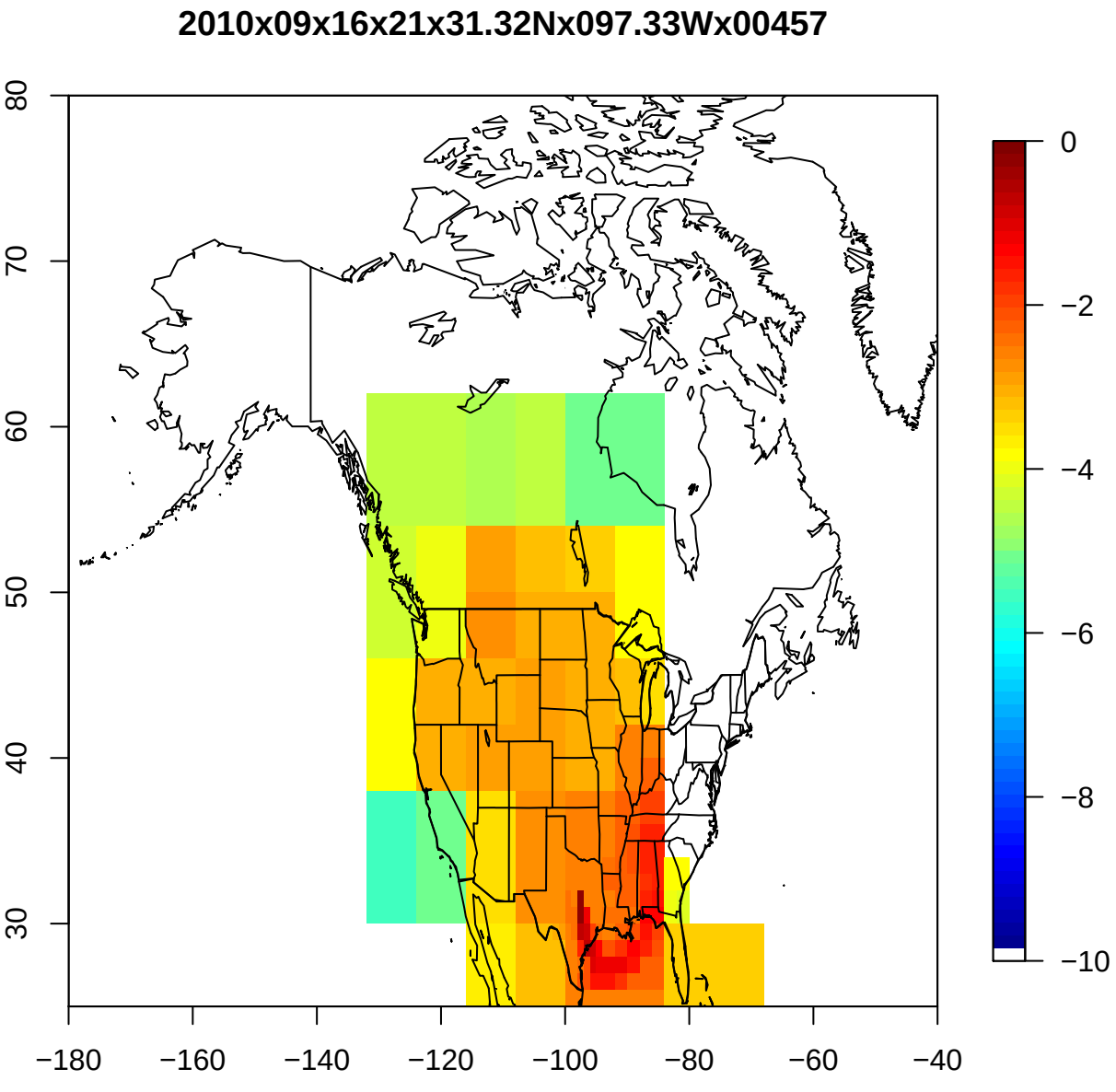
2010x09x16x21x31.32Nx097.33Wx00457
80
70
60
50
40
30
−180
−160
−140
−120
−100
−80
−60
−40
0
−2
−4
−6
−8
−10

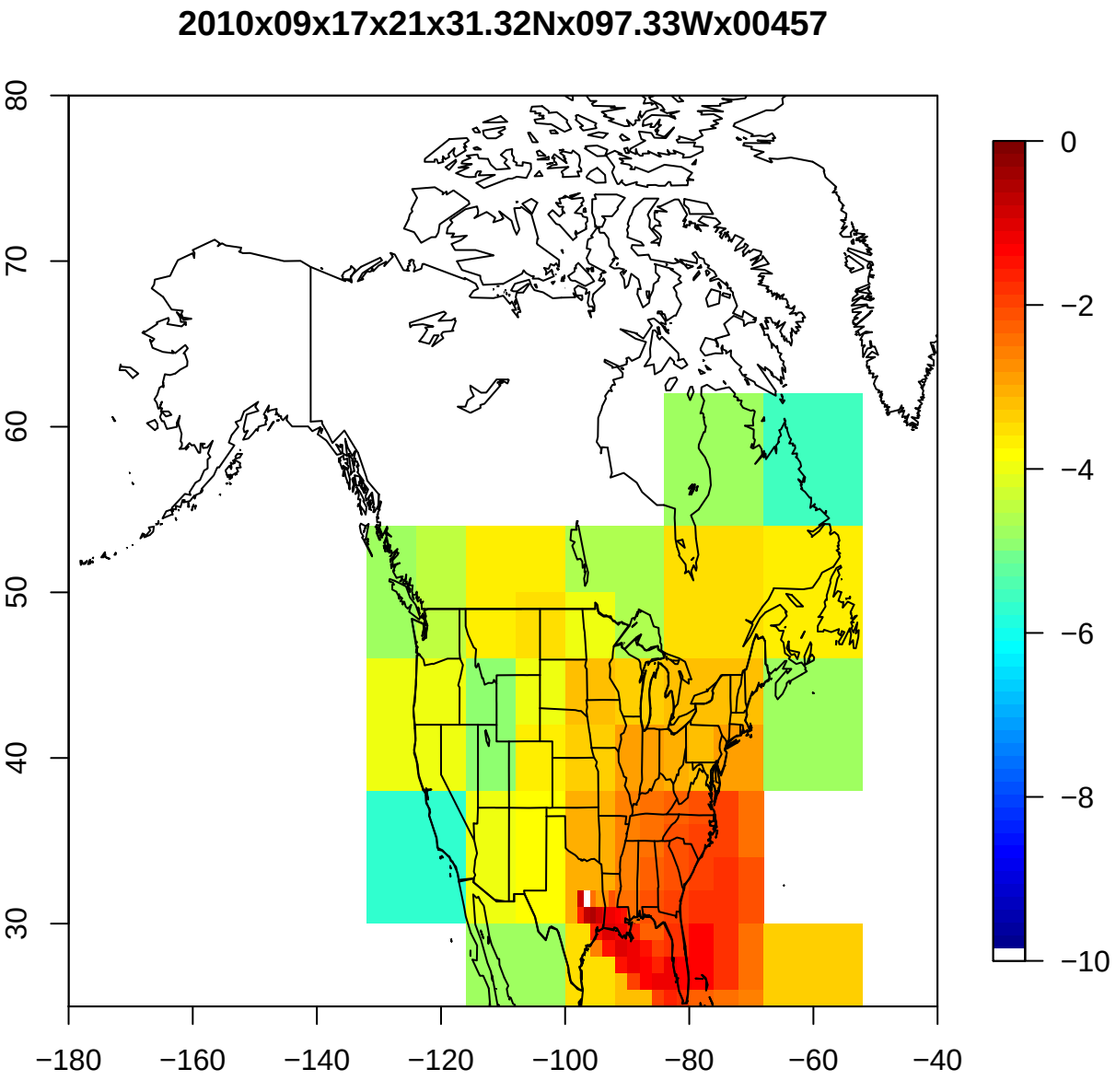
2010x09x17x21x31.32Nx097.33Wx00457
80
70
60
50
40
30
−180
−160
−140
−120
−100
−80
−60
−40
0
−2
−4
−6
−8
−10

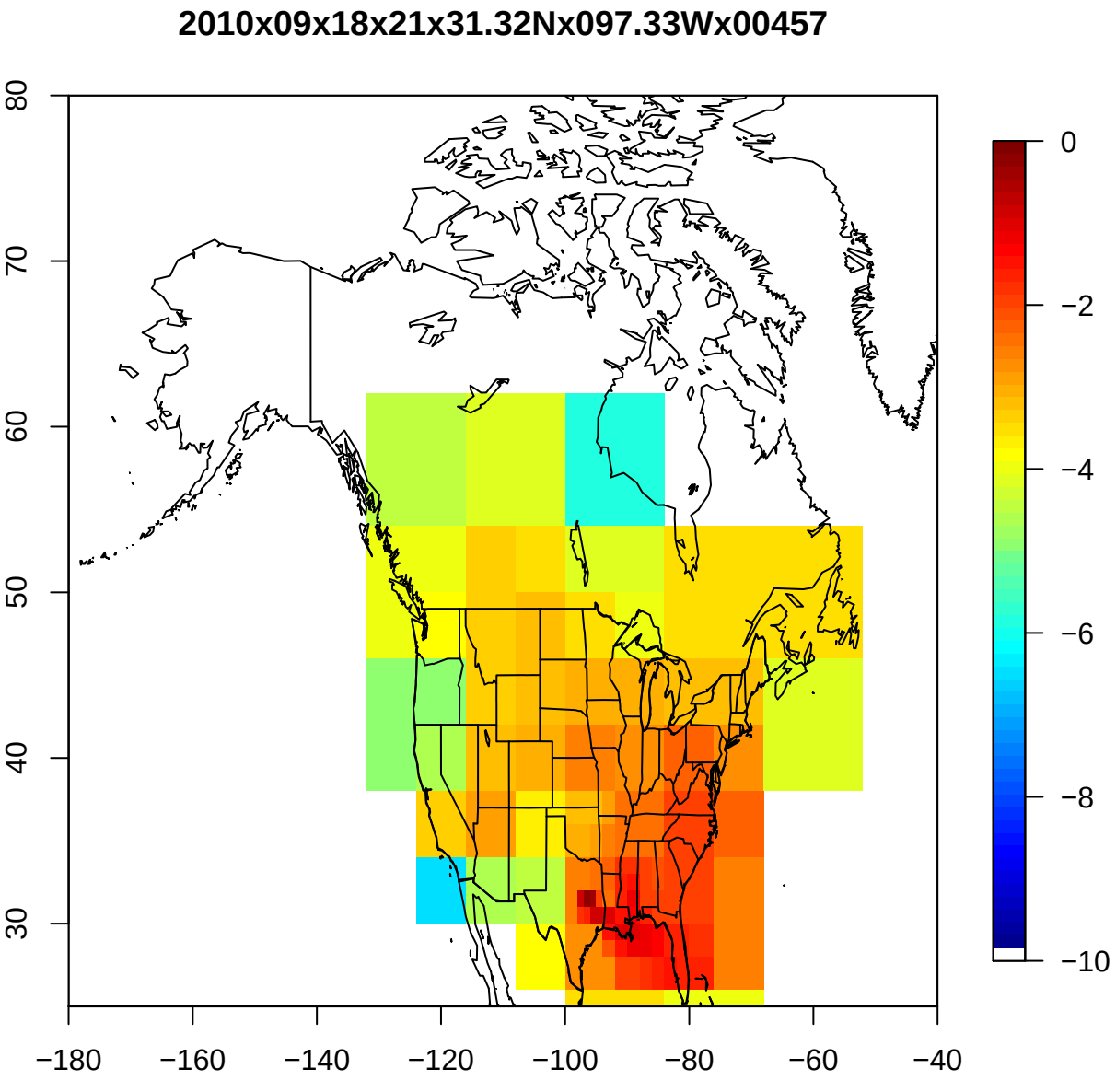
2010x09x18x21x31.32Nx097.33Wx00457
80
70
60
50
40
30
−180
−160
−140
−120
−100
−80
−60
−40
0
−2
−4
−6
−8
−10

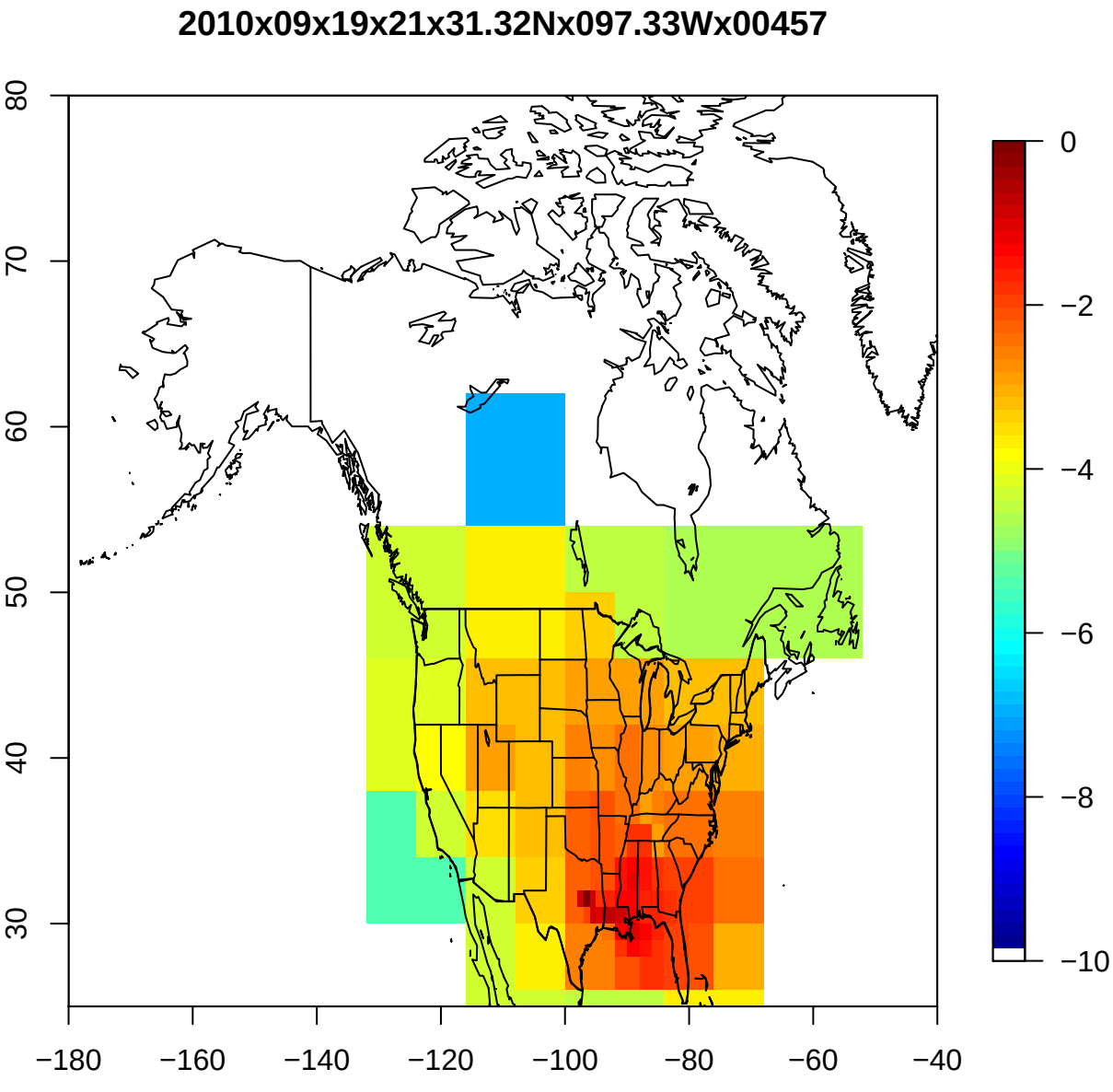
2010x09x19x21x31.32Nx097.33Wx00457
80
70
60
50
40
30
−180
−160
−140
−120
−100
−80
−60
−40
0
−2
−4
−6
−8
−10

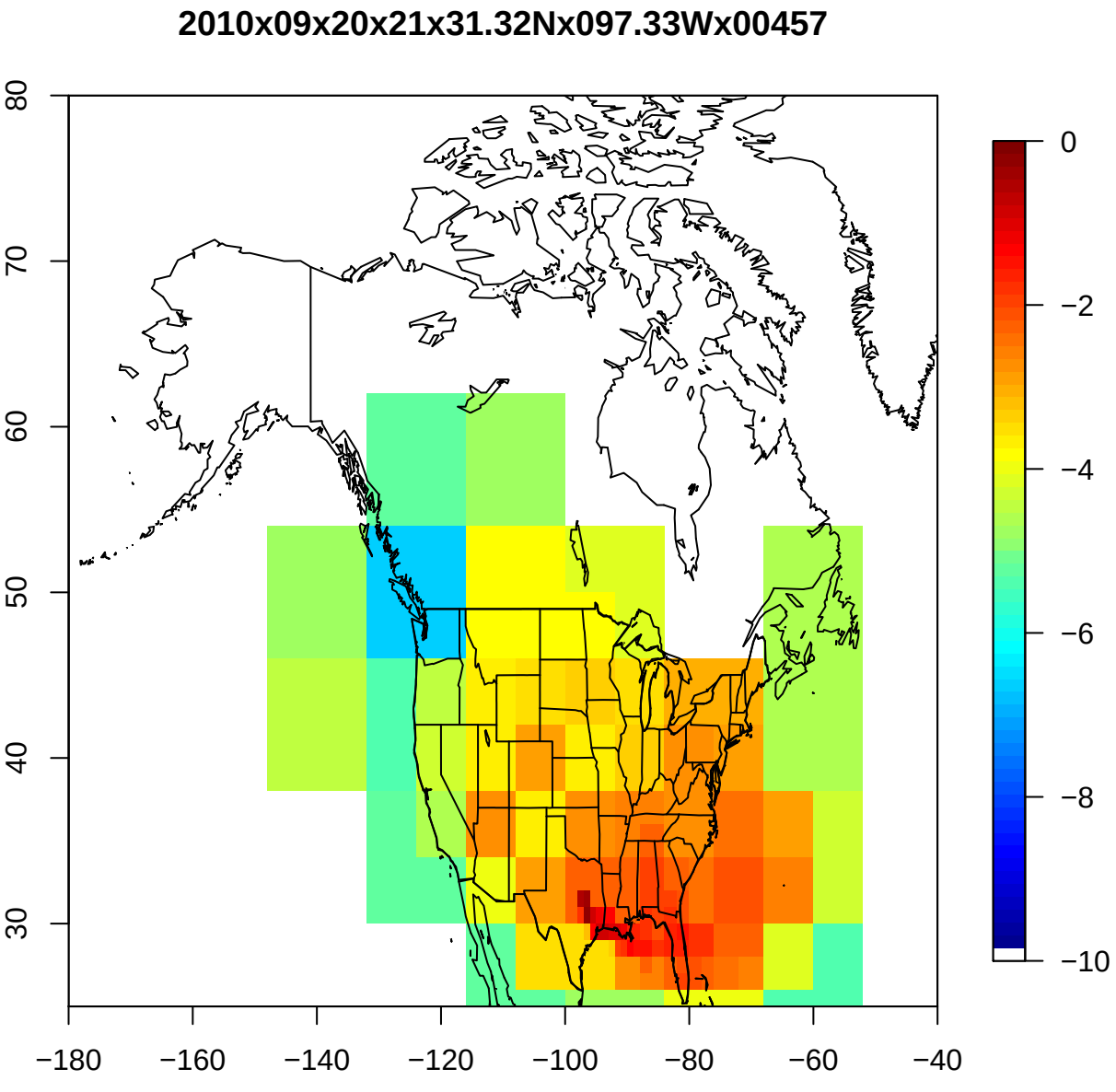
2010x09x20x21x31.32Nx097.33Wx00457
80
70
60
50
40
30
−180
−160
−140
−120
−100
−80
−60
−40
0
−2
−4
−6
−8
−10

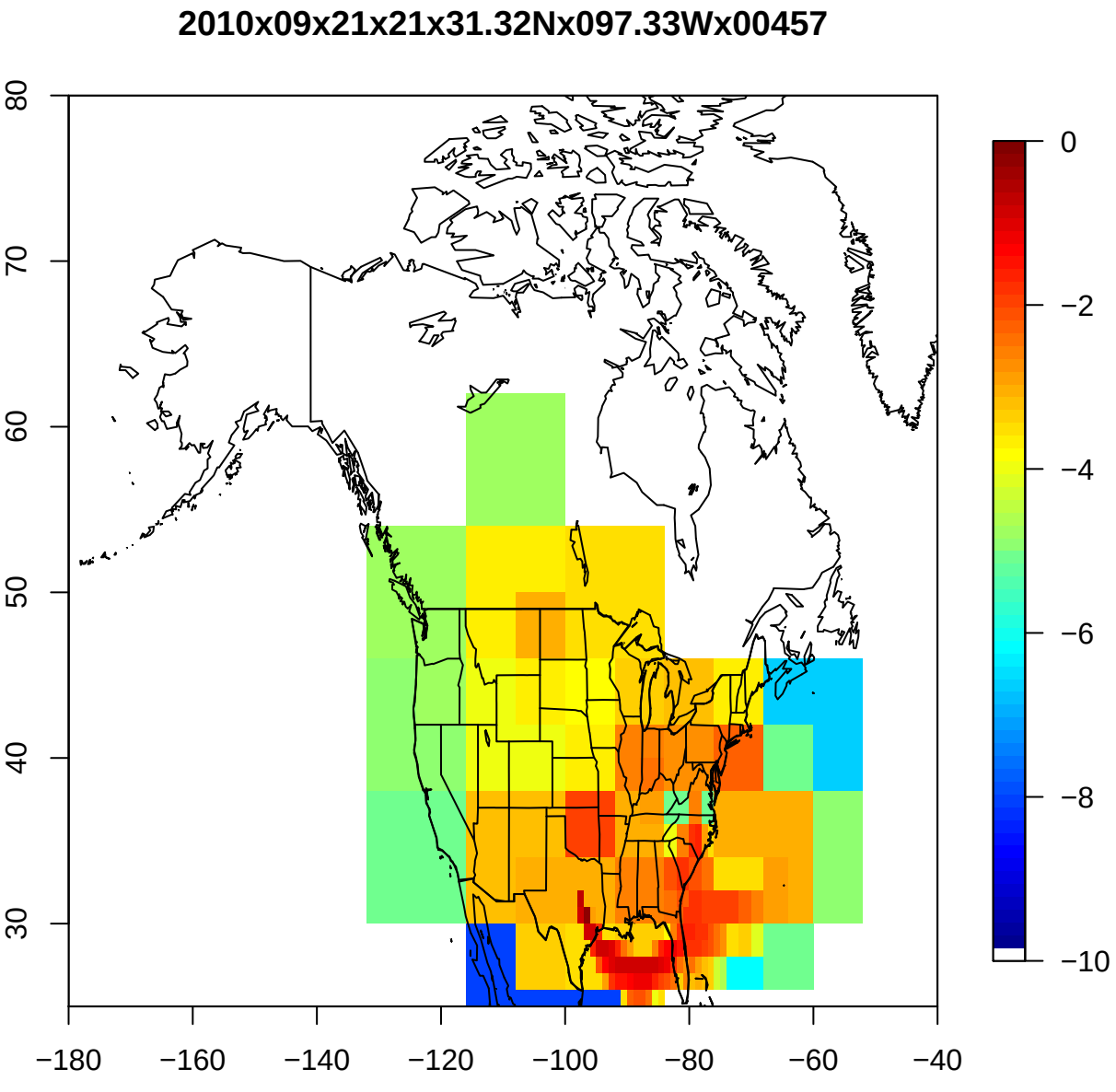
2010x09x21x21x31.32Nx097.33Wx00457
80
70
60
50
40
30
−180
−160
−140
−120
−100
−80
−60
−40
0
−2
−4
−6
−8
−10

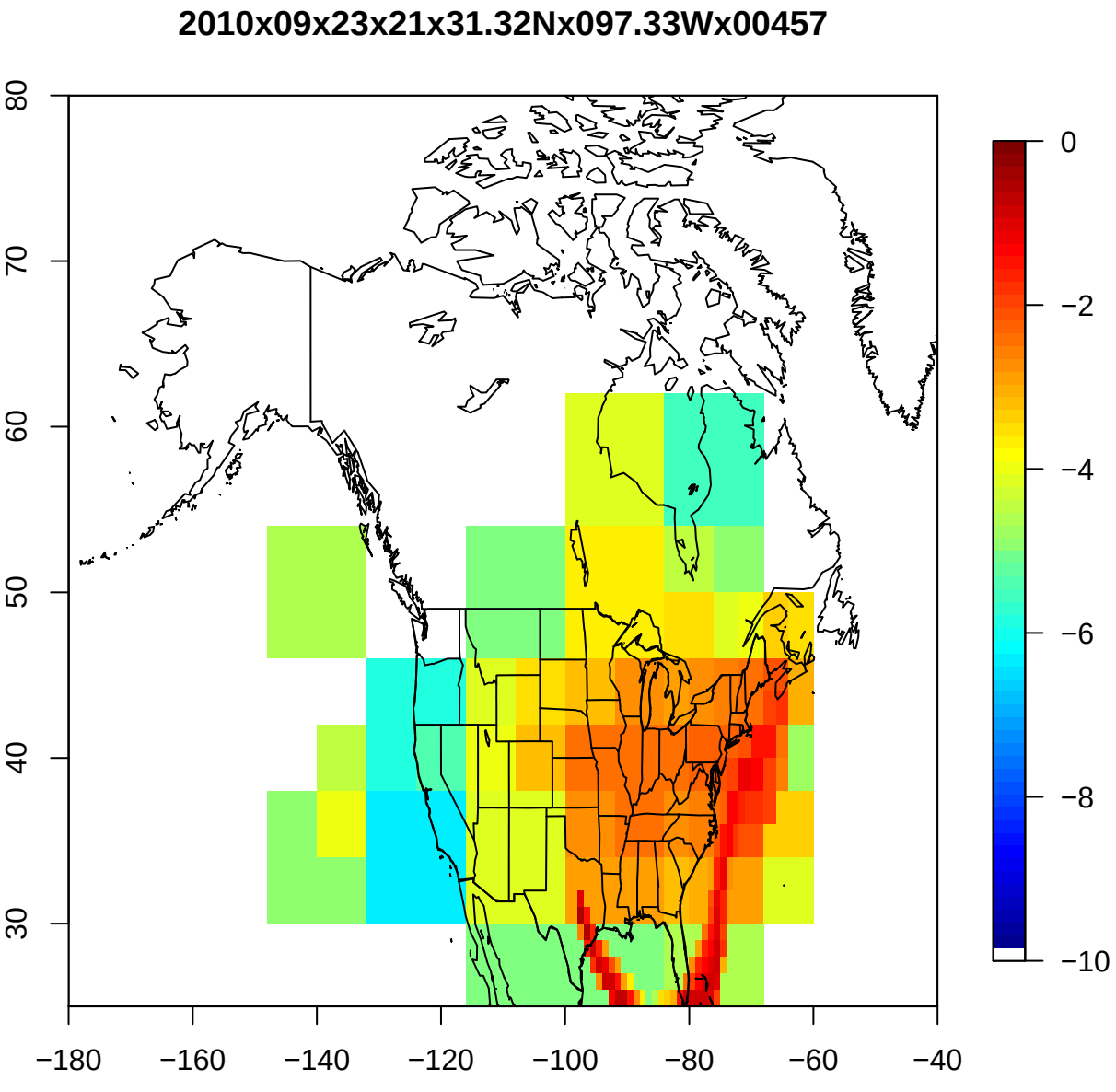
2010x09x23x21x31.32Nx097.33Wx00457
80
70
60
50
40
30
−180
−160
−140
−120
−100
−80
−60
−40
0
−2
−4
−6
−8
−10

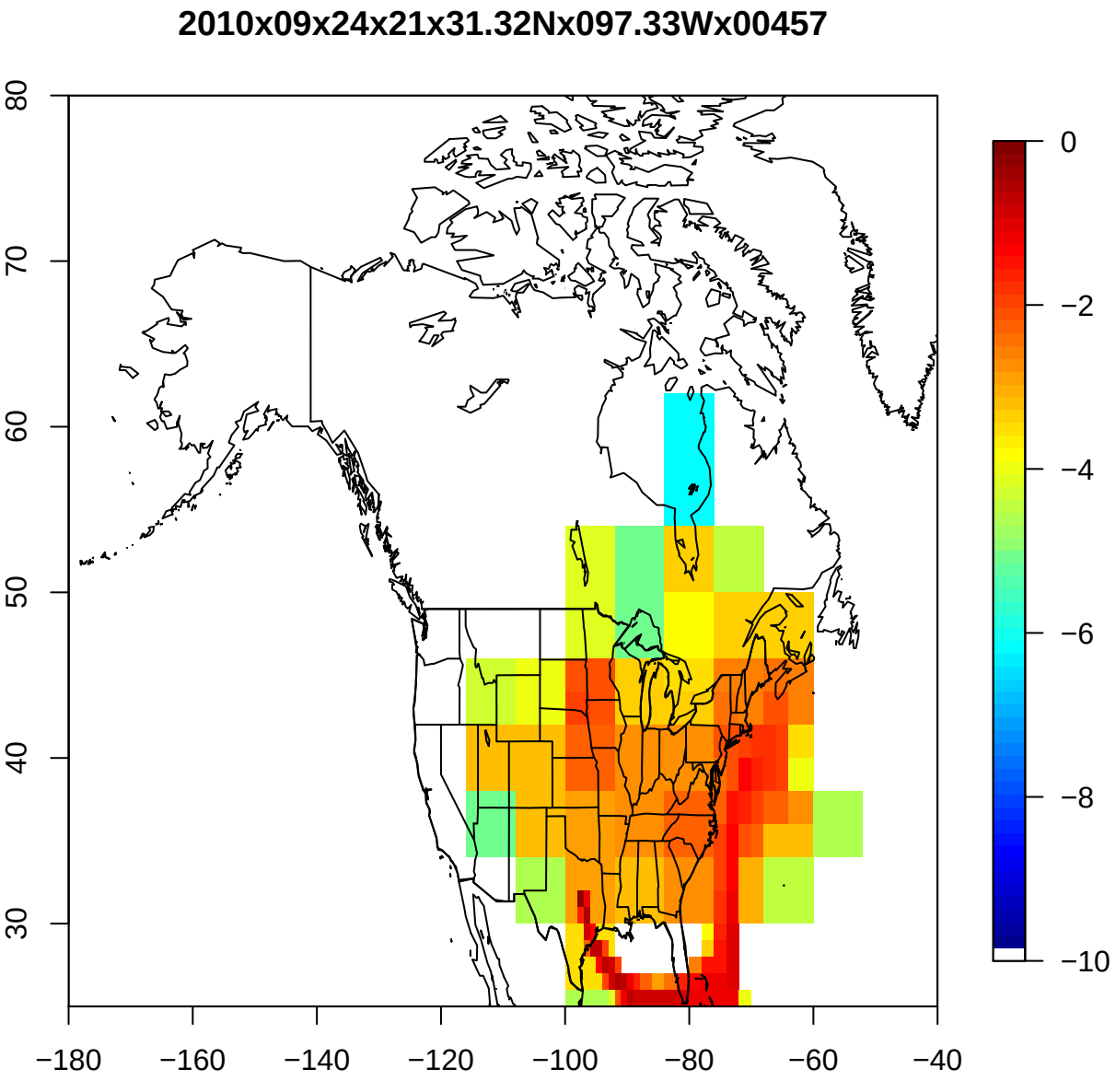
2010x09x24x21x31.32Nx097.33Wx00457
80
70
60
50
40
30
−180
−160
−140
−120
−100
−80
−60
−40
0
−2
−4
−6
−8
−10

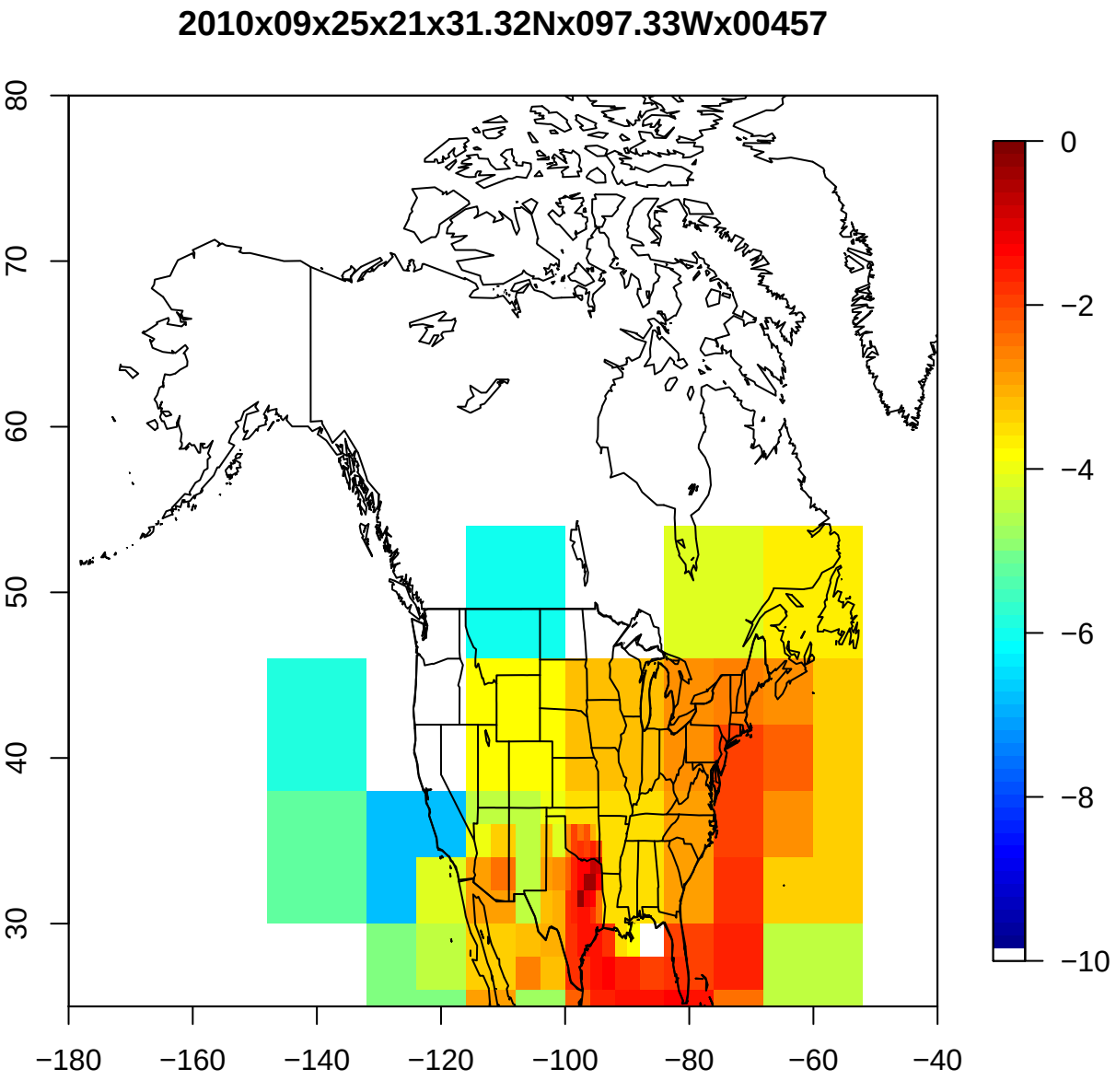
2010x09x25x21x31.32Nx097.33Wx00457
80
70
60
50
40
30
−180
−160
−140
−120
−100
−80
−60
−40
0
−2
−4
−6
−8
−10

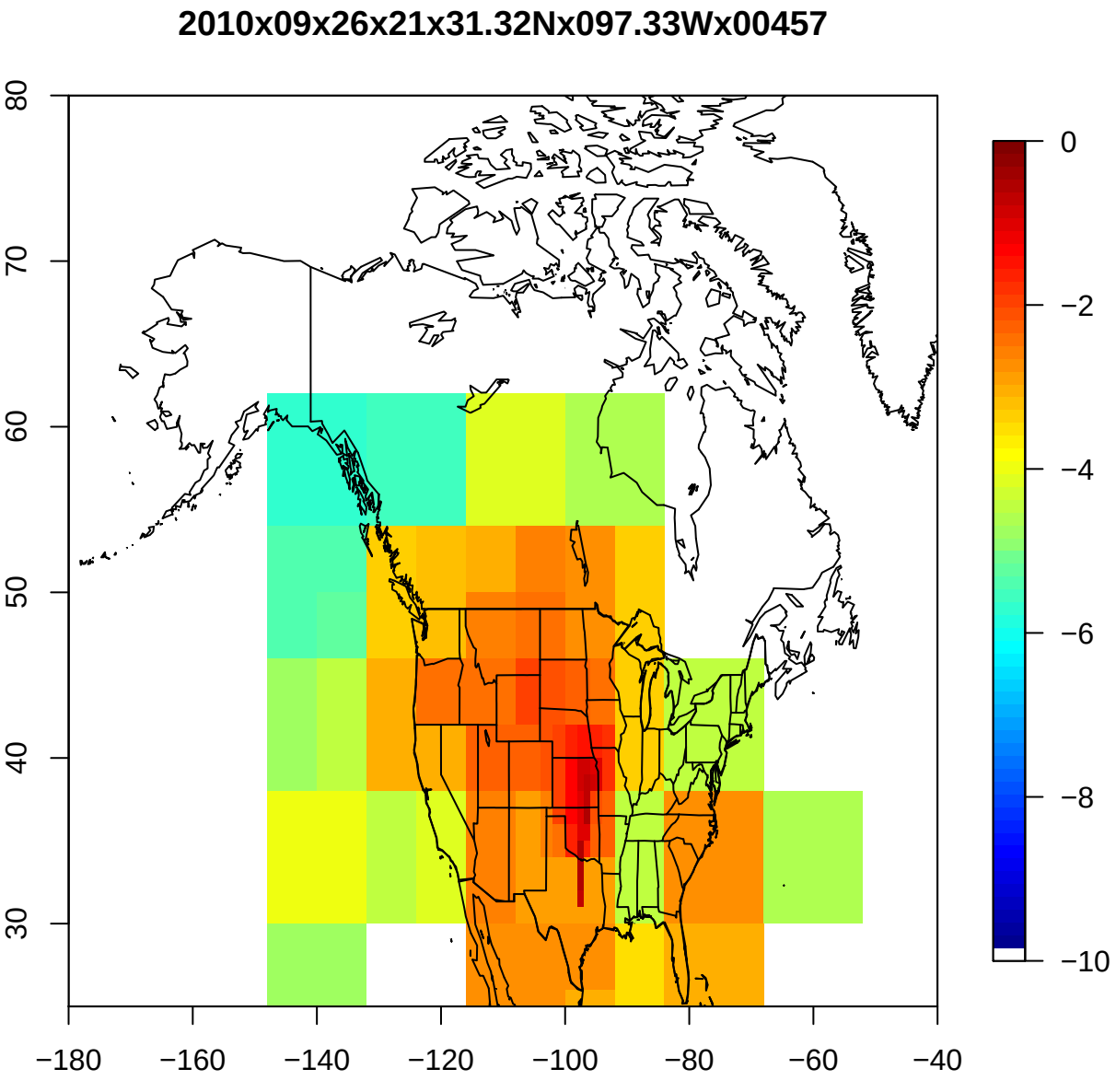
2010x09x26x21x31.32Nx097.33Wx00457
80
70
60
50
40
30
−180
−160
−140
−120
−100
−80
−60
−40
0
−2
−4
−6
−8
−10

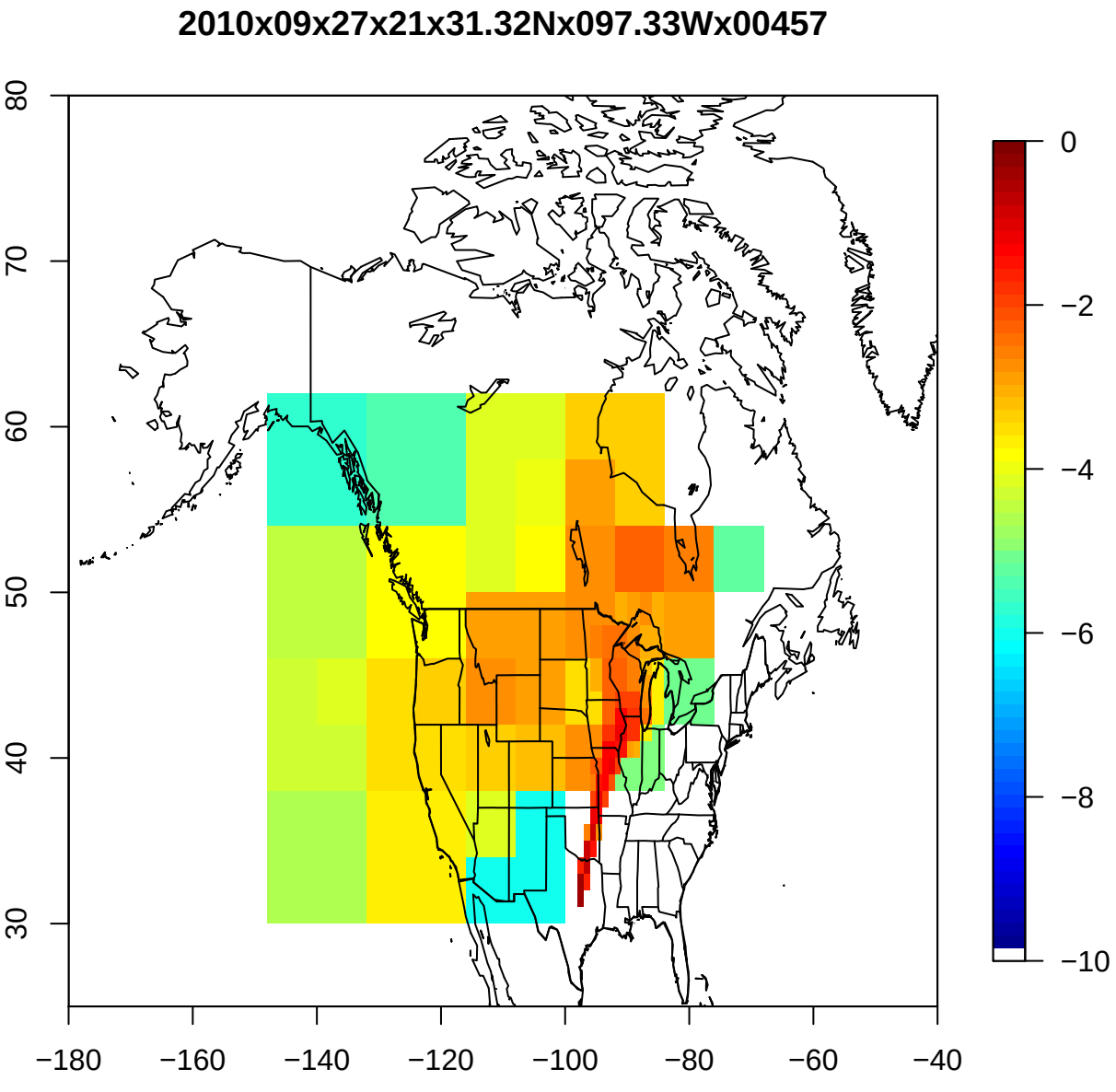
2010x09x27x21x31.32Nx097.33Wx00457
80
70
60
50
40
30
−180
−160
−140
−120
−100
−80
−60
−40
0
−2
−4
−6
−8
−10

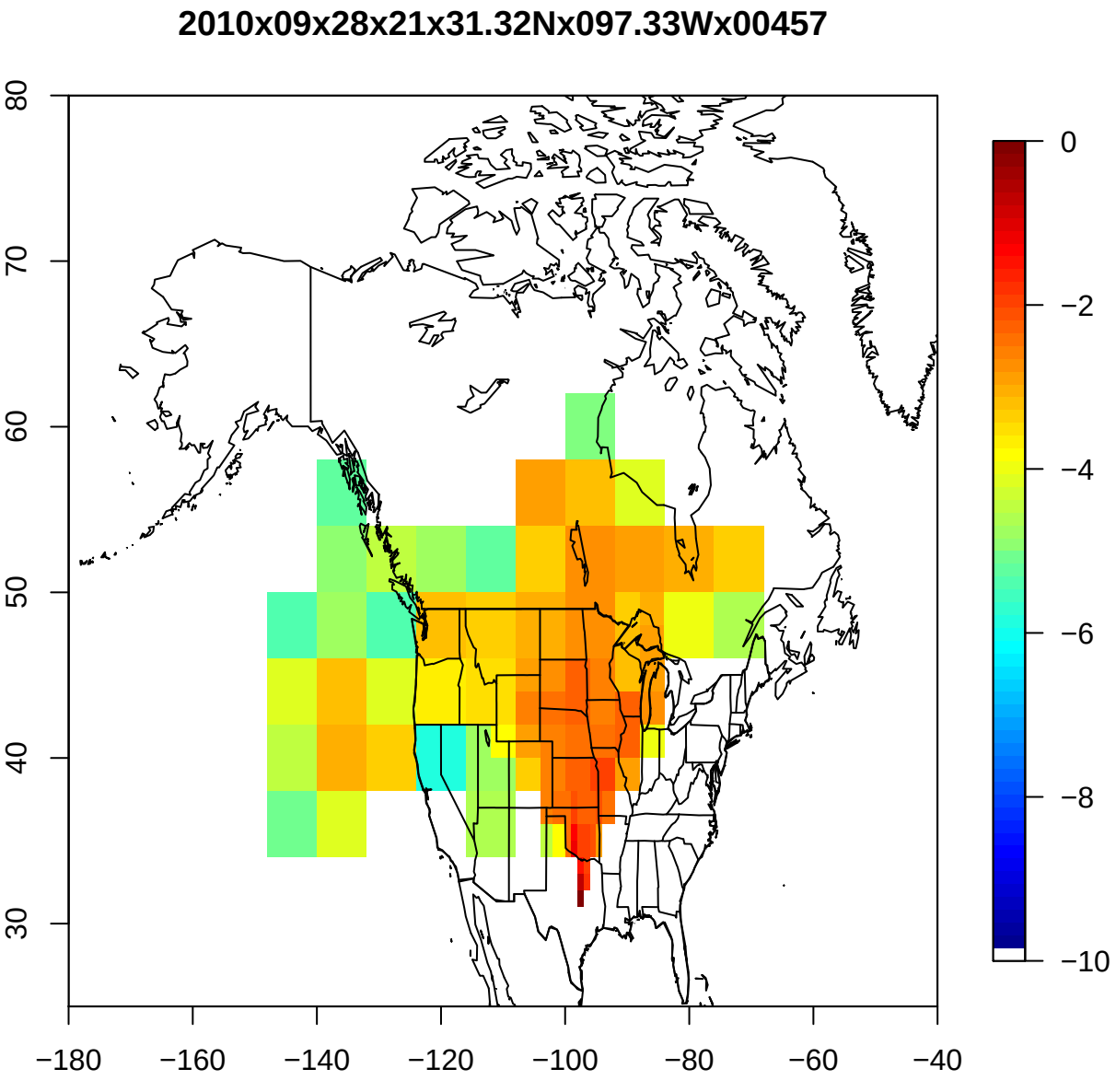
2010x09x28x21x31.32Nx097.33Wx00457
80
70
60
50
40
30
−180
−160
−140
−120
−100
−80
−60
−40
0
−2
−4
−6
−8
−10

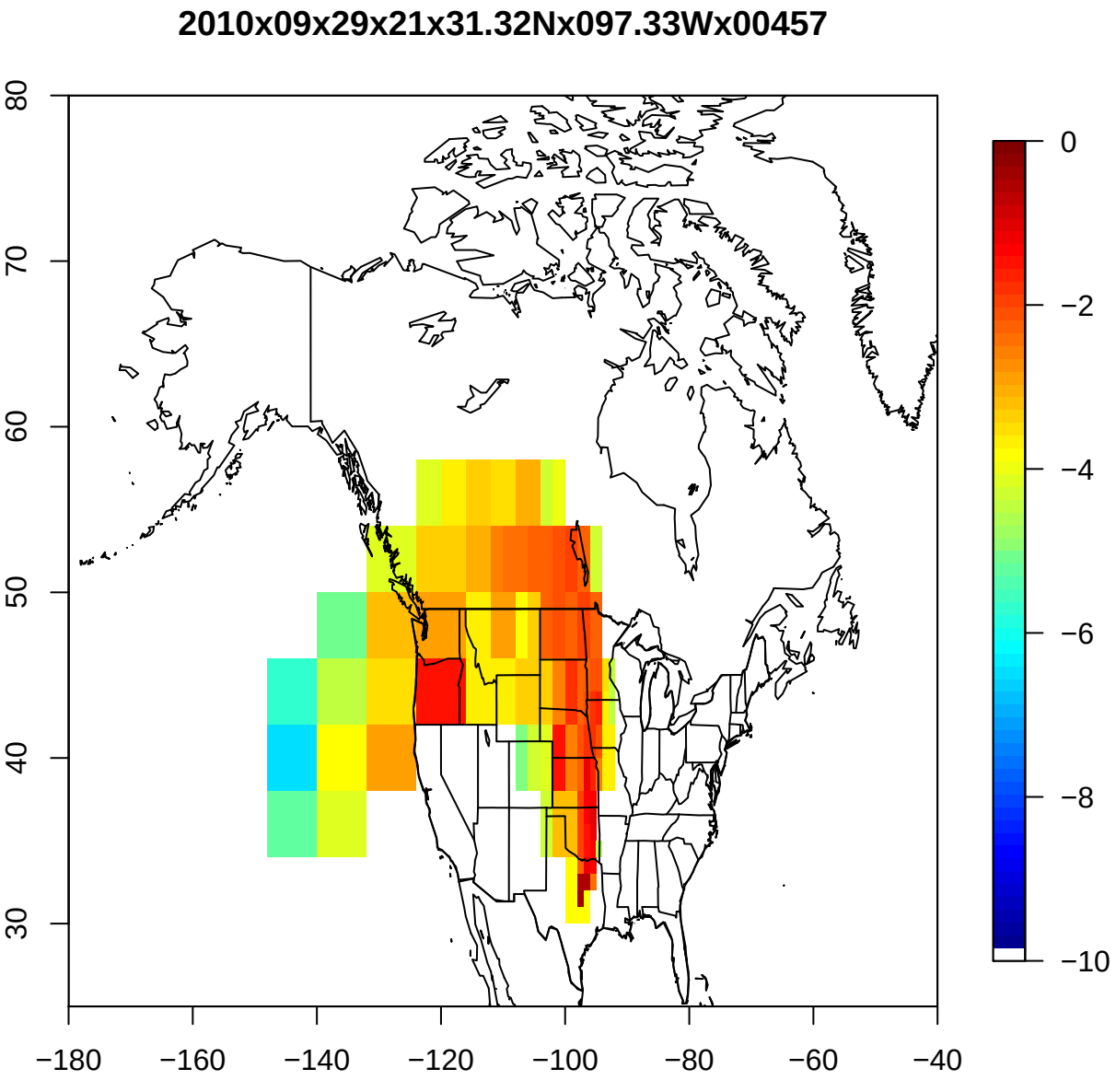
2010x09x29x21x31.32Nx097.33Wx00457
80
70
60
50
40
30
−180
−160
−140
−120
−100
−80
−60
−40
0
−2
−4
−6
−8
−10

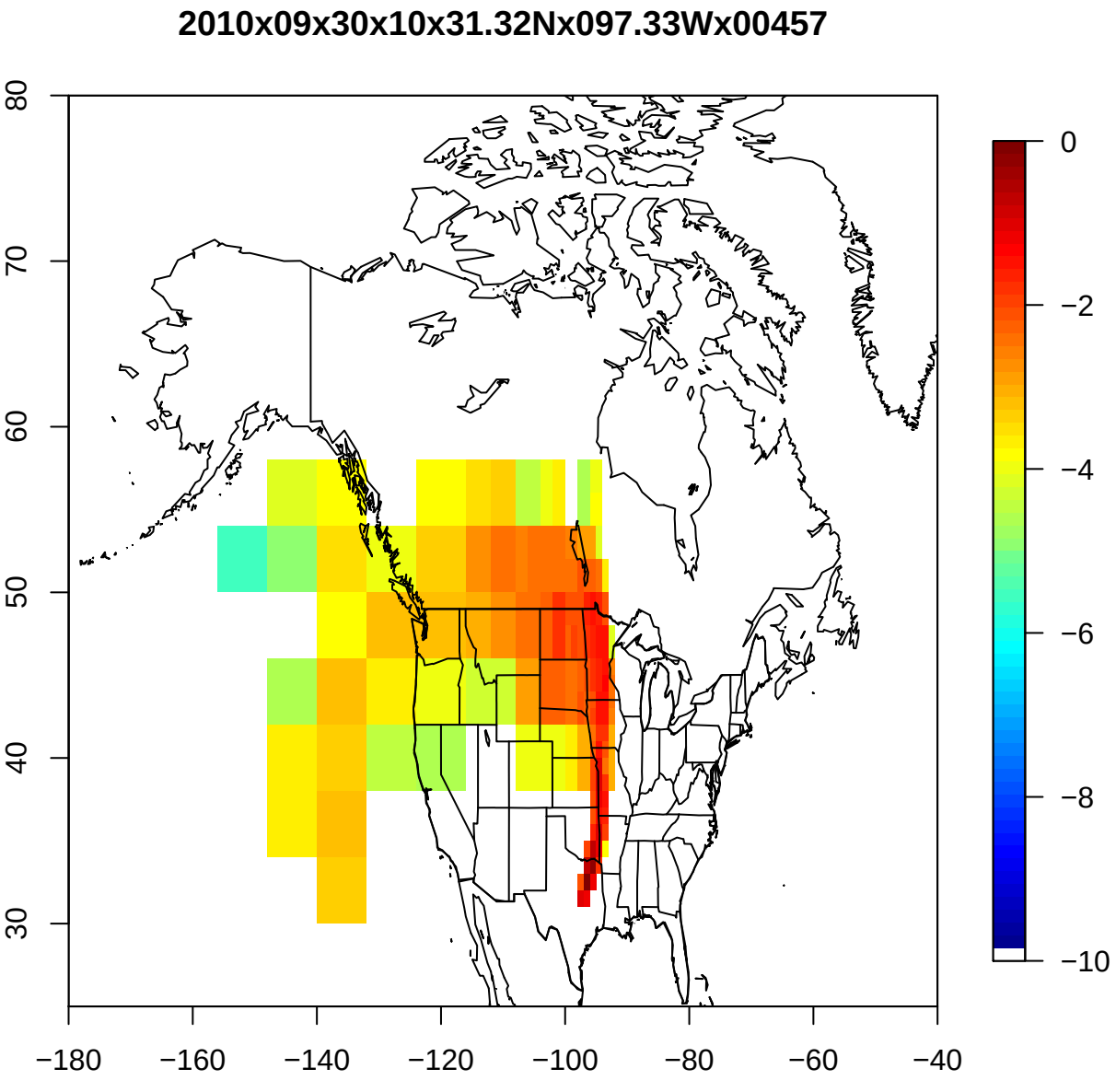
2010x09x30x10x31.32Nx097.33Wx00457
80
70
60
50
40
30
−180
−160
−140
−120
−100
−80
−60
−40
0
−2
−4
−6
−8
−10

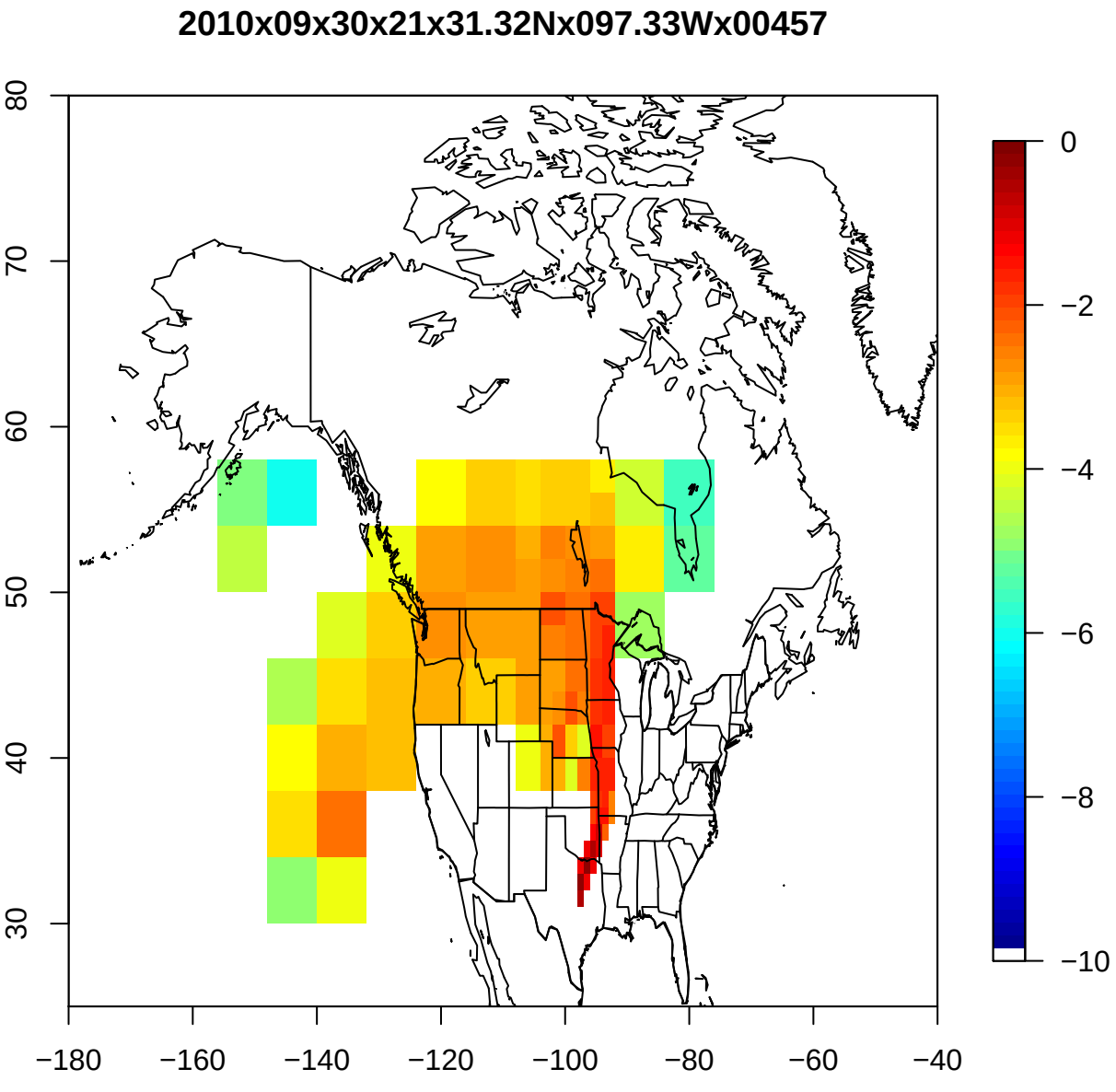
2010x09x30x21x31.32Nx097.33Wx00457
80
70
60
50
40
30
−180
−160
−140
−120
−100
−80
−60
−40
0
−2
−4
−6
−8
−10

2010x10x02x10x31.32Nx097.33Wx00457

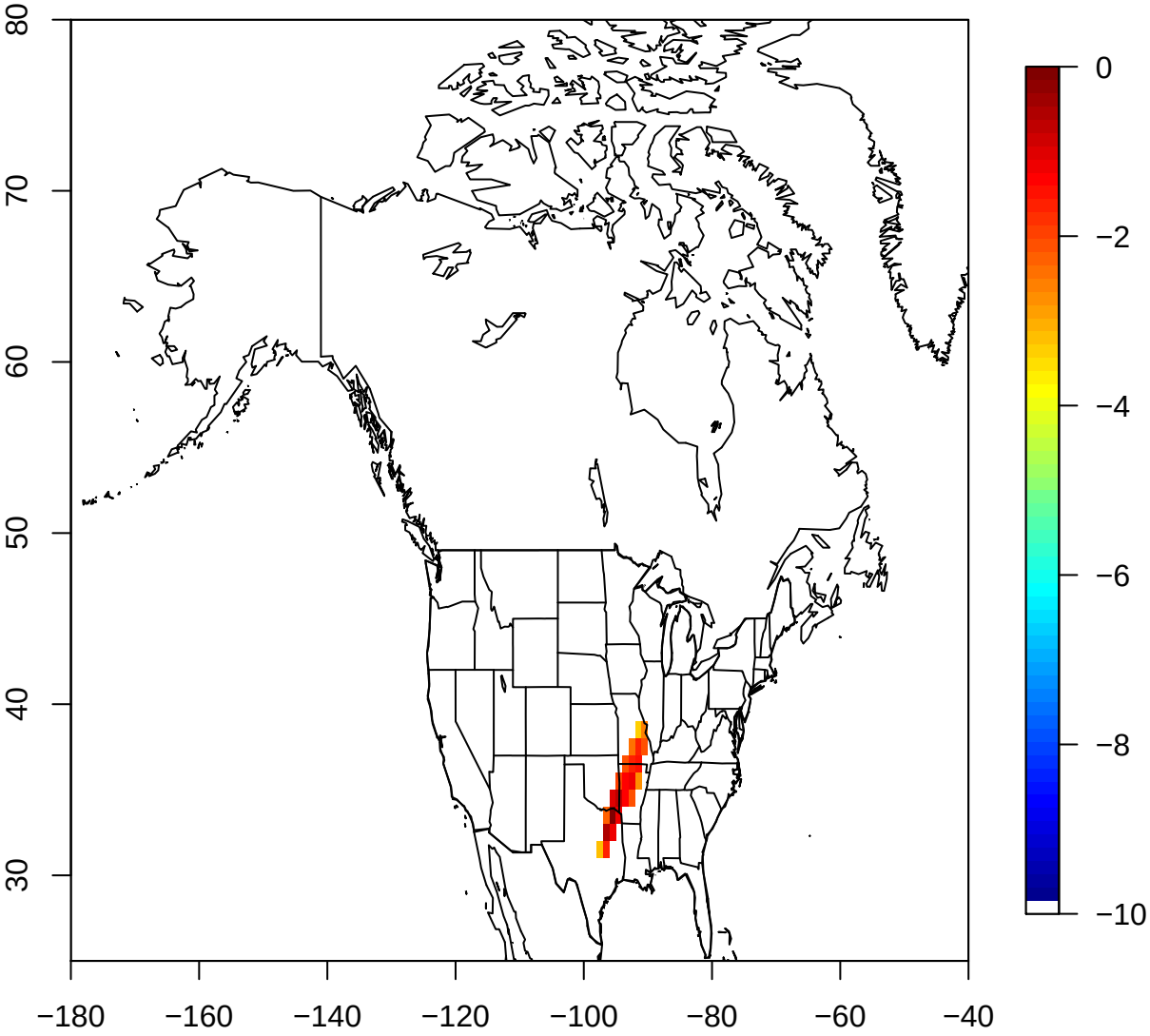

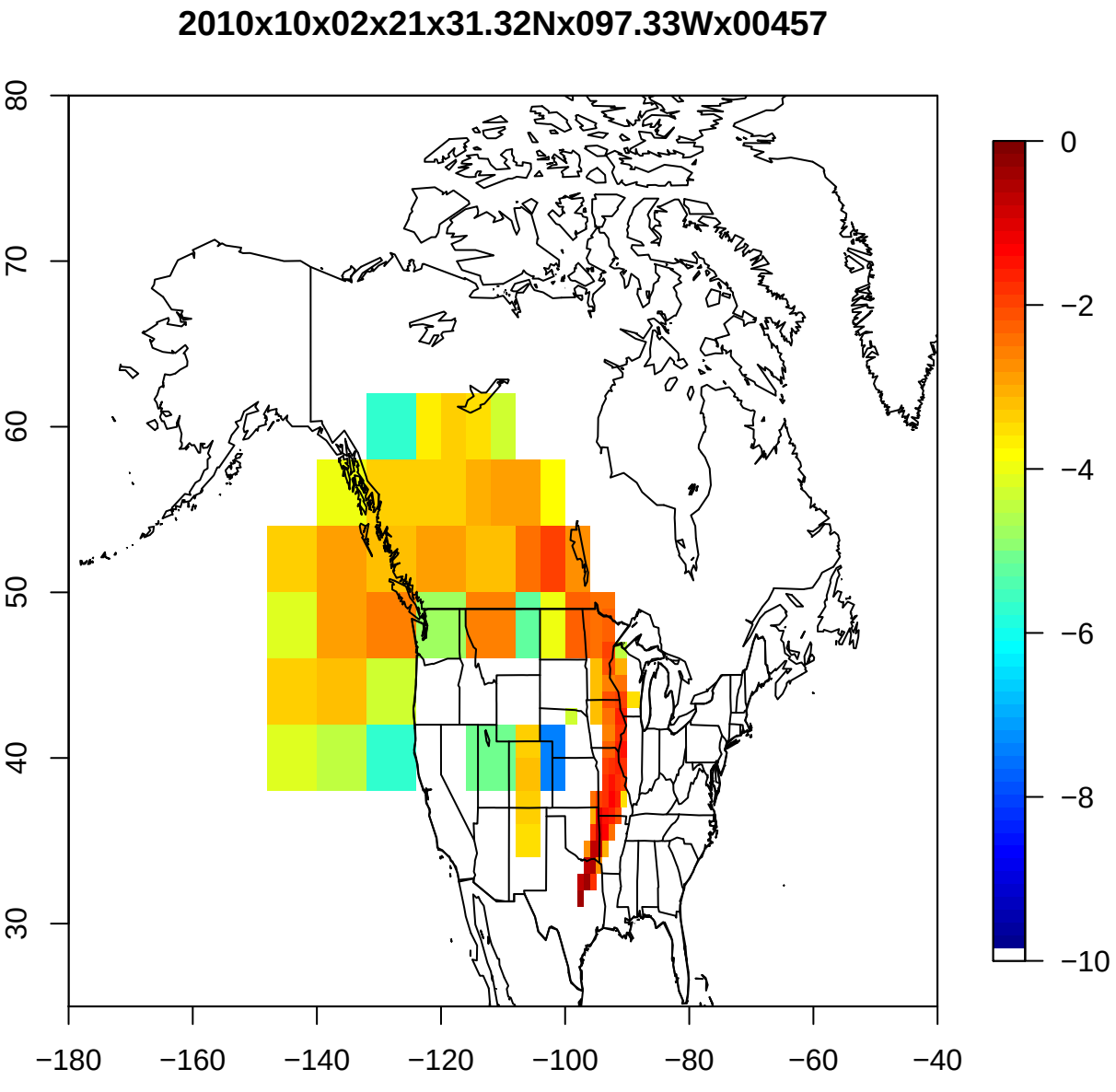
2010x10x02x21x31.32Nx097.33Wx00457
80
70
60
50
40
30
−180
−160
−140
−120
−100
−80
−60
−40
0
−2
−4
−6
−8
−10

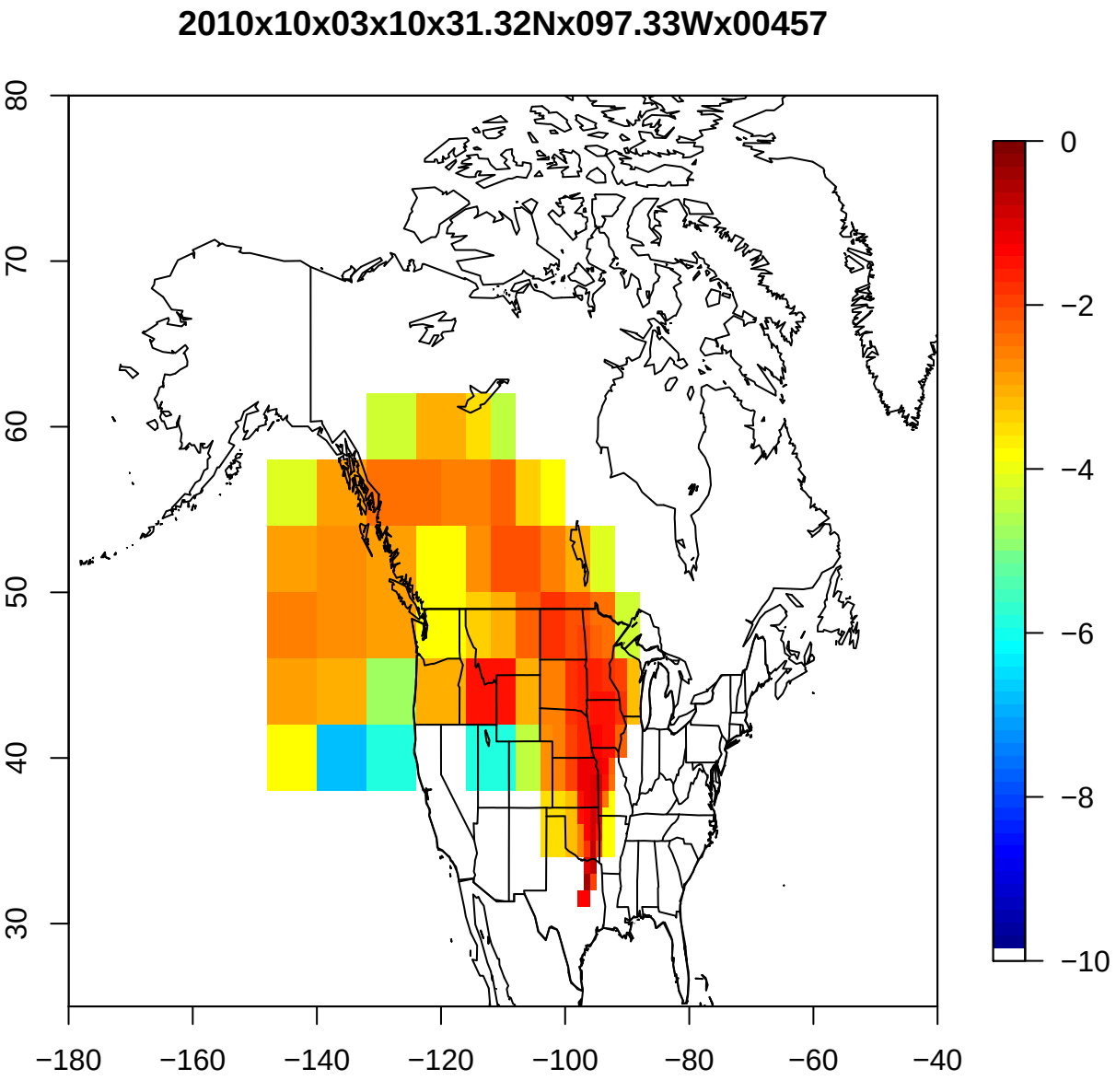
2010x10x03x10x31.32Nx097.33Wx00457
80
70
60
50
40
30
−180
−160
−140
−120
−100
−80
−60
−40
0
−2
−4
−6
−8
−10

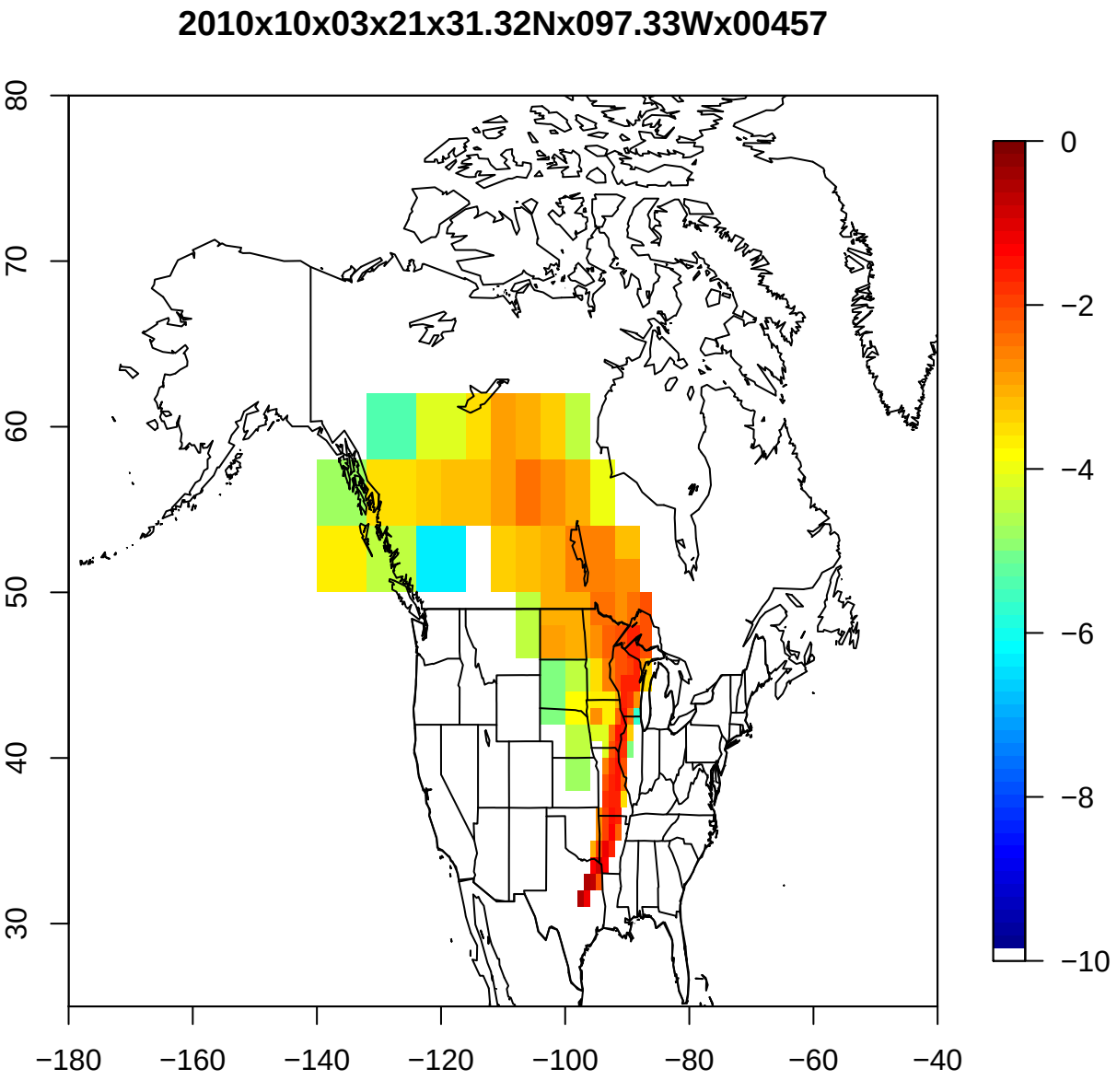
2010x10x03x21x31.32Nx097.33Wx00457
80
70
60
50
40
30
−180
−160
−140
−120
−100
−80
−60
−40
0
−2
−4
−6
−8
−10

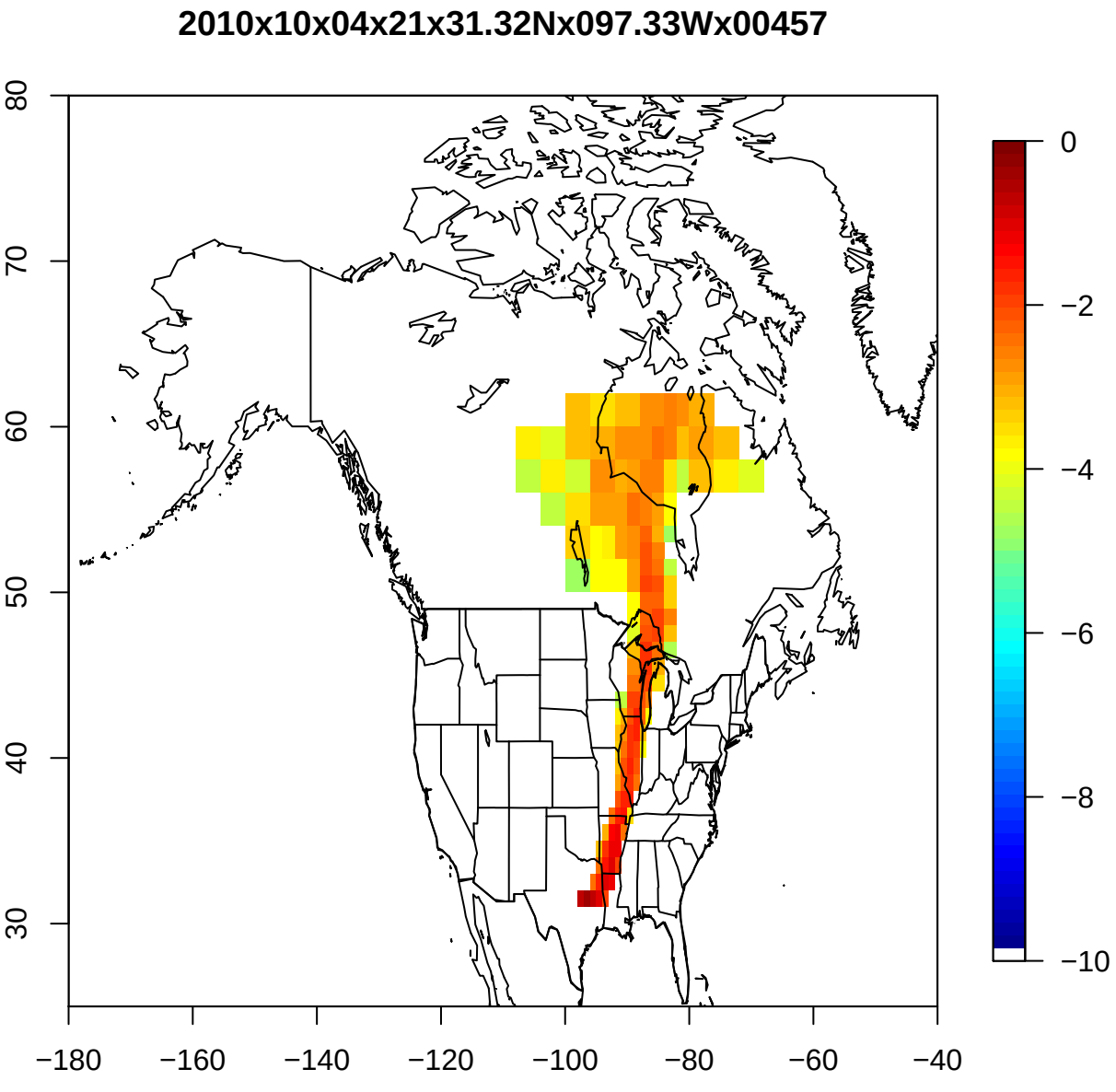
2010x10x04x21x31.32Nx097.33Wx00457
80
70
60
50
40
30
−180
−160
−140
−120
−100
−80
−60
−40
0
−2
−4
−6
−8
−10

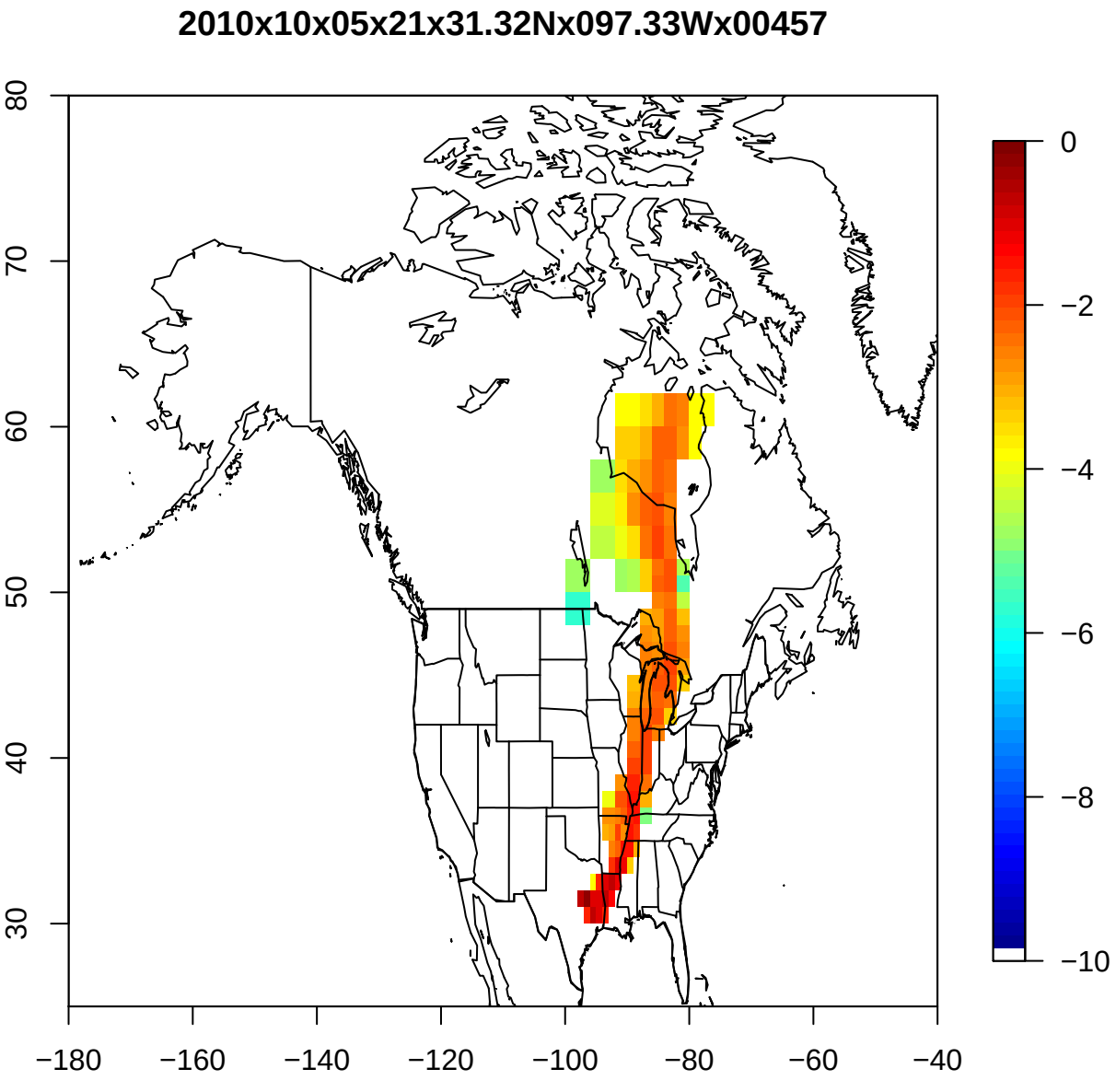
2010x10x05x21x31.32Nx097.33Wx00457
80
70
60
50
40
30
−180
−160
−140
−120
−100
−80
−60
−40
0
−2
−4
−6
−8
−10

2010x10x06x21x31.32Nx097.33Wx00457

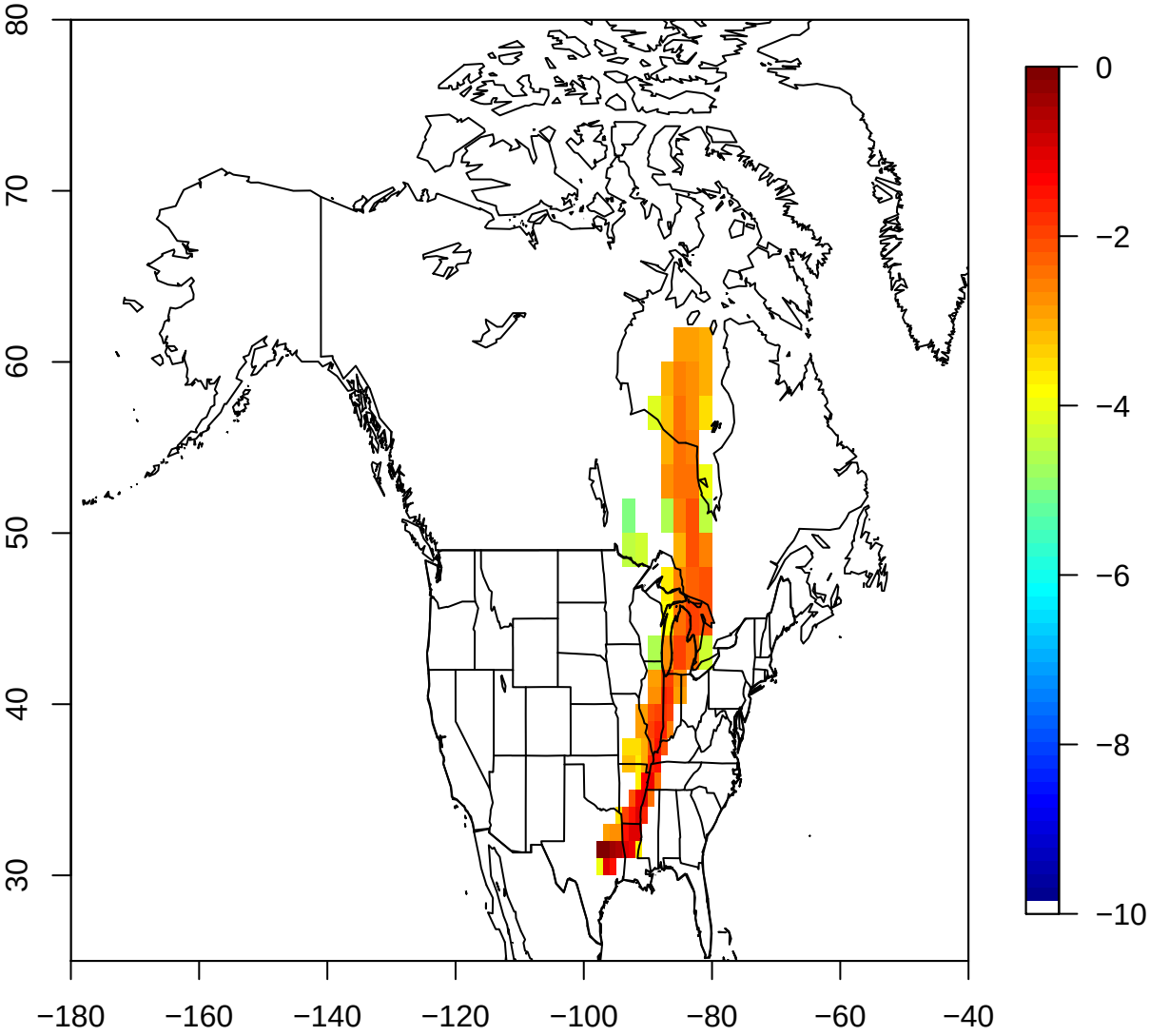

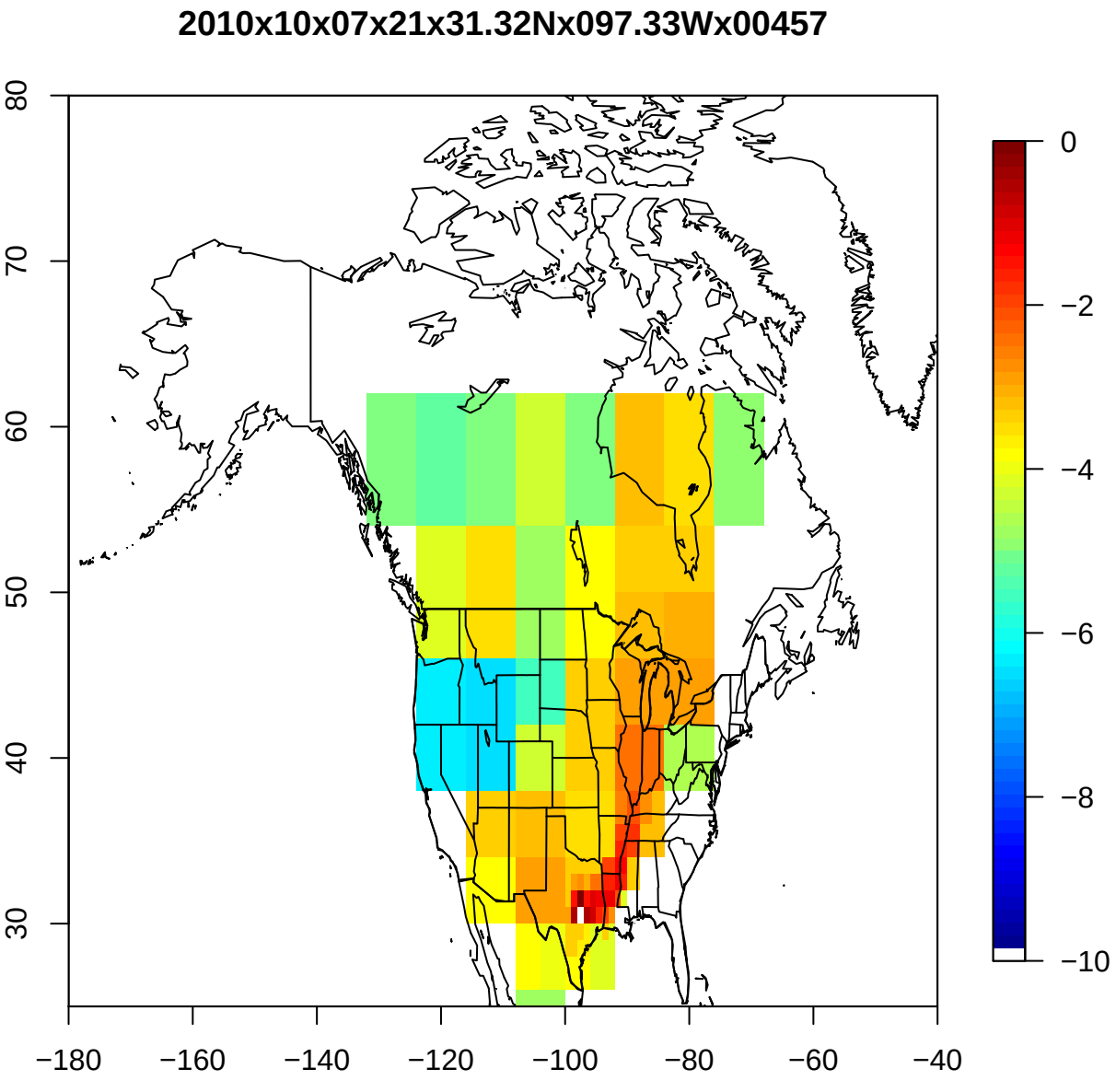
2010x10x07x21x31.32Nx097.33Wx00457
80
70
60
50
40
30
−180
−160
−140
−120
−100
−80
−60
−40
0
−2
−4
−6
−8
−10

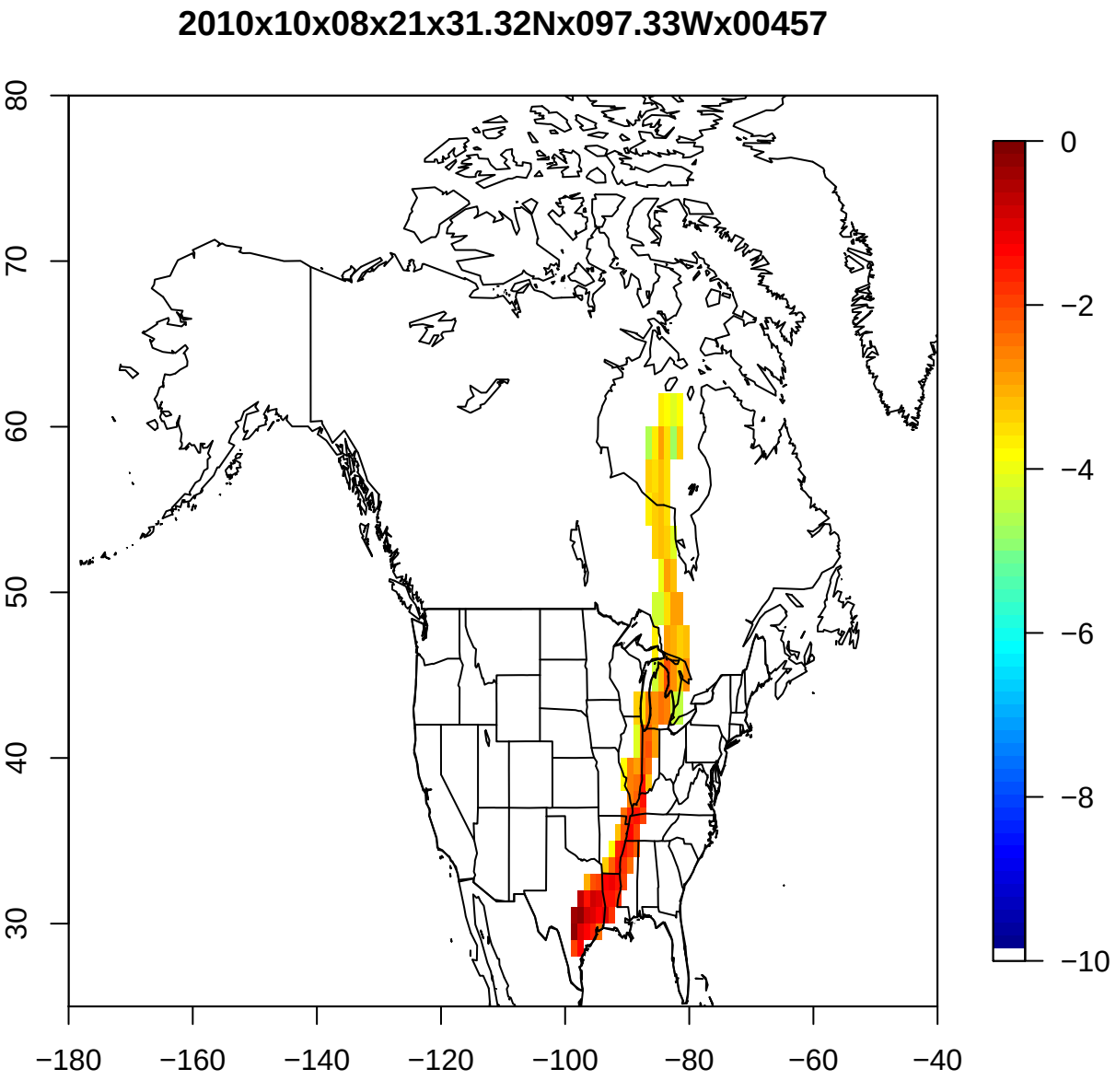
2010x10x08x21x31.32Nx097.33Wx00457
80
70
60
50
40
30
−180
−160
−140
−120
−100
−80
−60
−40
0
−2
−4
−6
−8
−10

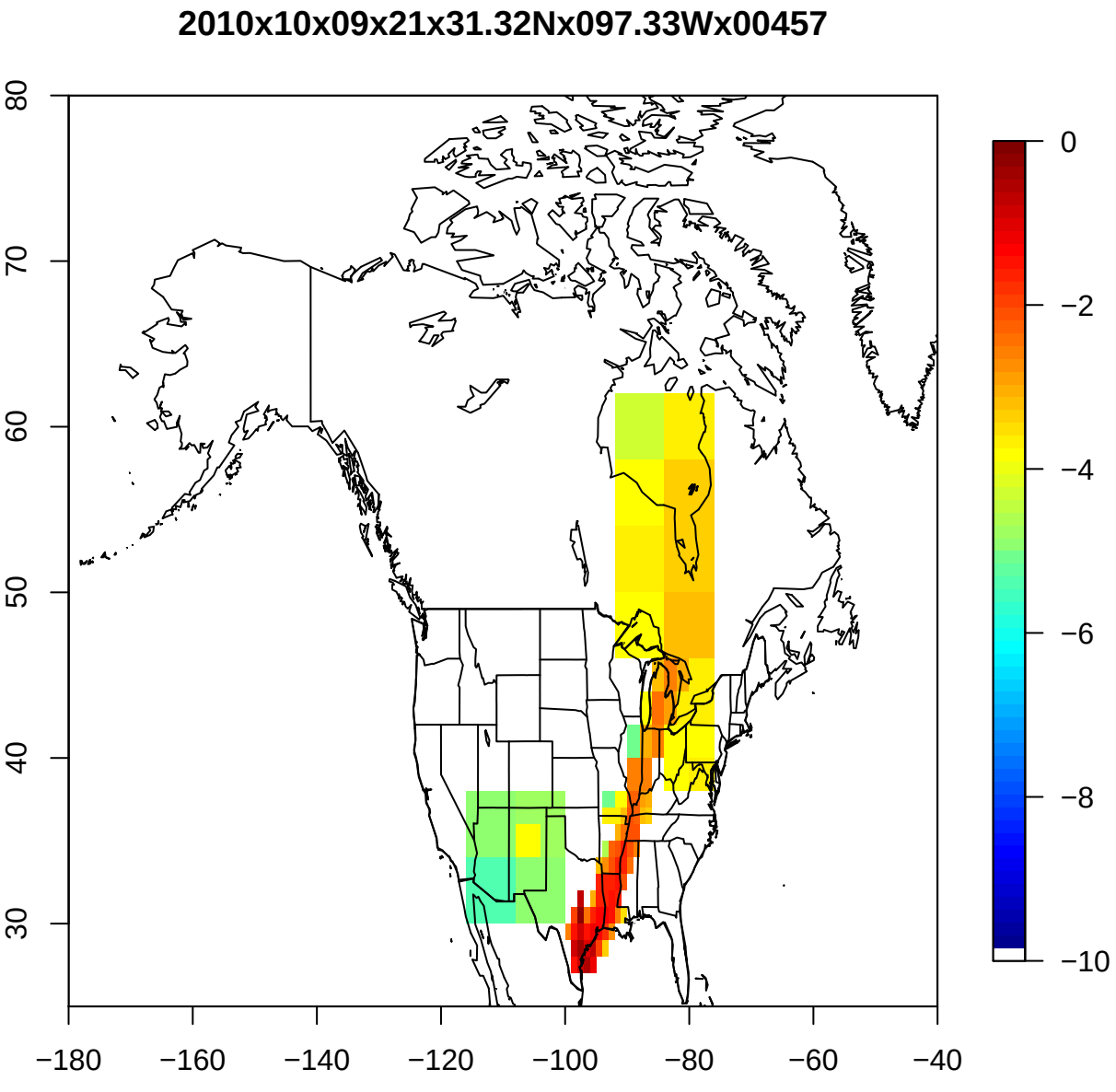
2010x10x09x21x31.32Nx097.33Wx00457
80
70
60
50
40
30
−180
−160
−140
−120
−100
−80
−60
−40
0
−2
−4
−6
−8
−10

Appendix 4: TCEQ Flask Intensive – High Confidence

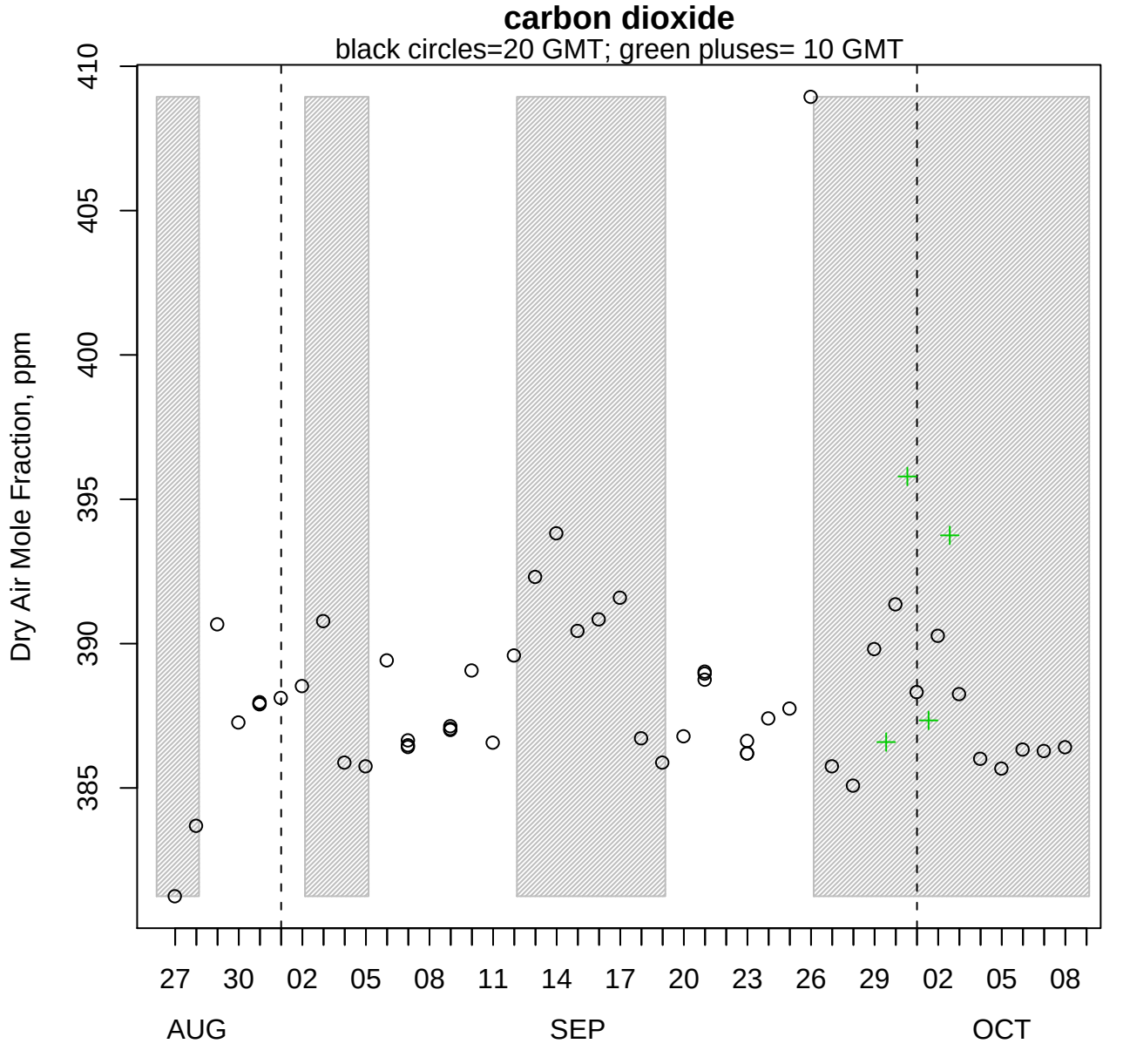

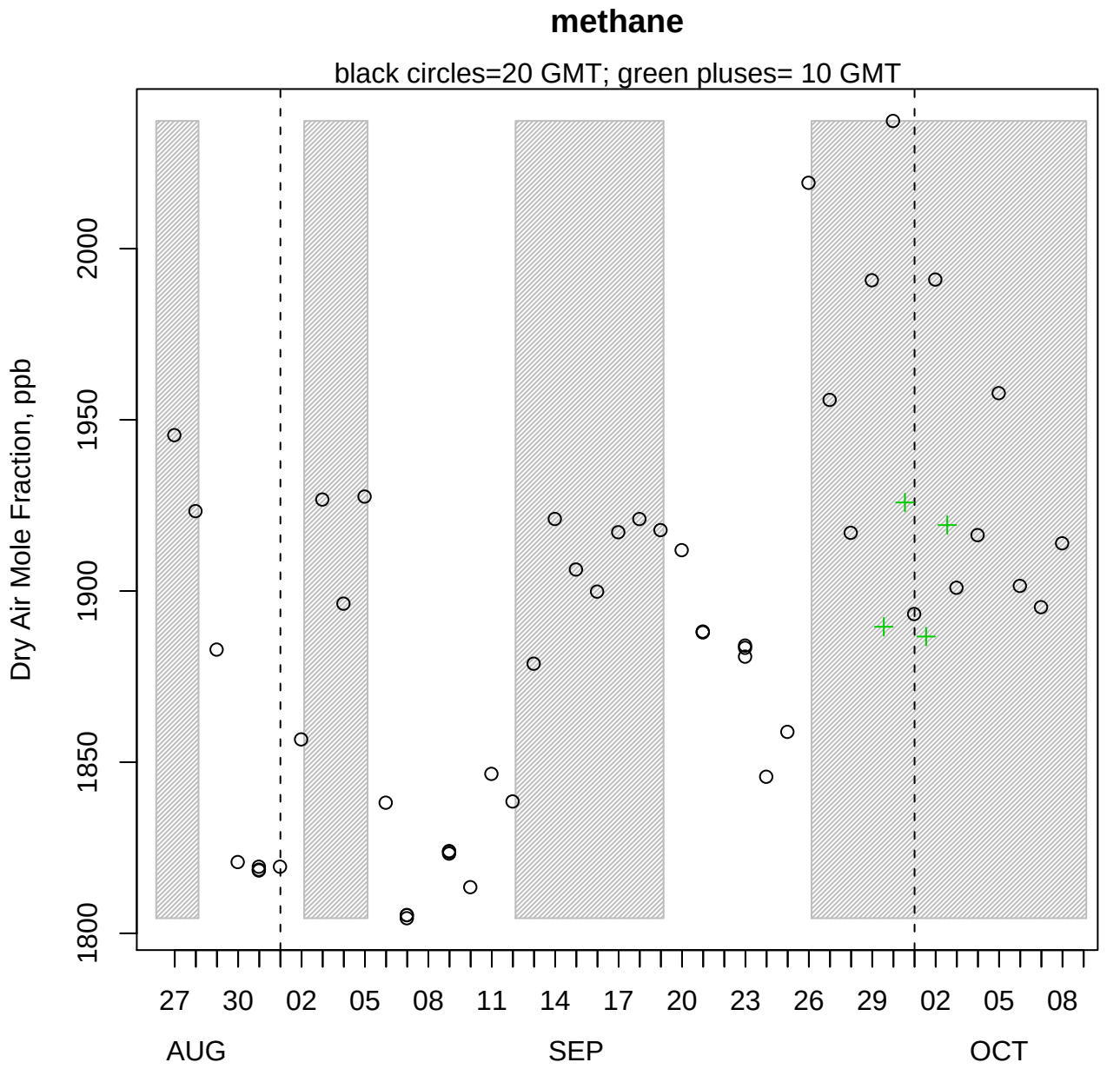
methane
black circles=20 GMT; green pluses= 10 GMT
Dry Air Mole Fraction, ppb
1800
1850
1900
1950
2000
27
30
02
05
08
11
14
17
20
23
26
29
02
05
08
AUG
SEP
OCT

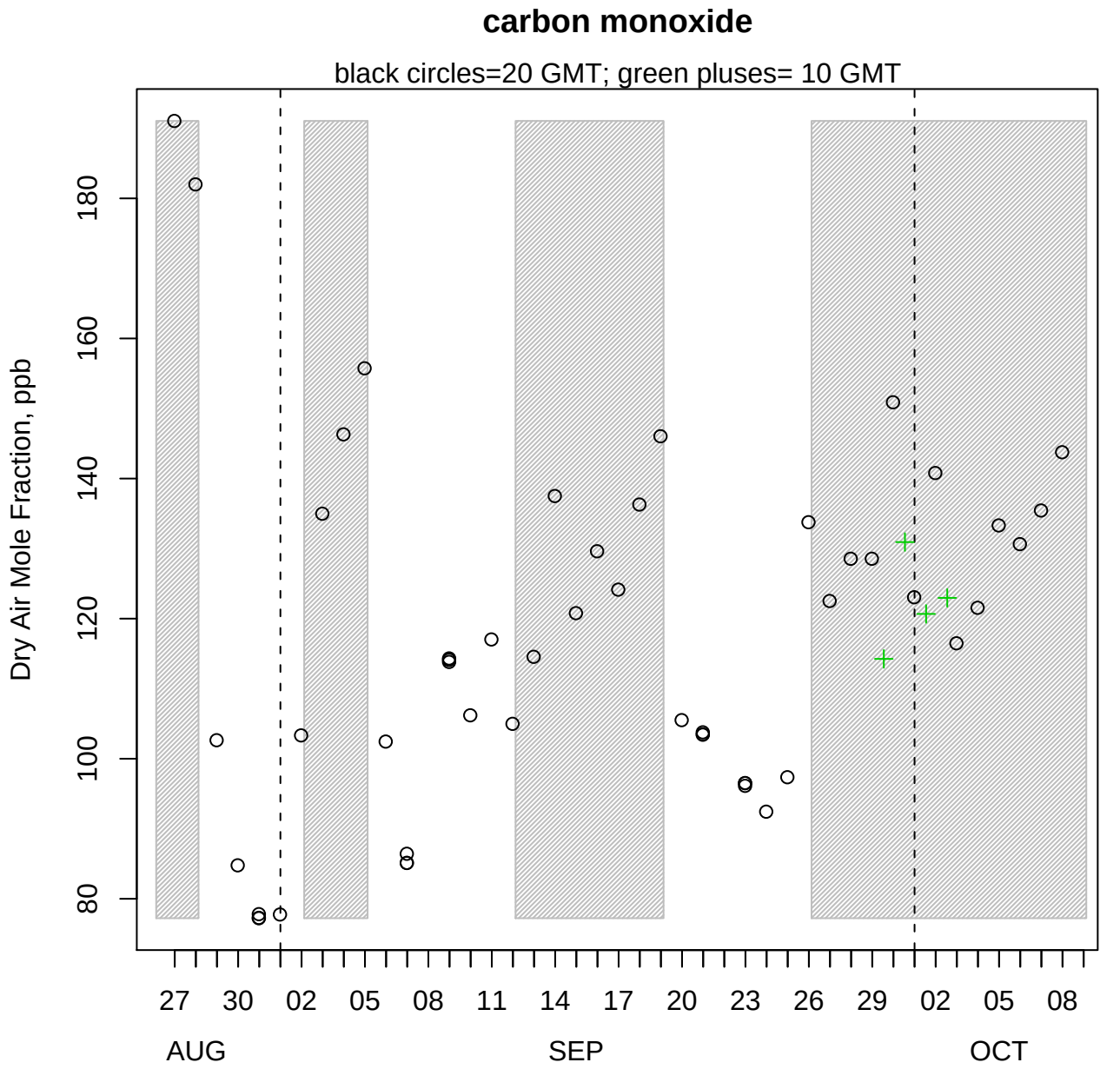
carbon monoxide
black circles=20 GMT; green pluses= 10 GMT
Dry Air Mole Fraction, ppb
80
100
120
140
160
180
27
30
02
05
08
11
14
17
20
23
26
29
02
05
08
AUG
SEP
OCT

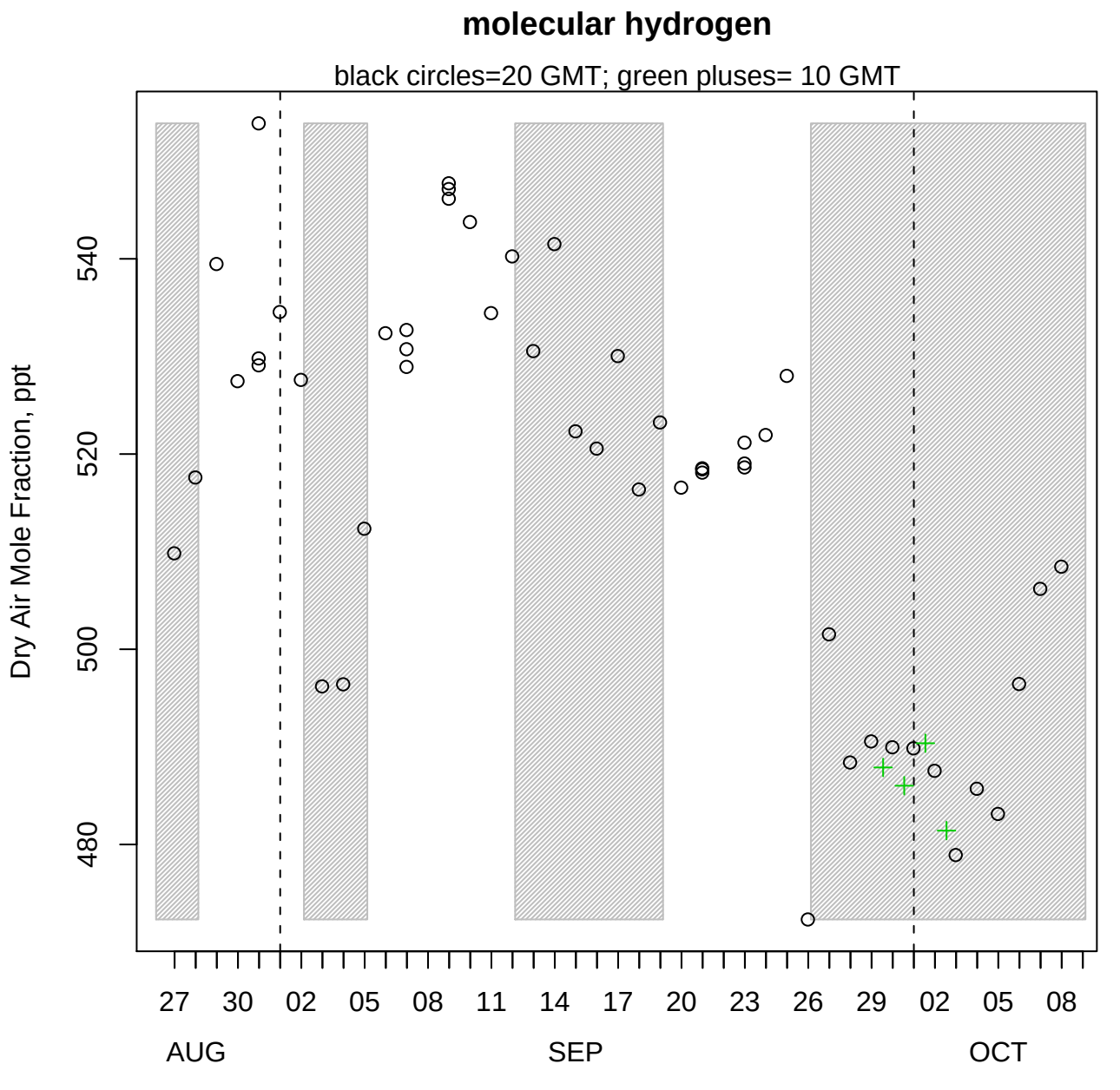
molecular hydrogen
black circles=20 GMT; green pluses= 10 GMT
Dry Air Mole Fraction, ppt
480
500
520
540
27
30
02
05
08
11
14
17
20
23
26
29
02
05
08
AUG
SEP
OCT

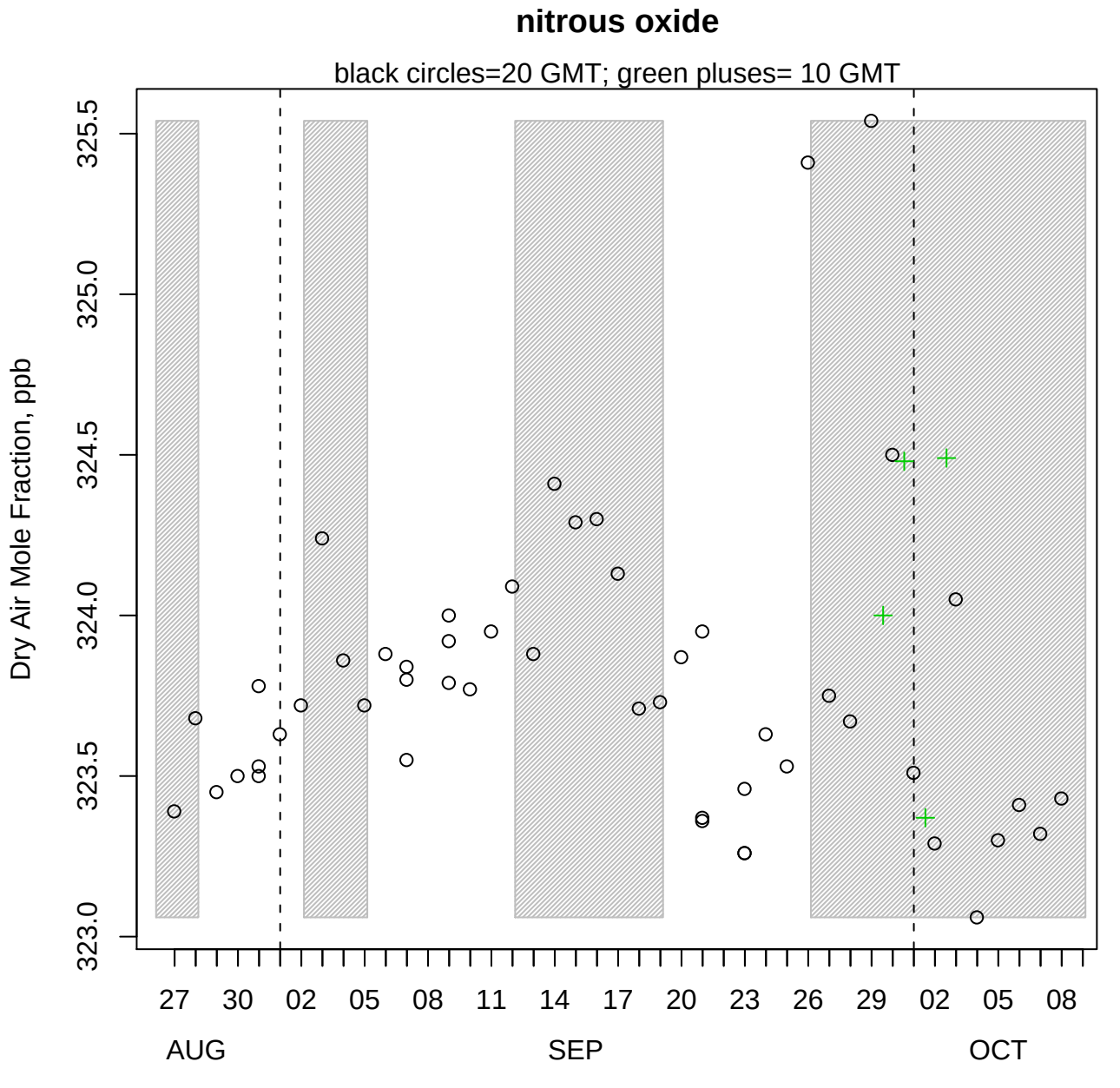
nitrous oxide
black circles=20 GMT; green pluses= 10 GMT
Dry Air Mole Fraction, ppb
325.5
325.0
324.5
324.0
323.5
323.0
27
30
02
05
08
11
14
17
20
23
26
29
02
05
08
AUG
SEP
OCT

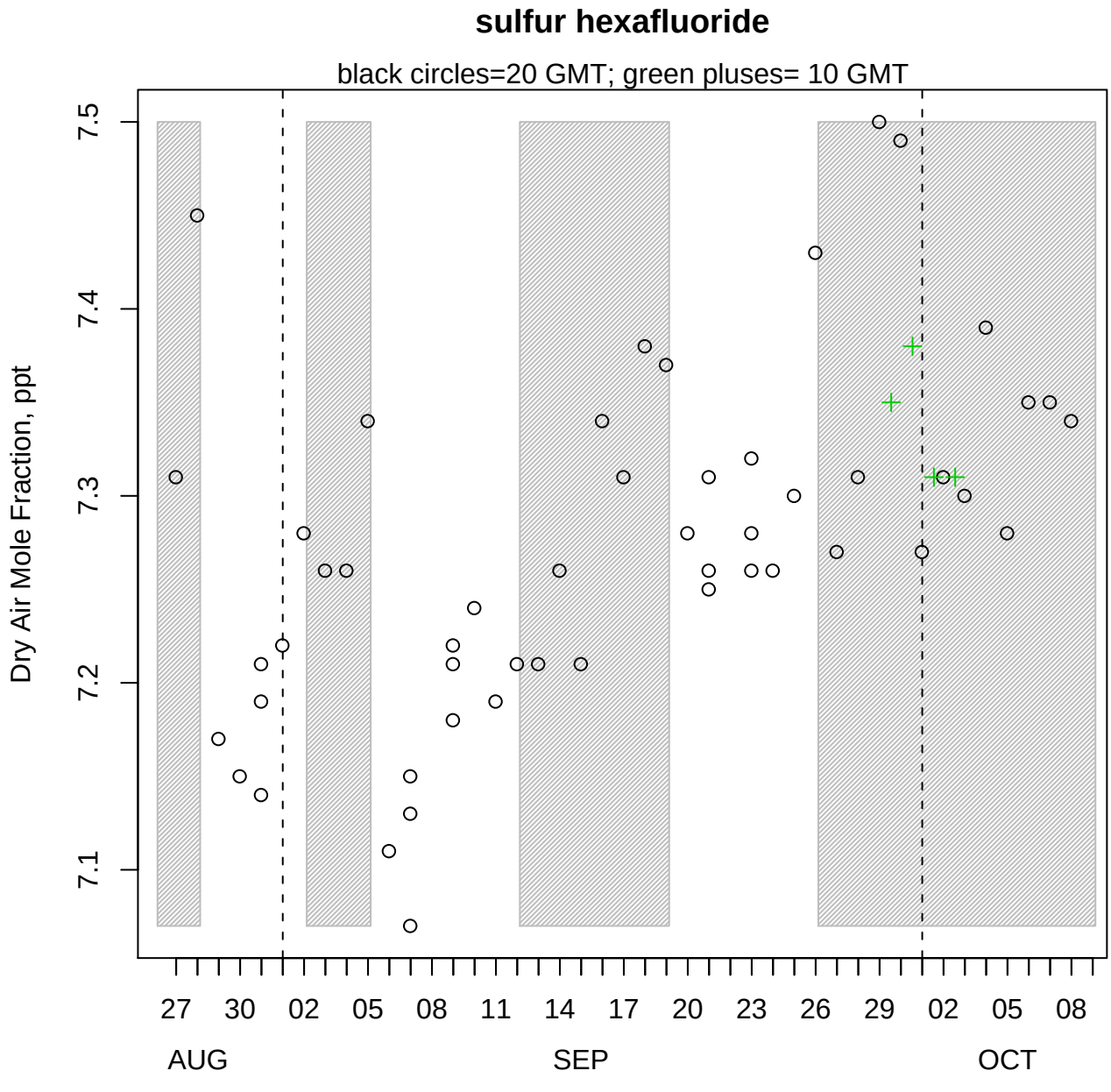
sulfur hexafluoride
black circles=20 GMT; green pluses= 10 GMT
Dry Air Mole Fraction, ppt
7.1
7.2
7.3
7.4
7.5
27
30
02
05
08
11
14
17
20
23
26
29
02
05
08
AUG
SEP
OCT

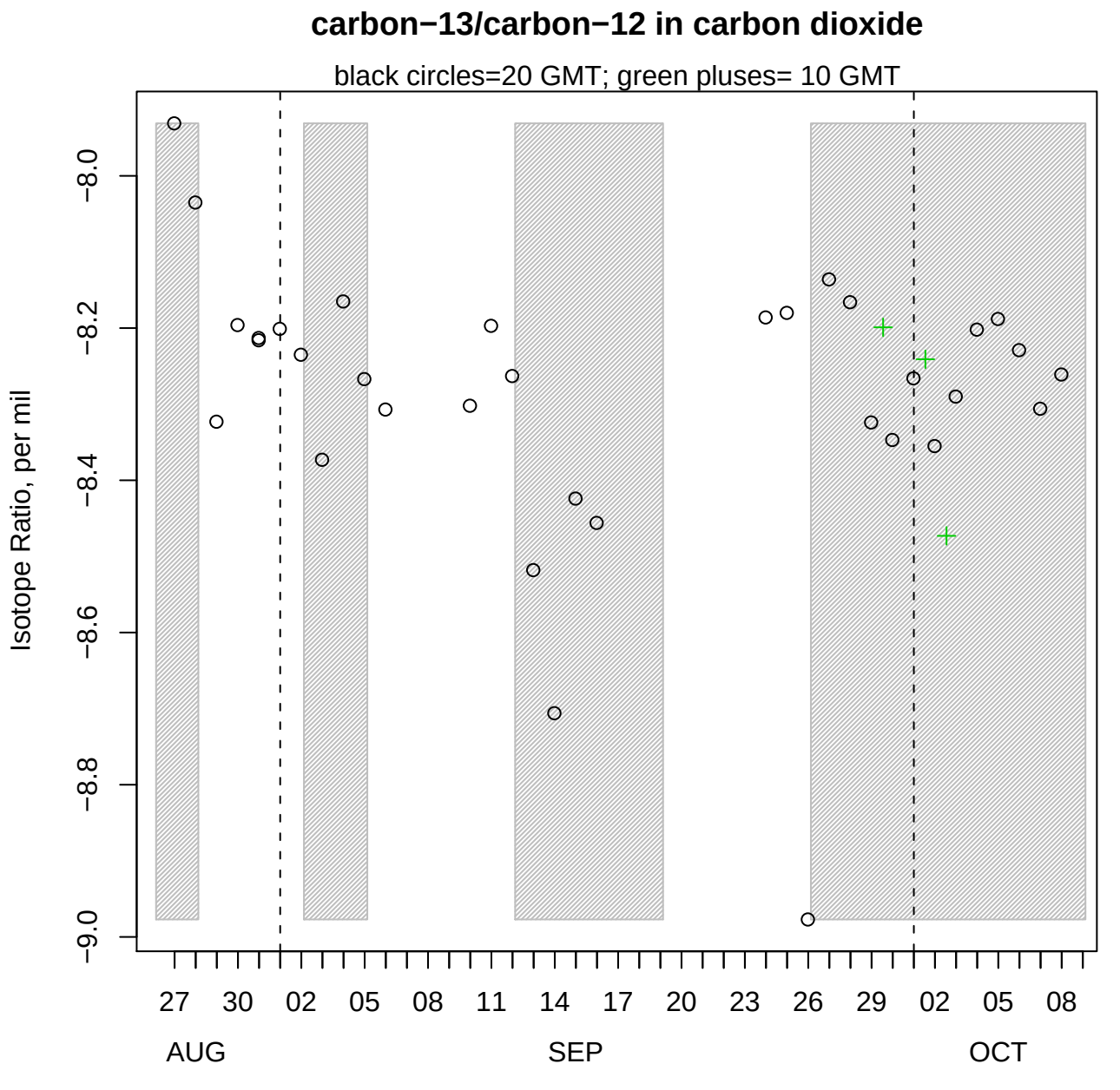
carbon−13/carbon−12 in carbon dioxide
black circles=20 GMT; green pluses= 10 GMT
Isotope Ratio, per mil
−8.0
−8.2
−8.4
−8.6
−8.8
−9.0
27
30
02
05
08
11
14
17
20
23
26
29
02
05
08
AUG
SEP
OCT

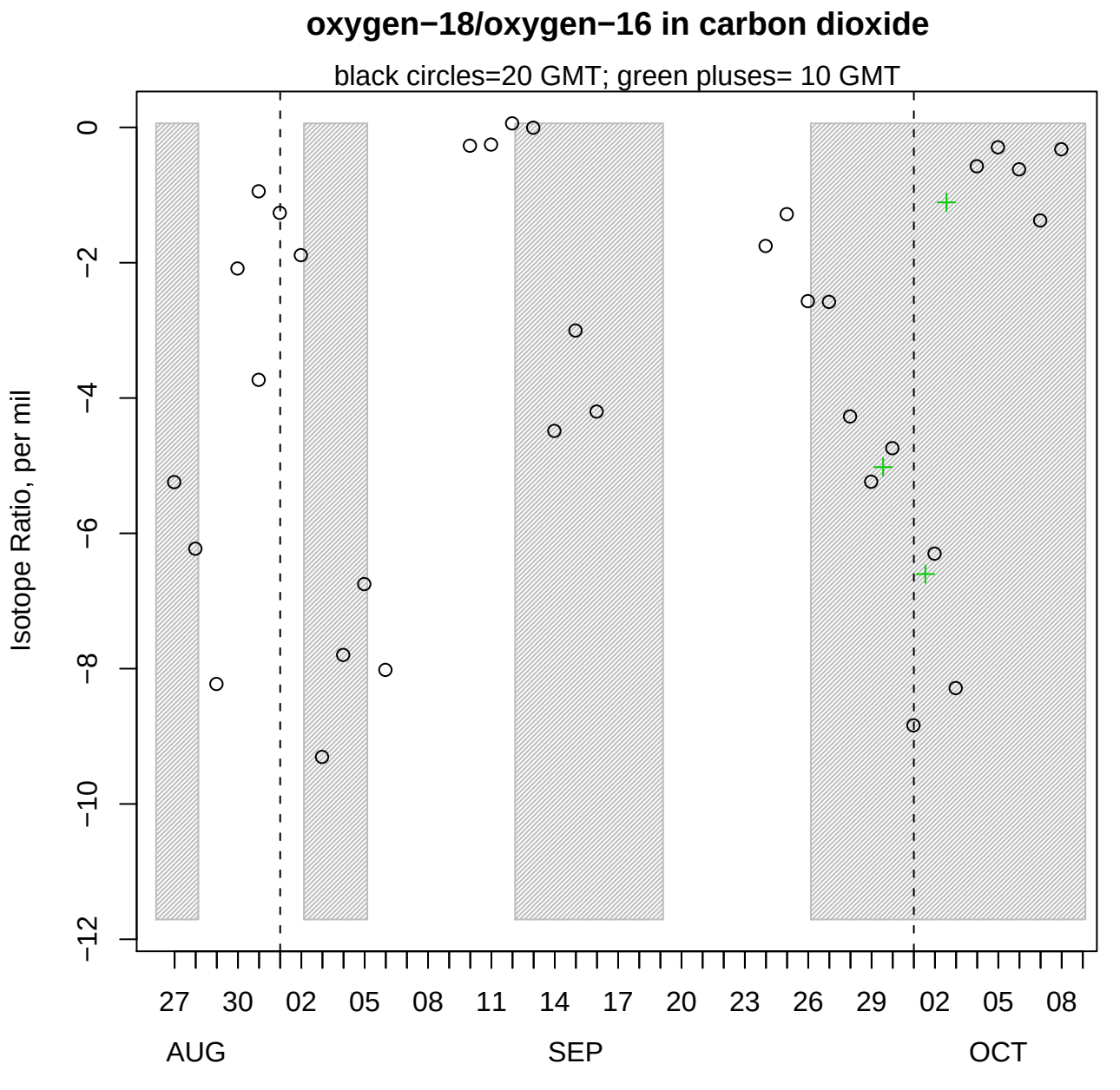
oxygen−18/oxygen−16 in carbon dioxide
black circles=20 GMT; green pluses= 10 GMT
Isotope Ratio, per mil
0
−2
−4
−6
−8
−10
−12
27
30
02
05
08
11
14
17
20
23
26
29
02
05
08
AUG
SEP
OCT

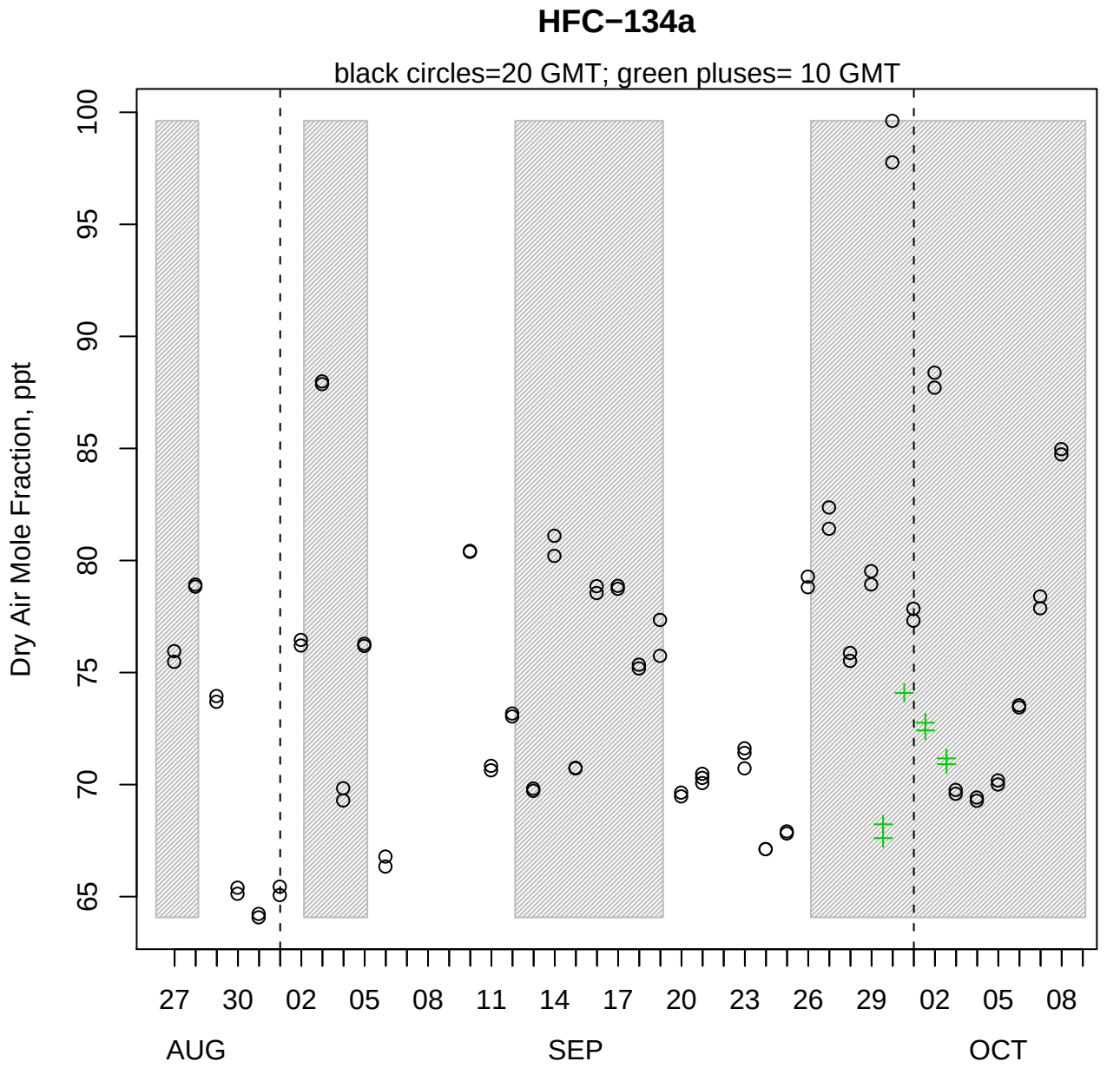
HFC−134a
black circles=20 GMT; green pluses= 10 GMT
Dry Air Mole Fraction, ppt
100
95
90
85
80
75
70
65
27
30
02
05
08
11
14
17
20
23
26
29
02
05
08
AUG
SEP
OCT

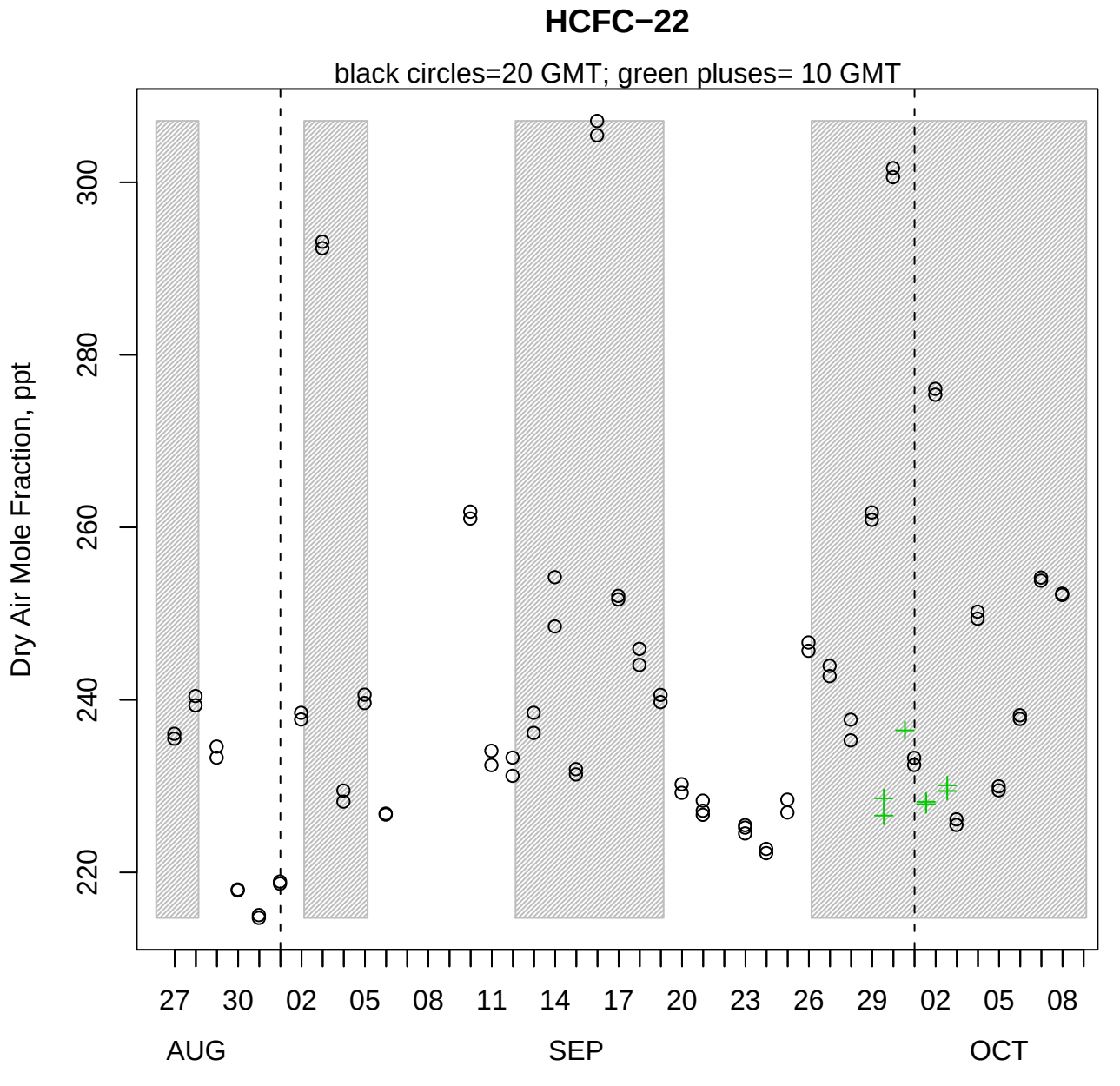
HCFC−22
black circles=20 GMT; green pluses= 10 GMT
Dry Air Mole Fraction, ppt
220
240
260
280
300
27
30
02
05
08
11
14
17
20
23
26
29
02
05
08
AUG
SEP
OCT

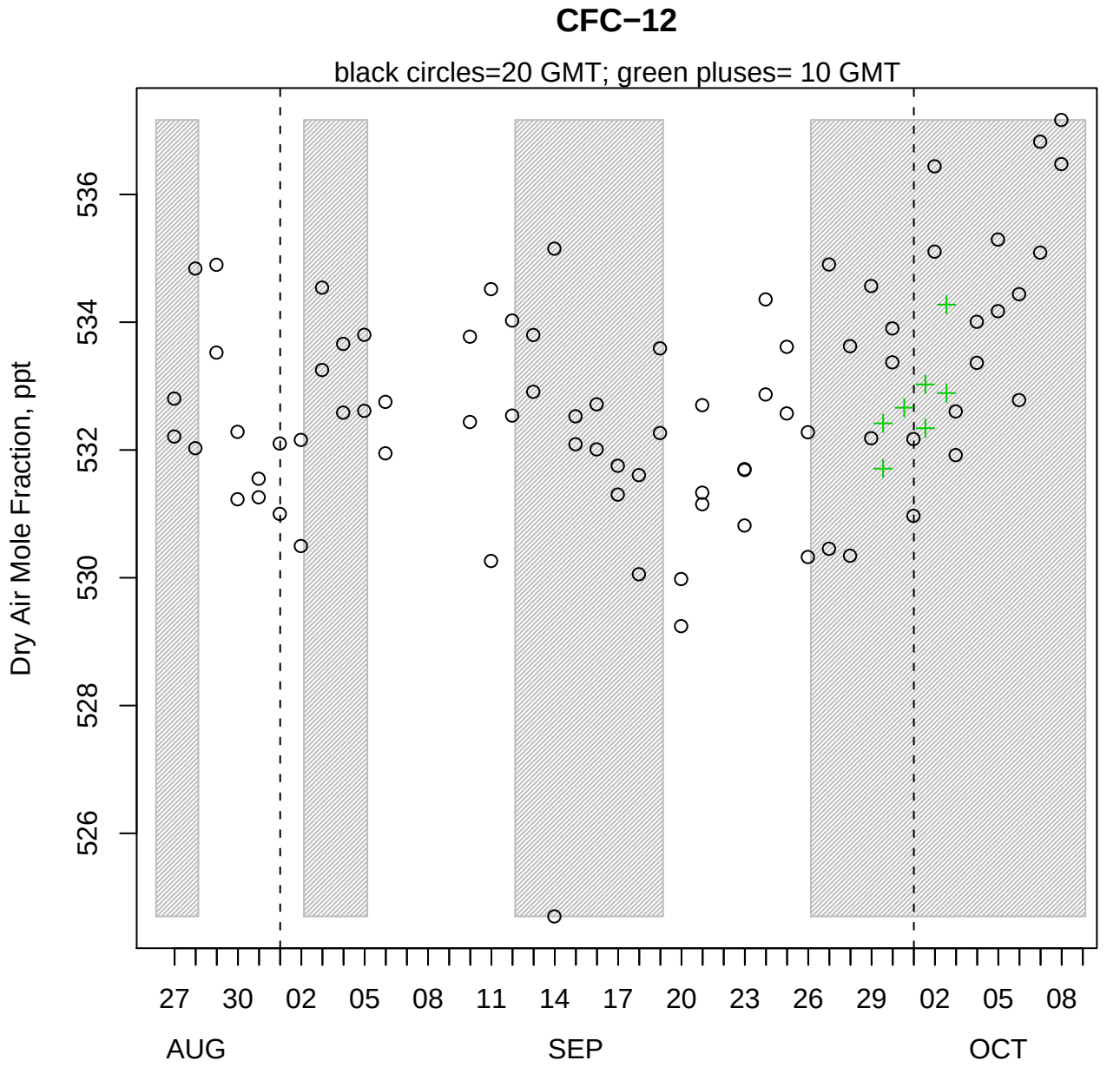
CFC−12
black circles=20 GMT; green pluses= 10 GMT
Dry Air Mole Fraction, ppt
526
528
530
532
534
536
27
30
02
05
08
11
14
17
20
23
26
29
02
05
08
AUG
SEP
OCT

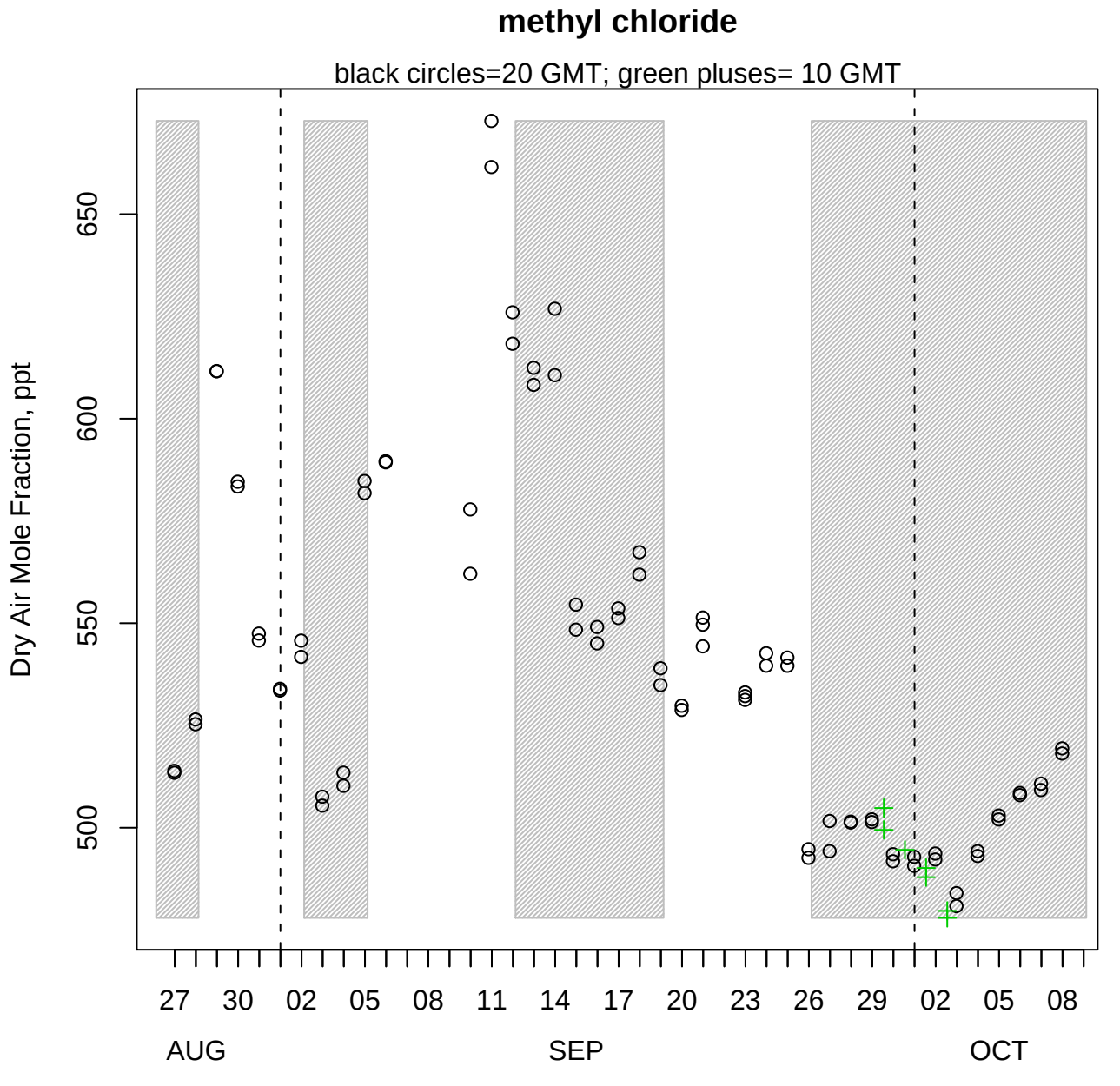
methyl chloride
black circles=20 GMT; green pluses= 10 GMT
Dry Air Mole Fraction, ppt
500
550
600
650
27
30
02
05
08
11
14
17
20
23
26
29
02
05
08
AUG
SEP
OCT

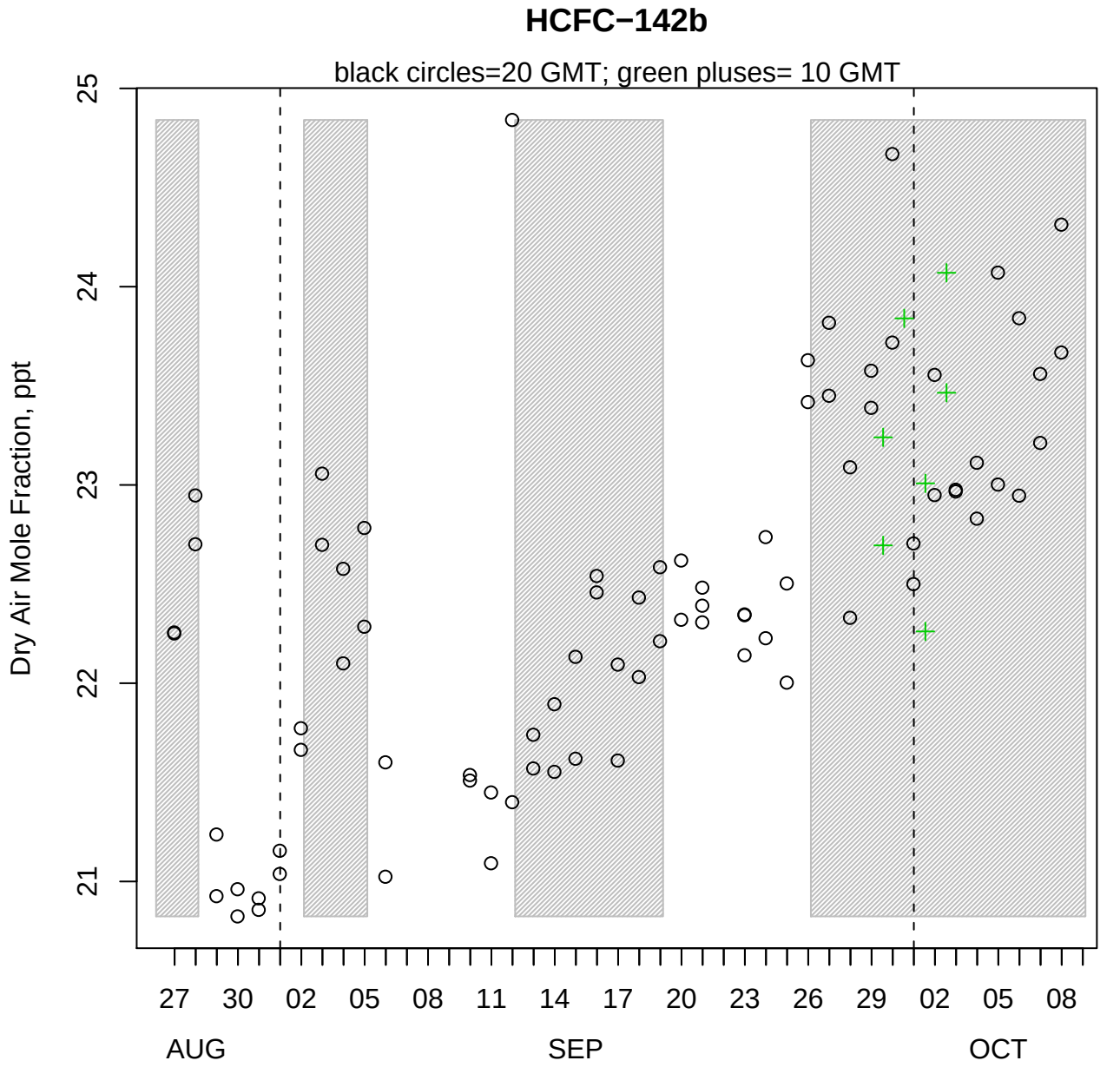
HCFC−142b
black circles=20 GMT; green pluses= 10 GMT
Dry Air Mole Fraction, ppt
25
24
23
22
21
27
30
02
05
08
11
14
17
20
23
26
29
02
05
08
AUG
SEP
OCT

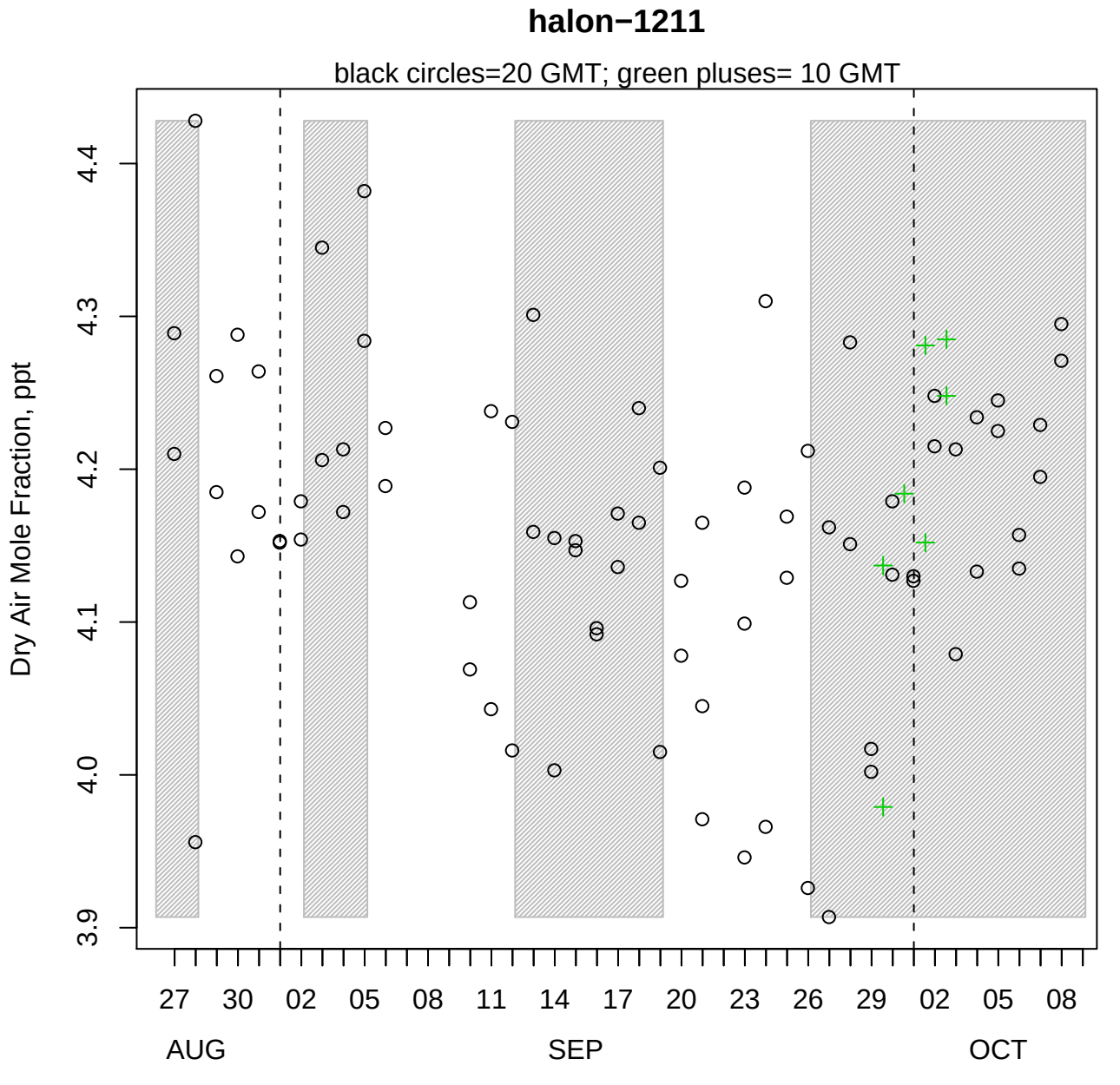
halon−1211
black circles=20 GMT; green pluses= 10 GMT
Dry Air Mole Fraction, ppt
3.9
4.0
4.1
4.2
4.3
4.4
27
30
02
05
08
11
14
17
20
23
26
29
02
05
08
AUG
SEP
OCT

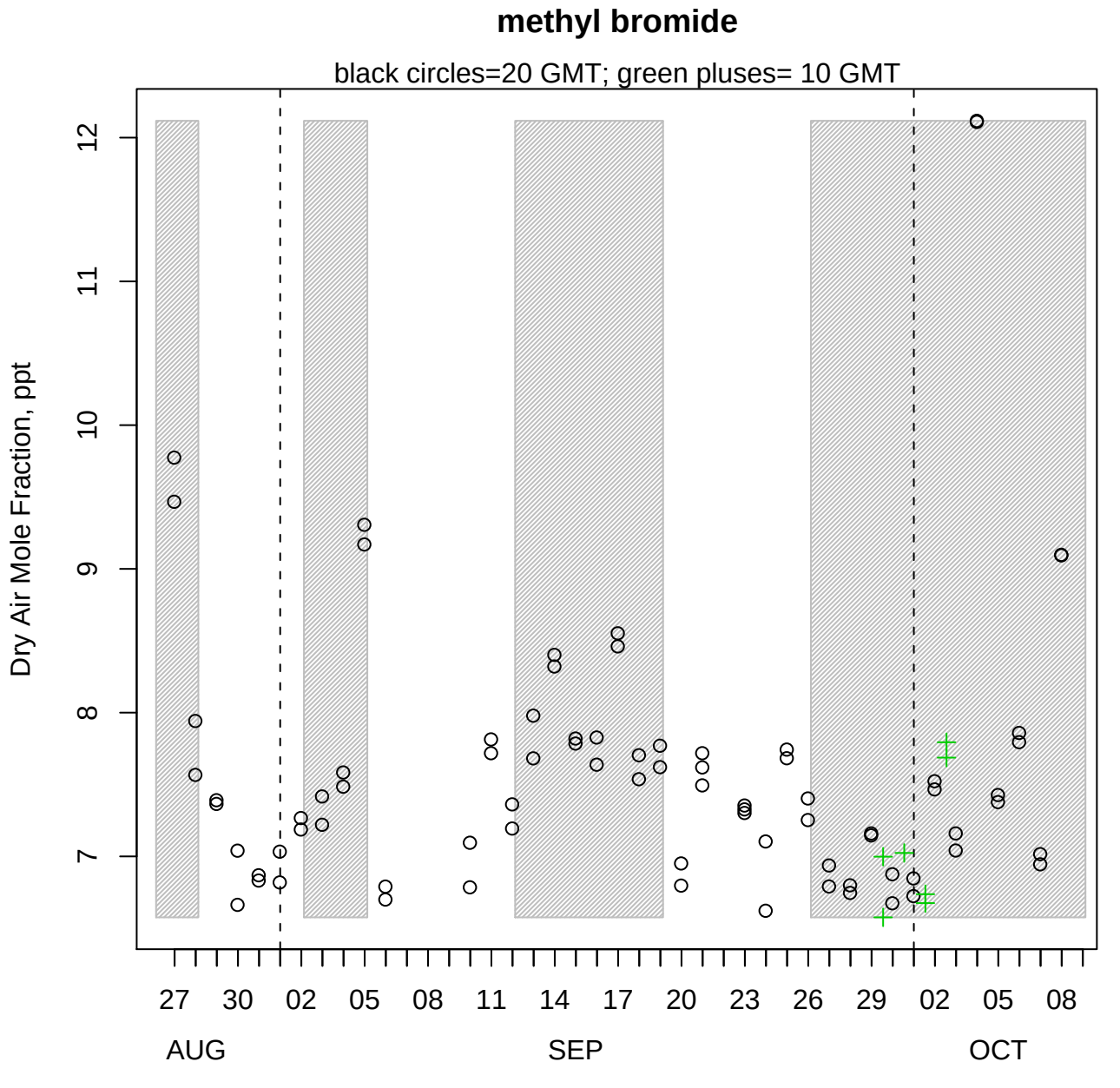
methyl bromide
black circles=20 GMT; green pluses= 10 GMT
Dry Air Mole Fraction, ppt
7
8
9
10
11
12
27
30
02
05
08
11
14
17
20
23
26
29
02
05
08
AUG
SEP
OCT

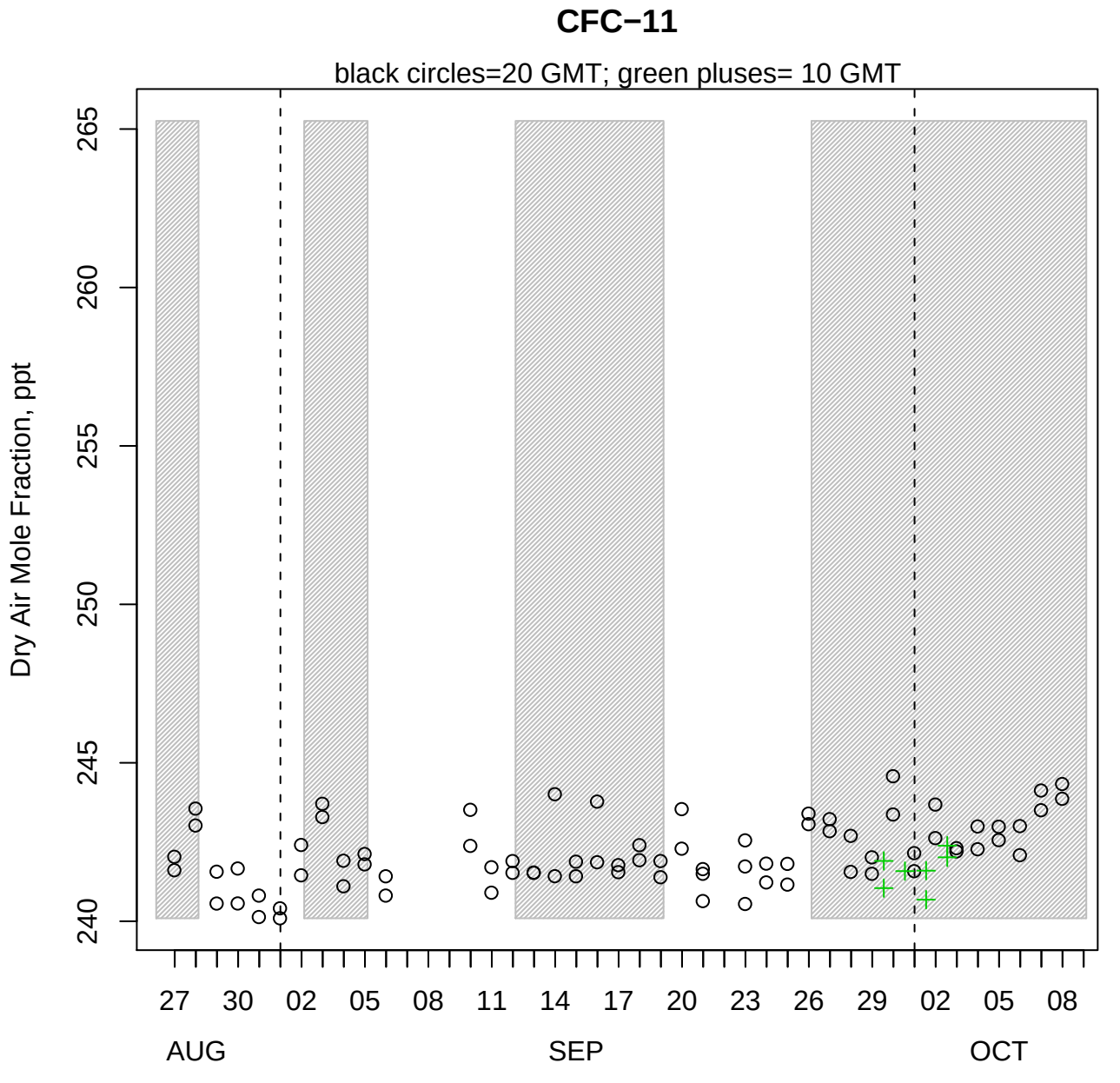
CFC−11
black circles=20 GMT; green pluses= 10 GMT
Dry Air Mole Fraction, ppt
265
260
255
250
245
240
27
30
02
05
08
11
14
17
20
23
26
29
02
05
08
AUG
SEP
OCT

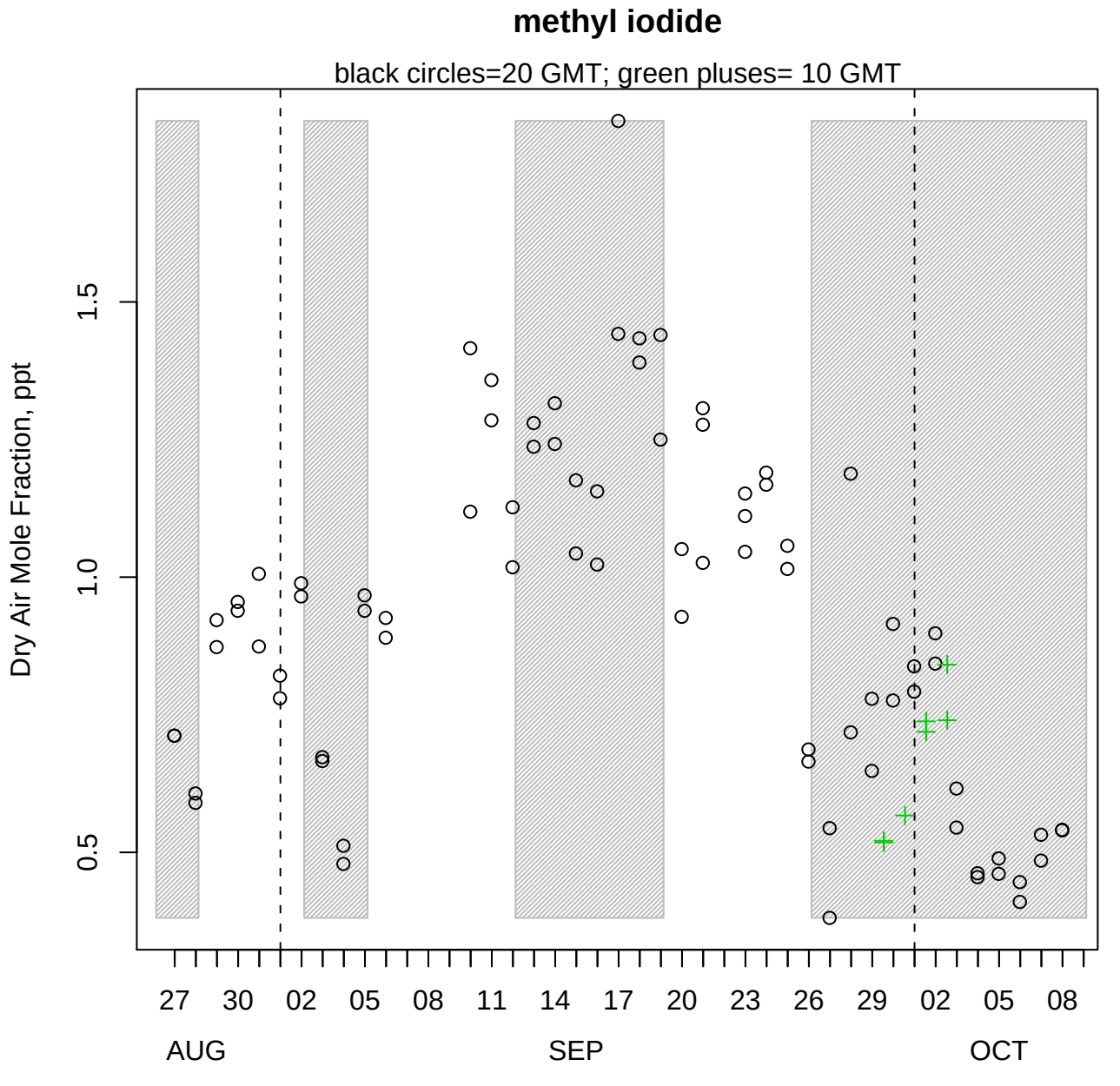
methyl iodide
black circles=20 GMT; green pluses= 10 GMT
Dry Air Mole Fraction, ppt
0.5
1.0
1.5
27
30
02
05
08
11
14
17
20
23
26
29
02
05
08
AUG
SEP
OCT

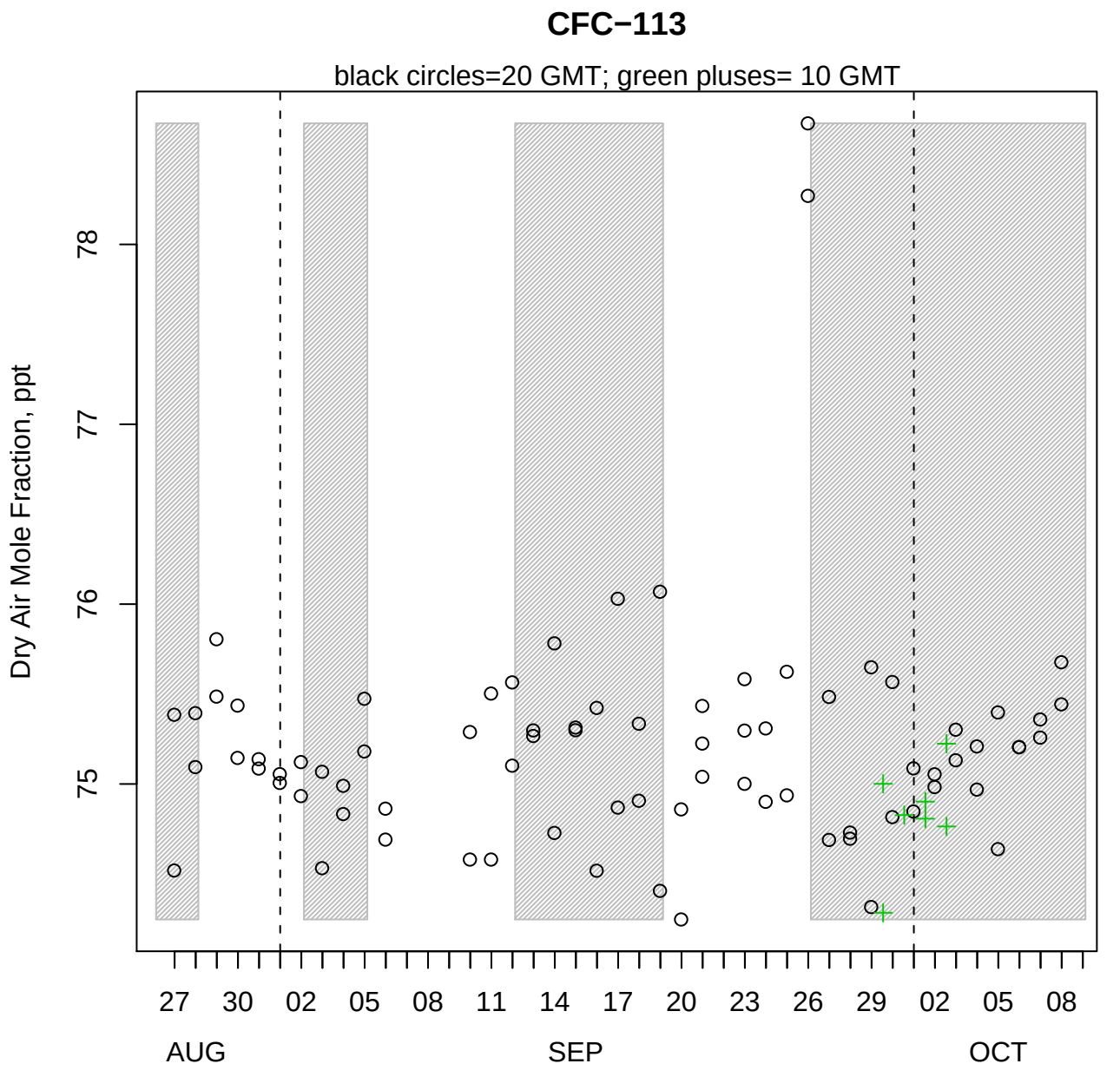
CFC−113
black circles=20 GMT; green pluses= 10 GMT
Dry Air Mole Fraction, ppt
75
76
77
78
27
30
02
05
08
11
14
17
20
23
26
29
02
05
08
AUG
SEP
OCT

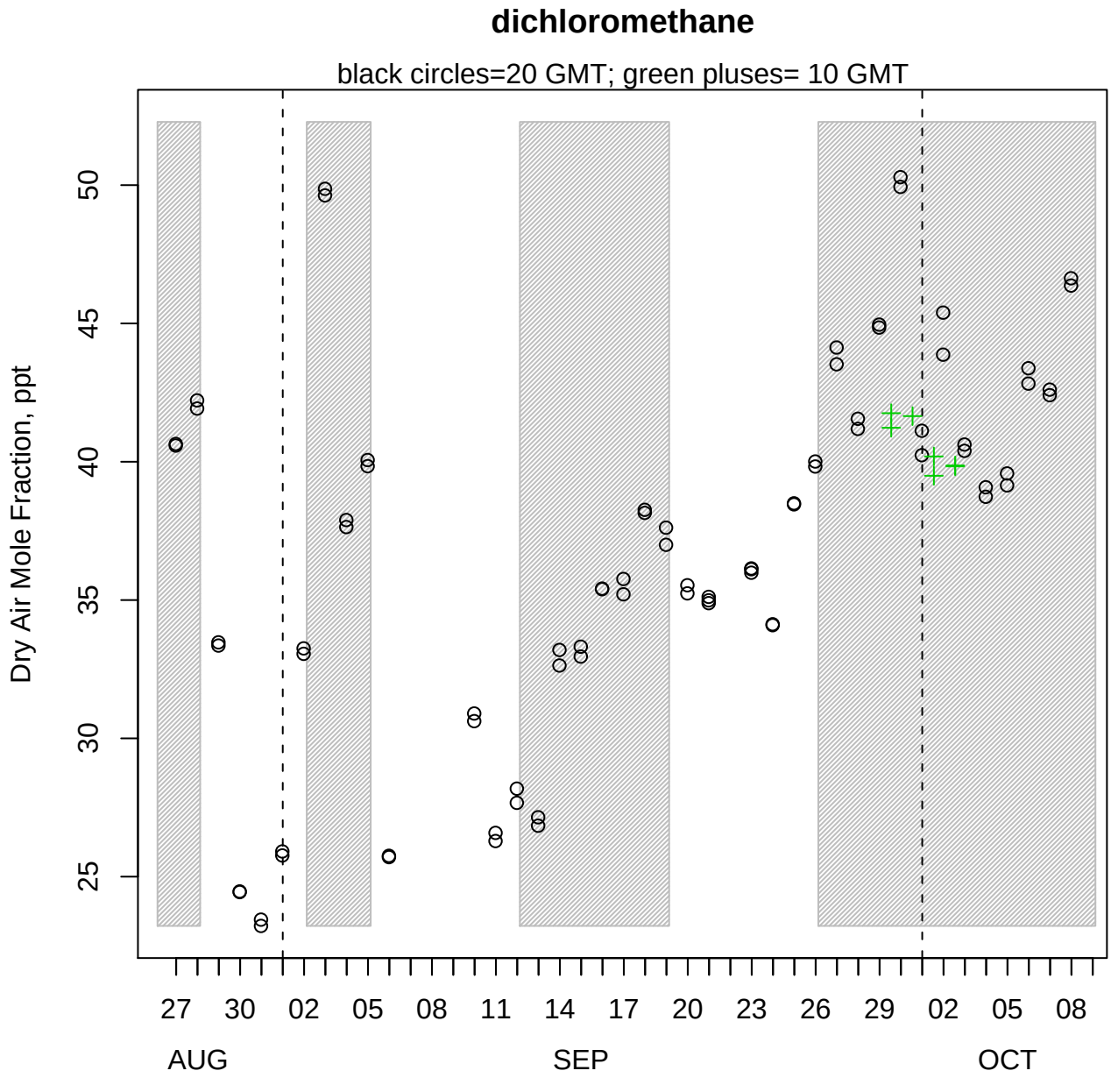
dichloromethane
black circles=20 GMT; green pluses= 10 GMT
Dry Air Mole Fraction, ppt
25
30
35
40
45
50
27
30
02
05
08
11
14
17
20
23
26
29
02
05
08
AUG
SEP
OCT

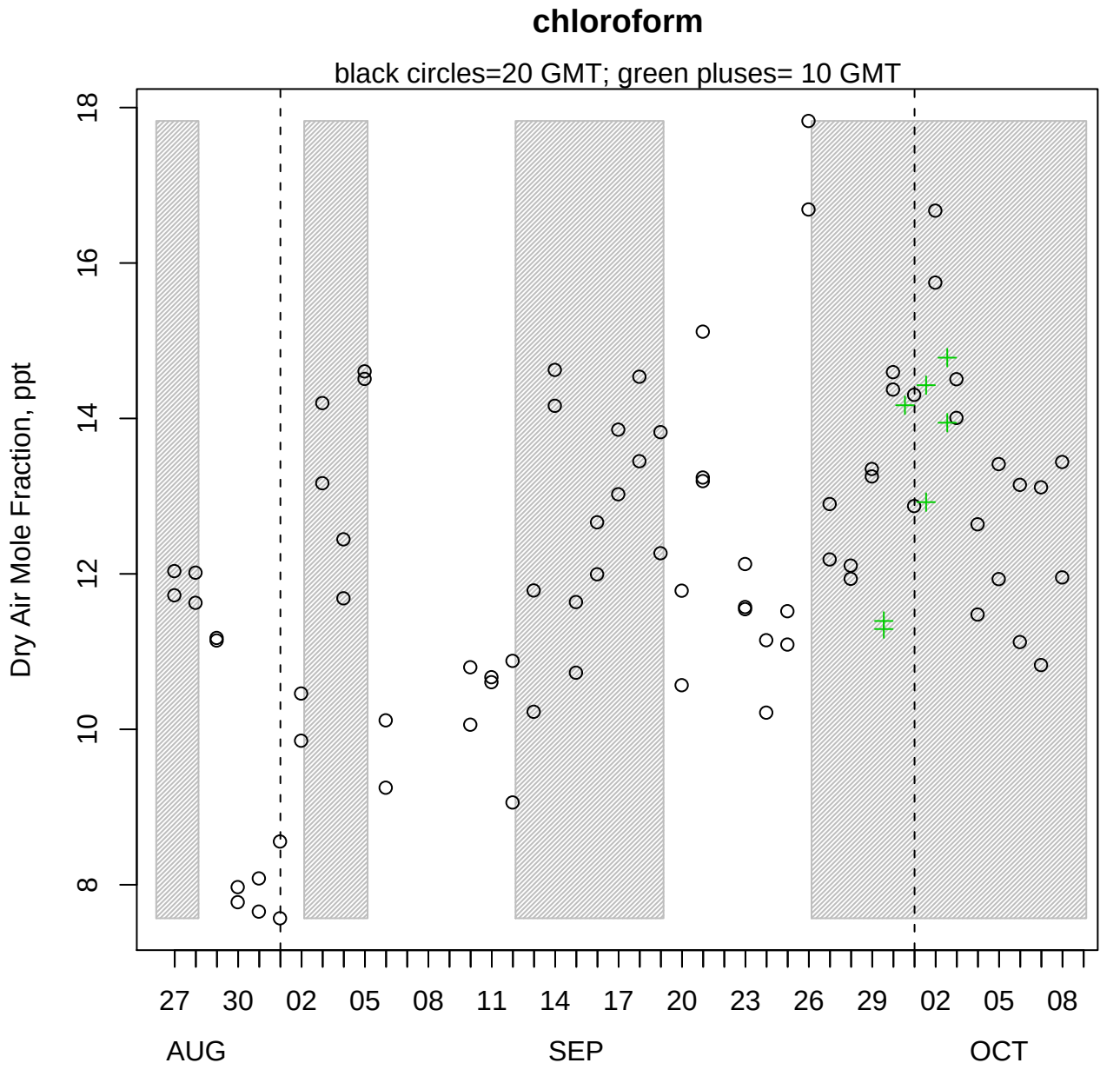
chloroform
black circles=20 GMT; green pluses= 10 GMT
Dry Air Mole Fraction, ppt
8
10
12
14
16
18
27
30
02
05
08
11
14
17
20
23
26
29
02
05
08
AUG
SEP
OCT

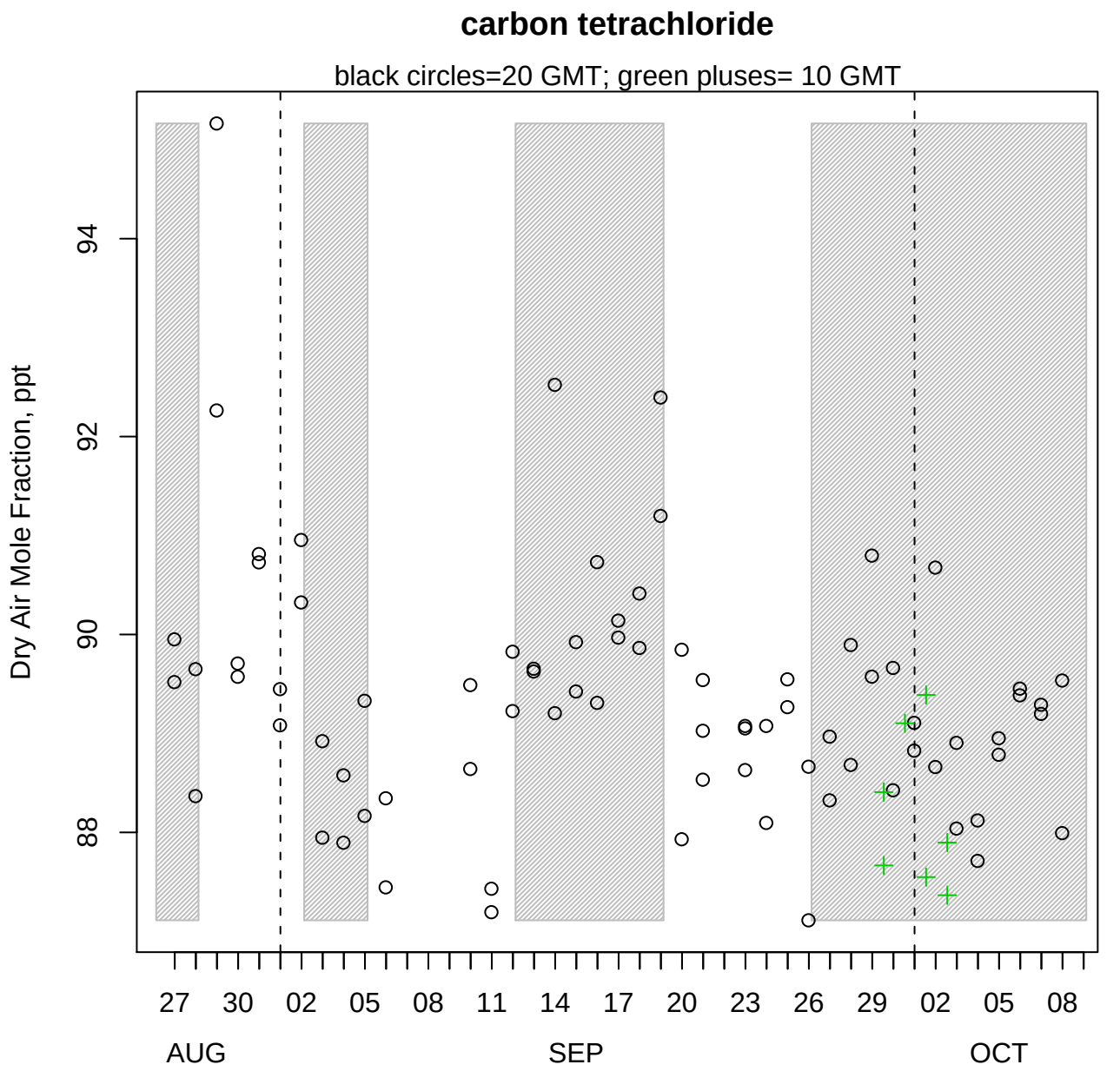
carbon tetrachloride
black circles=20 GMT; green pluses= 10 GMT
Dry Air Mole Fraction, ppt
88
90
92
94
27
30
02
05
08
11
14
17
20
23
26
29
02
05
08
AUG
SEP
OCT

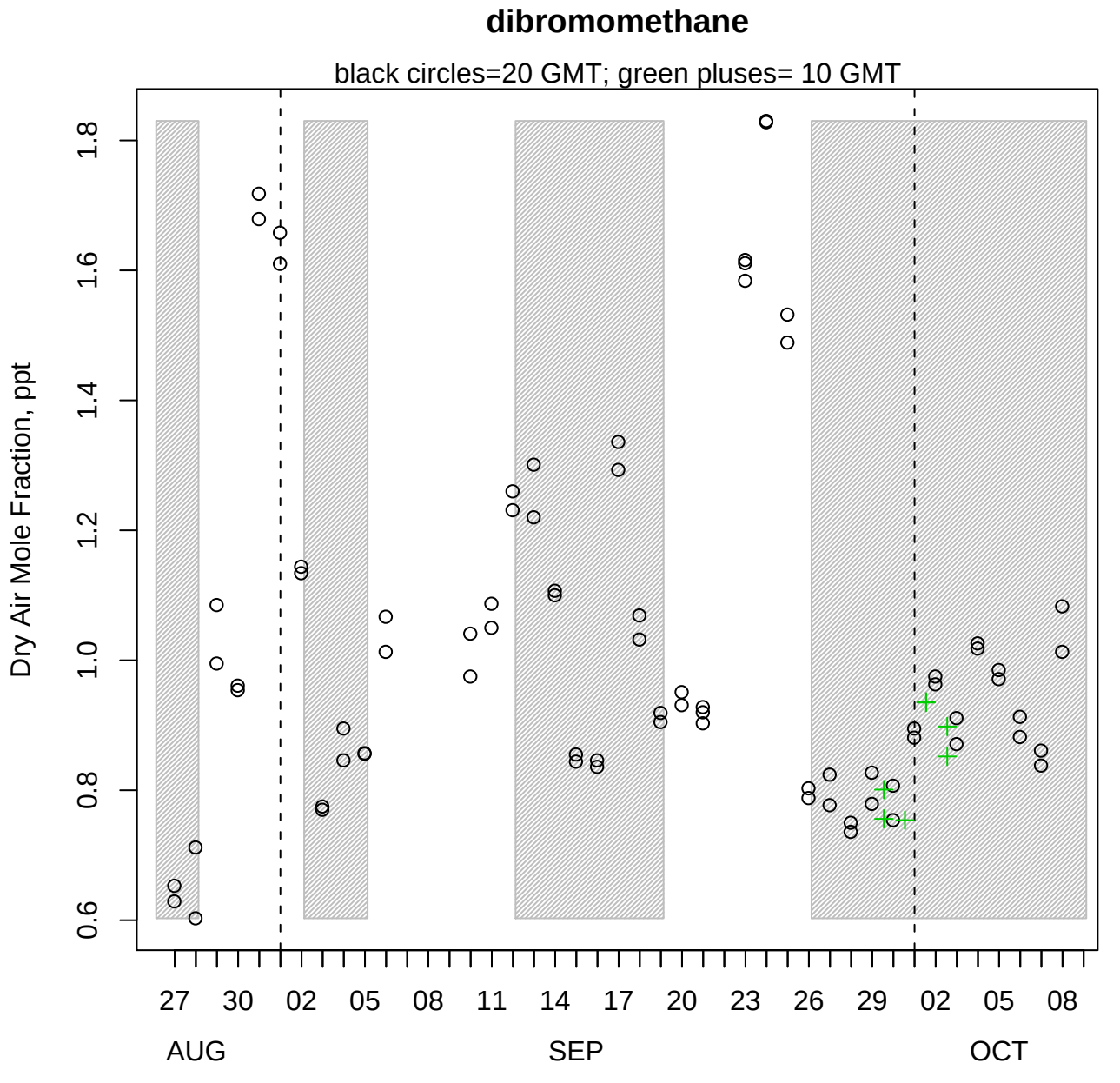
dibromomethane
black circles=20 GMT; green pluses= 10 GMT
Dry Air Mole Fraction, ppt
0.6
0.8
1.0
1.2
1.4
1.6
1.8
27
30
02
05
08
11
14
17
20
23
26
29
02
05
08
AUG
SEP
OCT

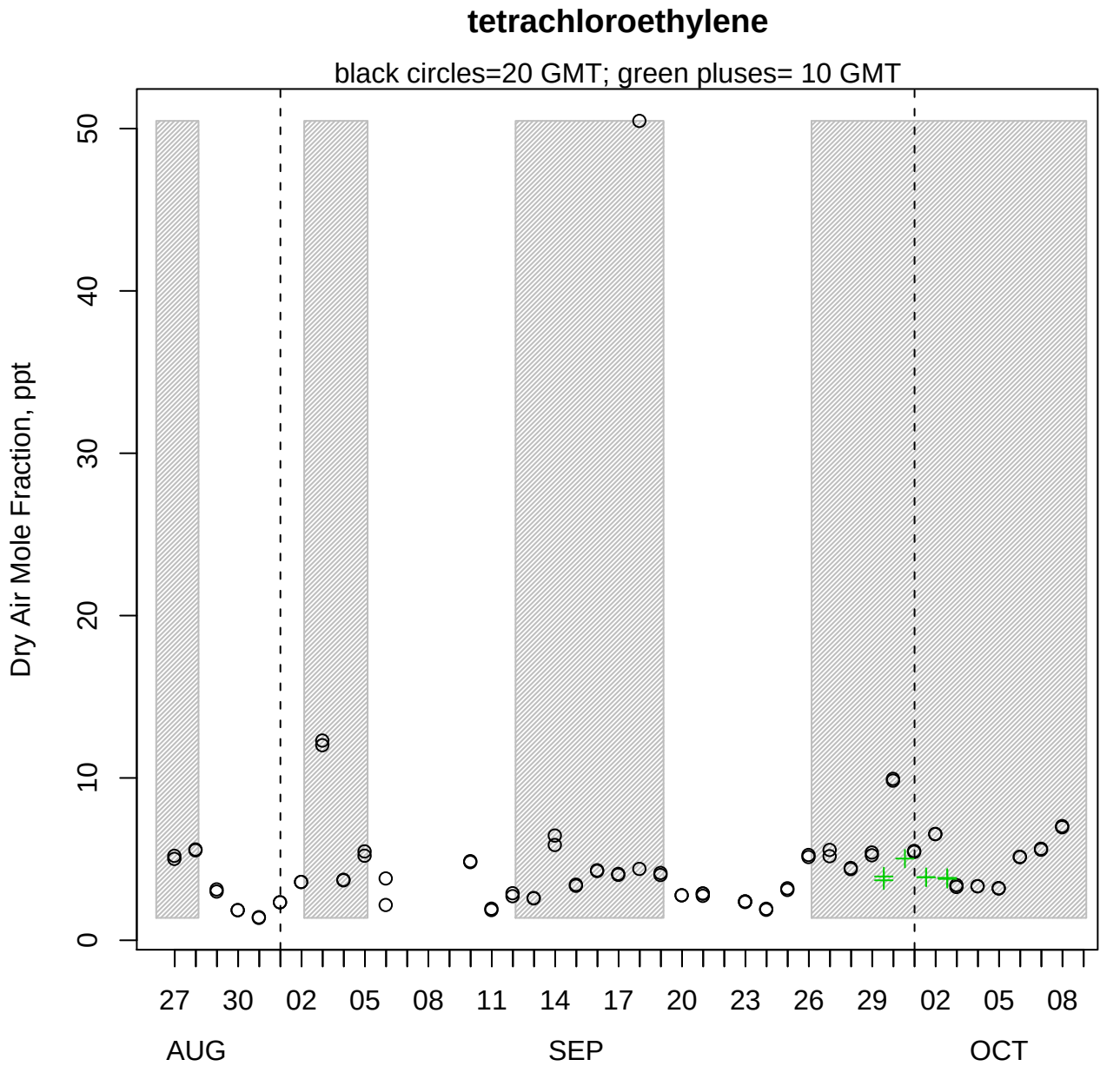
tetrachloroethylene
black circles=20 GMT; green pluses= 10 GMT
Dry Air Mole Fraction, ppt
0
10
20
30
40
50
27
30
02
05
08
11
14
17
20
23
26
29
02
05
08
AUG
SEP
OCT

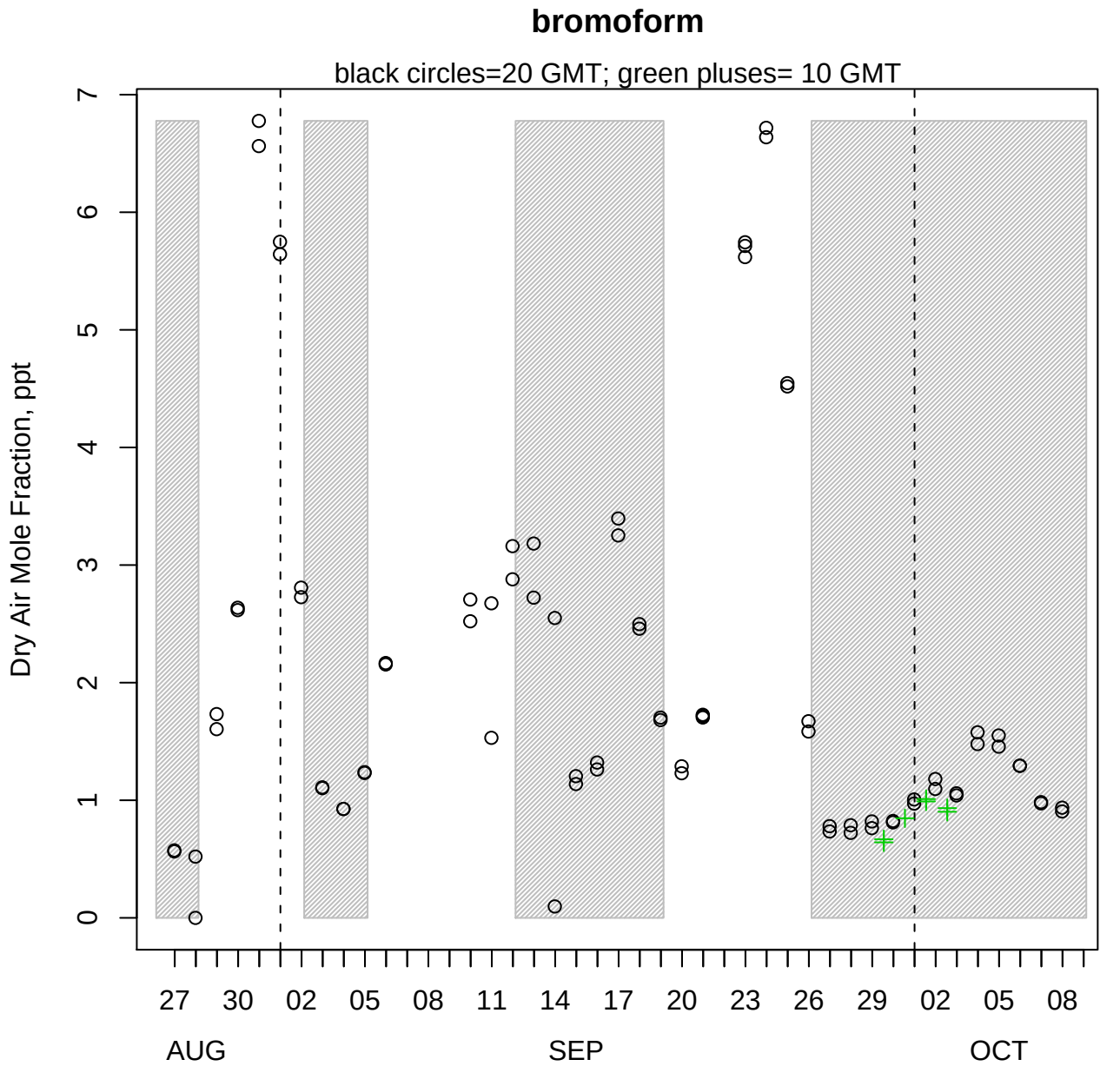
bromoform
black circles=20 GMT; green pluses= 10 GMT
Dry Air Mole Fraction, ppt
0
1
2
3
4
5
6
7
27
30
02
05
08
11
14
17
20
23
26
29
02
05
08
AUG
SEP
OCT

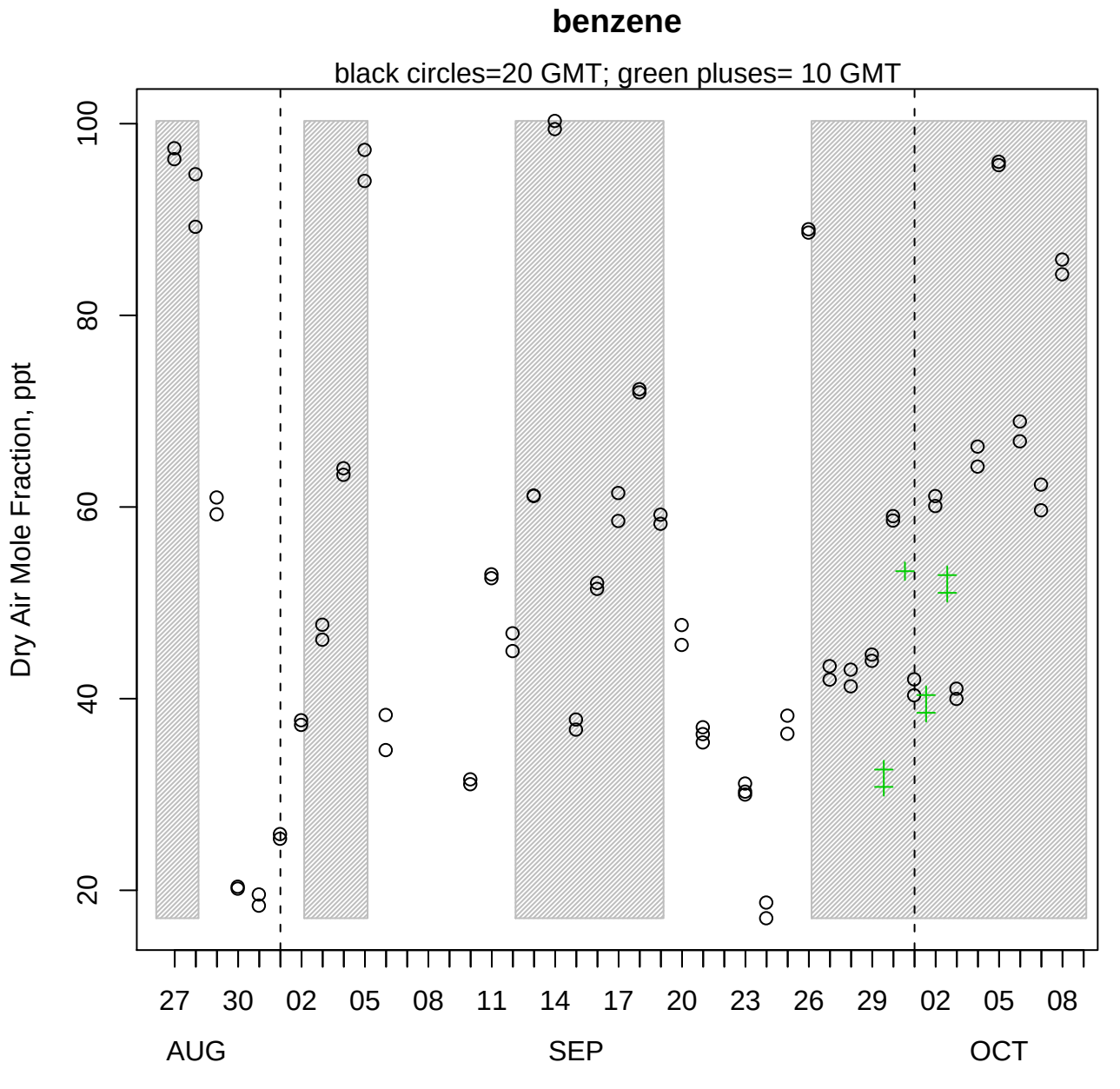
benzene
black circles=20 GMT; green pluses= 10 GMT
Dry Air Mole Fraction, ppt
100
80
60
40
20
27
30
02
05
08
11
14
17
20
23
26
29
02
05
08
AUG
SEP
OCT

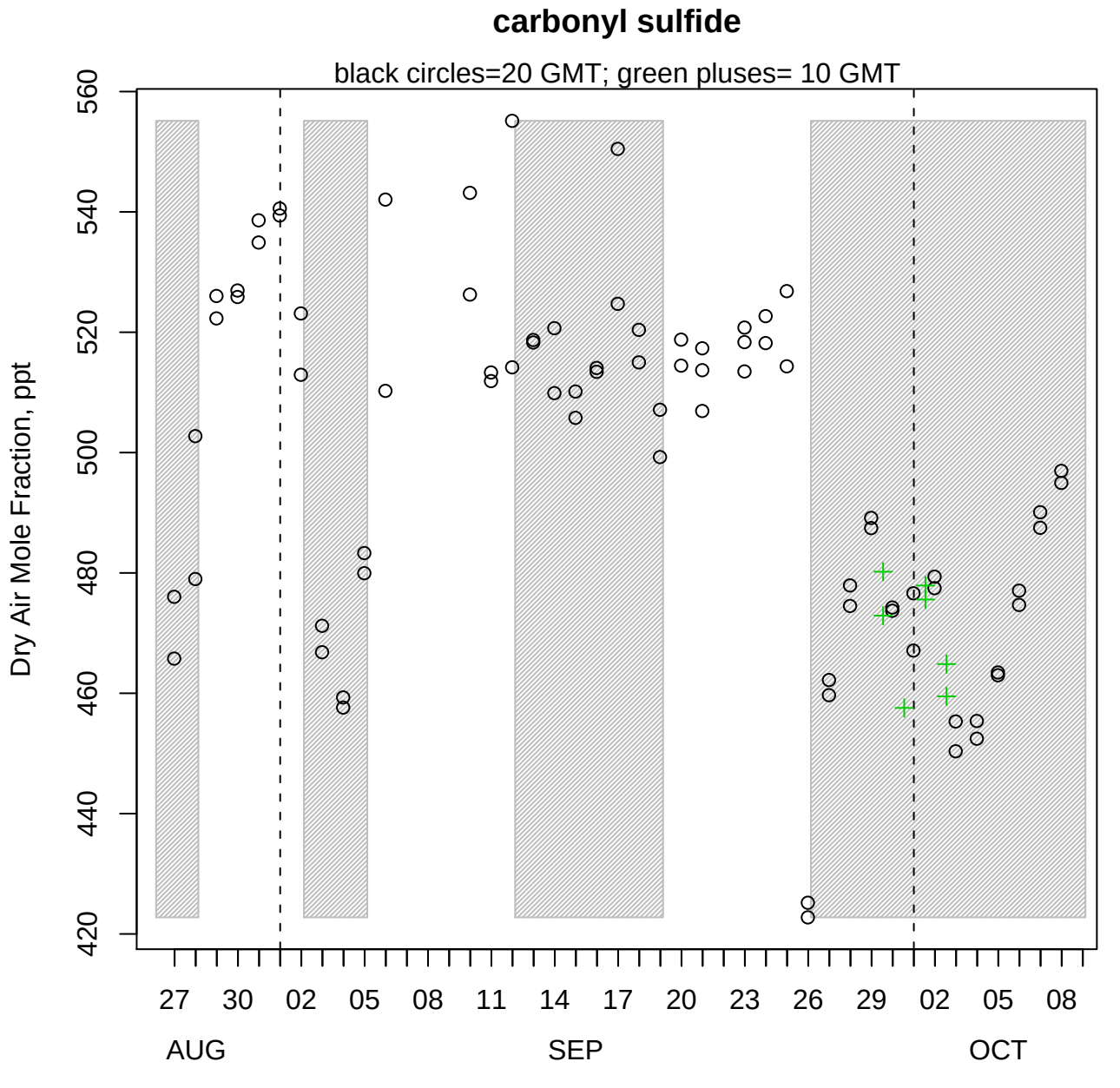
carbonyl sulfide
black circles=20 GMT; green pluses= 10 GMT
Dry Air Mole Fraction, ppt
560
540
520
500
480
460
440
420
27
30
02
05
08
11
14
17
20
23
26
29
02
05
08
AUG
SEP
OCT

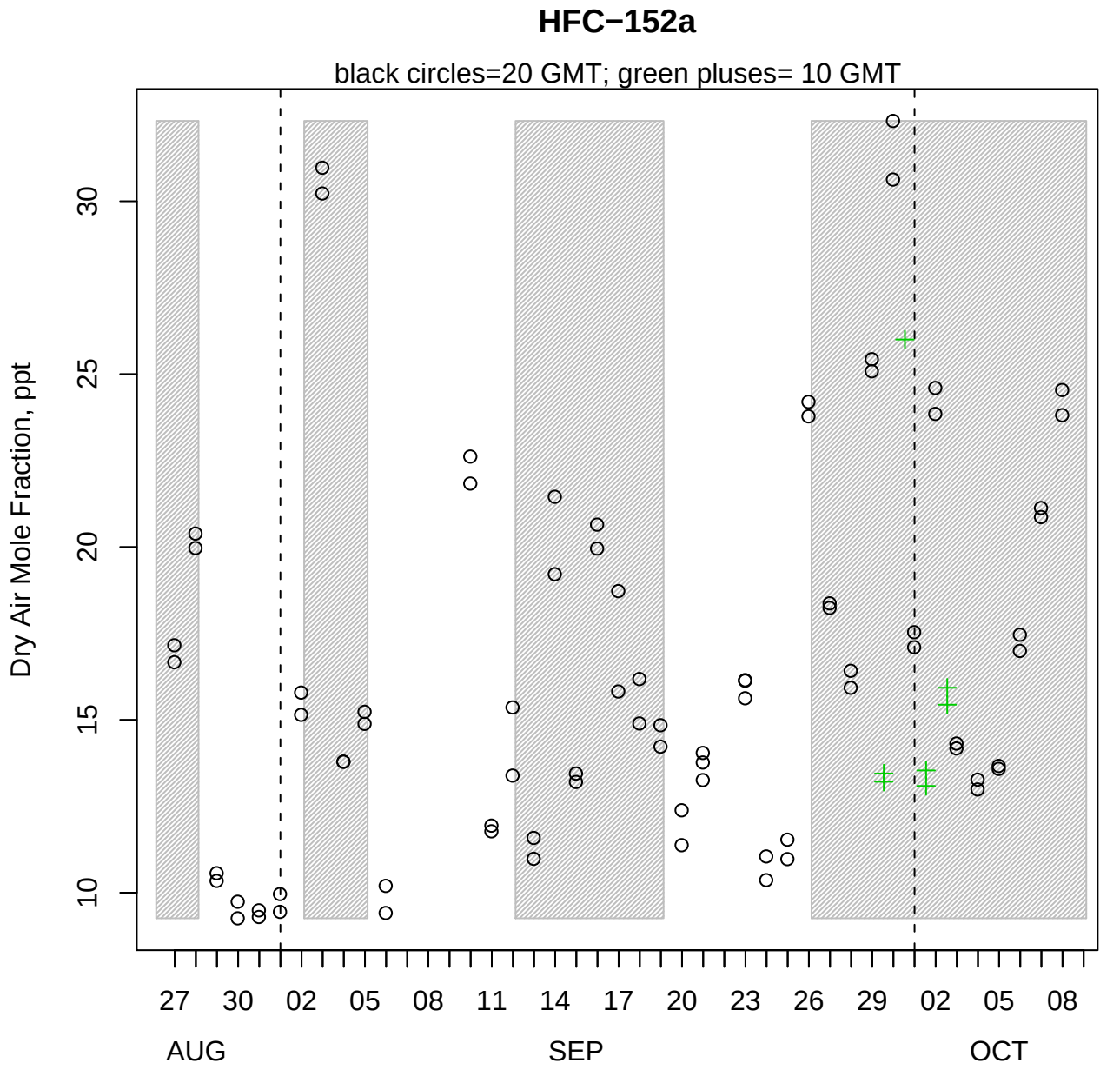
HFC−152a
black circles=20 GMT; green pluses= 10 GMT
Dry Air Mole Fraction, ppt
10
15
20
25
30
27
30
02
05
08
11
14
17
20
23
26
29
02
05
08
AUG
SEP
OCT

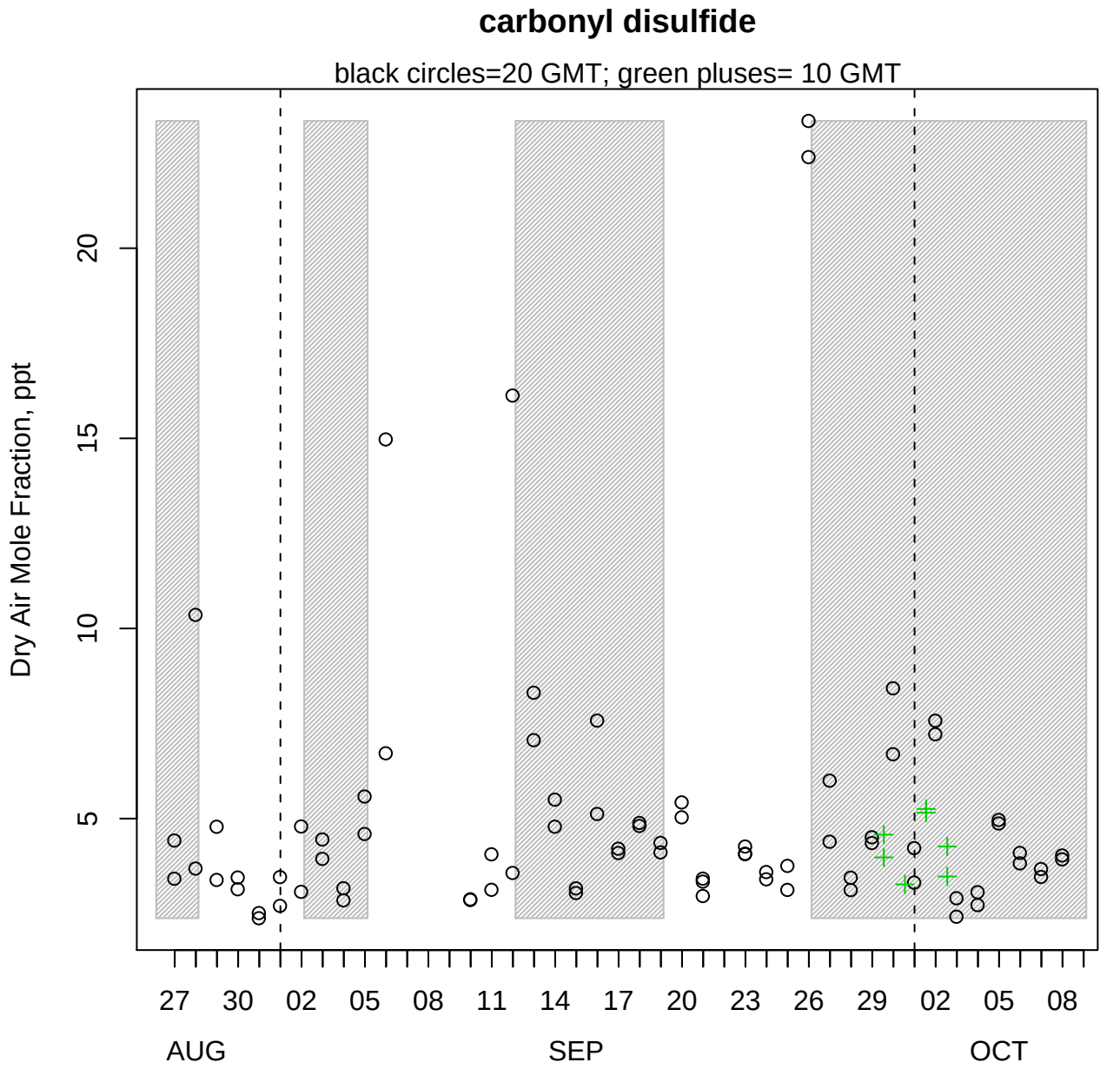
carbonyl disulfide
black circles=20 GMT; green pluses= 10 GMT
Dry Air Mole Fraction, ppt
5
10
15
20
27
30
02
05
08
11
14
17
20
23
26
29
02
05
08
AUG
SEP
OCT

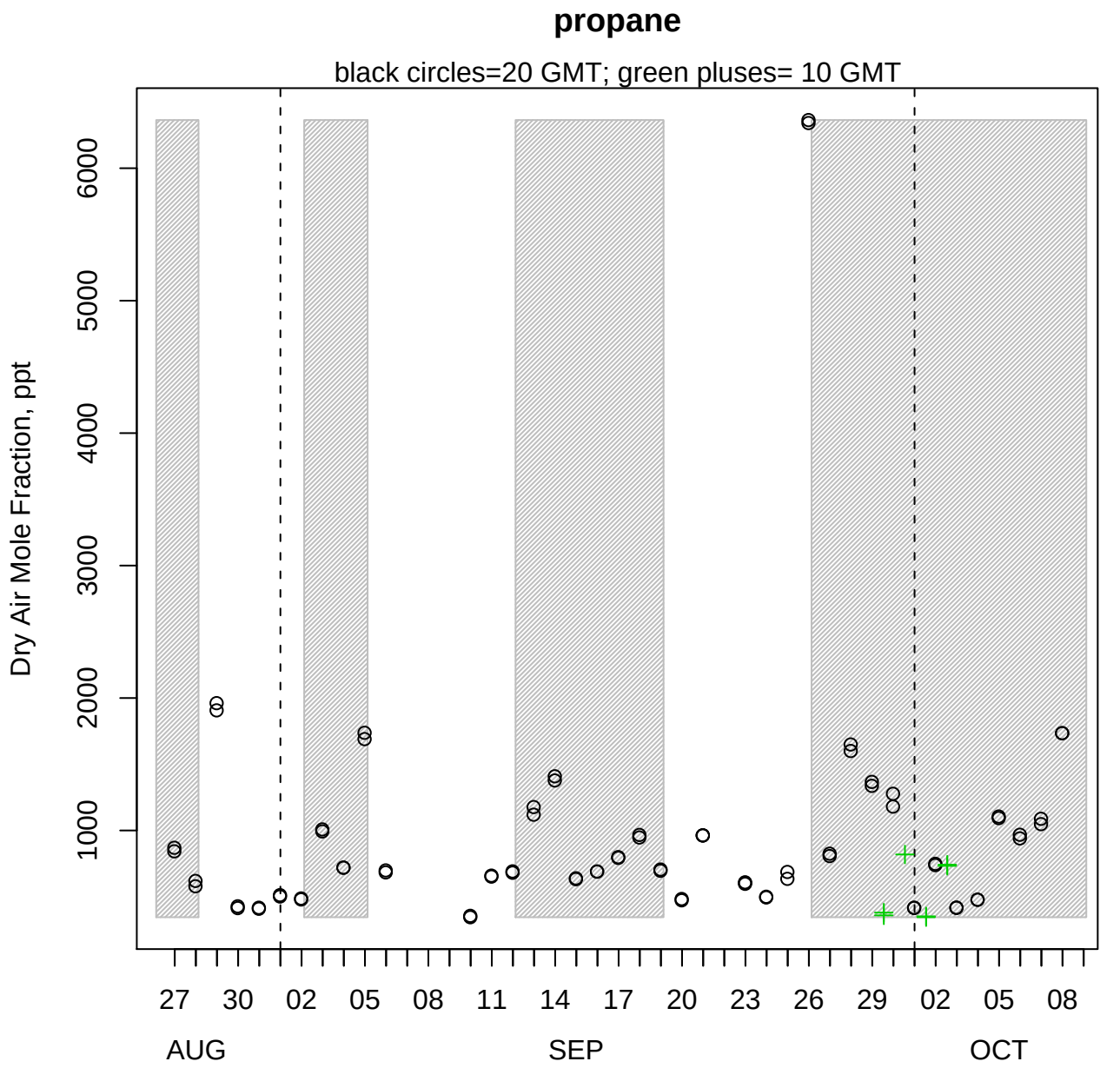
propane
black circles=20 GMT; green pluses= 10 GMT
Dry Air Mole Fraction, ppt
1000
2000
3000
4000
5000
6000
27
30
02
05
08
11
14
17
20
23
26
29
02
05
08
AUG
SEP
OCT

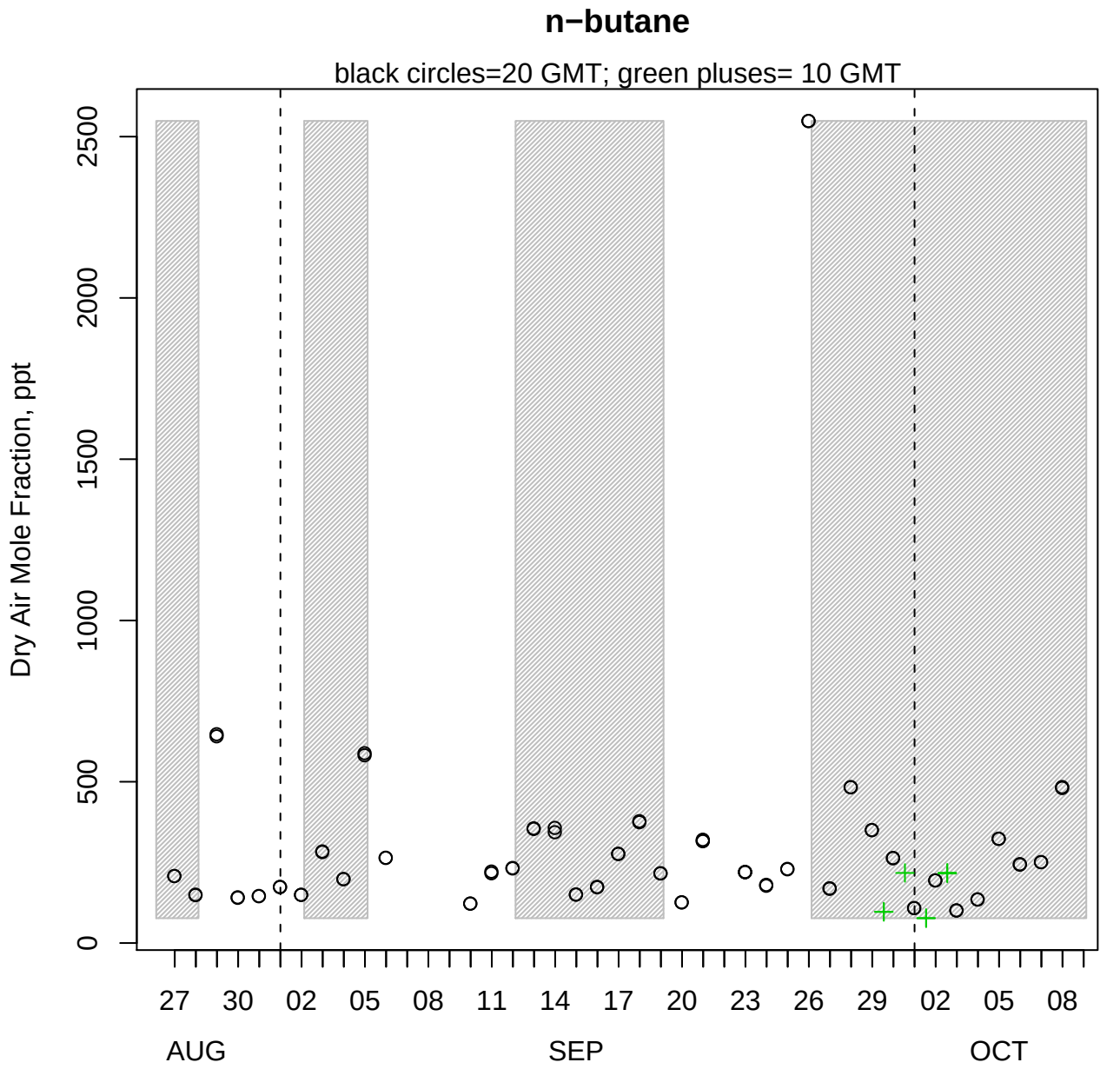
n−butane
black circles=20 GMT; green pluses= 10 GMT
Dry Air Mole Fraction, ppt
0
500
1000
1500
2000
2500
27
30
02
05
08
11
14
17
20
23
26
29
02
05
08
AUG
SEP
OCT

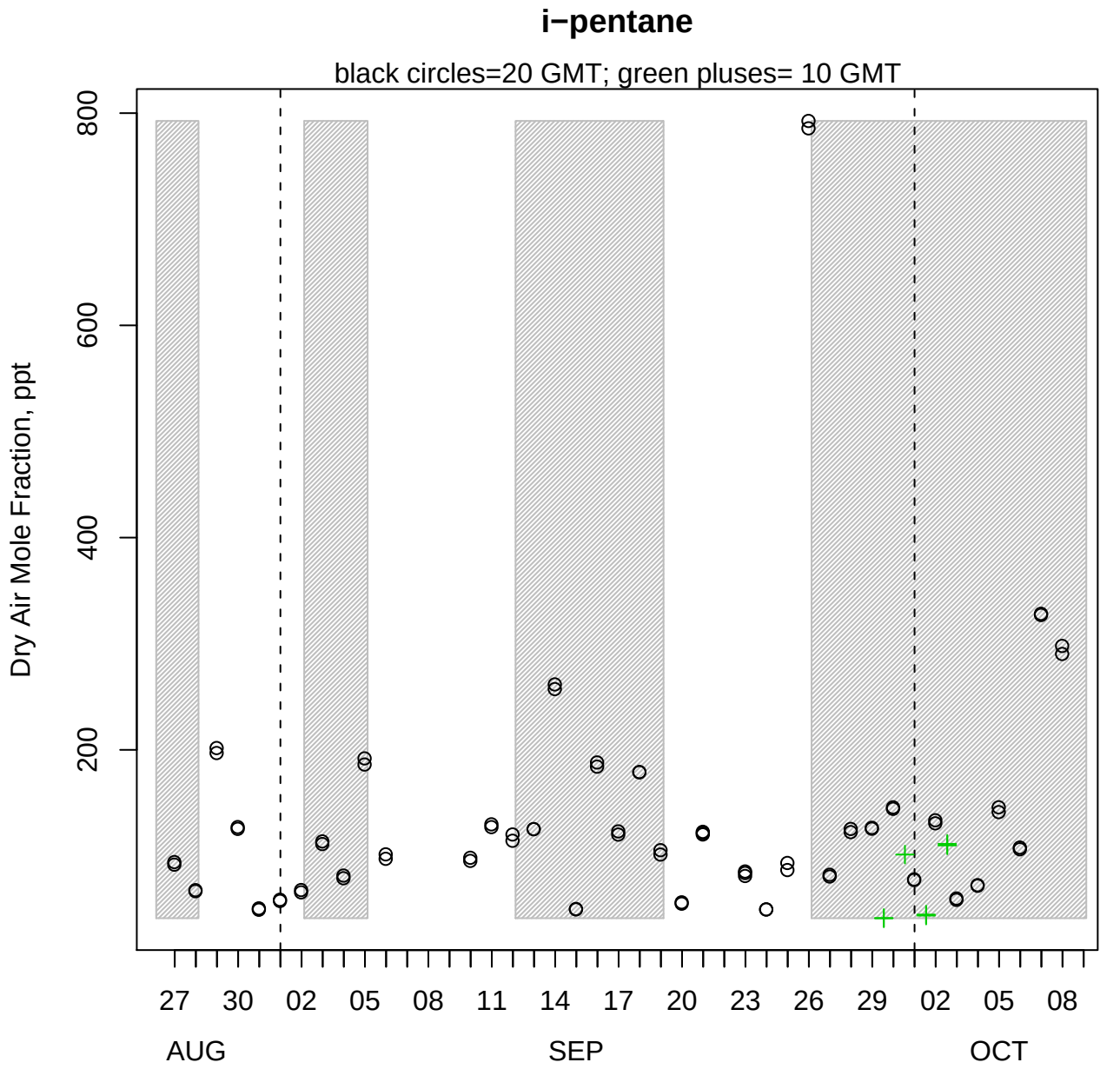
i−pentane
black circles=20 GMT; green pluses= 10 GMT
Dry Air Mole Fraction, ppt
800
600
400
200
27
30
02
05
08
11
14
17
20
23
26
29
02
05
08
AUG
SEP
OCT

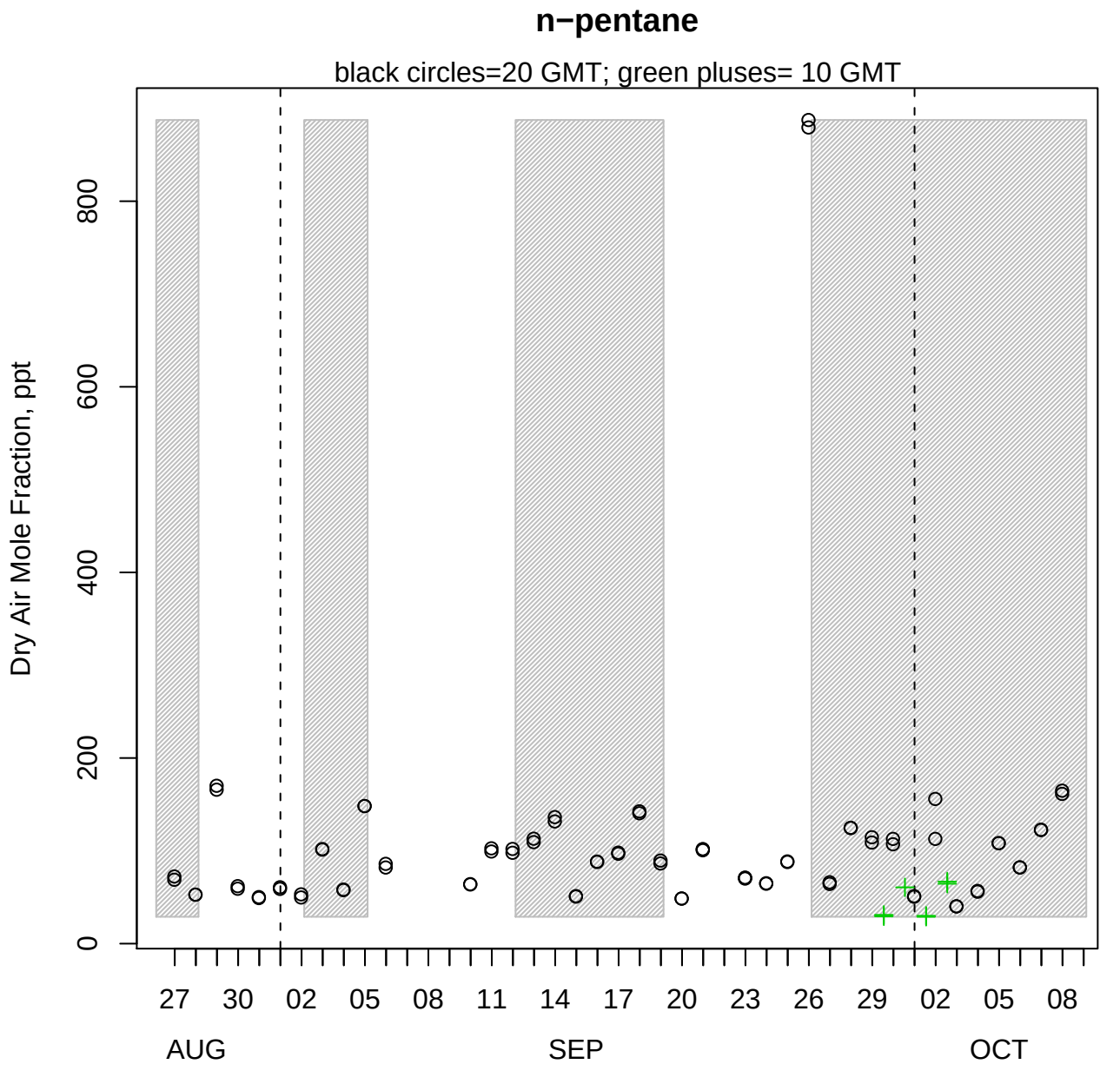
n−pentane
black circles=20 GMT; green pluses= 10 GMT
Dry Air Mole Fraction, ppt
0
200
400
600
800
27
30
02
05
08
11
14
17
20
23
26
29
02
05
08
AUG
SEP
OCT

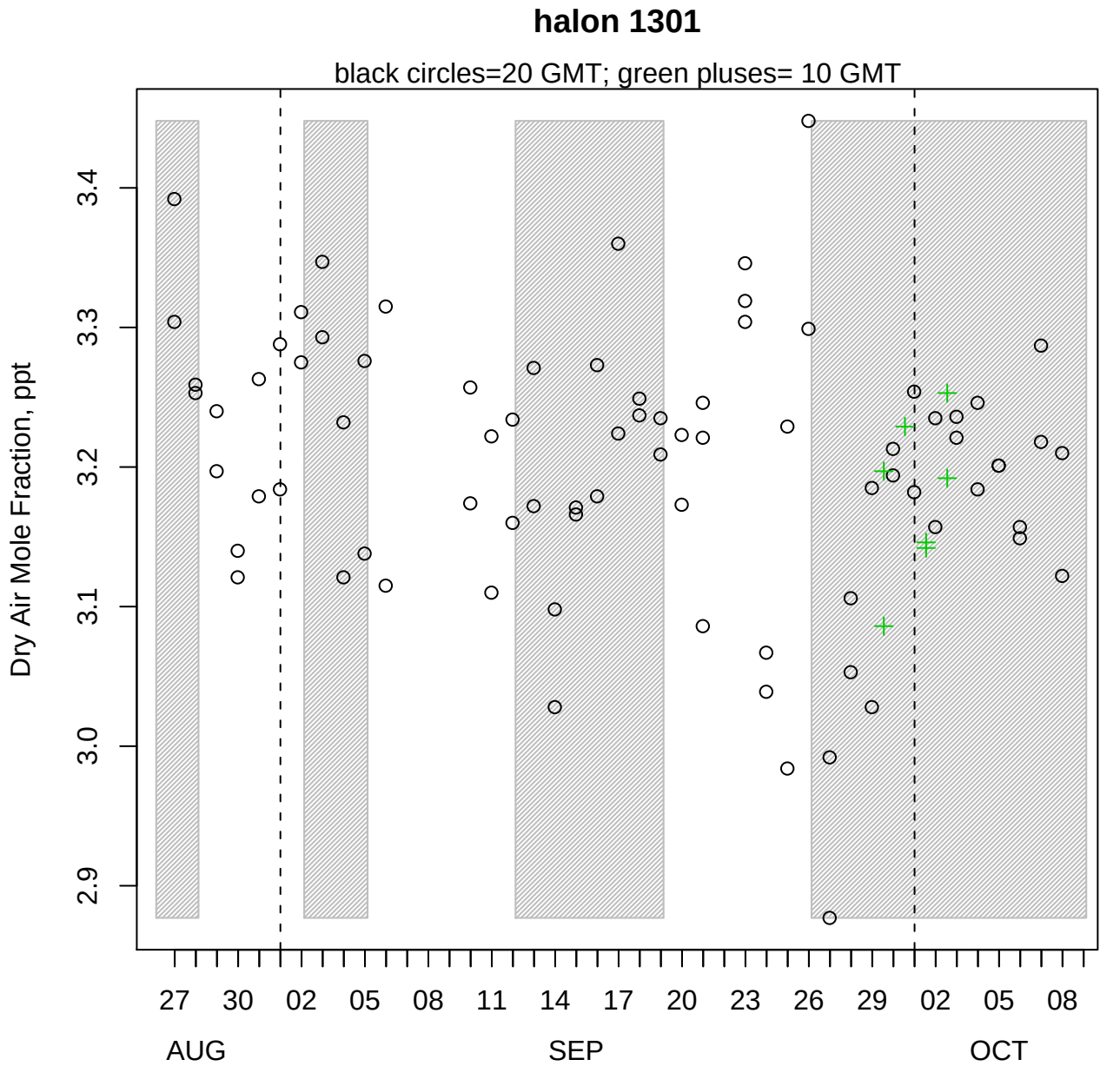
halon 1301
black circles=20 GMT; green pluses= 10 GMT
Dry Air Mole Fraction, ppt
2.9
3.0
3.1
3.2
3.3
3.4
27
30
02
05
08
11
14
17
20
23
26
29
02
05
08
AUG
SEP
OCT

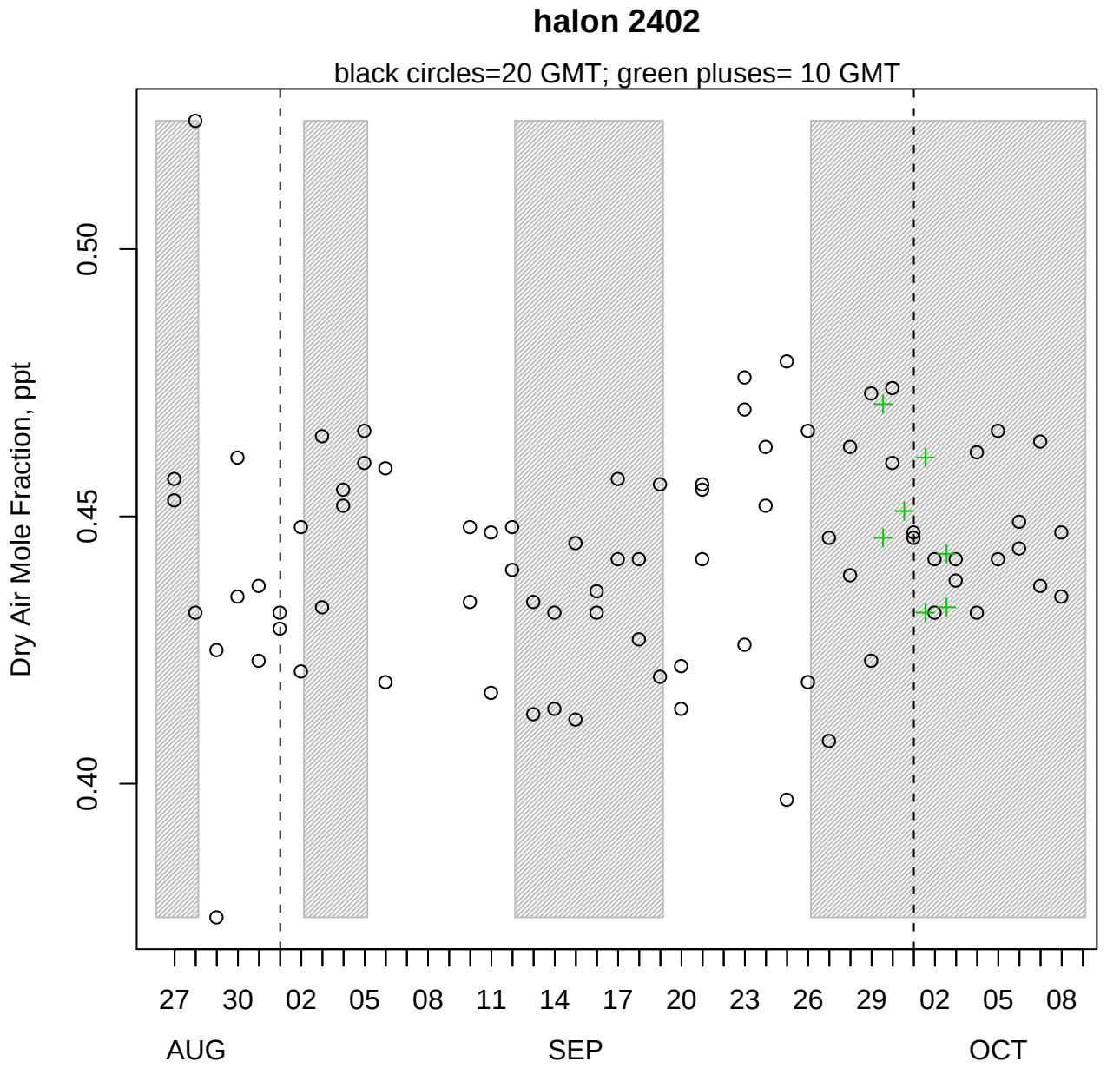
halon 2402
black circles=20 GMT; green pluses= 10 GMT
Dry Air Mole Fraction, ppt
0.40
0.45
0.50
27
30
02
05
08
11
14
17
20
23
26
29
02
05
08
AUG
SEP
OCT

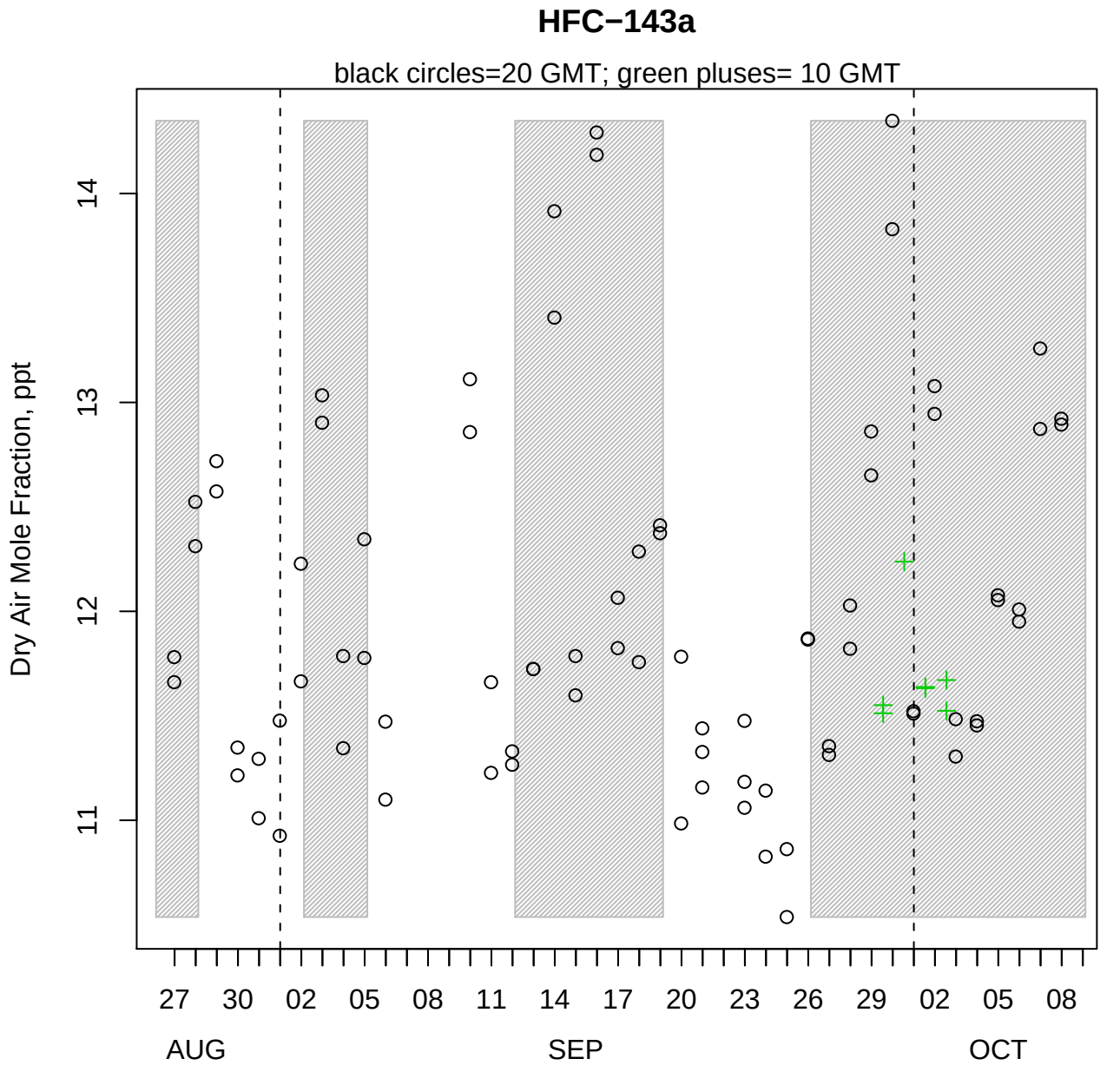
HFC−143a
black circles=20 GMT; green pluses= 10 GMT
Dry Air Mole Fraction, ppt
11
12
13
14
27
30
02
05
08
11
14
17
20
23
26
29
02
05
08
AUG
SEP
OCT

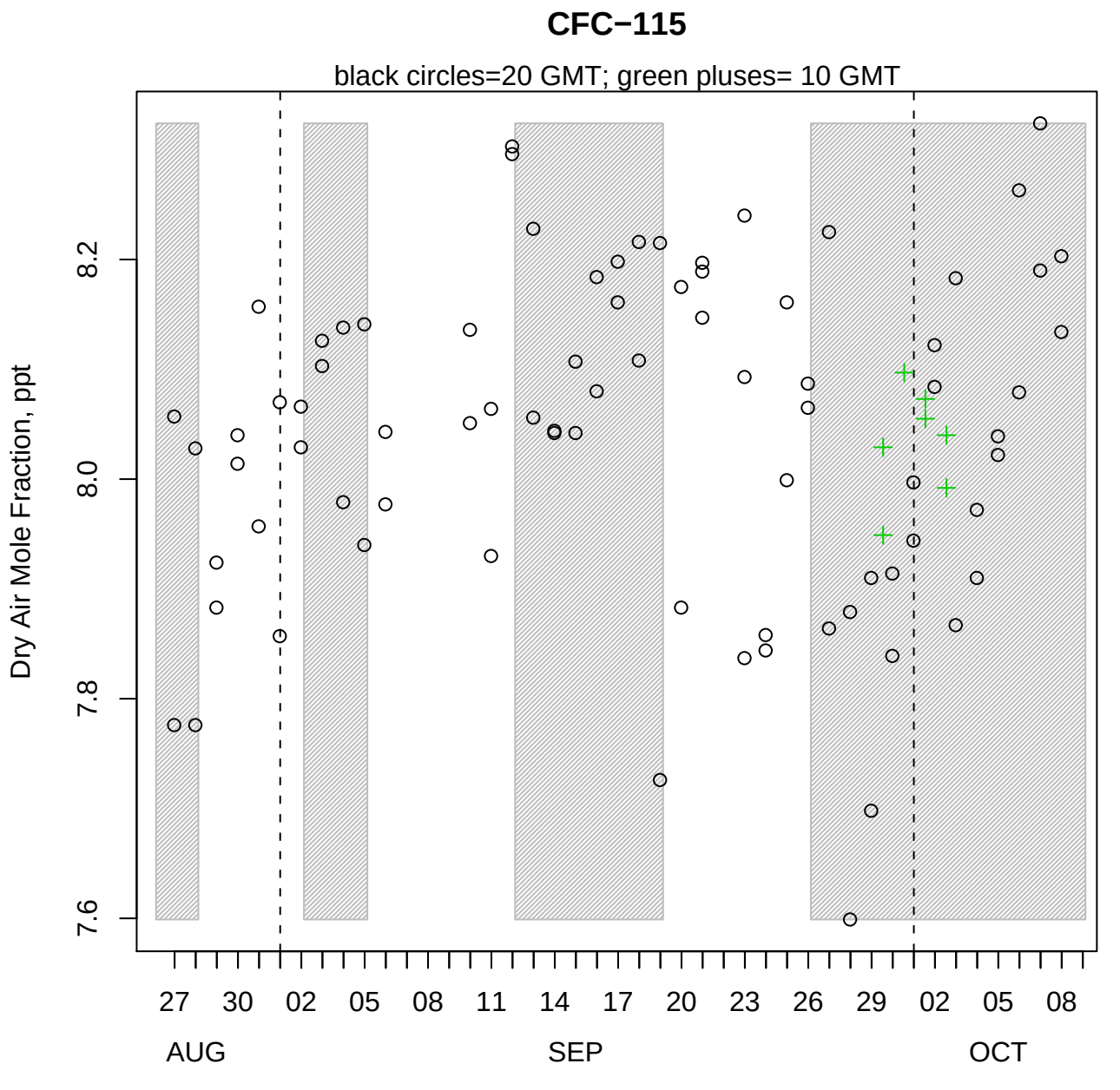
CFC−115
black circles=20 GMT; green pluses= 10 GMT
Dry Air Mole Fraction, ppt
7.6
7.8
8.0
8.2
27
30
02
05
08
11
14
17
20
23
26
29
02
05
08
AUG
SEP
OCT

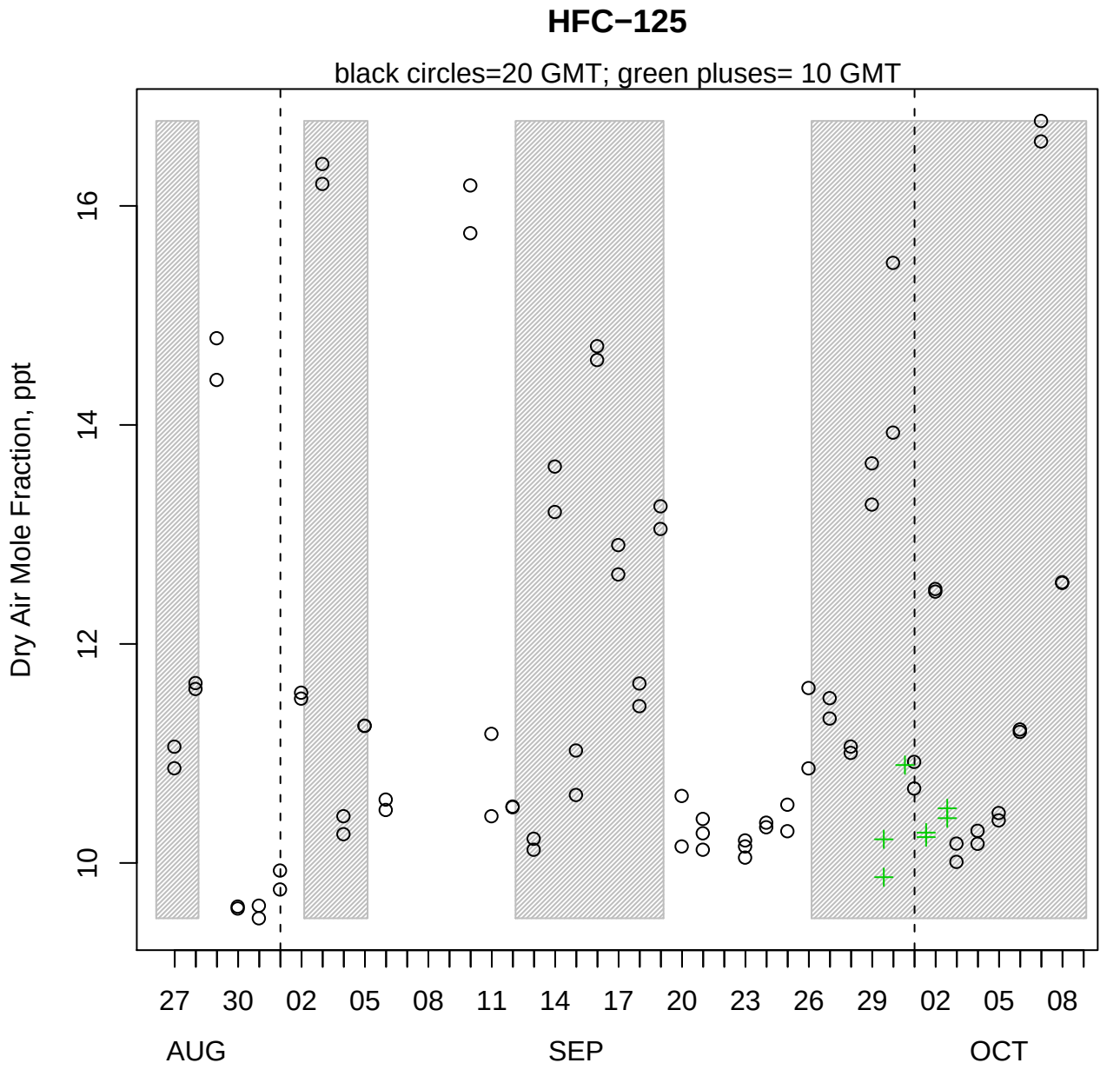
HFC−125
black circles=20 GMT; green pluses= 10 GMT
Dry Air Mole Fraction, ppt
10
12
14
16
27
30
02
05
08
11
14
17
20
23
26
29
02
05
08
AUG
SEP
OCT

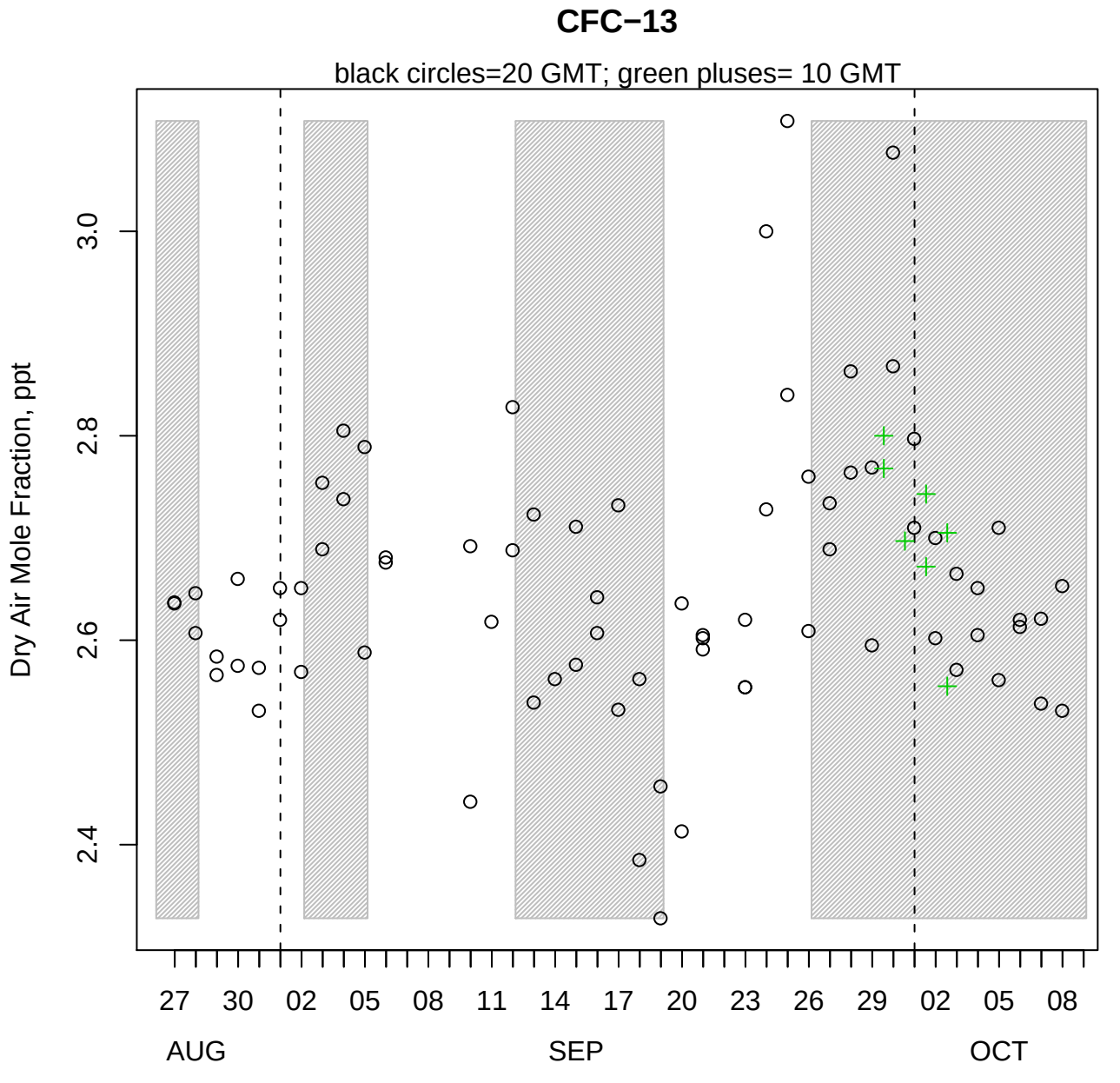
CFC−13
black circles=20 GMT; green pluses= 10 GMT
Dry Air Mole Fraction, ppt
3.0
2.8
2.6
2.4
27
30
02
05
08
11
14
17
20
23
26
29
02
05
08
AUG
SEP
OCT

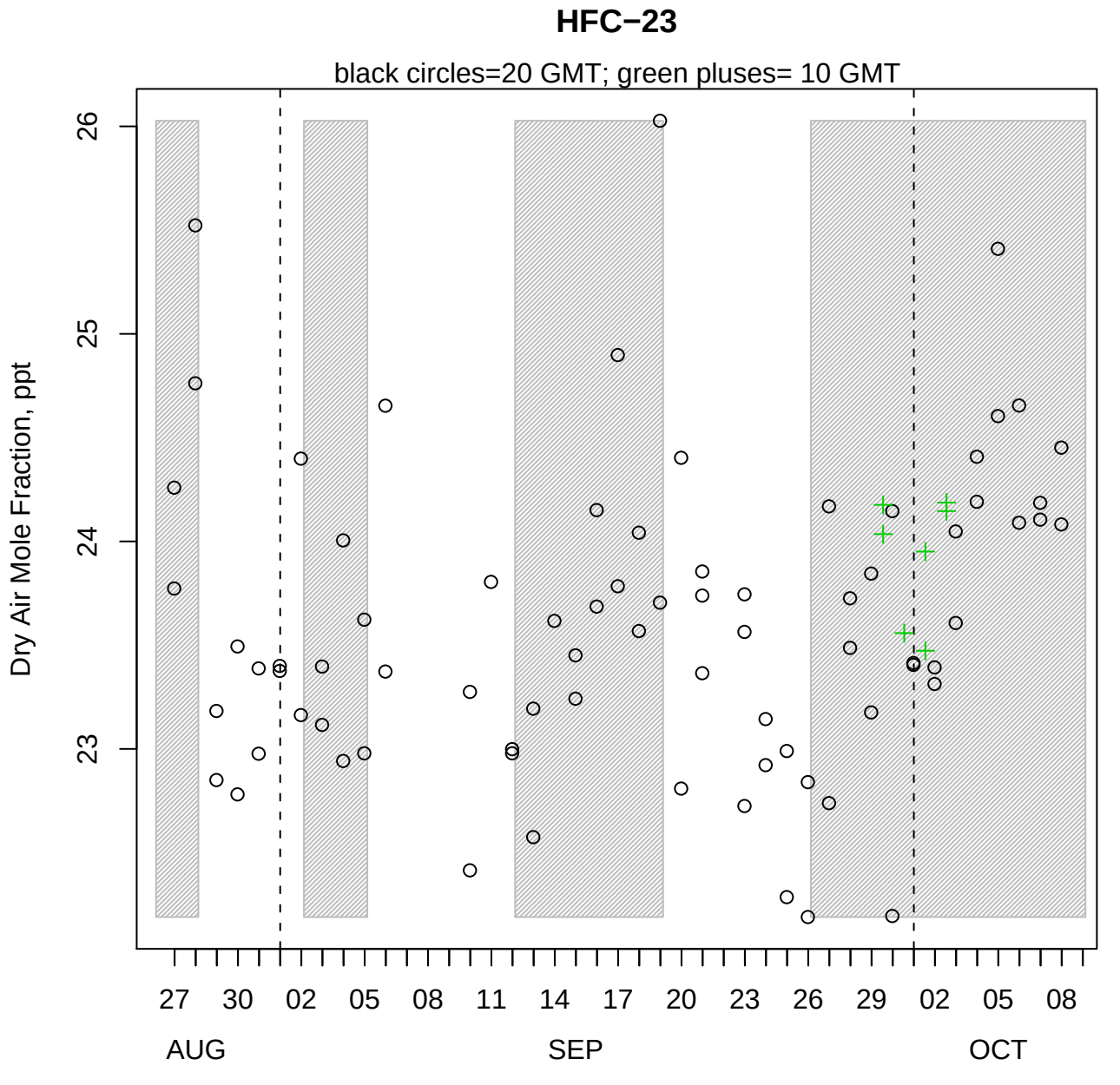
HFC−23
black circles=20 GMT; green pluses= 10 GMT
Dry Air Mole Fraction, ppt
23
24
25
26
27
30
02
05
08
11
14
17
20
23
26
29
02
05
08
AUG
SEP
OCT

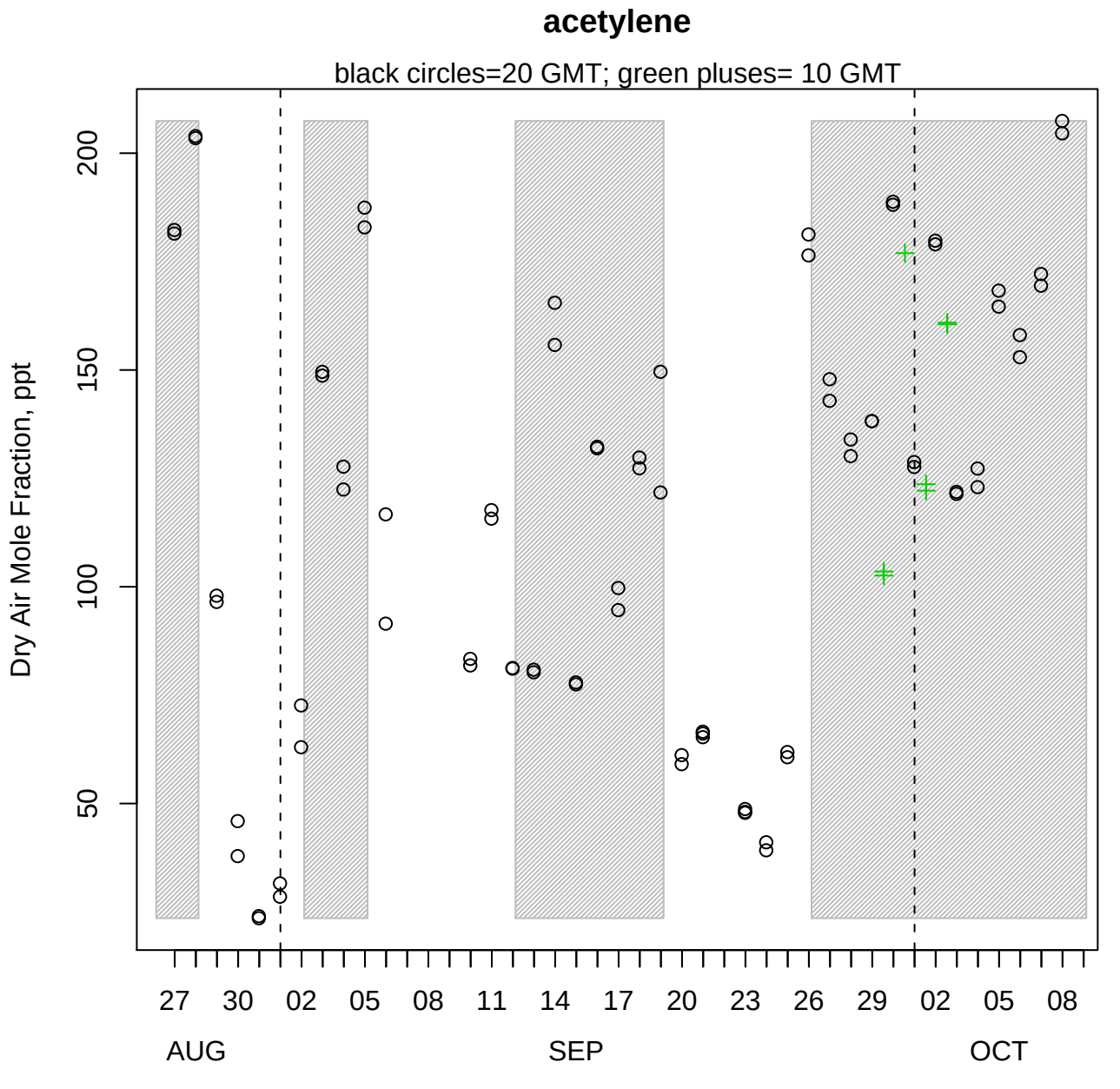
acetylene
black circles=20 GMT; green pluses= 10 GMT
Dry Air Mole Fraction, ppt
200
150
100
50
27
30
02
05
08
11
14
17
20
23
26
29
02
05
08
AUG
SEP
OCT

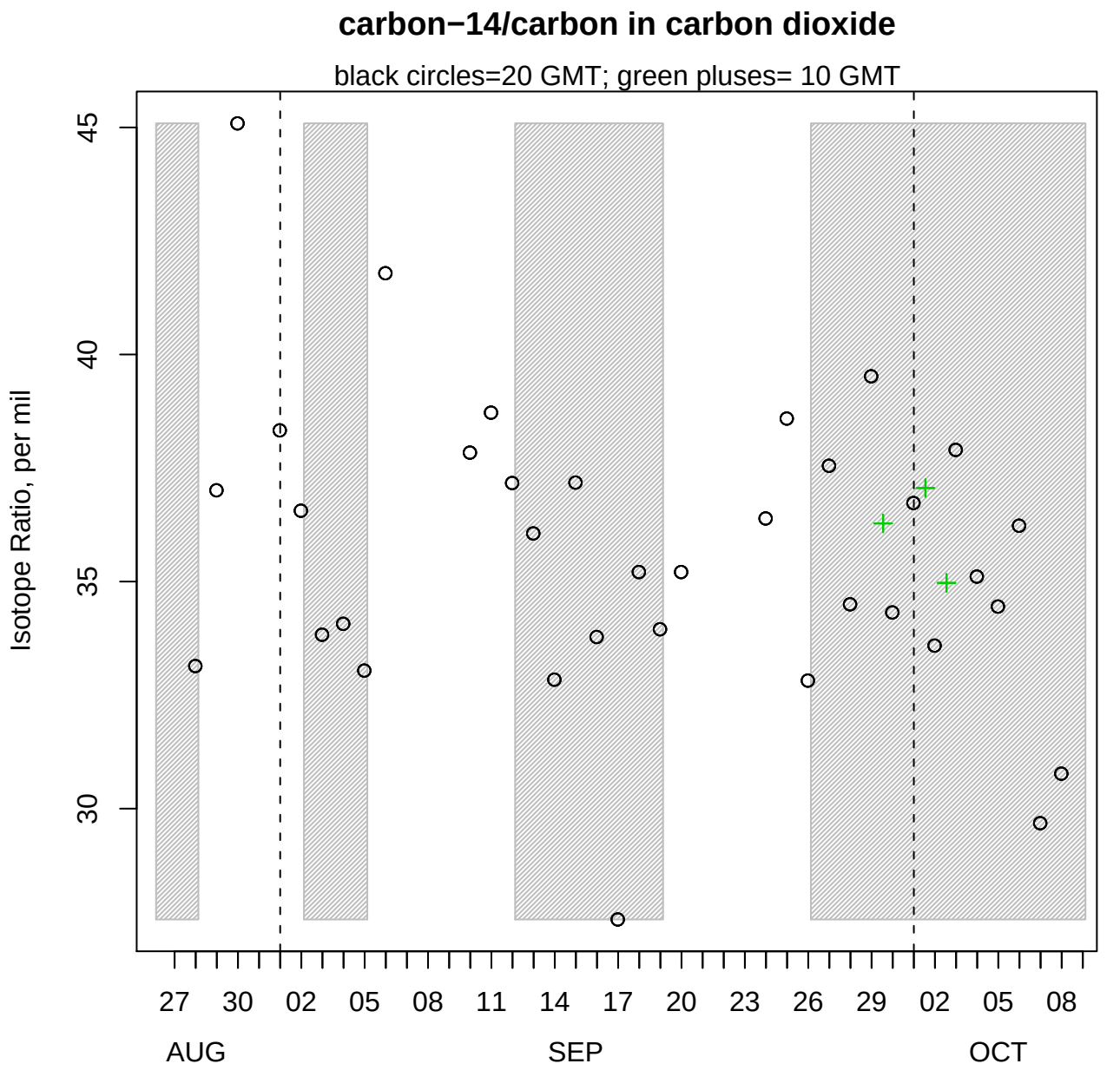
carbon−14/carbon in carbon dioxide
black circles=20 GMT; green pluses= 10 GMT
Isotope Ratio, per mil
45
40
35
30
27
30
02
05
08
11
14
17
20
23
26
29
02
05
08
AUG
SEP
OCT

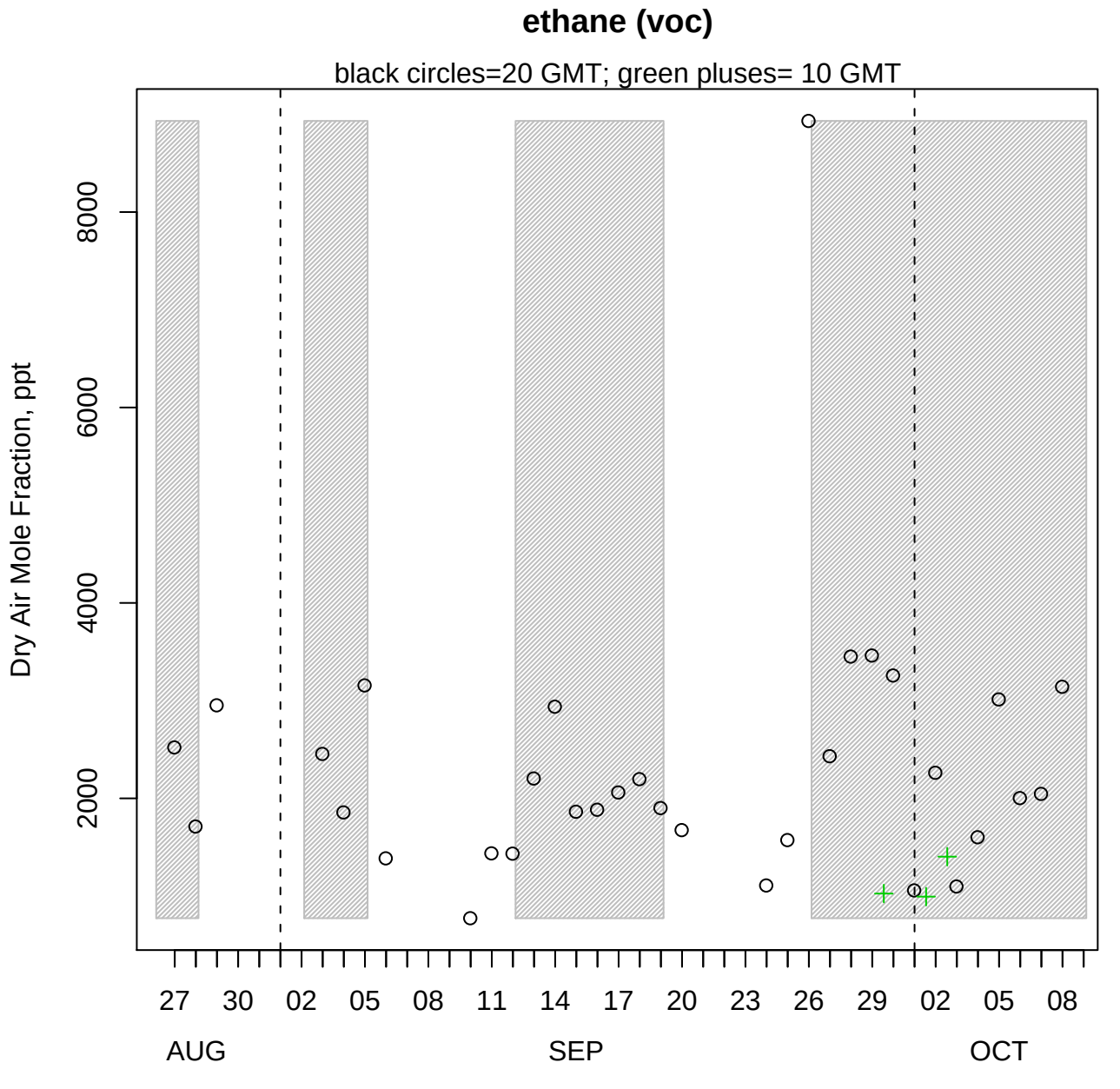
ethane (voc)
black circles=20 GMT; green pluses= 10 GMT
Dry Air Mole Fraction, ppt
2000
4000
6000
8000
27
30
02
05
08
11
14
17
20
23
26
29
02
05
08
AUG
SEP
OCT

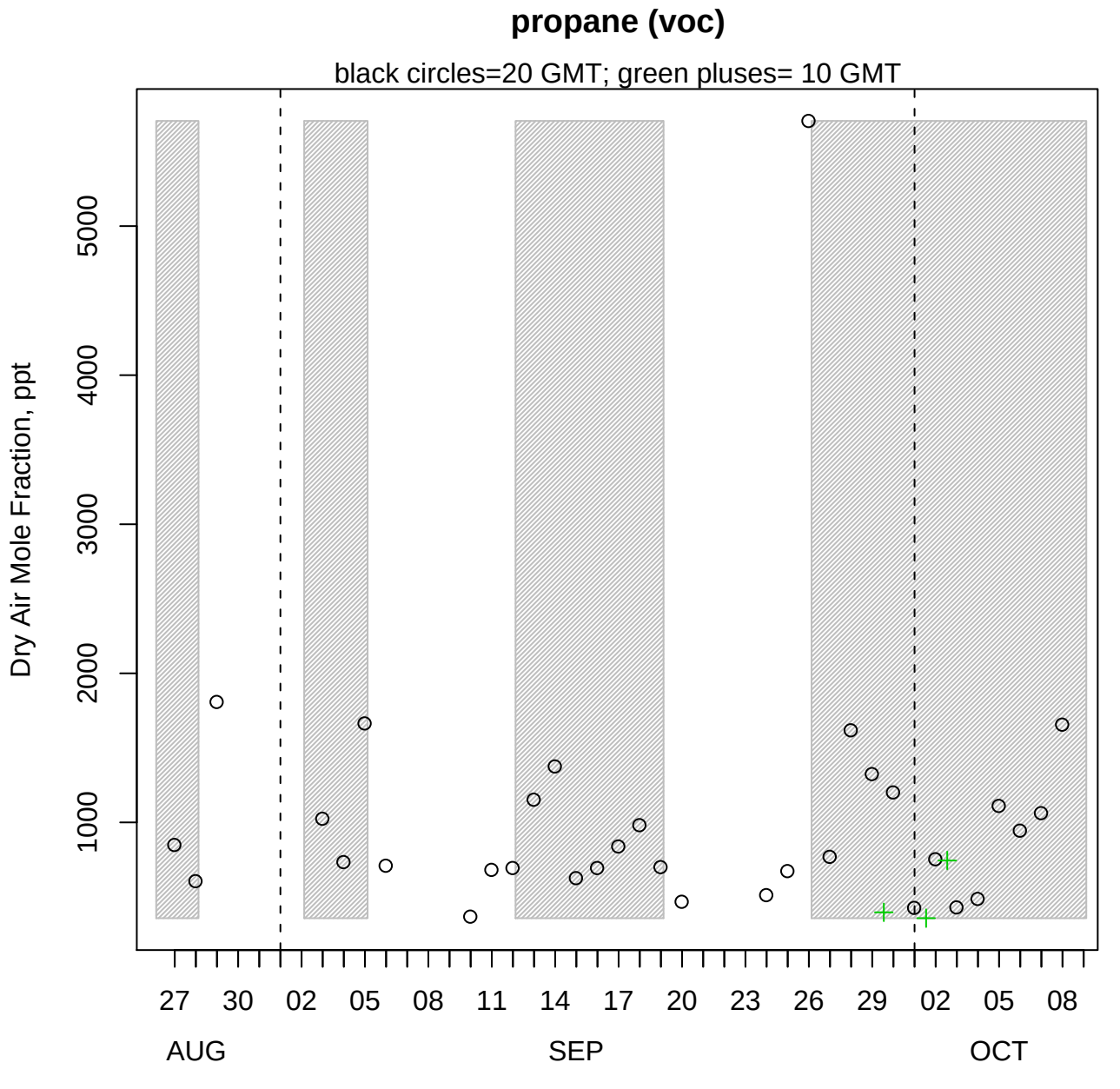
propane (voc)
black circles=20 GMT; green pluses= 10 GMT
Dry Air Mole Fraction, ppt
1000
2000
3000
4000
5000
27
30
02
05
08
11
14
17
20
23
26
29
02
05
08
AUG
SEP
OCT

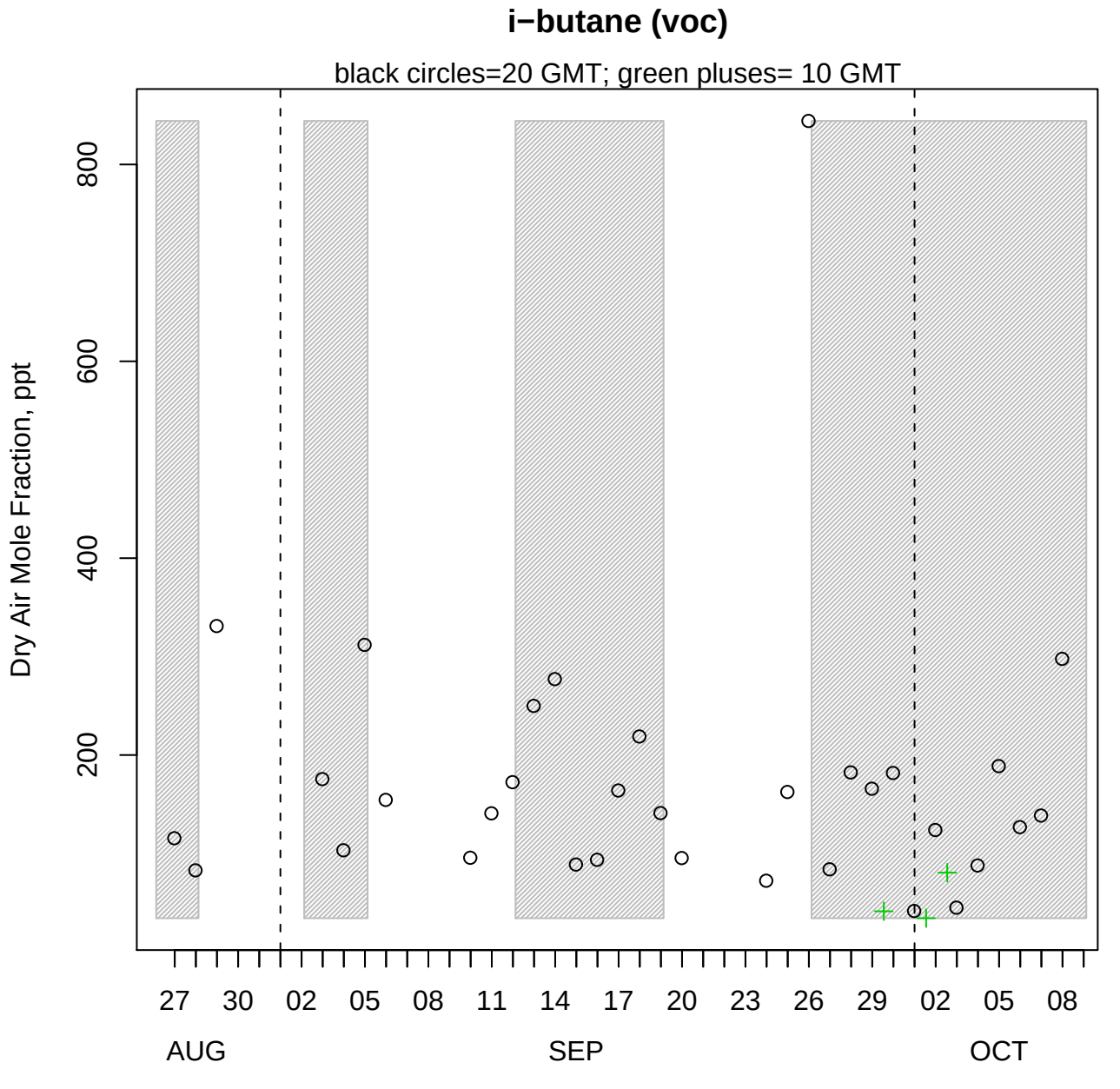
i−butane (voc)
black circles=20 GMT; green pluses= 10 GMT
Dry Air Mole Fraction, ppt
200
400
600
800
27
30
02
05
08
11
14
17
20
23
26
29
02
05
08
AUG
SEP
OCT

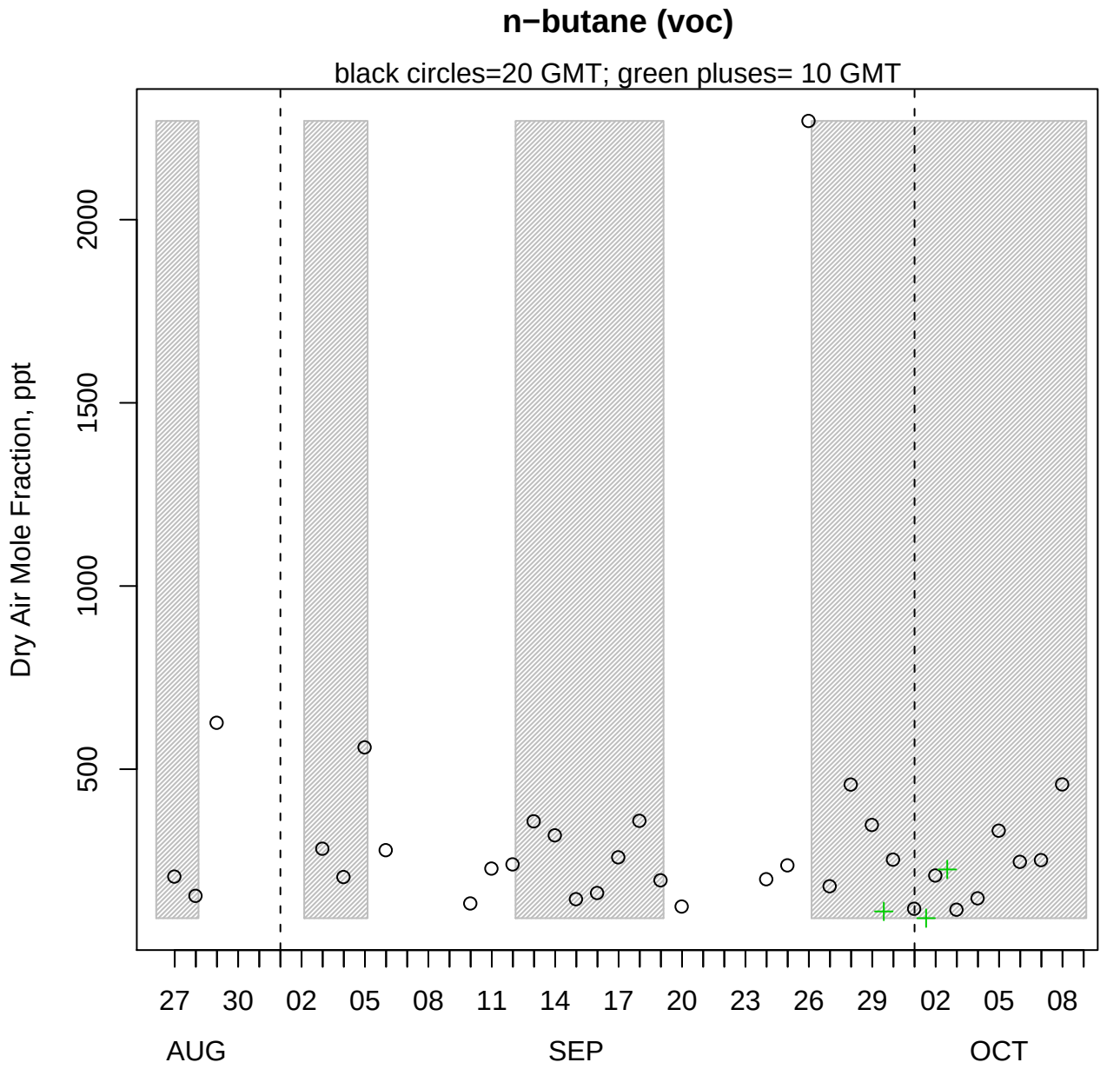
n−butane (voc)
black circles=20 GMT; green pluses= 10 GMT
Dry Air Mole Fraction, ppt
500
1000
1500
2000
27
30
02
05
08
11
14
17
20
23
26
29
02
05
08
AUG
SEP
OCT

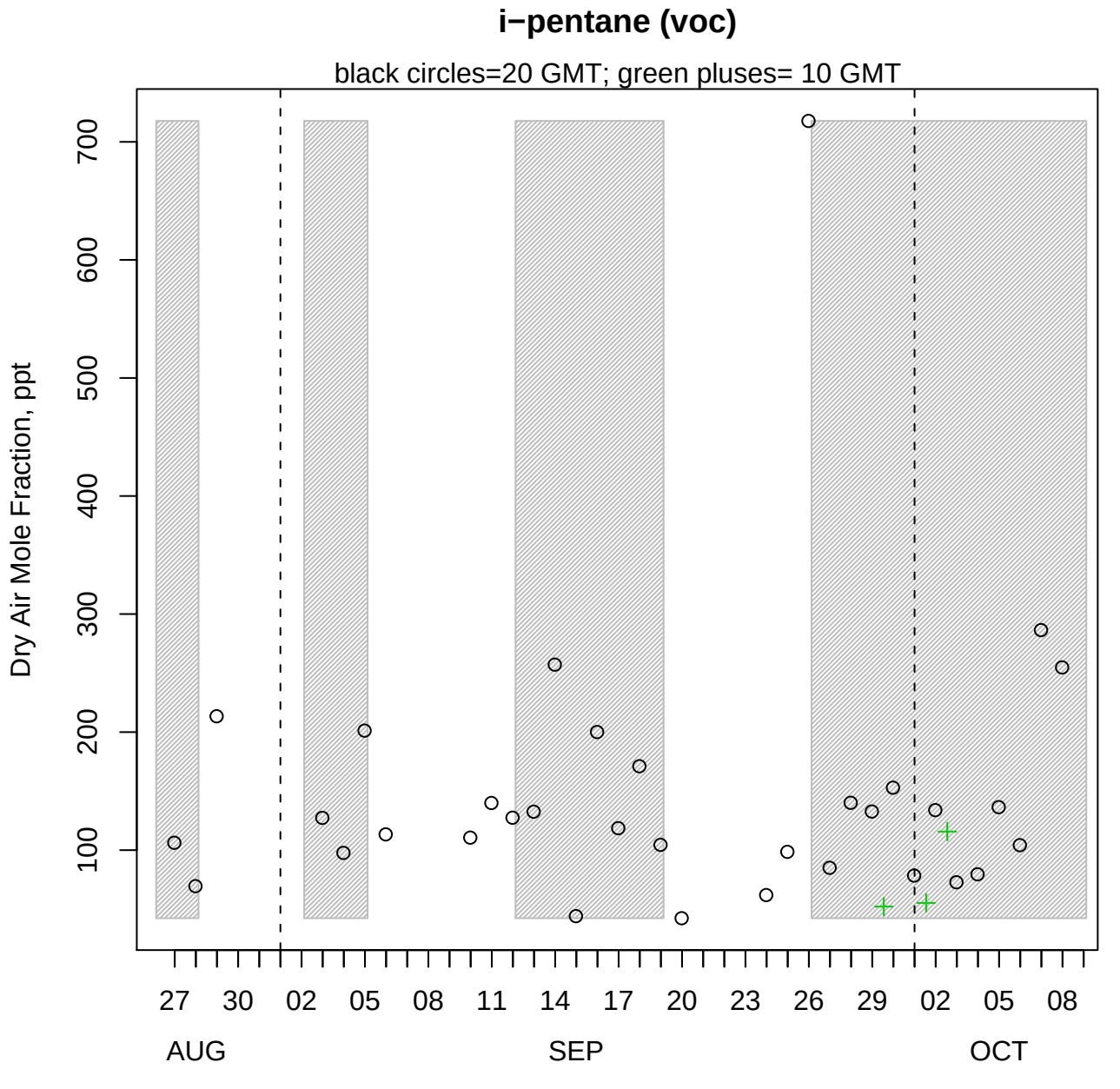
i−pentane (voc)
black circles=20 GMT; green pluses= 10 GMT
Dry Air Mole Fraction, ppt
100
200
300
400
500
600
700
27
30
02
05
08
11
14
17
20
23
26
29
02
05
08
AUG
SEP
OCT

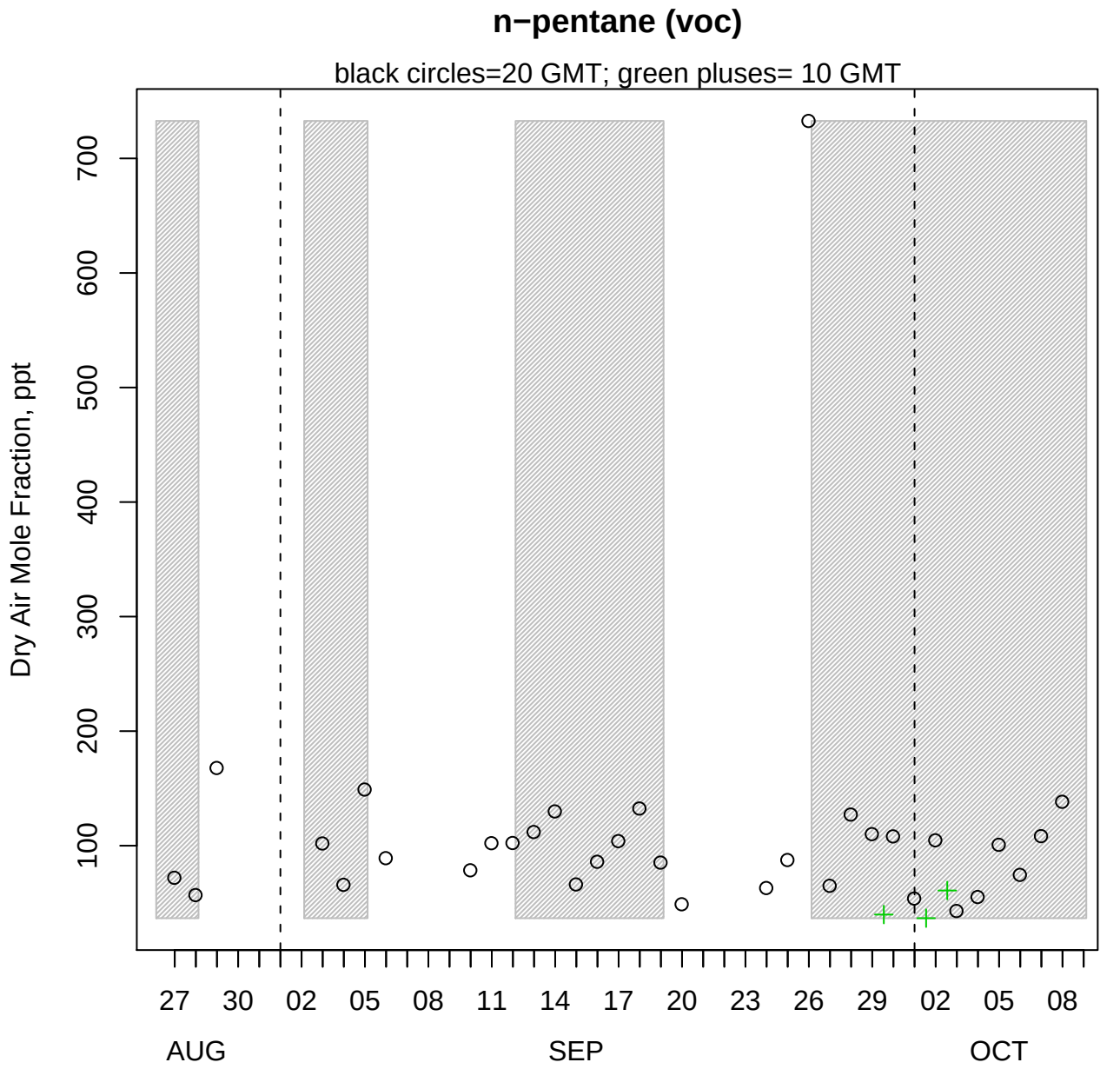
n−pentane (voc)
black circles=20 GMT; green pluses= 10 GMT
Dry Air Mole Fraction, ppt
100
200
300
400
500
600
700
27
30
02
05
08
11
14
17
20
23
26
29
02
05
08
AUG
SEP
OCT

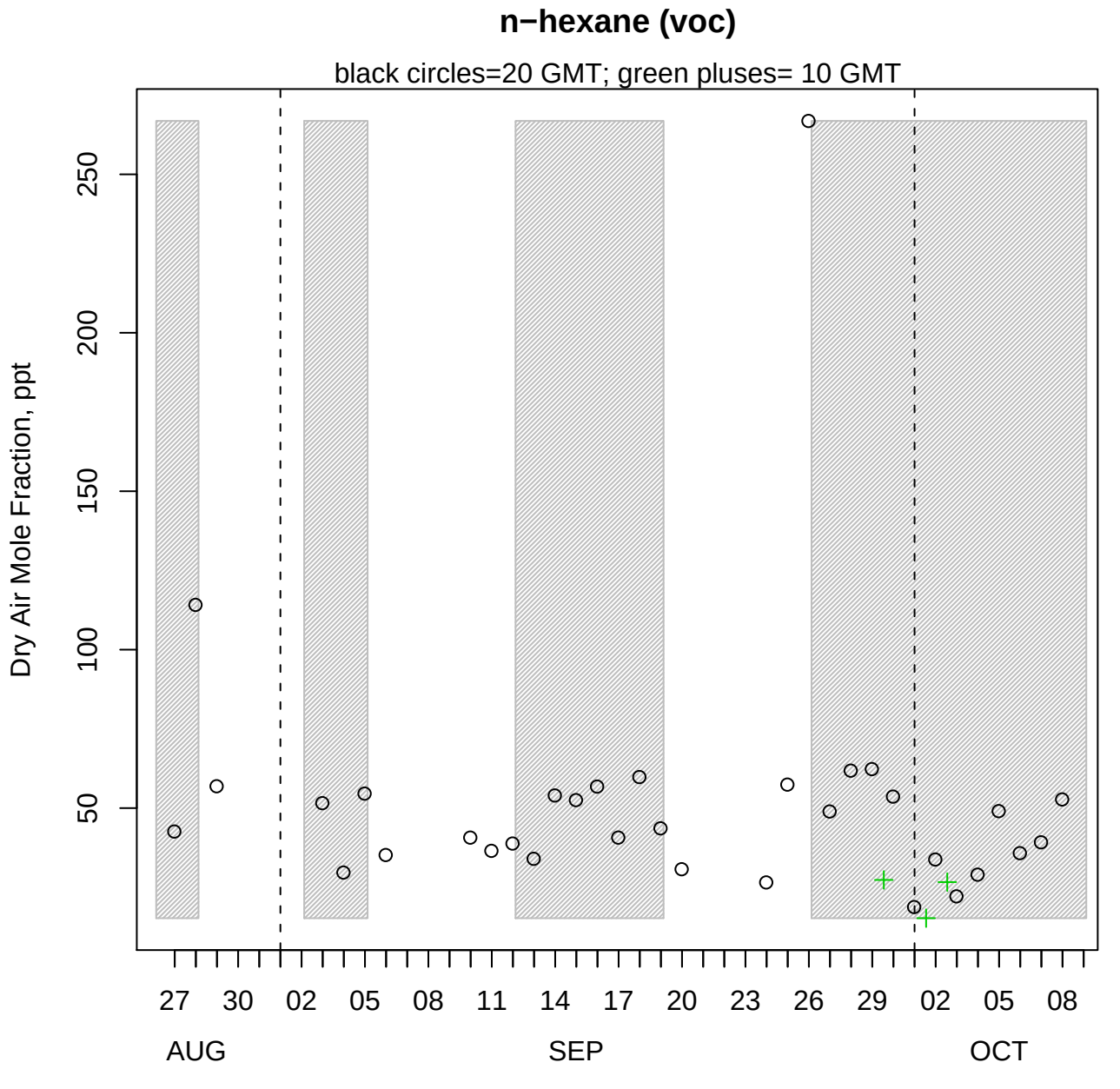
n−hexane (voc)
black circles=20 GMT; green pluses= 10 GMT
Dry Air Mole Fraction, ppt
50
100
150
200
250
27
30
02
05
08
11
14
17
20
23
26
29
02
05
08
AUG
SEP
OCT

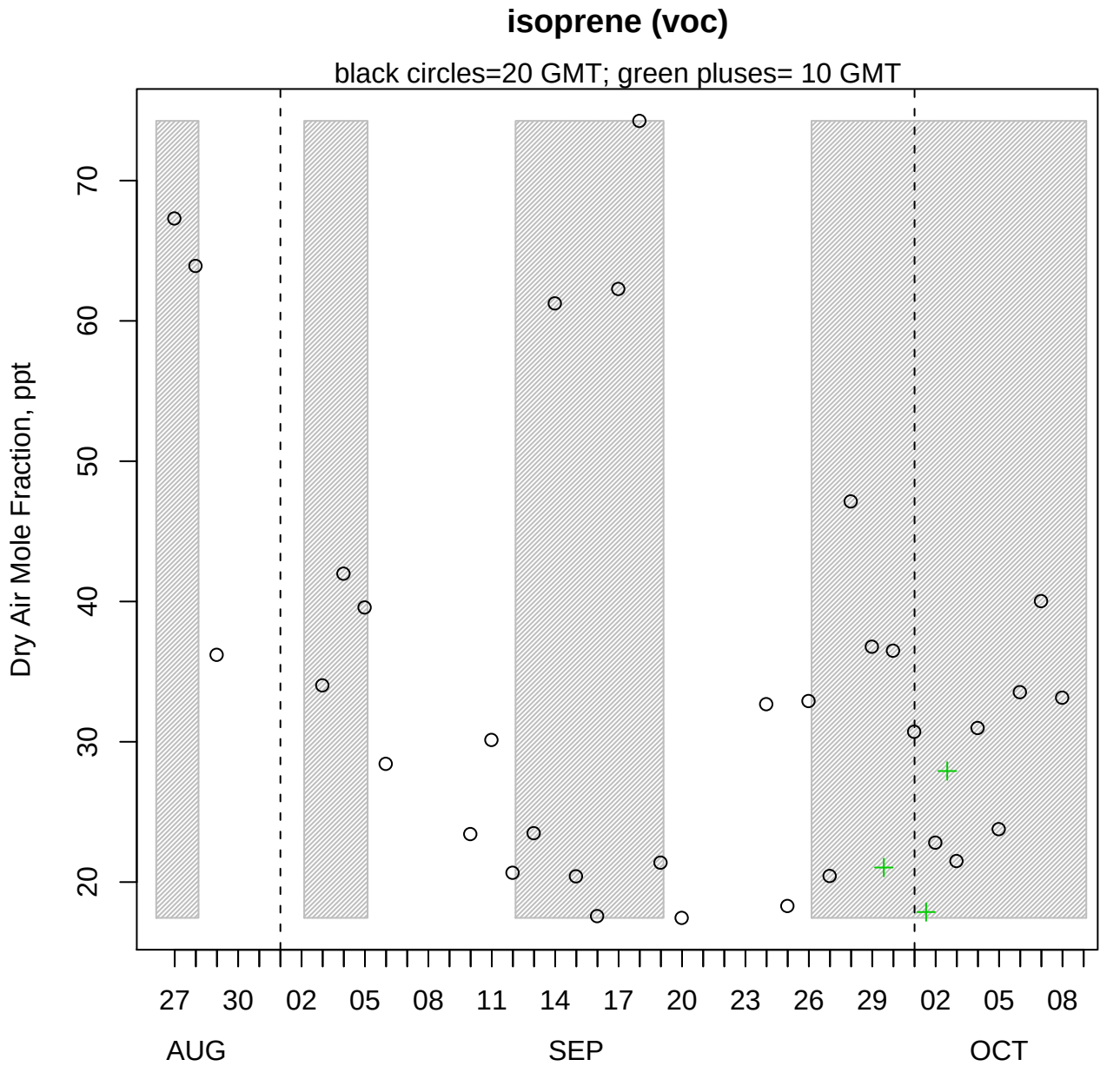
isoprene (voc)
black circles=20 GMT; green pluses= 10 GMT
Dry Air Mole Fraction, ppt
20
30
40
50
60
70
27
30
02
05
08
11
14
17
20
23
26
29
02
05
08
AUG
SEP
OCT

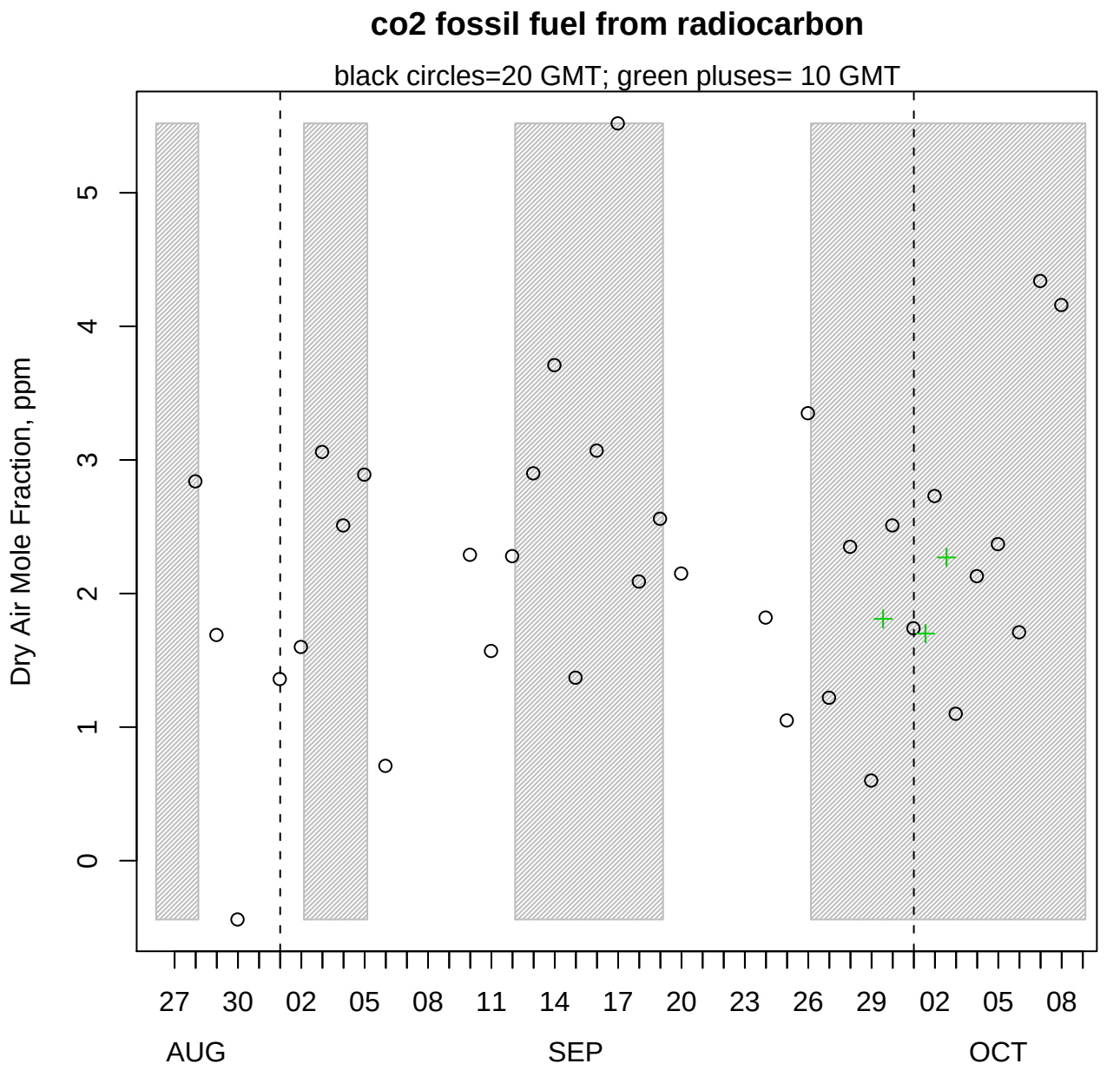
co2 fossil fuel from radiocarbon
black circles=20 GMT; green pluses= 10 GMT
Dry Air Mole Fraction, ppm
0
1
2
3
4
5
27
30
02
05
08
11
14
17
20
23
26
29
02
05
08
AUG
SEP
OCT